Analysis of Isogeometric Non-Symmetric FEM-BEM Couplings for the Simulation of Electromechanical Energy Converters

Analyse von isogeometrischen nicht-symmetrischen FEM-BEM Kopplungen zur Simulation elektromechanischer Energiewandler

Zur Erlangung des akademischen Grades Doktor-Ingenieur (Dr.-Ing.)
genehmigte Dissertation von Mehdi Elasmi aus Tunis, Tunesien
Fachbereich Elektrotechnik und Informationstechnik
Tag der Einreichung: 14.09.2021, Tag der Prüfung: 06.12.2021

1. Gutachten: Prof. Dr.-Ing. Stefan Kurz
2. Gutachten: Prof. Dr. rer. nat. Christoph Erath
3. Gutachten: Prof. Dr. rer. nat. Sebastian Schöps

Darmstadt – D 17

TECHNISCHE UNIVERSITÄT DARMSTADT

Fachbereich 18
Electromagnetism and Mathematical Modelling Group

Analysis of Isogeometric Non-Symmetric FEM-BEM Couplings for the Simulation of Electromechanical Energy Converters
Analyse von isogeometrischen nicht-symmetrischen FEM-BEM Kopplungen zur Simulation elektromechanischer Energiewandler

genehmigte Dissertation von Mehdi Elasmi aus Tunis, Tunesien
Fachbereich Elektrotechnik und Informationstechnik

1. Gutachten: Prof. Dr.-Ing. Stefan Kurz
2. Gutachten: Prof. Dr. rer. nat. Christoph Erath
3. Gutachten: Prof. Dr. rer. nat. Sebastian Schöps

Tag der Einreichung: 14.09.2021
Tag der Prüfung: 06.12.2021

Darmstadt – D 17

Bitte zitieren Sie dieses Dokument als:
URN: urn:nbn:de:tuda-tuprints-203294
URL: http://tuprints.ulb.tu-darmstadt.de/20329

Dieses Dokument wird bereitgestellt von tuprints,
E-Publishing-Service der TU Darmstadt
http://tuprints.ulb.tu-darmstadt.de
tuprints@ulb.tu-darmstadt.de

To my father

Erklärungen laut Promotionsordnung

§8 Abs. 1 lit. c PromO

Ich versichere hiermit, dass die elektronische Version meiner Dissertation mit der schriftlichen Version übereinstimmt.

§8 Abs. 1 lit. d PromO

Ich versichere hiermit, dass zu einem vorherigen Zeitpunkt noch keine Promotion versucht wurde. In diesem Fall sind nähere Angaben über Zeitpunkt, Hochschule, Dissertationsthema und Ergebnis dieses Versuchs mitzuteilen.

§9 Abs. 1 PromO

Ich versichere hiermit, dass die vorliegende Dissertation selbstständig und nur unter Verwendung der angegebenen Quellen verfasst wurde.

§9 Abs. 2 PromO

Die Arbeit hat bisher noch nicht zu Prüfungszwecken gedient.

Darmstadt, 14.09.2021

M. Elasmi

Zusammenfassung

Diese Arbeit befasst sich mit der Analyse von isogeometrischen nicht-symmetrischen Kopplungen der Methode der finiten Elemente (FEM, von engl. Finite Element Method) mit der direkten Randelementmethode (BEM, von engl. Boundary Element Method) für Aufgabestellungen, wie sie bei der Modellierung elektromechanischer Energiewandler vorkommen.

Das (elektro)magnetische Teilsystem eines solchen multiphysikalischen Problems lässt sich mit der Wirbelstromnäherung der Maxwellschen Gleichungen beschreiben. Sowohl das statische als auch das quasistationäre Verhalten des Systems werden in dieser Arbeit behandelt. Dafür werden Wirbelstromformulierungen auf Basis des magnetischen Vektorpotentials in zwei- und dreidimensionalen Lipschitz-Gebieten hergeleitet. Es werden dabei keine Einschränkungen bezüglich der Topologie der Gebiete vorausgesetzt.
Die FEM wird in solchen Gebieten eingesetzt, in denen nichtlineare Materialien zulässig sind. Im Gegensatz dazu ist die Anwendung der BEM auf Gebiete beschränkt, die lineares Materialverhalten aufweisen, da eine Fundamentallösung benötigt wird.

Es wird bei der vorliegenden Analyse von der Theorie Lipschitz-stetiger und streng monotoner Operatoren ausgegangen. Diesem theoretischen Rahmen entsprechen auch die physikalischen Eigenschaften der betrachteten nichtlinearen Materialien.
Um Wohlgestelltheit der Kopplungen zu zeigen, wird je nachdem entweder eine implizite Stabilisierung eingeführt (in zwei Dimensionen) oder eine Formulierung in geeigneten Quotientenräumen betrachtet (in drei Dimensionen). Außerdem wird die Quasioptimalität der Galerkin-Approximation nachgewiesen. Daraus werden Fehlerabschätzungen optimaler Ordnung für konforme B-Spline-Räume abgeleitet. Darüber hinaus weist der punktweise Fehler bezüglich Funktionalen der Lösung in BEM-Gebieten eine Verbesserung der Konvergenzraten auf, die unter bestimmten Bedingungen zur Verdopplung dieser Raten führt. Diese Eigenschaft wird Superkonvergenz genannt.
Zur Geometriemodellierung werden NURBS (von engl. Non-Uniform Rational B-Splines) benutzt, so dass keine weiteren numerischen Fehler durch die Approximation der Geometrie eingeführt werden. Zusätzlich erleichtert dieses Diskretisierungsverfahren die Durchführung von h- und p-Verfeinerungen.

Die theoretischen Resultate werden durch numerische Beispiele validiert. Zur Illustration des gekoppelten elektromechanischen Problems wird das magnetische mit dem mechanischen Teilsystem schwach gekoppelt. Die für die Kopplung benötigten Kräfte und/oder Drehmomente werden mittels des Maxwellschen Spannungstensors ausgehend von den Cauchy-Daten der Lösung des magnetischen Teilsystems berechnet. Bei den zeitabhängigen numerischen Beispielen wird die Zeitdiskretisierung mittels eines klassischen impliziten Euler-Verfahrens durchgeführt. Alle Resultate entsprechen den Erwartungen und den Referenzlösungen.

Abstract

The main contribution of this thesis consists in providing a rigorous analysis of non-symmetric isogeometric couplings of the Finite Element Method (FEM) and the direct Boundary Element Method (BEM) for some model problems that are relevant for the simulation of electromechanical energy converters.

The corresponding (electro)magnetic subsystem of such a multi-physics problem can be modeled by the eddy-current approximation of Maxwell's equations. We study this type of models in both the static and quasi-stationary case, which we formulate in terms of the magnetic vector potential in two-dimensional (2D) and three-dimensional (3D) Lipschitz domains with a general topology. We associate FEM with bounded domains that may be filled with non-linear materials, whereas BEM is applied for bounded and unbounded domains that contain linear materials, i.e., for which a fundamental solution is available.

Our analysis is based on the framework of strongly monotone and Lipschitz continuous operators, which also incorporates the required physical properties of the considered non-linear materials.
To establish well-posedness and stability of the continuous settings, we use either implicit stabilization (in two dimensions) or a formulation in appropriate quotient spaces (in three dimensions) depending on the specific model. Moreover, we show the quasi-optimality of the method with respect to a conforming Galerkin discretization. For the concrete discretization, we consider an isogeometric framework, in particular, we employ conforming B-Spline spaces for the approximation of the solution, and Non-Uniform Rational B-Splines (NURBS) for geometric modelling. This approach facilitates h- and p-refinements, and avoids the introduction of geometrical errors. In this setting, we derive a priori estimates, and discuss the possible improvement of the convergence rates (super-convergence) of the method, when the pointwise error in functionals of the solution (more precisely its Cauchy data) is evaluated in the BEM domain. This improvement may double the usual convergence rates under certain circumstances.

The theoretical findings are confirmed through several numerical examples. To validate our approach for the complete electromechanical system, we couple the (electro)magnetic and the mechanical subsystems weakly, and compute the needed forces and/or torques by using the Maxwell Stress Tensor (MST) method. For the sake of illustration, time derivatives are discretized by means of a classical implicit Euler scheme. The results of numerical experiments are in agreement with the expectations and the reference solutions.

Contents

List of figures

1 Introduction and motivation

> Energy cannot be created or destroyed, it can only be changed from one form to another.
>
> *A. Einstein*

Under electromechanical energy converters we understand every device that converts electrical energy into mechanical one, and vice versa. They are involved in a broad spectrum of applications, ranging from micro to macro scales, and from complex industrial processes to common household items used on a daily basis. For instance, food processors, refrigerators, microphones and loudspeakers, electric cars, and some types of power-plant facilities rely particularly on these devices. In general, a pattern can be recognized: The input energy, which is either electrical or mechanical is transferred to a coupling carrier field, usually a magnetic field, where it is temporarily stored and then released in terms of the other type of energy. Inevitably, some energy may dissipate during the process, e.g., in form of heat. For convenience, we classify these devices in two categories:

- Linear motion devices: the linear motion is caused by the (electromagnetic) force.
- Rotating machines: depending on the direction of conversion, they can be labeled either motors or generators. The former rely on the conversion of an electrical to mechanical energy, and vice versa for the latter.

We also use the term electric machines generically to designate both types. More details about the physical foundation of the topic and its significance can be found in [54]. The development and optimization of such machines requires first of all a good knowledge of their physical background. Indeed, it consists in a multi-physics problem with (electro)magnetism as the core physical field coupled at least with the corresponding mechanical equations. After having a suitable model at our disposal, its resolution poses the next challenge. An analytical solution is either too complex or not possible in general. Hence, we resort to numerical methods, which offer a relatively wide spectrum of approaches that may have advantages and disadvantages depending on the case and on the goal. The most widespread one is the Finite Element Method (FEM). It is well-established and advantageous in many cases, in particular, in the presence of non-linear materials and inhomogenities. For an introduction to mathematical modelling and FEM for this type of devices we refer, e.g., to [113]. However, FEM requires a domain discretization. Hence, considering unbounded or very thin domains may lead to difficulties. In these cases, the Boundary Element Method (BEM) turns out to be an attractive alternative, because it transfers a problem from the domain to the boundary. Nevertheless, BEM is reserved to linear problems with computable fundamental solutions. To cope with this, we opt for a coupling of FEM and BEM, which we discretize by using the isogeometric paradigm, i.e., by using the same type of basis functions for the geometric design and for the approximation of the solution. Typically, these basis functions are B-Splines and/or Non-Uniform Rational B-Splines (NURBS). We will further discuss the choice of our numerical approach in Section 1.2, but first we address the physical framework encountered in this

work. The current chapter is then concluded by Section 1.3, where we give an overview on the structure and content of this treatise.

1.1 Physical framework

In the following, we present the relevant equations that are needed to derive suitable model problems for machines that rely on electromechanical energy conversions. First, we start by introducing the governing equations in electromagnetism. These are based on the well-known Maxwell's equations. In particular, the considered regime for most electromechanical applications happens to be in the low-frequency range, see [66, Section 2.2]. In this case, the full set of Maxwell's equations can be reduced to the so called eddy-current model, which is also known as the magnetoquasistationary case. In addition, since non-linear materials are widely considered in this type of applications, we discuss their properties and the required assumptions that are needed for an appropriate physical model. Then, we address the underlying equations of motion along with the Maxwell Stress Tensor (MST) method, which we utilize for the computation of forces and torques. Last, we introduce the considered approach to couple the electrical and mechanical subsystems, which consists in a weak coupling that allows to solve the electromechanical problem sequentially.

1.1.1 Maxwell's equations

The publication of James Clerk Maxwell [85] is regarded as the foundation of classical electrodynamics. Thereby, he provided a mathematical model consisting in a set of partial differential equations that describe electromagnetic fields. In their modern formulation, as given, e.g., in [67], the differential form of Maxwell's equations reads

$$\operatorname{div} \boldsymbol{d}(\boldsymbol{x},t) = \varrho(\boldsymbol{x},t), \tag{1.1a}$$
$$\operatorname{div} \boldsymbol{b}(\boldsymbol{x},t) = 0, \tag{1.1b}$$
$$\mathbf{curl}\, \boldsymbol{e}(\boldsymbol{x},t) = -\partial_t \boldsymbol{b}(\boldsymbol{x},t), \tag{1.1c}$$
$$\mathbf{curl}\, \boldsymbol{h}(\boldsymbol{x},t) = \partial_t \boldsymbol{d}(\boldsymbol{x},t) + \boldsymbol{j}(\boldsymbol{x},t) \tag{1.1d}$$

for any $\boldsymbol{x} \in \mathbb{R}^3$ and $t > 0$. Equation (1.1a) is known as Gauß's law. It relates the electric flux density $\boldsymbol{d}(\boldsymbol{x},t)$ to its source, namely, the electric charge distribution $\varrho(\boldsymbol{x},t)$. The second equation (1.1b) is its equivalent for magnetism. It states the important result that the magnetic flux density $\boldsymbol{b}(\boldsymbol{x},t)$ is source free, hence, it points out to the absence of magnetic monopoles. Equations (1.1c) and (1.1d) are known as Faraday's and Ampère's law, respectively. They relate electric quantities to magnetic ones. In particular, (1.1c) means that a time-varying magnetic flux density induces a spatial variation of the electric field $\boldsymbol{e}(\boldsymbol{x},t)$, and vice-versa. Similarly, a time-varying electric flux density is always accompanied with a spatial variation of the magnetic field strength $\boldsymbol{h}(\boldsymbol{x},t)$. In addition, electric currents, denoted by $\boldsymbol{j}(\boldsymbol{x},t)$, also contribute to the last equation.
In certain situations, the consideration of the full set of Maxwell's equations is not necessary. Indeed, neglecting the term $\partial_t \boldsymbol{d}(\boldsymbol{x},t)$ for low-frequency applications yields a valid approximation, which is labeled in the literature as the magnetoquasistationary case or eddy-current approximation. Justifications about its validity are furnished in [11, 16, 105, 112]. Note that for our specific applications, the inductive and resistive effects are dominant. More generally, when the capacitive effects dominate, a different type of low-frequency approximation is required, see [112]. Indeed, eddy-current approximation is the standard model to choose

for the simulation of electric machines, see [102], for instance. We also refer to [99, Section 2.2–2.3] for an introduction to the subject. Therefore, the system (1.1) simplifies to[1]

$$\operatorname{div} \boldsymbol{e}(\boldsymbol{x},t) = \frac{\varrho(\boldsymbol{x},t)}{\varepsilon}, \tag{1.2a}$$

$$\mathbf{curl}\, \boldsymbol{e}(\boldsymbol{x},t) = -\partial_t \boldsymbol{b}(\boldsymbol{x},t), \tag{1.2b}$$

$$\mathbf{curl}\, \boldsymbol{h}(\boldsymbol{x},t) = \boldsymbol{j}(\boldsymbol{x},t), \tag{1.2c}$$

$$\operatorname{div} \boldsymbol{b}(\boldsymbol{x},t) = 0. \tag{1.2d}$$

Note that due to $\partial_t \boldsymbol{d}(\boldsymbol{x},t) = 0$, the electric charge distribution $\varrho(\boldsymbol{x},t)$ is constant in time, i.e., $\partial_t \varrho = 0$. This yields the continuity equation

$$\operatorname{div} \boldsymbol{j}(\boldsymbol{x},t) = 0.$$

Moreover, the electric charge distribution ϱ is decoupled from the magnetic field equations in this context. Hence, it can be computed in a post-processing step, see [112, Section 3.2].
These equations need to be supplemented by constitutive laws, which define the relation between field quantities and their fluxes. In the linear isotropic case, we have for the magnetic field

$$\boldsymbol{b}(\boldsymbol{x},t) = \mu \boldsymbol{h}(\boldsymbol{x},t), \tag{1.3}$$

where μ is a scalar known as the magnetic permeability. It is defined by $\mu = \mu_\mathrm{r}\mu_0$, where μ_r denotes the relative magnetic permeability of the material, and μ_0 is a physical constant called the vacuum permeability. In this context, we restrict ourselves throughout the thesis to the homogeneous case. In general, μ is a non-linear second-rank tensor. For simplicity, we consider an isotropic case, and focus on the non-linear dependency of μ on $\boldsymbol{h}(\boldsymbol{x},t)$, in particular on its magnitude, which we denote by H. Correspondingly, the magnitude of $\boldsymbol{b}(\boldsymbol{x},t)$ is designated by B. A positive or negative sign are also associated to the values B and H to indicate a specific field's direction.
With the aid of Figure 1.1, we showcase coarsely the response of a generic ferromagnetic material to an external magnetic field, and refer the reader, e.g., to [66, 102] for more details. For this, let us first assume that the material is not magnetized a priori. With magnetization, we mean the ability of a material to create an internal magnetic field, when it is subjected to an external one. For ferromagnetic materials the created field tends to align itself with the external one. This process is not only non-linear, but it also depends on the history of the magnetizing field; hence the name hysteresis. Note that because it relates B to H, the hysteresis loop is also called B-H curve. In the following, we use both terms interchangeably. A gradual increase of the external field strength H causes the magnitude of the induced one to increase following path (I), which is commonly known as initial magnetization curve. After reaching the plateau b_s, called magnetic saturation, the slope behaves like in vacuum. Next, applying a magnetic field in the opposite direction leads the material to demagnetize gradually according to path (II) until $B = 0$ for $H = -h_\mathrm{c}$. The magnetic coercivity h_c is hence the amount of magnetic field that needs to be subjected to a material in order to demagnetize it. Then the induced field increases in the opposite direction until saturation at $B = -b_\mathrm{s}$. Last, a repetition of the first step yields path (III) and closes the loop at $B = b_\mathrm{s}$. The slope of the secant between a specified point of the hysteresis and the origin corresponds to the permeability of the material, and its width, which is given by h_c, determines the type of the magnetic material. We characterize here two types: hard and soft magnetic materials. In Figure 1.2, we show a representative hysteresis loop for each one of these two categories as well as a possible approximation in the corresponding relevant domain. On one hand, hard materials are

[1] For (1.2a) we used the constitutive relation for the electric field $\boldsymbol{d}(\boldsymbol{x},t) = \varepsilon \boldsymbol{e}(\boldsymbol{x},t)$, where the electric permittivity ε is assumed to be a scalar.

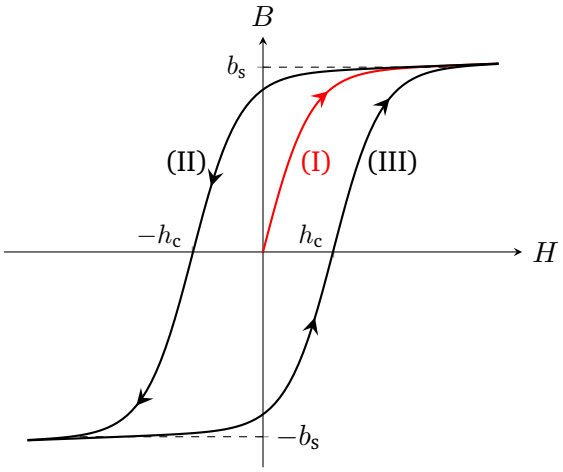

Figure 1.1: Illustration of a hysteresis loop for a ferromagnetic material. The paths (I)-(III) indicate the curves that are traced by the magnitude B of the induced magnetic flux density subjected to an increase-decrease-increase sequence of the magnetic field's magnitude H until saturation. The latter is designated by b_s, and the hysteresis' width by the magnetic coercivity h_c.

recognized by a large coercivity h_c and a high remanence b_r.[2] The latter provides information about the memorized magnetization in the material after removing the applied magnetic field, and thus, about the strongest possible magnetic field it can produce as a magnet. Therefore, hard materials are employed in electric machines for permanent magnetization. For simulation purposes, and by considering a properly designed permanent magnet for this class of applications, a line approximation, as depicted by the red line in Figure 1.2a, represents a sufficiently good approximation of the B-H curve, see [102, Section 3.1]. The restriction of the relevant magnetic characteristic to the second quadrant, i.e., for $B \geq 0$ and $H \leq 0$, is a result of the Ampère's law and the conservation of flux[3], see [66, Section 4.5.4] for a more extensive explanation. In this case, (1.3) can be rewritten as

$$\boldsymbol{b} = \mu \boldsymbol{h} + \boldsymbol{b}_r, \tag{1.4}$$

where $\boldsymbol{b}_r$ is the remanent magnetic flux density. Its relation to the coercive field $\boldsymbol{h}_c$ is stated by $\boldsymbol{b}_r = \mu \boldsymbol{h}_c$. On the other hand, soft magnetic materials are characterized by a narrow hysteresis with a low remanent flux density. Due to their high magnetic permeability, such materials are suitable to channel and guide the flux through them, e.g., to generate a force or create a magnetic field. They are employed in both Direct Current (DC) and Alternating Current (AC) applications. In particular, energy losses have to be taken into account in the latter regime. We mention the hysteresis loss, which is related to the area enclosed by the hysteresis loop, and eddy-current loss, which depends on the electric conductivity. Both sources can be counteracted with a relatively narrow hysteresis, and by laminating the material. Therefore, soft magnetic materials are widely considered, i.a., in electric machines, and for magnetic circuits. A good approximation for the material properties is provided by the initial magnetization curve, which is specified in Figure 1.2b by the red curve, see [66, Section 4.5]. This characteristic is in general not analytically predefined. It is rather

[2] We take as a representative example for our purpose and hence as a reference an NdFeB magnet, which is an alloy of Neodymium, iron, and boron.

[3] For an arbitrary closed contour γ consisting of γ_i and γ_e, such that γ_i is contained in the permanent magnet and γ_e in the surrounding air, the integral form of Ampère's law yields $H_i = -H_e \frac{l_e}{l_i}$. Thereby, l_e and l_i are the corresponding lengths of γ_e and γ_i, respectively. Moreover, by conservation of flux, B_i and B_e have the same direction along γ.

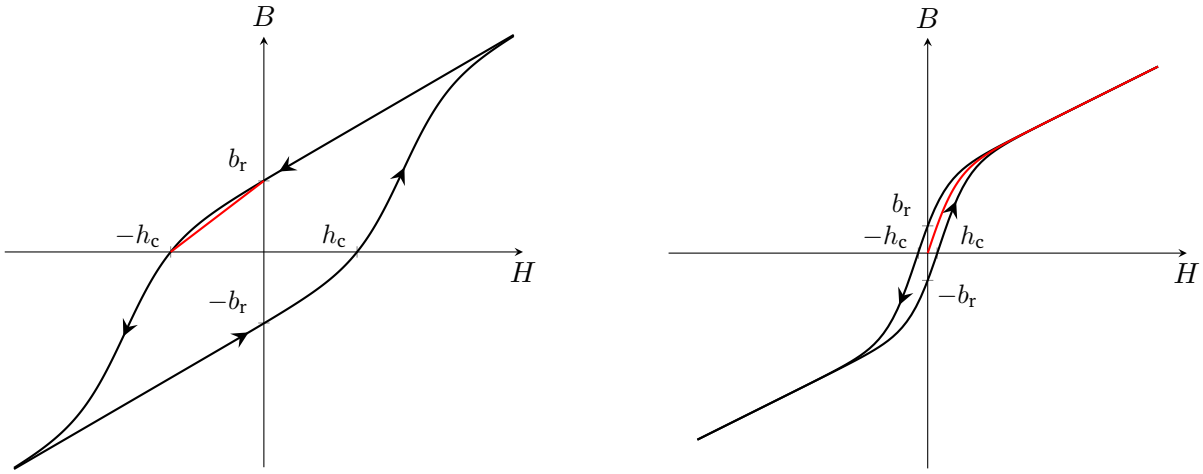

(a) hard magnetic material with a line approximation of the characteristic (in red)

(b) soft magnetic material with the initial magnetization curve (in red)

Figure 1.2: Examples of hysteresis loops for hard and soft magnetic materials.

constructed by interpolation and/or approximation starting from measured data, which are usually subject to measurement errors, see [91, Section 3.1] and the references cited therein. From now on, we reserve the term B-H curve exclusively for the approximations of hysteresis loops, as described above and illustrated by Figure 1.2b. In order to obtain a physically meaningful B-H curve, some assumptions have to be made, cf. [91, 96].

Definition 1.1 (Admissible B-H curve)**.** *We call a non-linear function $g : \mathbb{R}_0^+ \to \mathbb{R}_0^+$, $g(H) = B$ that describes a B-H curve admissible if it exhibits the following properties:*

- *g is continuously differentiable on $\mathbb{R}_0^+$,*
- *$g(0) = 0$,*
- *$g'(s) \geq \mu_0$, $\forall s \geq 0$,*
- *$\lim_{s\to\infty} g'(s) = \mu_0$.*

As an immediate consequence, if g is admissible then it is Lipschitz continuous and strongly monotone, i.e., for all $s, t \in \mathbb{R}_0^+$

$$\exists\, C_{\mathrm{L}}^g > 0 : \quad |g(s) - g(t)| \leq C_{\mathrm{L}}^g |s - t| \qquad \textit{(Lipschitz continuity)},$$
$$\exists\, C_{\mathrm{M}}^g > 0 : \quad (g(s) - g(t))\,(s - t) \geq C_{\mathrm{M}}^g\,(s - t)^2 \qquad \textit{(strong monotonicity)}$$

hold. In particular, $C_{\mathrm{L}}^g := \sup_{s\in\mathbb{R}_0^+} g'(s)$ and $C_{\mathrm{M}}^g = \mu_0$, see [91, Corollary 2.2].

Assumption 1.2. *Throughout this work, all considered B-H curves are assumed to be admissible in the sense of Definition 1.1.*

The permeability, which is related to g by

$$\mu(s) = \begin{cases} \dfrac{g(s)}{s}, & s > 0, \\ \lim\limits_{s\to 0} \dfrac{g(s)}{s}, & s = 0 \end{cases} \tag{1.5}$$

is continuous on $\mathbb{R}_0^+$. This can be readily seen for $s > 0$. For $s = 0$ we see that $\mu(0) := \lim\limits_{s\to 0} \dfrac{g(s)}{s} = g'(0)$, because $g(0) = 0$. Moreover, μ is bounded by $\mu_0 \leq \mu \leq C_{\mathrm{L}}^g$ as can be demonstrated analogously to the proof of [91, Corollary 2.2.6] by using the mean value theorem and L'Hôpital's rule. With this, the constitutive law for a soft magnetic material can be written as

$$\boldsymbol{b}(\boldsymbol{x}, t) = \mu(H)\boldsymbol{h}(\boldsymbol{x}, t). \tag{1.6}$$

Furthermore, we also need the inverse of the permeability. Indeed, the existence of an inverse function $g^{-1} : \mathbb{R}_0^+ \to \mathbb{R}_0^+$ of g follows from its strong monotonicity. In addition, g^{-1} satisfies similar properties as g. In particular, it is also strongly monotone and Lipschitz continuous with a monotonicity constant $C_{\mathrm{M}}^{g^{-1}} = (C_{\mathrm{L}}^g)^{-1}$ and a Lipschitz constant $C_{\mathrm{L}}^{g^{-1}} = (C_{\mathrm{M}}^g)^{-1} = \frac{1}{\mu_0} := \nu_0$, where ν_0 is the vacuum reluctivity. With this, we characterize the reluctivity of a magnetic material that is described by an admissible B-H curve g by

$$\nu(s) = \begin{cases} \dfrac{g^{-1}(s)}{s}, & s > 0, \\ \lim\limits_{s\to 0} \dfrac{g^{-1}(s)}{s}, & s = 0. \end{cases} \tag{1.7}$$

Analogously to μ, the reluctivity ν is continuously differentiable on $\mathbb{R}^+$, and bounded with $C_{\mathrm{M}}^{g^{-1}} \leq \nu \leq \nu_0$. We refer to [91, Corollary 2.2] for proofs of the assertions on g^{-1} and ν.

In the presence of conductive materials, we further state Ohm's law

$$\boldsymbol{j}(\boldsymbol{x}, t) = \kappa \boldsymbol{e}(\boldsymbol{x}, t), \tag{1.8}$$

where $\kappa \geq 0$ is another material constant, known as electrical conductivity. For simplicity, we restrict ourselves to the linear, isotropic, and homogeneous case. Note that (1.8) is considered only for passive conductive materials. Indeed, the Ohm's law as given above does not apply for active material, see [11, Section 1.2.2], where additionally to the explanation a more general formulation is furnished. Therefrom, a generalized Ohm's law reads

$$\boldsymbol{j}(\boldsymbol{x}, t) = \kappa \boldsymbol{e}(\boldsymbol{x}, t) + \boldsymbol{j}_{\mathrm{s}}(\boldsymbol{x}, t), \tag{1.9}$$

where $\boldsymbol{j}_{\mathrm{s}}(\boldsymbol{x}, t)$ is an imposed electric current density, which is specified as an input, and thus it is independent of the electromagnetic field. Moreover, note that (1.8) and (1.9) are only valid for conductors at rest. However, they can be extended to take into account moving domains that contain conductive materials. This will be addressed in the next subsection, which is devoted to motion.

Up to now, the presented setting is only valid in a local sense. For instance, let us consider a field, which is defined over two bounded domains Ω_1 and Ω_2 that share a common interface Γ_{12}, i.e., $\overline{\Omega}_1 \cap \overline{\Omega}_2 = \Gamma_{12}$. In this case, the field lines may be discontinuous across the interface Γ_{12}, even if the field itself is continuous over both domains separately. This arises, e.g., if Ω_1 and Ω_2 are filled with different materials. Provided

their existence, we denote by $\boldsymbol{n}_1$ and $\boldsymbol{n}_2$ the outward pointing normal vectors of Ω_1 and Ω_2, respectively. In addition, we choose $\boldsymbol{n} = \boldsymbol{n}_1 = -\boldsymbol{n}_2$ to be the reference direction. In the absence of surface currents, the continuity is only guaranteed in one component, namely,

$$(\boldsymbol{b}_1(\boldsymbol{x},t) - \boldsymbol{b}_2(\boldsymbol{x},t)) \cdot \boldsymbol{n}(\boldsymbol{x}) = 0, \tag{1.10a}$$
$$(\boldsymbol{h}_1(\boldsymbol{x},t) - \boldsymbol{h}_2(\boldsymbol{x},t)) \times \boldsymbol{n}(\boldsymbol{x}) = \boldsymbol{0}, \tag{1.10b}$$
$$(\boldsymbol{e}_1(\boldsymbol{x},t) - \boldsymbol{e}_2(\boldsymbol{x},t)) \times \boldsymbol{n}(\boldsymbol{x}) = \boldsymbol{0}, \tag{1.10c}$$
$$(\boldsymbol{j}_1(\boldsymbol{x},t) - \boldsymbol{j}_2(\boldsymbol{x},t)) \cdot \boldsymbol{n}(\boldsymbol{x}) = 0, \tag{1.10d}$$

cf. [11, Section 2.2.1]. These conditions, also known as jump conditions, mean that the normal component of the magnetic flux density $\boldsymbol{b}(\boldsymbol{x},t)$ and the electric current density $\boldsymbol{j}(\boldsymbol{x},t)$ as well as the tangential part of the magnetic and electric field $\boldsymbol{h}(\boldsymbol{x},t)$ and $\boldsymbol{e}(\boldsymbol{x},t)$ are continuous. Consequently, the other components can be discontinuous. In the presence of surface currents, which we express by $\boldsymbol{k}(\boldsymbol{x},t)$, the tangential component of $\boldsymbol{h}(\boldsymbol{x},t)$ is no longer continuous. Equation (1.10b) is then extended to include surface currents in the following way,

$$(\boldsymbol{h}_1(\boldsymbol{x},t) - \boldsymbol{h}_2(\boldsymbol{x},t)) \times \boldsymbol{n}(\boldsymbol{x}) = \boldsymbol{k}(\boldsymbol{x},t).$$

Remark 1.3. *Note that these results, as presented above, are in disagreement with the implicit regularity assumption that we made for* (1.2)*. Indeed, for the latter to be well-defined in a strong sense, the components of the involved fields should be differentiable in order to guarantee the existence of the corresponding differential operators. This is obviously not satisfied in the considered example due to the above discussed discontinuities. Nevertheless, this contradiction can be fixed if we resort to weaker regularity assumptions in a suitable mathematical setting for both interior or exterior domains and their related boundaries. This is the subject of Chapter 2.*

To complete the magnetoquasistationary setting, suitable decay conditions of the fields in unbounded domains should be stated. As demonstrated in [16, Proposition 3.1], if $(\boldsymbol{e}(\boldsymbol{x},t), \boldsymbol{h}(\boldsymbol{x},t))$ solves the eddy-current model (1.2) supplemented with

$$\boldsymbol{e}(\boldsymbol{x},t) = \mathcal{O}(|\boldsymbol{x}|^{-1}), \quad \text{uniformly for } |\boldsymbol{x}| \to \infty,$$
$$\boldsymbol{h}(\boldsymbol{x},t) = \mathcal{O}(|\boldsymbol{x}|^{-1}), \quad \text{uniformly for } |\boldsymbol{x}| \to \infty,$$

then they admit the following decay condition:

$$\boldsymbol{e}(\boldsymbol{x},t) = \mathcal{O}(|\boldsymbol{x}|^{-2}), \quad \text{uniformly for } |\boldsymbol{x}| \to \infty, \tag{1.12a}$$
$$\boldsymbol{h}(\boldsymbol{x},t) = \mathcal{O}(|\boldsymbol{x}|^{-2}), \quad \text{uniformly for } |\boldsymbol{x}| \to \infty. \tag{1.12b}$$

In the next subsection, we introduce the underlying equations of the mechanical subsystem, and the used method for the computation of forces and torques.

1.1.2 Equations of motion

In the context of electromechanical energy converters, motion is usually ruled by rigid-body dynamics. The term rigid implies that regardless of the involved external forces and torques, all deformations of the moving bodies can be neglected. The content of the current subsection is based on [75, 78, 81].
A trajectory is characterized by the kinematic variables $(\boldsymbol{x}, \dot{\boldsymbol{x}}, \ddot{\boldsymbol{x}}, \cdots)$, which correspond to the position of the

moving body, its velocity, acceleration, and if needed further time derivatives of $\boldsymbol{x}$.

Depending on the position of the reference frame as well as its dynamics, the kinematic variables take different representations. Conventionally, we distinguish two main approaches: the Lagrangian and the Eulerian description. First, the former describes motion as experienced by the material itself. In other words, the reference frame, which we denote by Σ_l, is attached to the moving body, e.g., such that its origin and axes coincide with the center of mass and the principle axes of inertia of the body, respectively. Note that the Lagrangian reference frame is not an inertial frame, in general.
Second, the Eulerian description is formulated from the perspective of a so called laboratory frame, whose movement is not accelerated and is independent of the body motion. The Eulerian reference frame is an inertial frame. We denote it by Σ_e. The center of mass of the moving body is represented in Σ_e by $\boldsymbol{x}_\mathrm{e}^0(t)$, for $t \geq 0$. Furthermore, we designate by $\boldsymbol{x}_\mathrm{e}$ and $\boldsymbol{x}_\mathrm{l}$ the coordinates in Σ_e and Σ_l, respectively. The position in Σ_e can be expressed as an affine transformation of the Lagrangian coordinates as follows

$$\boldsymbol{x}_\mathrm{e} = \boldsymbol{x}_\mathrm{e}^0(t) + \mathcal{T}(t)\boldsymbol{x}_\mathrm{l}. \tag{1.13}$$

Thereby, $\mathcal{T}(t)$ is an orthogonal transformation, which can be obtained by composing the corresponding rotation matrices associated to each Eulerian angle Ψ, Θ, and Φ, i.e., by $\mathcal{T}(t) = \mathcal{T}_\Psi(t)\mathcal{T}_\Theta(t)\mathcal{T}_\Phi(t)$ with $t \geq 0$. We refer to, e.g., [75, Section 2.3.1] for an explicit representation of $\mathcal{T}(t)$. Taking the derivative of (1.13) yields the velocity field in Σ_e, namely,

$$\dot{\boldsymbol{x}}_\mathrm{e}(\boldsymbol{x}_\mathrm{e}, t) := \partial_t \boldsymbol{x}_\mathrm{e} = \dot{\boldsymbol{x}}_\mathrm{e}^0(t) + \boldsymbol{\omega}_\mathrm{l} \times (\boldsymbol{x}_\mathrm{e} - \boldsymbol{x}_\mathrm{e}^0(t)), \tag{1.14}$$

where $\boldsymbol{\omega}_\mathrm{l}$ denotes the angular velocity, which can be computed from $\mathcal{T}(t)$ following [78].

As mentioned in the previous subsection, Ohm's law (1.8) does not take motion into account. Indeed, from the point of view of Σ_e, (1.8) need to be extended such that

$$\boldsymbol{j}(\boldsymbol{x}_\mathrm{e}, t) = \kappa \left(\boldsymbol{e}(\boldsymbol{x}_\mathrm{e}, t) + \dot{\boldsymbol{x}}_\mathrm{e}(\boldsymbol{x}_\mathrm{e}, t) \times \boldsymbol{b}(\boldsymbol{x}_\mathrm{e}, t) \right). \tag{1.15}$$

The velocity term $\dot{\boldsymbol{x}}_\mathrm{e}(\boldsymbol{x}_\mathrm{e}, t) \times \boldsymbol{b}(\boldsymbol{x}, t)$ results from the effect of the Lorentz force on moving charges, see [36, 78]. As for the rest of the model problem defined by (1.2) and (1.3), nothing changes. A similar result is proved also for the Lagrangian description, namely, the equations of the eddy-current model stay valid even when they are written with respect to such accelerated reference frame, see [79]. In addition, the velocity term in (1.15) vanishes in this case, since by definition the reference frame is fixed in the moving conducting body. Interestingly, a free choice of the reference frame can be made in our context, we refer to [75, 79, 81] for more details. Therefore, we can choose the Lagrangian description for moving bodies in order to avoid an explicit representation of the velocity field in the model problem, and for convenience also for the stationary parts. This allows a decoupling of the electrical and mechanical systems in the sense that they do not need to be handled simultaneously, as will be explained subsequently.

Motion is a result of external forces and torques exerted on the considered rigid body. Their relations to kinematics are given in terms of Lagrangian coordinates by the second Newton law's of motion [81, Section 1.7.1]

$$\boldsymbol{f}_\mathrm{M} = m\ddot{\boldsymbol{x}}_\mathrm{l} + \boldsymbol{\omega}_\mathrm{l} \times m\dot{\boldsymbol{x}}_\mathrm{l}, \tag{1.16a}$$
$$\boldsymbol{\tau}_\mathrm{M} = \boldsymbol{\Theta}\dot{\boldsymbol{\omega}}_\mathrm{l} + \boldsymbol{\omega}_\mathrm{l} \times \boldsymbol{\Theta}\boldsymbol{\omega}_\mathrm{l}, \tag{1.16b}$$

where on the left-hand sides $\boldsymbol{f}_{\mathrm{M}}$ and $\boldsymbol{\tau}_{\mathrm{M}}$ denote the total force and torque, respectively. On the right-hand sides m denotes the mass, and $\boldsymbol{\Theta}$ the inertia tensor. In particular, the considered trajectories for electromechanical energy converters are usually guided and limited to either a translation or rotation. In the case where only one degree of freedom is involved, (1.16) reduces to

$$f_{\mathrm{M}} = m\ddot{x}_{\mathrm{l}} \tag{1.17}$$

for a pure translation, and to

$$\tau_{\mathrm{M}} = \theta\dot{\omega}_{\mathrm{l}} \tag{1.18}$$

for a pure rotation around one specific axis. In the above equation, θ refers to the moment of inertia. In our context, the computation of the magnetic force and torque plays a central role, considering that they represent the coupling quantities of the electrical and mechanical systems. For this, we first define the magnetic part of the MST in empty space, cf. [75, Section 2.2], by

$$\boldsymbol{\mathcal{T}}_{\mathrm{M}} = \frac{1}{\mu_0}\boldsymbol{b}\otimes\boldsymbol{b} - \frac{|\boldsymbol{b}|^2}{2\mu_0}\mathrm{Id}, \tag{1.19}$$

where $\otimes$ denotes an outer product, and Id the identity operator. Then, we choose a surface Γ_{e} such that it encloses the Region Of Interest (ROI) where the magnetic force and/or torque are aimed at. As it will be clarified in the remainder of this work, independently of the ROI, which may contain non-linear materials, the points of the closed surface Γ_{e} are always chosen to be in air regions. Whence the validity of (1.19). With this, the magnetic force is obtained by computing the following surface integral

$$\boldsymbol{f}_{\mathrm{M}} = \int_{\Gamma_{\mathrm{e}}} \boldsymbol{\mathcal{T}}_{\mathrm{M}}\cdot\boldsymbol{n}\,\mathrm{d}\boldsymbol{x}, \tag{1.20}$$

and the torque is calculated by

$$\boldsymbol{\tau}_{\mathrm{M}} = \int_{\Gamma_{\mathrm{e}}} \boldsymbol{x}\times(\boldsymbol{\mathcal{T}}_{\mathrm{M}}\cdot\boldsymbol{n})\,\mathrm{d}\boldsymbol{x}. \tag{1.21}$$

Thereby, the integrals have to be understood with respect to Cartesian components.

With this, we address in the next subsection the considered coupling technique for the electrical and the mechanical subsystems.

1.1.3 The coupled electromechanical system

Usually, the electrical and the mechanical subsystems have to be solved simultaneously, since a change in the electrical state of the subsystem affects the mechanical one, and vice versa. In this case, we speak about a strong coupling. In general, a direct solution is challenging, because of the possible non-linearity of all involved unknowns in the electromechanical system. However, over a finite set of increasing time steps, the strongly coupled problem can be simplified and solved using suitable predictor–corrector methods, see [75, Section 4.6] and the literature cited therein for more details.

As an alternative, we opt for the simpler approach of weak coupling, which consists in solving the electrical and mechanical subsystems sequentially over a finite set of increasing time steps. To give sense to this simplification, smaller time steps have to be chosen, such that the force/torque and the electromagnetic field

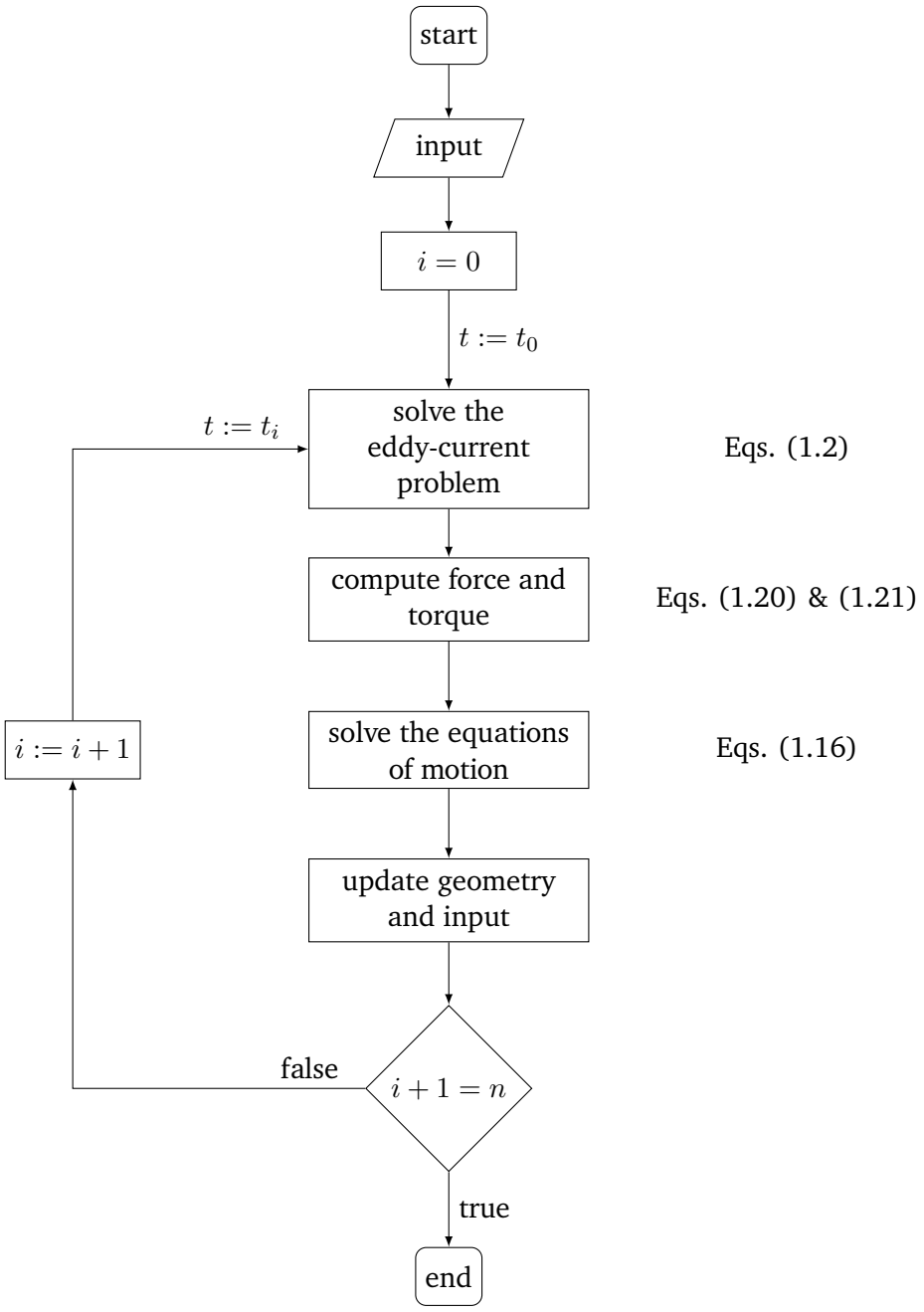

Figure 1.3: A flowchart representing the main blocks for the solution of an electromechanical problem over a set of n increasing time steps, i.e., $t_0 < \ldots < t_i < \ldots < t_{n-1}$.

can be assumed to be constant within two steps. In other words, the changes have to be small enough to be neglected, which depends on the concrete application. Then, the solution of the electromechanical problem follows the flowchart of Figure 1.3. Thereby, input refers to all the prescribed physical quantities that are needed to solve the electromechanical problem, such as the right-hand sides, the initial positions, the material profiles etc. Update geometry and input means the implementation of the body's new state after experiencing a motion, which is caused by the exerted force/torque. These information serve then as new

inputs to the eddy-current problem for the next iteration, and the loop is iterated until the last time step. For this, the force and torque are obtained by the MST method, i.e., by computing the surface integrals (1.20) and/or (1.21). The main subsystems of the coupled problem are represented by the eddy-current model and the equations of motion. The former consists of system (1.2) supplemented by the corresponding constitutive law depending on the material, i.e., (1.3), (1.4), or (1.6), Ohm's law (1.9), as well as further boundary and initial conditions that will be specified in the next chapters, whereas the latter is fully represented by the equations of motion (1.16) together with suitable initial conditions.

In general, the solution of the coupled problem can not be achieved analytically, especially for complicated geometries and inhomogenities. Therefore, we resort to numerical methods. Choosing suitable schemes is dependent on the specific problem. In the next section, we discuss this subject for our particular type of applications.

1.2 Choice of the numerical method

Let us recall the problem that we have at our disposal by means of a concrete example, consisting in a Permanent Magnet Synchronous Machine (PMSM). Due to its translational symmetry along the height of its cylindrical shape, we depict only a two-dimensional (2D) cross-section of the machine in Figure 1.4. It consists of two disjoint ring domains that are separated by a thin air gap. The outer and inner domains are called stator and rotor, respectively. Indeed, as the name suggests, the stator which contains the coils that carry the imposed currents is immobile, whereas the rotor possesses a rotational degree of freedom. Embedded in the latter are Permanent Magnets (PMs), which provide a permanent magnetic field. The core of the machine is constructed by stacked steel laminations, in order to reduce eddy-current losses. Both the PM and steel exhibit non-linear magnetic behavior, in particular, they can be classified as hard and soft magnetic materials, respectively, see also Figure 1.2. The rotor's motion results from a mechanical torque, which is due to the interaction of magnetic fields in the thin air gap. Note that these fields are produced by the PMs on the rotor's side, and by the currents that are passing through the coils on the stator's side.

This example is representative because it manifests the most challenging aspects that need to be taken into account in order to choose a suitable numerical method for the simulation of electromechanical energy converters. On one hand, we have two disjoint domains that contain non-linear materials. On the other hand, there is a gap that may be very thin, and which is filled by a linear material. A straightforward choice to deal with non-linearity and non-homogeneous equations would be FEM. It is well-established theoretically as well as numerically, and widely used for this type of applications. We refer to the textbooks [88, 102, 113] and to the manuscripts [11, 13, 60], for instance. FEM relies on a tessellation of the geometry into finite elements, such as tetrahedrons or hexahedrons, for example. This is called meshing, and it turns out to be a hurdle when it comes to the meshing of very thin domains. This becomes even more challenging if motion is included.

A way around this is provided by BEM. In particular, BEMs are more suitable for problems that are formulated in unbounded domains or in thin geometries, because they require only surface meshing. Indeed, by means of potential operators a representation formula can be derived. Further steps lead to Boundary Integral Equations (BIEs) that are formulated on the boundary. However, the existence of a fundamental solution is conditional to BEM. Hence, non-linear equations are excluded from its range of validity. Other apparent drawbacks of BEM have slowed down its popularity at first glance. Even though the matrices produced

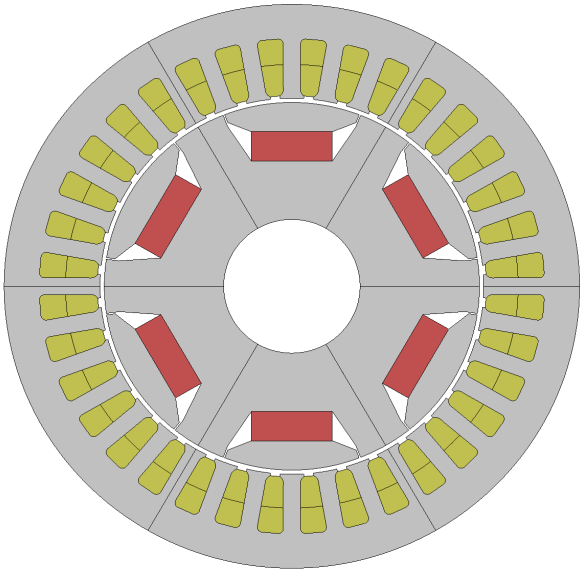

Figure 1.4: Cross-section of a 6-pole Permanent Magnet Synchronous Machine (PMSM), which consists of: Permanent Magnets (PMs) (red), coils (yellow), and a steel core (gray).

thereby are way smaller compared to FEM as the system's dimensionality is reduced, they are structurally dense, whereas the FEM matrix can be stored as a sparse matrix by choosing suitable basis functions for assembling. Moreover, the mathematical foundation of BEM for Maxwell's equations lacked for a long time an appropriate characterization of the corresponding trace spaces in a general Lipschitz setting. Nevertheless, thanks to [17, 18, 20] this problem has already been solved. Besides, the time and memory consuming assembling of BEM matrices can now be tackled by several fast assembling techniques, such as [8, 97, 98]. We also refer to [103, 109] for more BEM-related content.

Hence, an intuitive approach consists in coupling FEM and BEM. In relation to the PMSM example of Figure 1.4, FEM is considered in the rotor and the stator domains, whereas BEM is applied in thin air gap. As a consequence, disjoint domains can be modeled separately, which facilitates the incorporation of motion. Moreover, FEM-BEM couplings, thanks to the BEM part, are suitable for force and torque calculations with the MST method, as introduced above with Equations (1.19) to (1.21). Furthermore, an interesting feature can be observed: under some assumptions, the convergence of the numerical solution towards the exact one is ameliorated in the BEM domain and can even reach a doubling of the standard convergence rates of FEM with respect to h-refinements. A demonstration in the 2D static case is furnished in [42], and its validity in the three-dimensional (3D) case is discussed in [43].

Depending on the BIEs that are utilized to supplement the FEM part, three main coupling types that involve two unknowns arise: a direct symmetric coupling à la Costabel [30], an indirect non-symmetric one as proposed by Bielak and MacCamy in [9], and a direct non-symmetric coupling, called Johnson-Nédélec coupling, see [69]. Furthermore, an additional coupling with three unknowns, known as the three-field method, has been considered in [45].
FEM-BEM couplings are usually discretized by means of collocation or Galerkin techniques. Our focus will

be on the latter. In their classical form, the Galerkin couplings rely on a discretization with lowest order basis functions. However, one of the main goals of simulation for electromechanical devices is the calculation of forces and torques, which involves the computation a posteriori of derivatives of the solution. Thus, going up to higher order basis functions seems more favorable. Moreover, a good representation of the geometry is necessary in order to avoid an induced approximation error and to facilitate motion. For this, we consider an isogeometric framework, which was first proposed in [65]. The method is called Isogeometric Analysis (IGA), and it relies on B-Splines together with some of its extensions such as NURBS. These basis functions play a central role in Computer Aided Design (CAD) software, because they allow an exact representation of industry-relevant geometries. We refer the reader to [94] for an introduction to B-Splines and NURBS. In other terms, the isogeometric framework allows the unification of two processes that are typically separated, namely, design and analysis. This is achieved by employing the same type of basis functions for both steps. Moreover, we benefit from an efficient h-refinement that does not alter the original geometry. Furthermore, basis functions of arbitrarily high order can merely be computed thanks to the definition of B-Splines and NURBS. The refinement step with respect to the basis functions' order is called p-refinement. Several works considered IGA as an alternative to classical FEM and BEM for electromagnetic applications, we mention [10, 29, 119], for instance.

As implied by the PMSM example in this section, the 3D problem can indeed be reduced in some cases to a 2D one. Nevertheless, we are interested in both cases in this thesis. Furthermore, in order to solve the eddy-current problem, several formulations can be considered either with respect to the fields, which yields, e.g., an $\boldsymbol{e}$-based formulation or by invoking scalar and/or vector potentials. Here, we choose a vector potential formulation, see Chapter 3. Moreover, we study the magnetoquasistationary case as well as the static one, which might follow in a steady state context. In the following, we give a brief overview on some related works.

Related works In the 3D case, we refer to [61], where the mathematical foundation of the symmetric FEM-BEM coupling for an $\boldsymbol{e}$-based eddy-current model is provided. Moreover, a numerical validation for the symmetric and the indirect non-symmetric coupling with a vector potential formulation is furnished, e.g., in [71] for both the eddy-current and the magnetostatic case. For the latter, a direct coupling approach with a reduced magnetic potential can also be employed as in [14], for instance. The introduction of auxiliary quantities such as magnetic potentials is a widely considered approach to deal with magnetostatic problems. For instance, [52, 57, 101] are based on a total and/or reduced scalar magnetic potential. However, the stability of these methods depends on the considered permeability of the materials, and may deteriorate in some cases. This drawback was fixed in [74], where an alternative approach that consists in the consideration of a vector potential formulation for the FEM part, along with a total scalar magnetic potential in the exterior BEM domain was proposed. Nevertheless, this method is only valid for simply-connected domains. For more general topologies, a reduced scalar magnetic potential for the BEM part instead of the total one relaxes the topology assumption, see [95]. In the context of electromechanical energy converters, FEM-BEM couplings reveal to be promising alternatives, see, e.g., [75, 78, 81]. In the 2D case, we refer to [41, 56, 82, 106] and the references cited therein in the magnetoquasistatic regime, and to [6, 42, 46, 108], for instance, for the magnetostatic case. In the same context, [86] used the isogeometric FEM-BEM coupling with a collocation based discretization for magneto-mechanical problems in two dimensions. Moreover, see [77] for an application of FEM-BEM coupling on a watch stepping motor.
Regarding the mathematical foundation of IGA, we refer the reader to [24, 25] and [21, 119], where the approximation properties of B-Splines and their trace spaces are studied in the context of Maxwell's equations.

In the next section we describe the goals of this treatise and give an overview on its structure along with the content of each chapter.

1.3 Goal and structure of this treatise

In the preceding sections, we introduced the physical background and the numerical method that we consider in this work, respectively. Our main goal is to provide a rigorous mathematical analysis of direct non-symmetric FEM-BEM couplings for the simulation of electromechanical devices in the isogeometric framework. Moreover, we aim to verify the established theoretical findings numerically to highlight the practical relevance of the proposed method.
In the presence of symmetries, the physical problem can be reduced from 3D space to a 2D one. The governing equations of the obtained model problems are structurally different: in the 3D case, we deal with **curl curl** equations, whereas diffusion problems arise in the 2D one. Both cases are addressed in this thesis, which is organized as follows:

- Chapter 2 is dedicated to the introduction of the mathematical framework that is needed for a suitable formulation of the physical problems at hand. First, we address briefly the notion of connectedness, smoothness, and regularity. We follow up with the relevant Sobolev spaces in bounded domains and on the boundary as well as the corresponding Bochner spaces. Afterwards, we present the main theorems on monotone equations, which are crucial to show well-posedness of our non-linear problems. Then, we introduce the energy spaces and discuss their relations with respect to the differential operators for trivial and non-trivial topologies. Last, and in the same context, we give the corresponding trace spaces, the Green's identities, and some further fundamental results.

- In Chapter 3, we derive a vector potential formulation of the eddy-current model in interior and exterior domains separately. Then, we address the basics of Boundary Element Methods (BEMs). We introduce the considered representation formulae, we discuss the Boundary Integral Operators (BIOs) and their properties, and present the corresponding Boundary Integral Equations (BIEs). An essential tool in our analysis resides in estimating the double-layer operators by means of the Steklov-Poincaré operators. The chapter is concluded with an introduction to the isogeometric paradigm, where we also present the relevant discrete spaces for our method.

- Chapter 4 is devoted to the analysis of the non-symmetric coupling. We start it with the elliptic-elliptic interface problem, which arises, e.g., from the magnetostatic model in two dimensions. We establish well-posedness and provide a stability result for a specific type of practice-oriented non-linearities. Moreover, we state well-posedness of the discrete problem, and derive an a priori estimate with respect to h-refinements for an approximation via B-Spline spaces. Then, we use these results to extend the analysis to the parabolic-elliptic interface problem. With similar tools, we further analyze an additional class of Boundary Value Problems (BVPs) that are topologically similar to electromechanical devices, such as the PMSM of Figure 1.4. Besides well-posedness and stability, we also address the possible superconvergence of the solution when evaluated in the BEM domain. In other words, due to the integral nature of BEM, the convergence rates are ameliorated and may double under some circumstances. In the last section of this chapter, we analyze the 3D magnetostatic case, and provide analogous results as for the previous 2D problems.

- In the penultimate Chapter 5, we validate the theoretical results numerically by means of several academical but yet representative examples. Furthermore, we address the explicit computation of forces and torques, which play the role of the coupling quantities of the electrical and mechanical systems.
- We end the thesis in Chapter 6 with a conclusion on the proposed method. We address possible extensions and improvements that would contribute to the consolidation of the isogeometric FEM-BEM coupling as an attractive alternative for the simulation of electromechanical energy converters.

2 Mathematical framework

> As any human activity needs goals,
> mathematical research needs problems.
>
> D. Hilbert

In Remark 1.3, we evoked that the smoothness of vector fields in a componentwise sense is incompatible with an interface problem. Besides, if the bounded domain Ω is not globally smooth, the existence of a normal vector is not guaranteed in every point of its boundary. Hence, the specification of the domain's regularity is primordial. To cope with this, the problem has to be formulated in an appropriate mathematical setting. This represents the content of this chapter. Obviously, the fields have to be set in so called energy spaces, which are the standard Hilbert spaces for Maxwell-based Boundary Value Problems (BVPs), see [11, 60], for instance. For the time-dependent problem, we also introduce a class of Bochner spaces, which we define as a time-parameterized collection of energy spaces. In addition, the notion of quotient spaces turns out to be useful in the three-dimensional (3D) case, such that the problem can be formalized in the sense of equivalence classes [76]. The issue in the 3D case stems from the infinite-dimensional kernel of the **curl** operator. In other words, the uniqueness of a potential field can only be guaranteed up to a gradient. Furthermore, going to a boundary formulation requires the definition of suitable trace spaces. We use the results of [20], where a characterization of the relevant trace spaces is specified, along with the required trace and differential operators. The validity of the setting also includes Lipschitz domains. Moreover, we present some fundamental results such as Green's identities that are needed for the derivation of Boundary Integral Equations (BIEs). More details can be found, e.g., in [17, 22, 58, 109]. The chapter is organized as follows: In Subsection 2.1.1, we first clarify the meaning of connectedness, regularity and smoothness. Moreover, we define some relevant spaces that play a central role in the study of Partial Differential Equations (PDEs), and give an overview on the used notations. Then, we end the section with some fundamental results related to non-linear operators in Subsection 2.1.2. In Section 2.2, we introduce suitable Hilbert spaces endowed with graph norms that render the application of corresponding differential operators Lebesgue integrable, and discuss the elements of the de Rham complex, whose structure depends on the topological properties of the domain. In Section 2.3, we proceed similarly to introduce and characterize the corresponding trace spaces, along with the needed tangential differential operators and evidently the trace operators.

2.1 Fundamentals

This section consists of two parts. First, we first introduce the considered geometries, and briefly recall the notions of smoothness and regularity. Then, we introduce the spaces of test functions and distributions. Last, we provide a short introduction to Sobolev and Bochner spaces. As we go along, the notational conventions that we use will be highlighted. The content of the first part of this section consists of well-established definitions

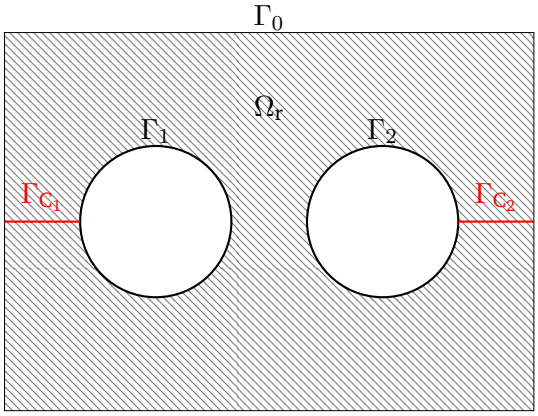

(a) a two-dimensional (2D) domain Ω_r with two holes. $\Gamma_r = \Gamma_0 \cup \Gamma_1 \cup \Gamma_2$ denotes the boundary of Ω_r and $\Gamma_C = \Gamma_{C_1} \cup \Gamma_{C_2}$ consists of the "cut" segments.

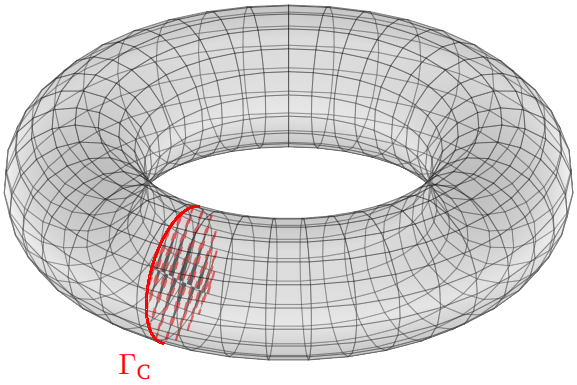

(b) a 3D domain Ω_t with one hole. Γ_C is the red "cut" surface.

Figure 2.1: Examples of non simply-connected 2D and 3D domains.

and results in the field of functional analysis. We rely for this mostly on [1, 34, 87, 109], for instance. Second, we introduce the main theorems on monotone operators, which are central in our analysis to prove well-posedness of the coupled problem. We refer to [122] for more details.

2.1.1 Preliminaries and notational conventions

Geometry Let $\Omega \subset \mathbb{R}^d$ with $d = 2, 3$ be a bounded domain, and let Γ denote its boundary. Unless specified, a domain Ω is implied to be open and connected, and Γ is assumed to consist of N_Γ connected components. For example, we illustrate in Figure 2.1a such a domain Ω_r with $d = 2$ and a boundary $\Gamma_r = \Gamma_0 \cup \Gamma_1 \cup \Gamma_2$, i.e., with $N_\Gamma = 3$. Obviously, Ω_r is connected but not simply-connected[1]. Nevertheless, Ω_r can be made simply-connected by "cutting" it along Γ_{C_1} and Γ_{C_2}. The necessary number of "cuts", which we denote throughout the thesis by N_C, can be determined in this case from the number of connected components of Γ by $N_C = N_\Gamma - 1 = 2$.
In the 3D case, a similar (but more involved) approach can be considered to gain a simply-connected domain from one that is only connected. For instance, the torus domain in Figure 2.1b, which we label Ω_t is connected but obviously not simply-connected, however $\Omega_t \backslash \Gamma_C$ is, as stated in [34, Section 5.2]. This idea will be formalized in Subsection 2.2.3.

Smoothness and Lipschitz continuity Let $D \in \{\mathbb{R}^d, \overline{\Omega}, \Gamma\}$ and $k \in \mathbb{N}_0$, we denote by $C^k(D)$ the space of k-times continuously differentiable functions over D, and by $C^\infty(D)$ the space of smooth functions, which consists of indefinitely continuously differentiable functions. To express the smoothness of a vector field

[1] We refer the reader, e.g., to [59, Chapter 1] and [64] for a formal definition of simply-connected domains.

$\boldsymbol{v} = (v_1, \ldots, v_d)$ over a domain D, we use $\boldsymbol{C}^k(D)$ and $\boldsymbol{C}^\infty(D)$, which have to be understood in a componentwise sense.

Furthermore, we say that a domain Ω is smooth, if its boundary Γ is represented by a family of smooth parametrizations. In other words, let us assume that there exists a regular tessellation of Γ, such that

$$\Gamma = \bigcup_{i=1}^{N_\tau} \overline{\tau}_i,$$

and for all $i, j = 1, \ldots, N_\tau$, $\overline{\tau}_i \cap \overline{\tau}_j$ is either empty, reduces to a single vertex, or consists of a whole common edge. Thereby, every boundary segment τ_i can be represented via a local parametrization

$$\tau_i = \{\boldsymbol{x} \in \mathbb{R}^d, \boldsymbol{\xi} \in \hat{\tau} : \boldsymbol{x} = \hat{\boldsymbol{p}}_i(\boldsymbol{\xi})\}, \tag{2.1}$$

where $\hat{\tau} \subset \mathbb{R}^{d-1}$ is an open parameter domain. With this, we say that Ω is smooth if all functions $\hat{\boldsymbol{p}}_i : \hat{\tau} \to \tau_i$ are of class $C^\infty(\Gamma)$. However, the smoothness assumption is too restrictive so that only a small class of geometries can be considered.

A more general concept of continuity can be reached by means of Hölder continuous parametrizations. For $k \in \mathbb{N}_0$ and $0 < \iota < 1$, we introduce the corresponding space

$$C^{k,\iota}(D) := \{v : v \in C^k(D), |v|_{0,\iota} < \infty\}.$$

Thereby, $|v|_{0,\iota}$ is a semi-norm defined by

$$|v|_{0,\iota} = \sum_{|\boldsymbol{\alpha}|=k} \sup_{\boldsymbol{x},\boldsymbol{y} \in D, \boldsymbol{x} \neq \boldsymbol{y}} \frac{|\partial_{\boldsymbol{x}}^{\boldsymbol{\alpha}} v(\boldsymbol{x}) - \partial_{\boldsymbol{y}}^{\boldsymbol{\alpha}} v(\boldsymbol{y})|}{|\boldsymbol{x} - \boldsymbol{y}|^\iota}. \tag{2.2}$$

The vectorial counterpart is defined analogously, and is denoted by $\boldsymbol{C}^{k,\iota}(D)$. In particular, for $k = 0$ and $\iota = 1$, we obtain the spaces $C^{0,1}(D)$ and $\boldsymbol{C}^{0,1}(D)$ of Lipschitz continuous functions and vector fields over D, respectively.

Analogously to the smooth case, we label a domain Ω Lipschitz, if Γ is represented by a family of Lipschitz continuous parametrizations, i.e., functions of class $C^{0,1}(\Gamma)$.

***L*^{p}-regularity** The regularity of a function can be described by differentiability and integrability in the sense of Lebesgue integrals. For this, we introduce Banach spaces of equivalence classes containing μ-measurable functions over a domain $D \in \{\mathbb{R}^d, \Omega, \Gamma\}, d = 2, 3$. Thereby, two functions are considered equal, if they differ only in a zero measure set, see [1] for instance. For $p \geq 1$, we define them by

$$L^p(D) = \{v \text{ is } \mu\text{-measurable} : \|v\|_{L^p(D)} < \infty\},$$

where μ is a Hausdorff measure and $\|\cdot\|_{L^p(D)}$ is the L^p-norm, which is computed for $v \in L^p(D)$ by

$$\|v\|_{L^p(D)} = \left(\int_D |v(\boldsymbol{x})|^p \, \mathrm{d}\boldsymbol{x} \right)^{\frac{1}{p}} \qquad \text{for } 1 \leq p < \infty,$$

$$\|v\|_{L^\infty(D)} = \operatorname*{ess\,sup}_{\boldsymbol{x}\in D} |v(\boldsymbol{x})| = \inf_{K\subset D,\mu(K)=0} \sup_{\boldsymbol{x}\in D\setminus K} |v(\boldsymbol{x})| \qquad \text{for } p=\infty.$$

For convenience, we write as integral measure generically $\mathrm{d}\boldsymbol{x}$ instead of $\mathrm{d}\mu$. However, note that the interpretation of $\mathrm{d}\boldsymbol{x}$ depends on the dimension of the considered manifold. For further reading we refer to [116, Section 2.3] and the literature cited therein. For $1 < p < \infty$, choosing q as the Hölder conjugate (or adjoint) of p, i.e.,

$$\frac{1}{p} + \frac{1}{q} = 1$$

yields the Hölder's inequality, namely, for $u \in L^p(D)$ and $v \in L^q(D)$, we have

$$\int_D |u(\boldsymbol{x})v(\boldsymbol{x})| \,\mathrm{d}\boldsymbol{x} \le \|u\|_{L^p(D)} \|v\|_{L^q(D)}, \tag{2.4}$$

and we say that $L^q(D)$ is dual to $L^p(D)$. In addition, we can express the norm of the dual space by means of the operator norm as

$$\|v\|_{L^q(D)} = \sup_{u\in L^p(D), u\neq 0} \frac{|\langle u, v\rangle_D|}{\|u\|_{L^p(D)}}, \quad v \in L^q(D),$$

where the notation $\langle\cdot,\cdot\rangle_D$ is called duality pairing that is evaluated over the domain D. It is computed for $u \in L^p(D)$ and $v \in L^q(D)$, with $L^q(D)$ dual to $L^p(D)$ by

$$\langle u, v\rangle_D = \int_D u(\boldsymbol{x})v(\boldsymbol{x}) \,\mathrm{d}\boldsymbol{x}.$$

For more details, and especially for the Banach dual spaces of $L^1(D)$ and $L^\infty(D)$, we refer to [1, Chapter 2]. Of particular interest for our purpose is the space of square integrable functions, which arises for $p = 2$. The space $L^2(D)$ is self dual, and it satisfies the Cauchy-Schwarz' inequality, which follows merely from (2.4) for $p = q = 2$

$$\int_D |u(\boldsymbol{x})v(\boldsymbol{x})| \,\mathrm{d}\boldsymbol{x} \le \|u\|_{L^2(D)} \|v\|_{L^2(D)}. \tag{2.5}$$

Furthermore, it is endowed with an inner product

$$(u, v)_D = \int_D u(\boldsymbol{x})v(\boldsymbol{x}) \,\mathrm{d}\boldsymbol{x},$$

which induces the norm

$$\|v\|_{L^2(D)} = \sqrt{(v, v)_D}.$$

Hence, it follows that $L^2(D)$ is a Hilbert space. Conform to our notation, we use $\boldsymbol{L}^p(D)$ to denote the space of equivalence classes of Lebesgue measurable vector fields $\boldsymbol{v}$ over D with respect to the $\boldsymbol{L}^p$-norm. Note that the previous definitions and results transfer accordingly from $L^p(D)$ to $\boldsymbol{L}^p(D)$.

Test function spaces and distributions Let $D \subseteq \mathbb{R}^d$ with $d = 2, 3$. We denote by $\mathcal{D}(D)$ the space of test functions, which consists of infinitely smooth functions with compact support in D, formally we define it by

$$\mathcal{D}(D) := \{\varphi \in C^\infty(D) : \operatorname{supp}\varphi \subset D \text{ compact}\} \qquad \text{with } \operatorname{supp}\varphi = \overline{\{\boldsymbol{x} \in D :\, \varphi(\boldsymbol{x}) \neq 0\}},$$

see [117, Definition V.1.9]. Note that $\mathcal{D}(D)$ is a vector space that is additionally equipped with a topology, which defines uniform convergence of sequences. We refer the reader to [117, Satz VIII.5.2] and [87] for

more details.

We call a linear map $V : \mathcal{D}(D) \to \mathbb{C}$ a distribution, if for all compact sets $K \subset D$, there exists a constant $C = C(K) > 0$ and $k \in \mathbb{N}_0$, which may depend on K such that

$$\forall \varphi \in \mathcal{D}(D),\ \operatorname{supp}\varphi \subset K : |V(\varphi)| \leq C \sum_{|\boldsymbol{\alpha}|\leq k} \sup_{\boldsymbol{x}\in K} |\partial^{\boldsymbol{\alpha}}_{\boldsymbol{x}} \varphi(\boldsymbol{x})| \tag{2.6}$$

with $\boldsymbol{\alpha} = (\alpha_1, \ldots, \alpha_d) \in \mathbb{N}_0^d$ being a multi-index. That is, for $\boldsymbol{x} = (x_1, \ldots, x_d)$ we have

$$|\boldsymbol{\alpha}| = \sum_{i=1}^{d} \alpha_i \quad \text{and} \quad \partial^{\boldsymbol{\alpha}}_{\boldsymbol{x}} \varphi(\boldsymbol{x}) = \frac{\partial^{|\boldsymbol{\alpha}|}\varphi(\boldsymbol{x})}{\partial^{\alpha_1} x_1 \ldots \partial^{\alpha_d} x_d}.$$

The evaluation of a distribution V on a test function $\varphi \in \mathcal{D}(D)$ is also denoted by angular brackets, namely,

$$V(\varphi) = \langle V, \varphi \rangle_D.$$

We collect distributions that are applied to a test function $\varphi \in \mathcal{D}(D)$ in $\mathcal{D}(D)'$. Note that the space of distributions $\mathcal{D}(D)'$ corresponds to the dual space of $\mathcal{D}(D)$.

In particular, we see in the following that a function $v \in L^2(D)$ can be identified with a distribution $V \in \mathcal{D}(D)'$. For an arbitrary compact subset $K \subset D$, and an arbitrary $\varphi \in \mathcal{D}(D)$ with $\operatorname{supp}\varphi \subset K$, we obtain by applying the Cauchy-Schwarz's inequality (2.5) that

$$|\,(v, \varphi)_D\,| \leq \|v\|_{L^2(D)} \|\varphi\|_{L^2(D)} \leq |K| \|v\|_{L^2(D)} \sup_{\boldsymbol{x}\in K} |\varphi(\boldsymbol{x})|.$$

Hence, the identification holds by (2.6), and we may write

$$\langle V, \varphi \rangle_D = (v, \varphi)_D \qquad \forall \varphi \in \mathcal{D}(D). \tag{2.7}$$

A distribution V that satisfies the representation (2.7) is called regular. Otherwise we call V singular, e.g., a Dirac distribution, which is defined by

$$\delta_{\boldsymbol{x}}(\varphi) = \langle \delta_{\boldsymbol{x}}, \varphi \rangle_D = \varphi(\boldsymbol{x}) \qquad \forall \varphi \in \mathcal{D}(D). \tag{2.8}$$

Given a distribution $V \in \mathcal{D}(D)'$, differentiation in a distributional sense is computed by [88, Equation 3.1]

$$\langle \partial^{\boldsymbol{\alpha}} V, \varphi \rangle_D = (-1)^{|\boldsymbol{\alpha}|} \langle V, \partial^{\boldsymbol{\alpha}} \varphi \rangle_D \qquad \forall \varphi \in \mathcal{D}(D). \tag{2.9}$$

This allows to find a weak derivative for a function that would be non-differentiable in a strong sense.
In addition, since we also need spaces for truncated test functions, we define

$$\mathcal{D}(\overline{\Omega}) := \{\varphi :\ \varphi = \psi_{|\overline{\Omega}},\ \psi \in \mathcal{D}(\mathbb{R}^d)\}.$$

In order to stick to our notational convention, we denote by $\boldsymbol{\varphi}$ and $\boldsymbol{V}$ a vector that contains test functions and distributions as components, respectively. Moreover, in the same componentwise sense, the space of test vector fields $\boldsymbol{\varphi}$ is designated by $\boldsymbol{\mathcal{D}}(D)$ and its dual by $\boldsymbol{\mathcal{D}}(D)'$, where D can be replaced by $\mathbb{R}^d$, $\overline{\Omega}$, or Ω.

Sobolev spaces The next step towards an appropriate mathematical setting for our purpose is delivered by Sobolev spaces. Indeed, they are Banach spaces, i.e., they are complete and normed; additionally, the corresponding norm allows the measurement of a function's or vector field's magnitude as well as its regularity by measuring the associated derivatives up to a given order. The latter are understood in a weak sense.
Sobolev spaces can be defined in different ways. In this work, we present a standard definition which is based on weak derivatives, and refer to [1, Chapter 3], [87, Chapter 3] for more details. With $p \geq 1$, $\boldsymbol{\alpha}$ a multi-index, and $k \in \mathbb{N}_0$, we denote by

$$W^{k,p}(\Omega) = \{v \in L^p(\Omega) : \partial^{\boldsymbol{\alpha}} v \in L^p(\Omega),\, \forall |\boldsymbol{\alpha}| \leq k\}$$

a Sobolev space defined over Ω. It can be equipped with the following norms

$$\begin{aligned} \|v\|_{W^{k,p}(\Omega)} &= \left(\sum_{|\boldsymbol{\alpha}| \leq k} \|\partial^{\boldsymbol{\alpha}} v\|^p_{L^p(\Omega)} \right)^{\frac{1}{p}} \qquad \text{for } 1 \leq p < \infty, \\ \|v\|_{W^{k,\infty}(\Omega)} &= \max_{|\boldsymbol{\alpha}| \leq k} \|\partial^{\boldsymbol{\alpha}} v\|_{L^\infty(\Omega)}. \end{aligned}$$

This definition can be extended to non-integer coefficients [87, Chapter 3]. Let $s = k + \iota$, where $\iota \in (0,1) \subset \mathbb{R}$. Moreover, k is the same as above, and $d = 2, 3$. For $1 \leq p < \infty$, we introduce the Slobodeckiĭ semi-norm

$$|v|_{W^{s,p}(\Omega)} = \left(\sum_{|\boldsymbol{\alpha}| = k} \int_\Omega \int_\Omega \frac{|\partial^{\boldsymbol{\alpha}}_{\boldsymbol{x}} v(\boldsymbol{x}) - \partial^{\boldsymbol{\alpha}}_{\boldsymbol{y}} v(\boldsymbol{y})|^p}{|\boldsymbol{x} - \boldsymbol{y}|^{d + p\iota}} \,\mathrm{d}\boldsymbol{x}\,\mathrm{d}\boldsymbol{y} \right)^{\frac{1}{p}}.$$

The semi-norm turns out to be the usual Hölder semi-norm as given in (2.2) for $p = \infty$. With this, we endow the Sobolev space of fractional order $W^{s,p}(\Omega)$ with the norm

$$\|v\|_{W^{s,p}(\Omega)} = \left(\|v\|^p_{W^{k,p}(\Omega)} + |v|^p_{W^{s,p}(\Omega)} \right)^{\frac{1}{p}} \qquad \text{for } 1 \leq p \leq \infty,$$

which renders it a Banach space.
In particular, we are interested in the case where $p = 2$. Indeed, similarly to the L^p-spaces, $W^{s,2}(\Omega)$ is a Hilbert space. We adopt therefore the notation $H^s(\Omega)$ for $W^{s,2}(\Omega)$. Note that this notation stems from a second definition of Hilbert spaces, which is based on the Fourier transform of distributions [87, Chapter 3]. For Lipschitz domains, we know from [109, Theorem 2.16] that both definitions are equivalent for all $s > 0$.
As previously, a Hilbert space is equipped with an inner product structure. It is expressed for $u, v \in H^k(\Omega)$ and $k \in \mathbb{N}_0$ by

$$(u, v)_{H^k(\Omega)} = \sum_{|\boldsymbol{\alpha}| \leq k} (\partial^{\boldsymbol{\alpha}} u, \partial^{\boldsymbol{\alpha}} v)_\Omega,$$

and for a fractional order $s = k + \iota$, with $\iota \in (0,1) \subset \mathbb{R}$ by

$$(u, v)_{H^s(\Omega)} = (u, v)_{H^k(\Omega)} + \sum_{|\boldsymbol{\alpha}| = k} \int_\Omega \int_\Omega \frac{\left(\partial^{\boldsymbol{\alpha}}_{\boldsymbol{x}} u(\boldsymbol{x}) - \partial^{\boldsymbol{\alpha}}_{\boldsymbol{y}} u(\boldsymbol{y})\right)\left(\partial^{\boldsymbol{\alpha}}_{\boldsymbol{x}} v(\boldsymbol{x}) - \partial^{\boldsymbol{\alpha}}_{\boldsymbol{y}} v(\boldsymbol{y})\right)}{|\boldsymbol{x} - \boldsymbol{y}|^{d + 2\iota}} \,\mathrm{d}\boldsymbol{x}\,\mathrm{d}\boldsymbol{y}.$$

Consequently, the following norm is induced for $s > 0$ and $v \in H^s(\Omega)$,

$$\|v\|_{H^s(\Omega)} = \sqrt{(v, v)_{H^s(\Omega)}}.$$

For $s = 0$, $H^0(\Omega)$ reduces to the space of square integrable functions, i.e., $L^2(\Omega)$.

In addition, we introduce Sobolev spaces, which are defined as the closure of $\mathcal{D}(\Omega)$ as follows

$$H_0^s(\Omega) = \overline{\mathcal{D}(\Omega)}^{\|\cdot\|_{H^s(\Omega)}}. \tag{2.11}$$

For $k \in \mathbb{N}_0$, $H_0^k(\Omega)$ can be understood as a Sobolev space $H^k(\Omega)$ with k weak derivatives in $L^2(\Omega)$ that vanish at the boundary of Ω. We will come back to this in the next subsection.

By setting $s > 0$, we define the Sobolev space $H^{-s}(\Omega)$ with negative exponents as the dual space of $H_0^s(\Omega)$, and endow it with the dual norm

$$\|u\|_{H^{-s}(\Omega)} = \sup_{v \in H_0^s(\Omega), v \neq 0} \frac{|\langle u, v \rangle_\Omega|}{\|v\|_{H_0^s(\Omega)}}.$$

Similarly, the dual space of $H^s(\Omega)$ corresponds to $H_0^{-s}(\Omega)$, cf. [109, Section 2.2]. Furthermore, let $\Omega^{\mathrm{e}} = \mathbb{R}^d \backslash \overline{\Omega}$ be an unbounded exterior domain. We need functions with local behavior. We collect them in

$$H^s_{\mathrm{loc}}(\Omega^{\mathrm{e}}) := \{v : \Omega^{\mathrm{e}} \to \mathbb{R} \,:\, v_{|K} \in H^s(K),\, \forall K \subset \Omega^{\mathrm{e}} \text{ compact}\}, \tag{2.12}$$

where $v_{|K}$ stands for the restriction of v to the set K. Note that for $s = 0$, the space of functions with local L^2-behavior is denoted by $L^2_{\mathrm{loc}}(\Omega^{\mathrm{e}})$.

Furthermore, we need Sobolev spaces on the boundary Γ. We recall here that Γ is Lipschitz. The construction of such spaces depends on the specific local parameterizations $\hat{\boldsymbol{p}}_i$ and the partition of Γ as introduced in (2.1). However, the corresponding norms are equivalent. For a more explicit explanation, see [109, Section 2.5]. We denote the Sobolev space defined over the boundary by $H^s(\Gamma)$. Note that for Lipschitz boundaries, the dependence on the parametrization limits the choice of s to $s \in [-1, 1]$. In the following, we provide a definition for $H^s(\Gamma)$ for completeness but refer the reader, e.g., to [109, Section 2.5] for more details. First, we introduce the corresponding Slobodeckiĭ semi-norm, which reads for $s \in (0, 1)$

$$|v|_{H^s(\Gamma)} = \left(\int_\Gamma \int_\Gamma \frac{|v(\boldsymbol{x}) - v(\boldsymbol{y})|^2}{|\boldsymbol{x} - \boldsymbol{y}|^{d-1+2s}} \,\mathrm{d}\boldsymbol{x}\,\mathrm{d}\boldsymbol{y} \right)^{\frac{1}{2}}.$$

Then, $H^s(\Gamma)$ is a Banach space when equipped with the norm

$$\|v\|_{H^s(\Gamma)} = \left(\|v\|^2_{L^2(\Gamma)} + |v|^2_{H^s(\Gamma)} \right)^{\frac{1}{2}},$$

where we used $H^0(\Gamma) = L^2(\Gamma)$. With this, the Sobolev space $H^s(\Gamma)$ can be defined as the closure of the space of smooth functions in the Sobolev-Slobodeckiĭ norm $\|\cdot\|_{H^s(\Gamma)}$, formally, we write

$$H^s(\Gamma) = \overline{\mathcal{C}^\infty(\Gamma)}^{\|\cdot\|_{H^s(\Gamma)}}.$$

Moreover, the dual space of $H^s(\Gamma)$ is denoted by $H^{-s}(\Gamma)$. Similarly to the domain spaces, $H^{-s}(\Gamma)$ is obtained

by the duality relation

$$\|u\|_{H^{-s}(\Gamma)} = \sup_{v \in H^s(\Gamma), v \neq 0} \frac{|\langle u, v \rangle_\Gamma|}{\|v\|_{H^s(\Gamma)}}.$$

As an alternative notation, we also designate by $H(D)'$ the dual space of some Banach space $H(D)$ defined over D.
Concerning vector-valued Sobolev spaces, i.e., spaces that contain vector fields, they are expressed as usual with a bold font, namely, we write $\boldsymbol{H}^{\pm s}(D)$ with $s > 0$ and $D \in \{\Omega, \Gamma\}$, and $\boldsymbol{L}^2_{\text{loc}}(\Omega^{\text{e}})$, $\boldsymbol{H}^s_{\text{loc}}(\Omega^{\text{e}})$ for the spaces with local behavior defined over an unbounded domain. Note that vector-valued Sobolev spaces have to be understood in a componentwise sense.

In this treatise, we also encounter spaces of functions that are defined over a time interval, whose instantaneous values consist of functions that lie in some Banach space H. Such spaces are known as Bochner spaces [48, Section 5.2.9]. We denote them here by using the following convention: For a specific time interval $T = [0, t_{\text{max}}]$, $t_{\text{max}} > 0$, and a space of instantaneous values $H(D)$, which is defined over a domain $D \in \{\Omega, \Gamma\}$, the corresponding Bochner space is expressed for $p \geq 1$ by

$$L^p(T; H(D)) := \{v \in L^p(T) : v(t) \in H(D), \forall t \in T\}.$$

In particular, we focus on the case $p = 2$. For $v \in L^2(T;\, H(D))$ with an instantaneous value $v(t) \in H(D)$ for $t \in T$, the Bochner space $L^2(T;\, H(D))$ can be equipped with its natural norm

$$\|v\|_{L^2(T;\, H(D))} = \left(\int_0^{t_{\text{max}}} \|v(t)\|^2_{H(D)} \, \mathrm{d}t \right)^{\frac{1}{2}}. \tag{2.13}$$

The dual space of a Bochner space that relates to $H(D)$ is understood as the time-parametrized collection of the dual spaces of $H(D)$, since $L^2(D)$ is self-dual. Concretely, we have

$$L^2(T;\, H(D)') := \{v \in L^2(T) : v(t) \in H(D)', \forall t \in T\}$$

as the dual space of $L^2(T;\, H(D))$. In the sense that the above defined Sobolev norms measure the spatial regularity of a function, we define a generic time-parameterized Sobolev space

$$L^2(\partial_t, T;\, H(D)) := \{v \in L^2(T;\, H(D)) : \partial_t v \in L^2(T;\, H(D)')\}, \tag{2.14}$$

and endow it with the norm

$$\|v\|_{L^2(\partial_t, T;\, H(D))} = \sqrt{\|v\|^2_{L^2(T;\, H(D))} + \|\partial_t v\|^2_{L^2(T;\, H(D)')}} \tag{2.15}$$

to allow the measurement of temporal regularity. Analogously to the weak derivatives in space, $\partial_t v$ exists in a weak sense. Note that we restrict ourselves here to the first time derivative, since it is sufficient for our purpose.
For consistency, Bochner spaces of a vector-valued Banach space $\boldsymbol{H}(D)$ are denoted by $\boldsymbol{L}^2(T;\, \boldsymbol{H}(D))$. In addition, the vector-valued counterpart of $L^2(\partial_t, T;\, H(D))$ is $\boldsymbol{L}^2(\partial_t, T;\, \boldsymbol{H}(D))$. The definitions can be adapted accordingly.

The next part is dedicated to the definition of quotient spaces, along with some important results for Hilbert spaces. In the following, let H denote a Hilbert space, and let $U \subset H$ be closed.

Theorem 2.1 (Best approximation in Hilbert spaces, [88, Theorem 2.7])**.** *For H and U as defined above, we have*

$$\forall v \in H,\, \exists!\, u \in U :\, \|v-u\|_H = \inf_{w\in U}\{\|v-w\|_H\}. \tag{2.16}$$

As a consequence, a direct sum decomposition can be stated. Two functions are said to be orthogonal in H, if for $u, v \in H$ their inner product vanishes, i.e., $(u, v)_H = 0$.

Theorem 2.2 (Projection theorem, [88, Theorem 2.9])**.** *For H and U as mentioned above, the orthogonal decomposition*

$$H = U \oplus U^\perp$$

holds. Thereby, $U^\perp$ is called the orthogonal complement of U in H. In other terms, we have

$$\forall v \in H,\, \exists!\, u \in U \text{ and } u^\perp \in U^\perp :\, v = u + u^\perp.$$

In particular, this result plays a central role to provide a characterization of quotient spaces, and in the Helmholtz decomposition, which we will encounter in the next section.

Definition 2.3 (Quotient space)**.** *A quotient space $[H] := H/U$ consists of the equivalence class*

$$[v] := \{v - w : w \in U\}, \quad v \in H.$$

Equipped with the best approximation norm (2.16)*, namely,*

$$\|[v]\|_{[H]} := \inf_{w\in U}\{\|v-w\|_H\}$$

the quotient space $[H]$ turns into a Banach space. Due to the uniqueness of the representation, which is stated in Theorem 2.1, and for ease of notation, we write $v := [v] \in [H]$. The interpretation of the elements of a quotient space should be clear from the context.

Corollary 2.4. *The quotient space $[H] := H/U$ can be identified with $U^\perp$, the orthogonal complement of U in H.*

Proof. By using the direct sum decomposition of Theorem 2.2 we define a canonical isomorphism $\iota : [H] \to U^\perp$, $v \mapsto v - u$, $u \in U$, which is well-defined and unique because of Theorem 2.1. Moreover, the same holds for the inverse mapping $\iota^{-1} : U^\perp \to [H], u^\perp \mapsto u^\perp + u$, $u \in U$. □

For instance, let $\mathrm{d} : H \to V$ be a differential operator with a non-trivial kernel $\ker(\mathrm{d})$. Thus, d is clearly not injective. As a workaround, we expect a representation in quotient spaces with respect to $\ker(\mathrm{d})$, i.e., $H/\ker(\mathrm{d})$ to enforce the injectivity of d by selecting representatives from the orthogonal complement space of $\ker(\mathrm{d})$, i.e., $\ker(\mathrm{d})^\perp$.

2.1.2 Main theorems on monotone operators and evolution equations

Motivated by the physical problem introduced in Chapter 1, non-linear problems, which are formulated either by elliptic or parabolic equations play a central role in this thesis. Fortunately, there is a standard theoretical framework that allows us to show well-posedness for such operator equations. This is provided in [122, Chapter 25 & 30], for instance. Here, we only state the main results that are relevant for our purpose.

Throughout this subsection, let H be a Hilbert space, and H' be its dual. First, let $\mathcal{A} : H \to H'$ be a non-linear operator, which is Lipschitz continuous and strongly monotone, i.e., for all $u, v \in H$

$$\exists\, C_{\mathrm{L}}^{\mathcal{A}} > 0 : \qquad \|\mathcal{A}u - \mathcal{A}v\|_{H'} \leq C_{\mathrm{L}}^{\mathcal{A}} \|u - v\|_H \quad \text{(Lipschitz continuity)}, \tag{2.17a}$$

$$\exists\, C_{\mathrm{M}}^{\mathcal{A}} > 0 : \quad \langle \mathcal{A}u - \mathcal{A}v, u - v \rangle \geq C_{\mathrm{M}}^{\mathcal{A}} \|u - v\|_H^2 \quad \text{(strong monotonicity)}. \tag{2.17b}$$

First, we state the main theorem on strongly monotone operators, which goes back to Zarantonello [120]. In particular, this is a crucial result for the study of non-linear elliptic equations.

Theorem 2.5 (Well-posedness, [122, Theorem 25.B])**.** *Let $f \in H'$, and let $\mathcal{A}$ be a non-linear operator that satisfies* (2.17)*. Then, the operator equation $\mathcal{A}u = f$ with $f \in H'$ admits a unique solution $u \in H$, which depends continuously on the right-hand side f.*

Remark 2.6. *Note that if we were only interested in well-posedness, then strict monotonicity instead of* (2.17b) *is sufficient to guarantee the existence and uniqueness of a solution [6, Remark 3]. The definition of strict monotonicity is provided in Appendix A, for convenience.*

Second, we consider the first order evolution equation

$$\partial_t u(t) + \mathcal{A}(t)u(t) = f(t). \tag{2.18}$$

Let V be defined as the pivot space of H and its dual H', i.e., such that (H, V, H') form a Gelfand triple with $H \subseteq V \subseteq H'$, see [118, Theorem 17.3]. Moreover, for the non-linear operator $\mathcal{A}(t) : H \to H'$, let the following properties hold:

1. For each $t \in (0, t_{\max})$, the operator $\mathcal{A}(t)$ is monotone, coercive, and hemicontinuous, see Appendix A for the corresponding definitions.
2. $\mathcal{A}(t)$ satisfies the following growth condition: There exists a non-negative function $C_1(t)$ and $C_2 > 0$ such that
$$\|\mathcal{A}(t)v(t)\|_{H'} \leq C_1(t) + C_2 \|v\|_H. \tag{2.19}$$
3. The function $t \mapsto \langle \mathcal{A}(t)v(t), w(t) \rangle$ is measurable on $(0, t_{\max})$ for all $v(t), w(t) \in H$.

For more details, we refer to [122, Section 30.2].

The main theorem on monotone first order evolution equations can be stated.

Theorem 2.7 (Well-posedness, [122, Theorem 30.A])**.** *In the framework given above by the properties* 1-3*, the operator equation* (2.18) *supplemented by an initial condition $u(0) = u_0 \in V$, and for a right-hand side $f \in L^2(T;\, H')$, admits a unique solution $u \in L^2(\partial_t, T;\, H)$.*

Remark 2.8. *Note that the initial condition $u(0) = u_0 \in V$ is meaningful, since $L^2(\partial_t, T; H)$ is continuously embedded in $C(T; H)$, see [121, Proposition 23.23] for more details.*

In particular, we will consider $u_0 = 0$ throughout this thesis for simplicity. Nevertheless, our analysis can be adapted to non-homogeneous initial conditions without complications.

Lemma 2.9. *Provided $\mathcal{A}(t)$ is strongly monotone, Lipschitz continuous, and hemicontinuous, then Theorem 2.7 applies.*

Proof. First, monotonicity and coercivity follow from the strong monotonicity, see Lemma A.3 for the latter. Then, the Lipschitz continuity induces a bound for $\mathcal{A}(t)$ in the sense of (2.19). In particular, for $v(0) = 0$, which is the concrete case we will consider, this can be established as follows

$$\begin{aligned}
\|\mathcal{A}(t)v(t)\|_{H'} &= \|\mathcal{A}(t)v(t) - \mathcal{A}(0)v(0) + \mathcal{A}(0)v(0)\|_{H'} \\
&\leq \|\mathcal{A}(t)v(t) - \mathcal{A}(0)v(0)\|_{H'} + \|\mathcal{A}(0)v(0)\|_{H'} \\
&\leq C_{\mathrm{L}}^{\mathcal{A}}\|v(t) - v(0)\|_H + \|\mathcal{A}(0)v(0)\|_{H'} \qquad \text{(with (2.17a))} \\
&\leq C_{\mathrm{G}}\left(1 + C_{\mathrm{L}}^{\mathcal{A}}\|v(t)\|_H\right)
\end{aligned}$$

with $C_{\mathrm{G}} = \max\left(1, \|\mathcal{A}(0)v(0)\|_{H'}\right)$. □

Remark 2.10. *In practice, i.e., with non-linear reluctivities given by an admissible B-H curve according to Definition 1.1, weak differentiability of the corresponding operator has been established, see [91, 99], for instance. In this regard, note that a Gâteaux (weak) differentiable operator is hemicontinuous. Indeed, provided it exists, the Gâteaux derivative of some functional g reads*

$$\mathrm{d}g(t)\tau = \lim_{\epsilon \to 0} \frac{g(t + \epsilon\tau) - g(t)}{\epsilon}.$$

In particular, we see that $\lim_{\epsilon \to 0} g(t + \epsilon\tau) = g(t)$ is guaranteed. That is, $g(t)$ is hemicontinuous. In addition, it is per definition strongly monotone and Lipschitz continuous. Therefore, choosing an admissible B-H curve in the sense of Definition 1.1 automatically covers the theoretical prerequisites of Lemma 2.9 and per extension of Theorem 2.7 as well as those of Theorem 2.5.

Remark 2.11. *Although the setting of Lemma 2.9 is less general than that of Theorem 2.7, it is more convenient/simple from a practical point of view because of Remark 2.10 as well as from an analysis perspective, since it allows us a straightforward transfer of results from elliptic to parabolic problems.*

In the next section, we introduce and address the properties of the natural spaces that arise in the context of Maxwell's equations.

2.2 Energy spaces and de Rham complex

Energy spaces provide a suitable functional setting for BVPs that are based on Maxwell's equations. In fact, they can be physically interpreted as spaces of potentials and fields with finite energies, which are measured by means of graph norms that are in turn induced by inner products. The first part is dedicated to their

introduction. Moreover, we give explicit integration by parts formulae. Indeed, they play a central role in the derivation and study of variational problems.
A fundamental feature of energy spaces consists in the fact that they form a sequence with respect to the appropriate differential operators, also known as de Rham complex. The structure of the sequence depends however on the topological properties of the domain. We start by considering an interior domain with a trivial topology. Then, we generalize the characterization of the spaces to a more general geometrical setting. We finish the subsection by discussing additional related spaces, namely, energy spaces with local behavior, and the time-parameterized counterparts.

2.2.1 Energy spaces

We recall that Ω is a bounded Lipschitz domain, and that Γ is its boundary. In particular, we consider $\Omega \in \mathbb{R}^3$. Analogously to (2.9), we first define the differential operators ∇, **curl**, and div in a distributional sense. Then, we introduce spaces that contain square integrable functions (vector fields) with weak derivatives in Ω, and give some fundamental characterizations and results.

Similarly to (2.7), we have:

- For $V \in \mathcal{D}(\Omega)'$ and $v \in L^2(\Omega)$,

$$\langle \nabla V, \boldsymbol{\varphi} \rangle_\Omega = -\langle V, \operatorname{div} \boldsymbol{\varphi} \rangle_\Omega = (\nabla v, \boldsymbol{\varphi})_\Omega = -(v, \operatorname{div} \boldsymbol{\varphi})_\Omega \qquad \forall \boldsymbol{\varphi} \in \boldsymbol{\mathcal{D}}(\Omega). \tag{2.20}$$

- For $\boldsymbol{U} \in \boldsymbol{\mathcal{D}}(\Omega)'$ and $\boldsymbol{u} \in \boldsymbol{L}^2(\Omega)$,

$$\langle \mathbf{curl}\, \boldsymbol{U}, \boldsymbol{\varphi} \rangle_\Omega = \langle \boldsymbol{U}, \mathbf{curl}\, \boldsymbol{\varphi} \rangle_\Omega = (\mathbf{curl}\, \boldsymbol{u}, \boldsymbol{\varphi})_\Omega = (\boldsymbol{u}, \mathbf{curl}\, \boldsymbol{\varphi})_\Omega \qquad \forall \boldsymbol{\varphi} \in \boldsymbol{\mathcal{D}}(\Omega). \tag{2.21}$$

- For $\boldsymbol{V} \in \boldsymbol{\mathcal{D}}(\Omega)'$ and $\boldsymbol{v} \in \boldsymbol{L}^2(\Omega)$,

$$\langle \operatorname{div} \boldsymbol{V}, \varphi \rangle_\Omega = -\langle \boldsymbol{V}, \nabla \varphi \rangle_\Omega = (\operatorname{div} \boldsymbol{v}, \varphi)_\Omega = -(\boldsymbol{v}, \nabla \varphi)_\Omega \qquad \forall \varphi \in \mathcal{D}(\Omega). \tag{2.22}$$

With this, we introduce the following energy spaces as in [35, Section IX.A.§1.2]

$$\begin{aligned} H(\nabla, \Omega) &:= \{v \in L^2(\Omega) : \nabla v \in \boldsymbol{L}^2(\Omega)\}, \\ \boldsymbol{H}(\mathbf{curl}, \Omega) &:= \{\boldsymbol{v} \in \boldsymbol{L}^2(\Omega) : \mathbf{curl}\, \boldsymbol{v} \in \boldsymbol{L}^2(\Omega)\}, \\ \boldsymbol{H}(\operatorname{div}, \Omega) &:= \{\boldsymbol{v} \in \boldsymbol{L}^2(\Omega) : \operatorname{div} \boldsymbol{v} \in L^2(\Omega)\}, \end{aligned}$$

where the differential operators ∇, **curl**, and div are understood in a weak sense as defined in (2.20), (2.21), and (2.22), respectively. Energy spaces are Hilbert spaces when equipped with the inner products

$$\begin{aligned} u, v \in H(\nabla, \Omega): &\qquad (u, v)_{H(\nabla,\Omega)} := (\boldsymbol{u}, \boldsymbol{v})_\Omega + (\nabla u, \nabla v)_\Omega, \\ \boldsymbol{u}, \boldsymbol{v} \in \boldsymbol{H}(\mathbf{curl}, \Omega): &\qquad (\boldsymbol{u}, \boldsymbol{v})_{\boldsymbol{H}(\mathbf{curl},\Omega)} := (\boldsymbol{u}, \boldsymbol{v})_\Omega + (\mathbf{curl}\, \boldsymbol{u}, \mathbf{curl}\, \boldsymbol{v})_\Omega, \\ \boldsymbol{u}, \boldsymbol{v} \in \boldsymbol{H}(\operatorname{div}, \Omega): &\qquad (\boldsymbol{u}, \boldsymbol{v})_{\boldsymbol{H}(\operatorname{div},\Omega)} := (\boldsymbol{u}, \boldsymbol{v})_\Omega + (\operatorname{div} \boldsymbol{u}, \operatorname{div} \boldsymbol{v})_\Omega, \end{aligned}$$

which induce the graph norms

$$
\begin{aligned}
v \in H(\nabla,\Omega): &\qquad \|v\|_{H(\nabla,\Omega)} := \sqrt{(v,v)_{H(\nabla,\Omega)}},\\
\boldsymbol{v} \in \boldsymbol{H}(\mathbf{curl},\Omega): &\qquad \|\boldsymbol{v}\|_{\boldsymbol{H}(\mathbf{curl},\Omega)} := \sqrt{(\boldsymbol{v},\boldsymbol{v})_{\boldsymbol{H}(\mathbf{curl},\Omega)}},\\
\boldsymbol{v} \in \boldsymbol{H}(\mathrm{div},\Omega): &\qquad \|\boldsymbol{v}\|_{\boldsymbol{H}(\mathrm{div},\Omega)} := \sqrt{(\boldsymbol{v},\boldsymbol{v})_{\boldsymbol{H}(\mathrm{div},\Omega)}},
\end{aligned}
$$

respectively. Therefore, they turn into Banach spaces with respect to these norms. An important result that is provided by the Riesz representation theorem allows us to identify the dual of a Hilbert space H, denoted by H', with itself. Hence, writing a duality pairing $\langle V, v\rangle$ with $V \in H'$ and $v \in H$, as an inner product (u, v) with $u, v \in H$ is meaningful, see [87, Theorem 2.30].
For notational consistency, note that we changed the notation of $H^1(\Omega)$ to $H(\nabla,\Omega)$.

The following density results play a central role in the study of energy spaces.

Lemma 2.12 ([27, Lemma 1 & 2])**.** *The following properties hold:*

- $\mathcal{D}(\overline{\Omega})$ *is dense in* $H(\nabla,\Omega)$.
- $\boldsymbol{\mathcal{D}}(\overline{\Omega})$ *is dense in* $\boldsymbol{H}(\mathrm{div},\Omega)$ *and* $\boldsymbol{H}(\mathbf{curl},\Omega)$.

With this, an assertion can be first proved for smooth functions, then extended continuously by density to energy spaces.

As motivated in Section 1.1, the model problems that we will consider in this thesis may involve non-linear operators. To take this into account in our analysis, we characterize in the following the considered class of non-linear operators.

Assumption 2.13 (Lipschitz continuous and strongly monotone operators)**.** *Let* $\mathcal{U} : \boldsymbol{L}^2(\Omega) \to \boldsymbol{L}^2(\Omega)$ *be a possibly non-linear operator. We assume* $\mathcal{U}$ *to be Lipschitz continuous and strongly monotone:*

- *Lipschitz continuity:*

$$
\exists\, C_{\mathrm{L}}^{\mathcal{U}} > 0: \quad \|\mathcal{U}\boldsymbol{v} - \mathcal{U}\boldsymbol{w}\|_{\boldsymbol{L}^2(\Omega)} \leq C_{\mathrm{L}}^{\mathcal{U}} \|\boldsymbol{v} - \boldsymbol{w}\|_{\boldsymbol{L}^2(\Omega)} \qquad \forall \boldsymbol{v}, \boldsymbol{w} \in \boldsymbol{L}^2(\Omega). \tag{2.23}
$$

- *Strong monotonicity:*

$$
\exists\, C_{\mathrm{M}}^{\mathcal{U}} > 0: \quad (\mathcal{U}\boldsymbol{v} - \mathcal{U}\boldsymbol{w}, \boldsymbol{v} - \boldsymbol{w})_{\Omega} \geq C_{\mathrm{M}}^{\mathcal{U}} \|\boldsymbol{v} - \boldsymbol{w}\|^2_{\boldsymbol{L}^2(\Omega)} \qquad \forall \boldsymbol{v}, \boldsymbol{w} \in \boldsymbol{L}^2(\Omega). \tag{2.24}
$$

In the process of deriving weak formulations, integration by parts represents a crucial tool. For this, we first define the corresponding trace operators that map domain functions or vector fields to the boundary, cf. [116].

Definition 2.14 (Trace operators)**.** *Let Ω be a Lipschitz domain with a connected boundary Γ. Moreover, we denote by $\boldsymbol{n}(\boldsymbol{x})$ an outward pointing normal vector with respect to Ω that is evaluated at $\boldsymbol{x} \in \Gamma$, and assume that $\boldsymbol{n}(\boldsymbol{x})$ exists almost everywhere (a.e.) on Γ. Then, we define the space of tangential vector fields*

$$\boldsymbol{L}^2_{\mathrm{t}}(\Gamma) = \{\boldsymbol{v} \in \boldsymbol{L}^2(\Gamma) : \boldsymbol{v} \cdot \boldsymbol{n} = 0, \text{ a.e. on } \Gamma\}, \tag{2.25}$$

and the trace operators:

- *Standard trace:* $\gamma_0 : \mathcal{D}(\overline{\Omega}) \to L^2(\Gamma)$, $\varphi(\boldsymbol{x}) \mapsto \lim\limits_{\Omega \ni \boldsymbol{y} \to \boldsymbol{x}} \varphi(\boldsymbol{y})$.
- *Conormal derivative:* $\gamma_1^{\mathcal{U}} : \mathcal{D}(\overline{\Omega}) \to L^2(\Gamma)$, $\varphi(\boldsymbol{x}) \mapsto \lim\limits_{\Omega \ni \boldsymbol{y} \to \boldsymbol{x}} \mathcal{U}\nabla\varphi(\boldsymbol{y}) \cdot \boldsymbol{n}(\boldsymbol{x})$.
- *Vector restriction trace:* $\boldsymbol{\gamma}_0 : \boldsymbol{\mathcal{D}}(\overline{\Omega}) \to \boldsymbol{L}^2(\Gamma)$, $\boldsymbol{\varphi}(\boldsymbol{x}) \mapsto \lim\limits_{\Omega \ni \boldsymbol{y} \to \boldsymbol{x}} \boldsymbol{\varphi}(\boldsymbol{y})$.
- *Normal trace:* $\gamma_{\boldsymbol{n}} : \boldsymbol{\mathcal{D}}(\overline{\Omega}) \to L^2(\Gamma)$, $\boldsymbol{\varphi}(\boldsymbol{x}) \mapsto \lim\limits_{\Omega \ni \boldsymbol{y} \to \boldsymbol{x}} \boldsymbol{\varphi}(\boldsymbol{y}) \cdot \boldsymbol{n}(\boldsymbol{x})$.
- *Tangential trace [2]:* $\boldsymbol{\gamma}_\times : \boldsymbol{\mathcal{D}}(\overline{\Omega}) \to \boldsymbol{L}^2_{\mathrm{t}}(\Gamma)$, $\boldsymbol{\varphi}(\boldsymbol{x}) \mapsto \lim\limits_{\Omega \ni \boldsymbol{y} \to \boldsymbol{x}} \boldsymbol{\varphi}(\boldsymbol{y}) \times \boldsymbol{n}(\boldsymbol{x})$.
- *Dirichlet trace [3]:* $\boldsymbol{\gamma}_{\mathrm{D}} : \boldsymbol{\mathcal{D}}(\overline{\Omega}) \to \boldsymbol{L}^2_{\mathrm{t}}(\Gamma)$, $\boldsymbol{\varphi}(\boldsymbol{x}) \mapsto \lim\limits_{\Omega \ni \boldsymbol{y} \to \boldsymbol{x}} \boldsymbol{n}(\boldsymbol{x}) \times (\boldsymbol{\varphi}(\boldsymbol{y}) \times \boldsymbol{n}(\boldsymbol{x}))$.
- *Neumann trace:* $\boldsymbol{\gamma}_{\mathrm{N}}^{\mathcal{U}} : \boldsymbol{\mathcal{D}}(\overline{\Omega}) \to \boldsymbol{L}^2_{\mathrm{t}}(\Gamma)$, $\boldsymbol{\varphi}(\boldsymbol{x}) \mapsto \lim\limits_{\Omega \ni \boldsymbol{y} \to \boldsymbol{x}} \mathcal{U}\,\mathbf{curl}\,\boldsymbol{\varphi}(\boldsymbol{y}) \times \boldsymbol{n}(\boldsymbol{x})$.

Thereby, $\mathcal{U}$ is a possibly non-linear operator according to Assumption 2.13. To simplify the notation, if $\mathcal{U} = \mathrm{Id}$ we write $\boldsymbol{\gamma}_{\mathrm{N}}$ and γ_1 instead of $\boldsymbol{\gamma}_{\mathrm{N}}^{\mathcal{U}}$ and $\gamma_1^{\mathcal{U}}$, respectively.

Then, the following characterizations for generalized integration by parts formulae can be stated.

Theorem 2.15 (Integration by parts)**.** *Let Ω be a bounded Lipschitz domain with a connected boundary Γ, and let $\boldsymbol{v} \in \boldsymbol{H}(\mathbf{curl}, \Omega)$ and $\boldsymbol{w} \in \boldsymbol{H}(\mathrm{div}, \Omega)$. Then, there exist unique distributions $\boldsymbol{\gamma}_\times\, \boldsymbol{v}\delta_\Gamma$ and $\gamma_{\boldsymbol{n}}\boldsymbol{w}\delta_\Gamma$ such that*

$$\left\langle \boldsymbol{\gamma}_\times\, \boldsymbol{v}\delta_\Gamma, \boldsymbol{\varphi} \right\rangle_\Gamma = (\boldsymbol{v}, \mathbf{curl}\,\boldsymbol{\varphi})_\Omega - (\mathbf{curl}\,\boldsymbol{v}, \boldsymbol{\varphi})_\Omega, \tag{2.26a}$$

$$\langle \gamma_{\boldsymbol{n}}\boldsymbol{w}\delta_\Gamma, \varphi \rangle_\Gamma = (\mathrm{div}\,\boldsymbol{w}, \varphi)_\Omega + (\boldsymbol{w}, \nabla\varphi)_\Omega \tag{2.26b}$$

[2] also known as rotated tangential trace.

[3] if $\boldsymbol{\gamma}_\times$ is labeled rotated tangential trace, then $\boldsymbol{\gamma}_{\mathrm{D}}$ is usually called tangential trace.

hold for all $\varphi \in \mathcal{D}(\overline{\Omega})$ *and* $\boldsymbol{\varphi} \in \boldsymbol{\mathcal{D}}(\overline{\Omega})$*. Thereby,* δ_Γ *denotes a Dirac distribution with support* Γ*, cf.* (2.8)*. For instance,*

$$\langle \gamma_{\boldsymbol{n}} \boldsymbol{w} \delta_\Gamma, \varphi \rangle_\Gamma = \langle \gamma_{\boldsymbol{n}} \boldsymbol{w}, \varphi_{|\Gamma} \rangle_\Gamma.$$

Proof. First, we derive the formulae for distributions. The divergence theorem, see [88, Theorem 3.19] is our starting point for the proof. For convenience, it states that for $\boldsymbol{u} \in \boldsymbol{C}^1(\overline{\Omega})$,

$$\int_\Omega \operatorname{div} \boldsymbol{u} \, \mathrm{d}\boldsymbol{x} = \int_\Gamma \boldsymbol{u}_{|\Gamma} \cdot \boldsymbol{n} \, \mathrm{d}\boldsymbol{x}. \tag{2.27}$$

It is obvious that this result holds also for $\boldsymbol{u} \in \boldsymbol{\mathcal{D}}(\overline{\Omega})$. With this, (2.26b) follows by choosing $\boldsymbol{u} := \boldsymbol{w}\varphi$. For (2.26a), we set $\boldsymbol{u} := \boldsymbol{v} \times \boldsymbol{\varphi}$ and use the vector identity $\operatorname{div}(\boldsymbol{v} \times \boldsymbol{\varphi}) = \boldsymbol{\varphi} \cdot \mathbf{curl}\, \boldsymbol{v} - \boldsymbol{v} \cdot \mathbf{curl}\, \boldsymbol{\varphi}$.
Then, by applying Cauchy-Schwarz's inequality to the right-hand sides of (2.26a) and (2.26b), respectively, we can merely establish well-posedness of the distributions $\boldsymbol{\gamma}_\times \boldsymbol{v}\delta_\Gamma$ and $\gamma_{\boldsymbol{n}} \boldsymbol{w} \delta_\Gamma$ in the sense of (2.6). Now using the density results of Lemma 2.12 closes the proof. For more details and explicit proofs, we refer to [116] and [35, Section IX.A.§1.2]. □

Remark 2.16. *By using similar arguments as for* (2.26b) *but for a fixed* $\boldsymbol{w} \in \boldsymbol{H}(\operatorname{div}, \Omega)$*, the existence of the standard trace* $\gamma_0 w$ *can be established for* $w \in H(\nabla, \Omega)$*, see [116, Section 2.5].*

In the following, we further derive two spaces that contain the solutions of the **curl curl** and the Laplace equations.

$$\begin{aligned} \boldsymbol{H}(\mathbf{curl}\ \mathbf{curl}, \Omega) &:= \{\boldsymbol{v} \in \boldsymbol{L}^2(\Omega) : \ \mathbf{curl}\, \mathbf{curl}\, \boldsymbol{v} \in \boldsymbol{L}^2(\Omega)\}, \\ H(\Delta, \Omega) &:= \{v \in L^2(\Omega) : \ \Delta v \in L^2(\Omega)\}, \end{aligned}$$

where $\Delta = \operatorname{div} \nabla$ denotes the Laplace operator. Similar to the energy spaces defined above, the spaces $\boldsymbol{H}(\mathbf{curl}\ \mathbf{curl}, \Omega)$ and $H(\Delta, \Omega)$ turn to Hilbert spaces when equipped with the inner products

$$\begin{aligned} \boldsymbol{u}, \boldsymbol{v} \in \boldsymbol{H}(\mathbf{curl}\ \mathbf{curl}, \Omega) : \quad & (\boldsymbol{u}, \boldsymbol{v})_{\boldsymbol{H}(\mathbf{curl}\ \mathbf{curl}, \Omega)} := (\boldsymbol{u}, \boldsymbol{v})_\Omega + (\mathbf{curl}\, \boldsymbol{u}, \mathbf{curl}\, \boldsymbol{v})_\Omega, \\ u, v \in H(\Delta, \Omega) : \quad & (u, v)_{H(\Delta, \Omega)} := (u, v)_\Omega + (\Delta u, \Delta v)_\Omega, \end{aligned}$$

which induce the norms

$$\begin{aligned} \boldsymbol{v} \in \boldsymbol{H}(\mathbf{curl}\ \mathbf{curl}, \Omega) : \quad & \|\boldsymbol{v}\|_{\boldsymbol{H}(\mathbf{curl}\ \mathbf{curl}, \Omega)} := \sqrt{(\boldsymbol{v}, \boldsymbol{v})_{\boldsymbol{H}(\mathbf{curl}\ \mathbf{curl}, \Omega)}}, \\ v \in H(\Delta, \Omega) : \quad & \|v\|_{H(\Delta, \Omega)} := \sqrt{(v, v)_{H(\Delta, \Omega)}}, \end{aligned}$$

respectively. For these spaces, we also find appropriate integration by parts formulae.

Corollary 2.17. *Let* Ω *be a bounded Lipschitz domain with a connected boundary* Γ*, and* $\mathcal{U}$ *a possibly non-linear operator according to Assumption 2.13. Then, there exist unique distributions* $\gamma_1^{\mathcal{U}} w\delta_\Gamma$ *and* $\boldsymbol{\gamma}_{\mathrm{N}}^{\mathcal{U}} \boldsymbol{w}\delta_\Gamma$ *such that:*

- *For* $w \in H(\Delta, \Omega)$*, it holds*

$$(\operatorname{div} \mathcal{U} \nabla w, \psi)_\Omega + (\mathcal{U} \nabla w, \nabla \psi)_\Omega = \langle \gamma_1^{\mathcal{U}} w \delta_\Gamma, \psi \rangle_\Gamma \quad \forall \psi \in \mathcal{D}(\overline{\Omega}). \tag{2.28}$$

- *For $\boldsymbol{w} \in \boldsymbol{H}(\mathbf{curl}\,\mathbf{curl}, \Omega)$, it holds*

$$(\mathcal{U}\,\mathbf{curl}\,\boldsymbol{w}, \mathbf{curl}\,\boldsymbol{\varphi})_\Omega - (\mathbf{curl}\,\mathcal{U}\,\mathbf{curl}\,\boldsymbol{w}, \boldsymbol{\varphi})_\Omega = \left\langle \boldsymbol{\gamma}_{\mathrm{N}}^{\mathcal{U}}\,\boldsymbol{w}\delta_\Gamma, \boldsymbol{\varphi}\right\rangle_\Gamma \quad \forall \boldsymbol{\varphi} \in \boldsymbol{\mathcal{D}}(\overline{\Omega}). \tag{2.29}$$

Proof. The first assertion (2.28) follows similarly to (2.26b) by setting $\boldsymbol{w} := \mathcal{U}\nabla w$ with $w \in H(\Delta, \Omega)$. Analogously, the second assertion arises by choosing $\boldsymbol{v} := \mathcal{U}\,\mathbf{curl}\,\boldsymbol{w}$ in (2.26a), which yields (2.29) for $\boldsymbol{w} \in \boldsymbol{H}(\mathbf{curl}\,\mathbf{curl}, \Omega)$. □

By taking boundary conditions into account, we introduce the subspaces

$$H_\lambda(\nabla, \Omega) := \{v \in H(\nabla, \Omega) : \gamma_0 v = \lambda\}, \tag{2.30a}$$
$$\boldsymbol{H}_{\boldsymbol{\lambda}}(\mathbf{curl}, \Omega) := \{\boldsymbol{v} \in \boldsymbol{H}(\mathbf{curl}, \Omega) : \boldsymbol{\gamma}_\times\,\boldsymbol{v} = \boldsymbol{\lambda}\}, \tag{2.30b}$$
$$\boldsymbol{H}_\lambda(\mathrm{div}, \Omega) := \{\boldsymbol{v} \in \boldsymbol{H}(\mathrm{div}, \Omega) : \gamma_{\boldsymbol{n}}\boldsymbol{v} = \lambda\}. \tag{2.30c}$$

The mapping properties of the trace operators applied to elements from $H(\nabla, \Omega)$, $\boldsymbol{H}(\mathbf{curl}, \Omega)$, and $\boldsymbol{H}(\mathrm{div}, \Omega)$ will be specified explicitly in the Section 2.3. Nevertheless, we already know from Theorem 2.15 and Remark 2.16 that they exist. In particular, we can define energy spaces with homogeneous boundary conditions, i.e., $H_0(\nabla, \Omega)$, $\boldsymbol{H}_{\mathbf{0}}(\mathbf{curl}, \Omega)$, and $\boldsymbol{H}_0(\mathrm{div}, \Omega)$ similarly to (2.11) by

$$H_0(\nabla, \Omega) = \overline{\mathcal{D}(\Omega)}^{\|\cdot\|_{H(\nabla,\Omega)}}, \quad \boldsymbol{H}_{\mathbf{0}}(\mathbf{curl}, \Omega) = \overline{\boldsymbol{\mathcal{D}}(\Omega)}^{\|\cdot\|_{\boldsymbol{H}(\mathbf{curl},\Omega)}}, \quad \boldsymbol{H}_0(\mathrm{div}, \Omega) = \overline{\boldsymbol{\mathcal{D}}(\Omega)}^{\|\cdot\|_{\boldsymbol{H}(\mathrm{div},\Omega)}},$$

see [88, Theorem 3.25 & Theorem 3.33]. Furthermore, in case we have a boundary with several connected components, it is convenient to specify the part of the boundary, on which a boundary condition is assigned. With Γ_i denoting some connected subset of Γ, we write

$$H_\lambda(\nabla, \Omega, \Gamma_i) := \{v \in H(\nabla, \Omega) : \gamma_0 v = \lambda \text{ on } \Gamma_i\}, \tag{2.31a}$$
$$\boldsymbol{H}_{\boldsymbol{\lambda}}(\mathbf{curl}, \Omega, \Gamma_i) := \{\boldsymbol{v} \in \boldsymbol{H}(\mathbf{curl}, \Omega) : \boldsymbol{\gamma}_\times\,\boldsymbol{v} = \boldsymbol{\lambda} \text{ on } \Gamma_i\}, \tag{2.31b}$$
$$\boldsymbol{H}_\lambda(\mathrm{div}, \Omega, \Gamma_i) := \{\boldsymbol{v} \in \boldsymbol{H}(\mathrm{div}, \Omega) : \gamma_{\boldsymbol{n}}\boldsymbol{v} = \lambda \text{ on } \Gamma_i\}. \tag{2.31c}$$

The spaces $H(\nabla, \Omega)$, $\boldsymbol{H}(\mathbf{curl}, \Omega)$, and $\boldsymbol{H}(\mathrm{div}, \Omega)$ are related by the differential operators ∇, **curl**, and div, such that they form a sequence

$$H(\nabla, \Omega) \xrightarrow{\nabla} \boldsymbol{H}(\mathbf{curl}, \Omega) \xrightarrow{\mathbf{curl}} \boldsymbol{H}(\mathrm{div}, \Omega) \xrightarrow{\mathrm{div}} L^2(\Omega).$$

The structure of the sequence depends on the topological properties of Ω. Hence, we distinguish in the following between simply-connected domains, and connected ones that (sloppily speaking) may possess holes, which we will specify later and refer to as topologically non-trivial. We refer, e.g., to [3, 12, 55, 60] for more reading.

2.2.2 De Rham complex for trivial topologies

A trivial topology can be represented by a simply-connected domain $\Omega \subset \mathbb{R}^3$ with a connected boundary Γ, see [11, Section 5.1.4]. In other words, the domain Ω has a trivial topology if it is contractible to a point.

In Figure 2.2, we visualize the structure of the de Rham complex, where the mentioned spaces form an exact sequence. It is the case when Ω has a trivial topology, see [4, 11]. The rectangles schematize a splitting of

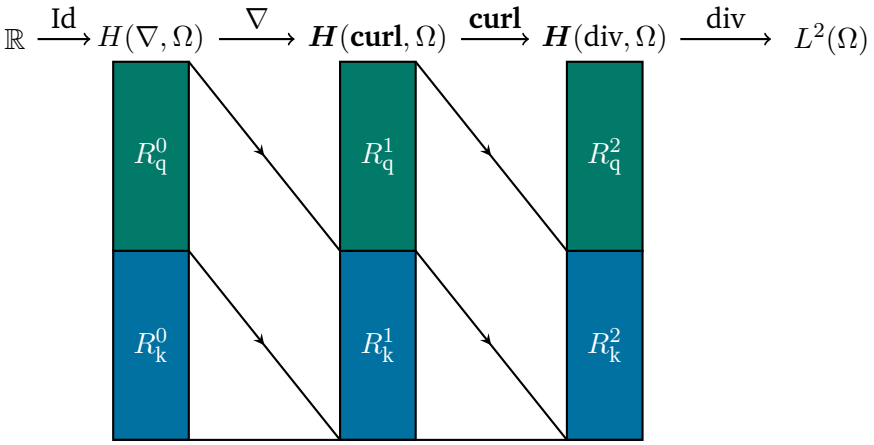

Figure 2.2: De Rham complex for a topologically trivial domain.

the function domains on which the differential operators ∇, **curl**, and div act: The green areas R^0_{q}, R^1_{q}, and R^2_{q} represent each the domain's elements that map to a non-zero element in the kernel of the succeeding operator in the sequence, which we illustrate with the blue areas R^0_{k}, R^1_{k}, and R^2_{k}, respectively. This gives rise to the closed subspaces

$$
\begin{aligned}
H(\nabla\mathbf{0},\Omega) &:= \{v \in H(\nabla,\Omega) : \nabla v = \mathbf{0}\},\\
\boldsymbol{H}(\mathbf{curl}\,\mathbf{0},\Omega) &:= \{\boldsymbol{v} \in \boldsymbol{H}(\mathbf{curl},\Omega) : \mathbf{curl}\,\boldsymbol{v} = \mathbf{0}\},\\
\boldsymbol{H}(\mathrm{div}\,0,\Omega) &:= \{\boldsymbol{v} \in \boldsymbol{H}(\mathrm{div},\Omega) : \mathrm{div}\,\boldsymbol{v} = 0\},
\end{aligned}
$$

and we say that the elements of $H(\nabla\mathbf{0},\Omega)$, $\boldsymbol{H}(\mathbf{curl}\,\mathbf{0},\Omega)$, and $\boldsymbol{H}(\mathrm{div}\,0,\Omega)$ are closed. Obviously, we also notice that the image of each differential operator coincides with the kernel of the next one in the sequence. In other words, we have

$$
\begin{aligned}
\mathbb{R} &= \ker(\nabla), && \text{(2.33a)}\\
\mathrm{Im}(\nabla) &= \ker(\mathbf{curl}), && \text{(2.33b)}\\
\mathrm{Im}(\mathbf{curl}) &= \ker(\mathrm{div}), && \text{(2.33c)}\\
\mathrm{Im}(\mathrm{div}) &= L^2(\Omega), && \text{(2.33d)}
\end{aligned}
$$

where $\mathrm{Im}(\cdot)$ denotes the image and $\ker(\cdot)$ the kernel of an operator. In terms of spaces, the relations in (2.33) translate to

$$
\begin{aligned}
\mathbb{R} &= H(\nabla\mathbf{0},\Omega), && \text{(2.34a)}\\
\nabla(H(\nabla,\Omega)) &= \boldsymbol{H}(\mathbf{curl}\,\mathbf{0},\Omega), && \text{(2.34b)}\\
\mathbf{curl}(\boldsymbol{H}(\mathbf{curl},\Omega)) &= \boldsymbol{H}(\mathrm{div}\,0,\Omega), && \text{(2.34c)}\\
\mathrm{div}(\boldsymbol{H}(\mathrm{div},\Omega)) &= L^2(\Omega). && \text{(2.34d)}
\end{aligned}
$$

As a direct consequence, we present the following result, which establishes the existence of potentials.

Theorem 2.18 (Existence of potentials)**.** *For a bounded topologically trivial Lipschitz domain Ω, we have,*

$$\boldsymbol{v} \in \boldsymbol{H}(\mathbf{curl}, \Omega): \quad \mathbf{curl}\, \boldsymbol{v} = \mathbf{0} \Rightarrow \quad \exists\, \varphi \in H(\nabla, \Omega) \ : \boldsymbol{v} = \nabla \varphi, \tag{2.35a}$$

$$\boldsymbol{v} \in \boldsymbol{H}(\mathrm{div}, \Omega): \quad \mathrm{div}\, \boldsymbol{v} = 0 \ \Rightarrow \exists\, \boldsymbol{w} \in \boldsymbol{H}(\mathbf{curl}, \Omega) : \boldsymbol{v} = \mathbf{curl}\, \boldsymbol{w}. \tag{2.35b}$$

We call a function φ and a vector field $\boldsymbol{w}$ that are obtained as above a scalar potential and vector potential, respectively.

Proof. The result is standard and can be found, e.g., in [55] and [115, Theorem 2.19]. □

It is evident that the potentials defined above are not unique. Indeed, because of (2.33), there exists a whole class of scalar potentials of the form $\varphi := \psi + C$, with $\psi \in H(\nabla, \Omega)$ and $C \in \mathbb{R}$ that satisfy the right-hand side of (2.35a). Similarly, all vector potentials of the form $\boldsymbol{w} := \boldsymbol{u} + \nabla \varphi$, with $\boldsymbol{u} \in \boldsymbol{H}(\mathbf{curl}, \Omega)$, $\varphi \in H(\nabla, \Omega)$ are possible representations of divergence free fields. In order to guarantee the uniqueness of potentials, further conditions have to be prescribed for a specific choice of the constant C. We present for instance one possible choice of unique potentials, and refer, e.g., to [3, 55], for more extensive results.

Corollary 2.19. *For a bounded topologically trivial Lipschitz domain Ω, it follows that*

$$\boldsymbol{v} \in \boldsymbol{H}(\mathbf{curl}\, \mathbf{0}, \Omega) \Rightarrow \exists!\, \varphi \in H(\nabla, \Omega) : \boldsymbol{v} = \nabla \varphi \quad \textit{with } (\varphi, 1)_\Omega = 0, \tag{2.36a}$$

$$\boldsymbol{v} \in \boldsymbol{H}(\mathrm{div}\, 0, \Omega) \ \Rightarrow \exists!\, \boldsymbol{w} \in \boldsymbol{H}(\mathbf{curl}, \Omega) \cap \boldsymbol{H}(\mathrm{div}, \Omega) : \boldsymbol{v} = \mathbf{curl}\, \boldsymbol{w} \quad \textit{with } \mathrm{div}\, \boldsymbol{w} = 0 \textit{ and } \gamma_{\boldsymbol{n}} \boldsymbol{w} = 0. \tag{2.36b}$$

Conditions that fix the choice of potentials are called gauge conditions.

Proof. The relation (2.36a) is straightforward, because the condition $(\varphi, 1)_\Omega = 0$ yields a potential that is orthogonal to the constants. Hence, the kernel is removed by definition. The proof of (2.36b) can be obtained, e.g., by adapting the more general result of [88, Theorem 3.38] for topologically trivial domains. □

For convenience, we define the space of divergence free vector fields with vanishing normal traces

$$\boldsymbol{H}_0(\mathrm{div}\, 0, \Omega) := \{\boldsymbol{v} \in \boldsymbol{H}(\mathrm{div}\, 0, \Omega) : \ \gamma_{\boldsymbol{n}} \boldsymbol{v} = 0\}, \tag{2.37}$$

and note that $\boldsymbol{w}$ as given in (2.36b) is an element of $\boldsymbol{H}(\mathbf{curl}, \Omega) \cap \boldsymbol{H}_0(\mathrm{div}\, 0, \Omega)$. The subspaces $H(\nabla \mathbf{0}, \Omega)$, $\boldsymbol{H}(\mathbf{curl}\, \mathbf{0}, \Omega)$, and $\boldsymbol{H}(\mathrm{div}\, 0, \Omega)$ are closed subsets of Hilbert spaces. Hence, Theorem 2.2 applies. We denote the corresponding quotient spaces by

$$\begin{aligned}
[H(\nabla, \Omega)] &:= \quad H(\nabla, \Omega)/H(\nabla \mathbf{0}, \Omega) \quad = H(\nabla, \Omega)/\mathbb{R}, \\
[\boldsymbol{H}(\mathbf{curl}, \Omega)] &:= \boldsymbol{H}(\mathbf{curl}, \Omega)/\boldsymbol{H}(\mathbf{curl}\, \mathbf{0}, \Omega) = \boldsymbol{H}(\mathbf{curl}, \Omega)/\nabla(H(\nabla, \Omega)), \\
[\boldsymbol{H}(\mathrm{div}, \Omega)] &:= \ \boldsymbol{H}(\mathrm{div}, \Omega)/\boldsymbol{H}(\mathrm{div}\, 0, \Omega) \ = \boldsymbol{H}(\mathrm{div}, \Omega)/\,\mathbf{curl}(\boldsymbol{H}(\mathbf{curl}, \Omega)).
\end{aligned}$$

For visualization, the quotient spaces $[H(\nabla, \Omega)]$, $[\boldsymbol{H}(\mathbf{curl}, \Omega)]$, and $[\boldsymbol{H}(\mathrm{div}, \Omega)]$ correspond to the regions R^0_{q}, R^1_{q}, and R^2_{q} in Figure 2.2. With this, Corollary 2.19 can be rewritten in terms of quotient spaces.

Corollary 2.20. *For a bounded topologically trivial Lipschitz domain Ω, it results that*

$$\boldsymbol{v} \in \boldsymbol{H}(\mathbf{curl}\, \mathbf{0}, \Omega) \Rightarrow \ \exists!\, \varphi \in [H(\nabla, \Omega)] \quad : \boldsymbol{v} = \nabla \varphi, \tag{2.38a}$$

$$\boldsymbol{v} \in \boldsymbol{H}(\operatorname{div} 0, \Omega) \quad \Rightarrow \exists! \, \boldsymbol{w} \in [\boldsymbol{H}(\mathbf{curl}, \Omega)] : \boldsymbol{v} = \mathbf{curl}\, \boldsymbol{w}. \tag{2.38b}$$

Proof. It is sufficient to show that these formulations and the ones in Corollary 2.19 are equivalent. First, by Corollary 2.4, we identify $[H(\nabla, \Omega)]$ with $H(\nabla \mathbf{0}, \Omega)^\perp$, and $[\boldsymbol{H}(\mathbf{curl}, \Omega)]$ with $\boldsymbol{H}(\mathbf{curl}\, \mathbf{0}, \Omega)^\perp$. Per definition of the orthogonal complement, there holds

$$\forall \varphi \in H(\nabla \mathbf{0}, \Omega)^\perp \text{ and } C \in H(\nabla \mathbf{0}, \Omega) = \mathbb{R}, \quad (\varphi, C)_\Omega = 0, \tag{2.39}$$

which coincides with the gauge condition in (2.36a).
Then, for the second equivalence, we know from (2.35a) that for $\boldsymbol{w}_0 \in \boldsymbol{H}(\mathbf{curl}\, \mathbf{0}, \Omega)$ there exists a $\varphi \in H(\nabla, \Omega)$ such that $\boldsymbol{w}_0 = \nabla \varphi$. With this, orthogonality of $\boldsymbol{w} \in \boldsymbol{H}(\mathbf{curl}\, \mathbf{0}, \Omega)^\perp$ and $\nabla \varphi \in \boldsymbol{H}(\mathbf{curl}\, \mathbf{0}, \Omega)$ means

$$(\boldsymbol{w}, \nabla \varphi)_\Omega = 0. \tag{2.40}$$

The integration by parts (2.26b) extends by continuity to $\varphi \in H(\nabla, \Omega)$ because of the density of $\mathcal{D}(\overline{\Omega})$ in $H(\nabla, \Omega)$, see Lemma 2.12 and Remark 2.16. Then, we see from

$$(\boldsymbol{w}, \nabla \varphi)_\Omega = \langle \gamma_{\boldsymbol{n}} \boldsymbol{w}, \, \gamma_0 \varphi \rangle_\Gamma - (\operatorname{div} \boldsymbol{w}, \varphi)_\Omega$$

that for $\boldsymbol{w}$ to be an element of the orthogonal complement $\boldsymbol{H}(\mathbf{curl}\, \mathbf{0}, \Omega)$ in $\boldsymbol{L}^2(\Omega)$, it has to satisfy $\operatorname{div} \boldsymbol{w} = 0$ and $\gamma_{\boldsymbol{n}} \boldsymbol{w} = 0$. Hence, $\boldsymbol{H}(\mathbf{curl}\, \mathbf{0}, \Omega)^\perp \subseteq \boldsymbol{H}(\mathbf{curl}, \Omega) \cap \boldsymbol{H}_0(\operatorname{div} 0, \Omega)$. Similarly, the reverse inclusion follows merely by means of integration by parts. Therefore, $\boldsymbol{H}(\mathbf{curl}\, \mathbf{0}, \Omega)^\perp$, thus $[\boldsymbol{H}(\mathbf{curl}, \Omega)]$, can be identified with $\boldsymbol{H}(\mathbf{curl}, \Omega) \cap \boldsymbol{H}_0(\operatorname{div} 0, \Omega)$. □

A similar de Rham complex can also be derived for energy spaces with homogeneous boundary conditions, see [27, Theorem 7].

2.2.3 De Rham complex for non-trivial topologies

The general type of de Rham complex arises when Ω has a more general topology. In particular, we consider $\Omega \subset \mathbb{R}^3$ to be connected but not simply-connected, for instance, as visualized in Figure 2.1. First, let us introduce the notion of pseudo-Lipschitz domains, and refer to [3, 88] for more details.

Definition 2.21 (Pseudo-Lipschitz, [3, Definition 3.1])**.** *Let $B_d(\boldsymbol{x}_0; r)$ denote the d-dimensional ball with center $\boldsymbol{x}_0$ and radius r. We consider $d = 2, 3$. A domain Ω is pseudo-Lipschitz, if we have*

$$\forall \boldsymbol{x} \in \partial\Omega, \, \exists \, n_{\boldsymbol{x}} \in \{1, 2\}, \, \exists \, r_0 > 0 : \, \forall \, 0 < \rho < r_0, \, \Omega \cap B_d(\boldsymbol{x}; \rho) = \{\omega_k\}_{k=1}^{n_{\boldsymbol{x}}} \text{ with } \omega_k \text{ connected and Lipschitz.}$$

Until now, we assumed the existence of a set of N_C connected surfaces $\{\Gamma_{\mathrm{C}_k}\}_{k=1}^{N_\mathrm{C}}$ that render a connected domain simply-connected. In the following, we formalize this idea and specify the requirements that should be fulfilled to account as an admissible interior cut.

Definition 2.22 (Interior cuts, [88, Section 3.7])**.** *We call Γ_{C_k} with $k = 1, \ldots, N_\mathrm{C}$, interior cuts of Ω if the following properties are satisfied for all $k = 1, \ldots, N_\mathrm{C}$:*

- *Γ_{C_k} are open parts of smooth surfaces.*
- *$\partial\Gamma_{\mathrm{C}_k} \subset \partial\Omega$.*

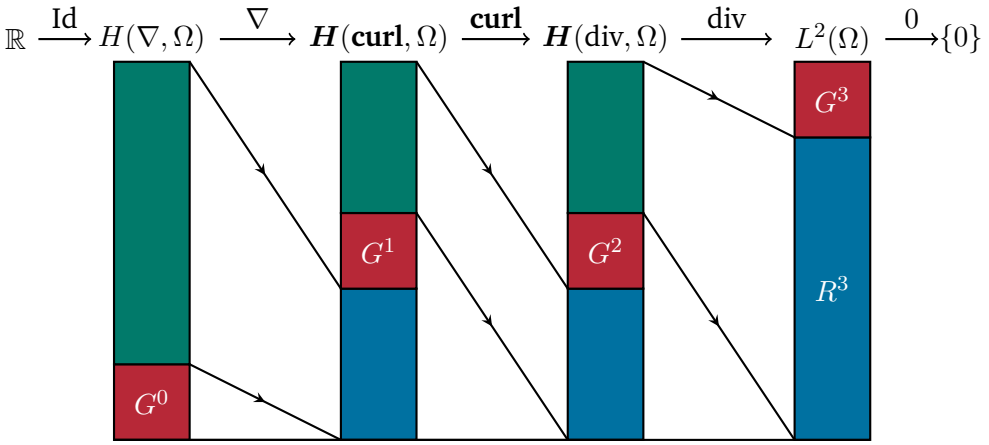

Figure 2.3: De Rham complex for a topologically non-trivial domain with cohomology (in red).

- *All surfaces* Γ_{C_k} *are disjoint.*
- $\Omega \setminus \bigcup_{k=1}^{N_C} \Gamma_{C_k}$ *is simply-connected and pseudo-Lipschitz.*

Remark 2.23 ([3, Remark 3.2])**.** *Definition 2.21 on pseudo-Lipschitz domains allows the consideration of cuts in multiply-connected Lipschitz domains. Let us consider a domain* Ω *with boundary* Γ*. Then, in the neighborhood of* $\boldsymbol{x} \in \Gamma$*, which is specified by a* d*-dimensional ball with positive radius and center* $\boldsymbol{x}$*,* $n_{\boldsymbol{x}} = 1$ *arises if the considered intersection of the neighborhood of* $\boldsymbol{x}$ *with* Ω *lies completely on one side of* Γ*, whereas* $n_{\boldsymbol{x}} = 2$ *means that the latter lies on both sides. For an illustration, see Figure 2.1a, where we find* $n_{\boldsymbol{x}} = 1$*, e.g., for* $\boldsymbol{x} \in \Gamma_0$ *and* $n_{\boldsymbol{x}} = 2$ *on* Γ_{C_1}*. Note also that pseudo-Lipschitz domains possess the cone property.*

As highlighted in Figure 2.3, we see that additional partitions arise in this case comparing to Figure 2.2. The corresponding subspaces of G^0, G^1, and G^2 contribute as well to the kernels of ∇, **curl** and div in $H(\nabla,\Omega)$, $\boldsymbol{H}(\mathbf{curl},\Omega)$ and $\boldsymbol{H}(\mathrm{div},\Omega)$, respectively. Moreover, the div operator maps the elements of $\boldsymbol{H}(\mathrm{div},\Omega)$ to a subspace of $L^2(\Omega)$ denoted by R^3. The orthogonal complement of R^3 in $L^2(\Omega)$ is represented by G^3. From [27, Theorem 7], we know indeed that the equalities in (2.33) change to inclusions, i.e.,

$$\begin{aligned} \mathbb{R} &\subseteq \ker(\nabla), \\ \mathrm{Im}(\nabla) &\subseteq \ker(\mathbf{curl}), \\ \mathrm{Im}(\mathbf{curl}) &\subseteq \ker(\mathrm{div}), \\ \mathrm{Im}(\mathrm{div}) &\subseteq L^2(\Omega). \end{aligned}$$

Moreover, the images of the differential operators on left-hand sides form closed subsets in the corresponding kernels [35, Section IX.A.§1.3]. In particular, $\ker(\mathbf{curl})$ and $\ker(\mathrm{div})$ being closed can be expressed by means of Theorem 2.2, which leads to

$$\boldsymbol{H}(\mathbf{curl}\,0,\Omega) = \ker(\mathbf{curl}) = \nabla H(\nabla,\Omega) \oplus (\nabla H(\nabla,\Omega))^{\perp,0}, \tag{2.42a}$$

$$\boldsymbol{H}(\mathrm{div}\,0,\Omega) = \ker(\mathrm{div}) \;\; = \mathbf{curl}\,\boldsymbol{H}(\mathbf{curl},\Omega) \oplus (\mathbf{curl}\,\boldsymbol{H}(\mathbf{curl},\Omega))^{\perp,0}. \tag{2.42b}$$

Thereby, orthogonality is understood in the $\boldsymbol{H}(\mathbf{curl},\Omega)$, and $\boldsymbol{H}(\mathrm{div},\Omega)$ sense, respectively. Note that the subspaces $(\nabla H(\nabla,\Omega))^{\perp,0}$ and $(\mathbf{curl}\,\boldsymbol{H}(\mathbf{curl},\Omega))^{\perp,0}$ are the orthogonal complements of $\nabla H(\nabla,\Omega)$ and $\mathbf{curl}\,\boldsymbol{H}(\mathbf{curl},\Omega)$ in the corresponding null-spaces $\boldsymbol{H}(\mathbf{curl}\,\mathbf{0},\Omega)$ and $\boldsymbol{H}(\mathrm{div}\,0,\Omega)$, respectively. Hence, to avoid a notational conflict with the orthogonal decomposition in the whole spaces $\boldsymbol{H}(\mathbf{curl},\Omega)$ and $\boldsymbol{H}(\mathrm{div},\Omega)$, we used the notation $(\cdot)^{\perp,0}$ instead of $(\cdot)^{\perp}$.
The spaces $(\nabla H(\nabla,\Omega))^{\perp,0}$ and $(\mathbf{curl}\,\boldsymbol{H}(\mathbf{curl},\Omega))^{\perp,0}$ are isomorphic to the first and second de Rham cohomology spaces (or groups), respectively. We label them

$$\mathbb{H}_1(\Omega) := (\nabla H(\nabla,\Omega))^{\perp,0}, \tag{2.43a}$$
$$\mathbb{H}_2(\Omega) := (\mathbf{curl}\,\boldsymbol{H}(\mathbf{curl},\Omega))^{\perp,0}. \tag{2.43b}$$

In addition to $\boldsymbol{H}_0(\mathrm{div}\,0,\Omega)$, which we defined in (2.37), we introduce

$$\boldsymbol{H}_{\mathbf{0}}(\mathbf{curl}\,\mathbf{0},\Omega) := \{\boldsymbol{v}\in\boldsymbol{H}(\mathbf{curl}\,\mathbf{0},\Omega) : \boldsymbol{\gamma}_\times\,\boldsymbol{v}=\mathbf{0}\}.$$

The spaces $\boldsymbol{H}_0(\mathrm{div}\,0,\Omega)$ and $\boldsymbol{H}_{\mathbf{0}}(\mathbf{curl}\,\mathbf{0},\Omega)$ correspond to the orthogonal complements of $(\nabla H(\nabla,\Omega))^{\perp}$ and $(\mathbf{curl}\,\boldsymbol{H}(\mathbf{curl},\Omega))^{\perp}$ in $\boldsymbol{H}(\mathbf{curl},\Omega)$ and $\boldsymbol{H}(\mathrm{div},\Omega)$, respectively. This can be established similarly to the proof of Corollary 2.20 by a direct application of the integration by parts formulae of Theorem 2.15 and by using the density arguments of Lemma 2.12 to extend the assertion to the corresponding energy spaces. For convenience, we write

$$\boldsymbol{H}_{\mathbf{0}}(\mathbf{curl}\,\mathbf{0},\Omega) = (\mathbf{curl}\,\boldsymbol{H}(\mathbf{curl},\Omega))^{\perp},$$
$$\boldsymbol{H}_0(\mathrm{div}\,0,\Omega) = (\nabla H(\nabla,\Omega))^{\perp}.$$

Therefore, the cohomology spaces $\mathbb{H}_1(\Omega)$ and $\mathbb{H}_2(\Omega)$ can be further characterized as follows

$$\mathbb{H}_1(\Omega) = \boldsymbol{H}(\mathbf{curl}\,\mathbf{0},\Omega)\cap\boldsymbol{H}_0(\mathrm{div}\,0,\Omega), \tag{2.45a}$$
$$\mathbb{H}_2(\Omega) = \boldsymbol{H}_{\mathbf{0}}(\mathbf{curl}\,\mathbf{0},\Omega)\cap\boldsymbol{H}(\mathrm{div}\,0,\Omega). \tag{2.45b}$$

We refer to [27, Definition 2.4] and [60] for more details about the cohomology spaces, and in addition to [35, Section IX.A.§1.3] for a more concrete characterization of the corresponding spaces associated to the regions in Figure 2.3. Therefrom, we also know that $\mathbb{H}_1(\Omega)$ and $\mathbb{H}_2(\Omega)$ contain harmonic Neumann and Dirichlet vector fields, respectively. Moreover, their dimensions are finite, and match with the first and second Betti numbers of Ω, i.e.,

$$\dim\mathbb{H}_1(\Omega) = \beta_1(\Omega),$$
$$\dim\mathbb{H}_2(\Omega) = \beta_2(\Omega).$$

Betti numbers are topological invariants that are defined as the dimensions of the respective cohomology spaces. In our connected 3D case, $\beta_1(\Omega)$ and $\beta_2(\Omega)$ correspond to N_{C} as in Definition 2.22 and to the number of connected boundaries N_Γ minus one, respectively, cf. [88, Theorem 3.42 & 3.43]. Informally, $\beta_1(\Omega)$ can be interpreted as the number of one-dimensional (1D) or "circular" holes, and $\beta_2(\Omega)$ as the number of 2D or "surface" holes. Note that $\beta_0(\Omega)$ and $\beta_3(\Omega)$ can also be defined: $\beta_0(\Omega)$ designates the number of connected components of Ω, thus, $\beta_0(\Omega)=1$, whereas $\beta_3(\Omega)=0$, see [4].

The last pieces of the puzzle reside in the characterization of the orthogonal complements of $\boldsymbol{H}(\mathbf{curl}\,\mathbf{0},\Omega)$ and $\boldsymbol{H}(\mathrm{div}\,0,\Omega)$ in $\boldsymbol{H}(\mathbf{curl},\Omega)$ and $\boldsymbol{H}(\mathrm{div},\Omega)$, respectively. They arise when inspecting the properties of the

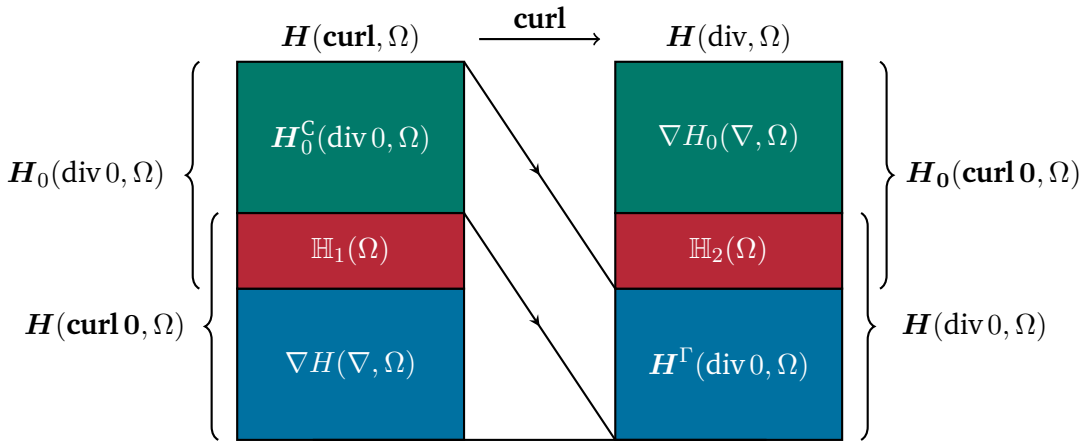

Figure 2.4: Orthogonal decompositions of $\boldsymbol{H}(\mathbf{curl},\Omega)$ and $\boldsymbol{H}(\mathrm{div},\Omega)$. The **curl** isomorphism (2.48) is represented by the arrows.

curl-operator. Let $\boldsymbol{H}_0^{\mathsf{C}}(\mathrm{div}\,0,\Omega)$ and $\boldsymbol{H}^{\Gamma}(\mathrm{div}\,0,\Omega)$ denote the subspaces of $\boldsymbol{H}(\mathrm{div}\,0,\Omega)$ with vanishing fluxes through the individual cuts and boundary pieces, respectively, i.e.,

$$\boldsymbol{H}_0^{\mathsf{C}}(\mathrm{div}\,0,\Omega) := \{\boldsymbol{v}\in\boldsymbol{H}(\mathrm{div}\,0,\Omega):\ \langle\gamma_{\boldsymbol{n}}\boldsymbol{v},1\rangle_{\Gamma_{C_k}}=0\quad\forall\,k=1,\dots,N_{\mathsf{C}}\},$$
$$\boldsymbol{H}^{\Gamma}(\mathrm{div}\,0,\Omega) := \{\boldsymbol{v}\in\boldsymbol{H}(\mathrm{div}\,0,\Omega):\ \langle\gamma_{\boldsymbol{n}}\boldsymbol{v},1\rangle_{\Gamma_{k}}=0\quad\forall\,k=1,\dots,N_{\Gamma}\}.$$

Theorem 2.24 (Isomorphisms of the **curl**-operator, cf. [12, Theorem 1 & 2])**.** *Let $\boldsymbol{H}(\mathbf{curl},\Omega)\cap\boldsymbol{H}_0^{\mathsf{C}}(\mathrm{div}\,0,\Omega)$ and $\boldsymbol{H}^{\Gamma}(\mathrm{div}\,0,\Omega)$ be endowed with the $\boldsymbol{H}(\mathbf{curl},\Omega)$ and $\boldsymbol{L}^2(\Omega)$ norms, respectively. Then, the operator*

$$\mathbf{curl}:\ \boldsymbol{H}(\mathbf{curl},\Omega)\cap\boldsymbol{H}_0^{\mathsf{C}}(\mathrm{div}\,0,\Omega)\to\boldsymbol{H}^{\Gamma}(\mathrm{div}\,0,\Omega) \tag{2.48}$$

is a homeomorphism. Furthermore, the same property holds also with

$$\mathbf{curl}:\ \boldsymbol{H}_{\mathbf{0}}(\mathbf{curl},\Omega)\cap\boldsymbol{H}^{\Gamma}(\mathrm{div}\,0,\Omega)\to\boldsymbol{H}_0^{\mathsf{C}}(\mathrm{div}\,0,\Omega). \tag{2.49}$$

Interestingly, notice the apparent correspondence (symmetry) of the structures of the spaces in (2.48) and (2.49). In fact, as explained in [12, Section 3.3], (2.49) is an isomorphism in a dual structure of the de Rham complex, which can be represented, e.g., as the sequence of energy spaces with homogeneous boundary conditions. In Figures 2.4 and 2.5, we illustrate the above mentioned observation along with the relevant orthogonal subspaces of $\boldsymbol{H}(\mathbf{curl},\Omega)$ and $\boldsymbol{H}(\mathrm{div},\Omega)$ on one hand, and $\boldsymbol{H}_{\mathbf{0}}(\mathbf{curl},\Omega)$ and $\boldsymbol{H}_0(\mathrm{div},\Omega)$ on the other hand. We refer, e.g., to [88] for more details on the decomposition of spaces with homogeneous boundary conditions.

As a consequence of Theorem 2.24, we state the following result.

Corollary 2.25. *For $\boldsymbol{v}\in\boldsymbol{H}^{\Gamma}(\mathrm{div}\,0,\Omega)$, there exists a unique $\boldsymbol{w}\in\boldsymbol{H}(\mathbf{curl},\Omega)\cap\boldsymbol{H}_0^{\mathsf{C}}(\mathrm{div}\,0,\Omega)$ with $\boldsymbol{v}=\mathbf{curl}\,\boldsymbol{w}$. Moreover, there exists $C_1>0$ such that*

$$\|\boldsymbol{v}\|_{\boldsymbol{H}(\mathbf{curl},\Omega)}\le C_1\|\mathbf{curl}\,\boldsymbol{w}\|_{\boldsymbol{L}^2(\Omega)}.$$

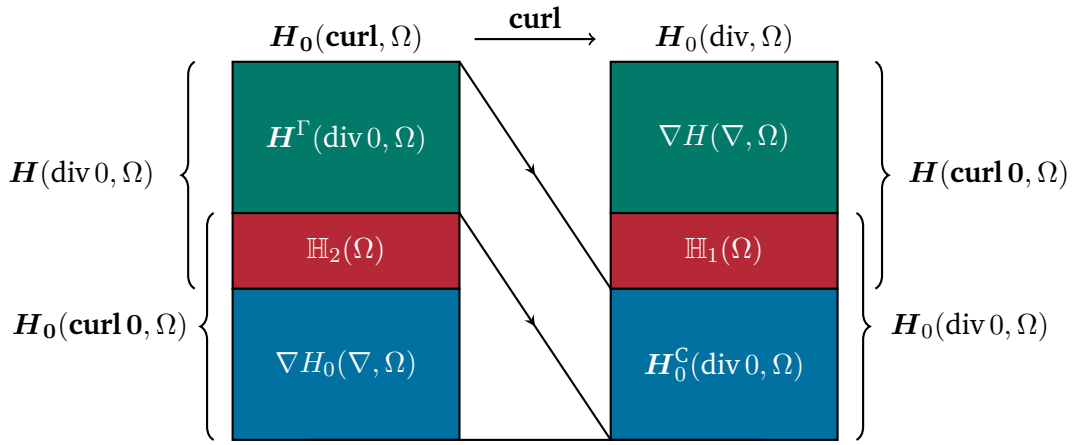

Figure 2.5: Orthogonal decompositions of $\boldsymbol{H_0}(\mathbf{curl},\Omega)$ and $\boldsymbol{H}_0(\mathrm{div},\Omega)$. The **curl** isomorphism (2.49) is represented by the arrows.

Reversely, a vector field $\boldsymbol{w} \in \boldsymbol{H}(\mathbf{curl},\Omega) \cap \boldsymbol{H}_0^{\mathsf{C}}(\mathrm{div}\,0,\Omega)$ implies that $\boldsymbol{v}$ is an element of $\boldsymbol{H}^{\Gamma}(\mathrm{div}\,0,\Omega)$, and there exists $C_2 > 0$ such that

$$\|\mathbf{curl}\,\boldsymbol{w}\|_{\boldsymbol{L}^2(\Omega)} \leq C_2 \|\boldsymbol{v}\|_{\boldsymbol{H}(\mathbf{curl},\Omega)}.$$

In addition, similar results hold for $\boldsymbol{v} \in \boldsymbol{H}_0^{\mathsf{C}}(\mathrm{div}\,0,\Omega)$ and $\boldsymbol{w} \in \boldsymbol{H_0}(\mathbf{curl},\Omega) \cap \boldsymbol{H}^{\Gamma}(\mathrm{div}\,0,\Omega)$.

Proof. The assertions are a direct consequence of Theorem 2.24. For instance, the results can also be obtained from [3, Theorem 3.12 & 3.17] or as a special case of the more general setting in [50, Lemma 3.1]. □

Altogether, we come to the well-known Helmholtz (Hodge) decompositions.

Theorem 2.26 (Helmholtz decompositions)**.** *Every vector field $\boldsymbol{u} \in \boldsymbol{L}^2(\Omega)$ admits the following orthogonal decomposition,*

$$\boldsymbol{u} = \mathbf{curl}\,\boldsymbol{v} + \nabla\varphi + \boldsymbol{\eta}_1 \tag{2.50}$$

with unique $\varphi \in H(\nabla,\Omega)$ (up to a constant), $\boldsymbol{\eta}_1 \in \mathbb{H}_1(\Omega)$, and $\boldsymbol{v} \in \boldsymbol{H_0}(\mathbf{curl},\Omega) \cap \boldsymbol{H}^{\Gamma}(\mathrm{div}\,0,\Omega)$. Alternatively, it holds for any $\boldsymbol{u} \in \boldsymbol{L}^2(\Omega)$ that

$$\boldsymbol{u} = \mathbf{curl}\,\boldsymbol{v} + \nabla\varphi + \boldsymbol{\eta}_2 \tag{2.51}$$

with unique $\varphi \in H_0(\nabla,\Omega)$, $\boldsymbol{\eta}_2 \in \mathbb{H}_2(\Omega)$, and $\boldsymbol{v} \in \boldsymbol{H}(\mathbf{curl},\Omega) \cap \boldsymbol{H}_0^{\mathsf{C}}(\mathrm{div}\,0,\Omega)$.

Proof. The decompositions are readily obtained by using Theorem 2.24 together with the orthogonal decompositions illustrated in Figure 2.4 and its "dual" in Figure 2.5. For convenience, we also refer, e.g, to [88, Theorem 3.45, Remark 3.46] and [35, Corollary IX.A.§1.6]. □

Remark 2.27. *For a topologically trivial domain Ω, the Helmholtz decompositions given above reduce to*

$$\forall \boldsymbol{u} \in \boldsymbol{L}^2(\Omega), \exists!\, \varphi \in H(\nabla,\Omega) \text{ and } \boldsymbol{v} \in \boldsymbol{H_0}(\mathbf{curl},\Omega) \cap \boldsymbol{H}(\mathrm{div}\,0,\Omega): \quad \boldsymbol{u} = \mathbf{curl}\,\boldsymbol{v} + \nabla\varphi,$$
$$\forall \boldsymbol{u} \in \boldsymbol{L}^2(\Omega), \exists!\, \varphi \in H_0(\nabla,\Omega) \text{ and } \boldsymbol{v} \in \boldsymbol{H}(\mathbf{curl},\Omega) \cap \boldsymbol{H}_0(\mathrm{div}\,0,\Omega): \quad \boldsymbol{u} = \mathbf{curl}\,\boldsymbol{v} + \nabla\varphi.$$

Note that in the first statement, φ is unique up to a constant.

In addition, the orthogonal decompositions

$$\begin{aligned}\boldsymbol{H}(\mathbf{curl},\Omega) &= \boldsymbol{H}(\mathbf{curl}\,\mathbf{0},\Omega) \oplus (\boldsymbol{H}(\mathbf{curl},\Omega) \cap \boldsymbol{H}_0^{\mathsf{C}}(\operatorname{div}0,\Omega)),\\ \boldsymbol{H}_{\mathbf{0}}(\mathbf{curl},\Omega) &= \boldsymbol{H}_{\mathbf{0}}(\mathbf{curl}\,\mathbf{0},\Omega) \oplus (\boldsymbol{H}_{\mathbf{0}}(\mathbf{curl},\Omega) \cap \boldsymbol{H}^{\Gamma}(\operatorname{div}0,\Omega))\end{aligned}$$

motivate the consideration of quotient spaces for analysis purposes. By Corollary 2.4, we obtain the identifications

$$[\boldsymbol{H}(\mathbf{curl},\Omega)] \cong \boldsymbol{H}(\mathbf{curl},\Omega) \cap \boldsymbol{H}_0^{\mathsf{C}}(\operatorname{div}0,\Omega), \tag{2.52a}$$

$$[\boldsymbol{H}_{\mathbf{0}}(\mathbf{curl},\Omega)] \cong \boldsymbol{H}_{\mathbf{0}}(\mathbf{curl},\Omega) \cap \boldsymbol{H}^{\Gamma}(\operatorname{div}0,\Omega). \tag{2.52b}$$

With this, we close the discussion about the existence and uniqueness of potentials in dependence of the topology. For more details, and more exhaustive contents, we refer the interested reader to [3, 27, 35, 55, 60]. Similar results for spaces with mixed and non-homogeneous boundary conditions are provided in [49] and [50].

In this work, Ω^{e} may be bounded or unbounded. For the latter case, we recall the definition of $H^s_{\mathrm{loc}}(\Omega^{\mathrm{e}})$ in (2.12). With $s=1$, we refer to this space as the local $H^1(\Omega^{\mathrm{e}})$ space, i.e., $H^1(K)$ for every compact subset K of Ω^{e}. Accordingly to the notation used for the energy spaces, we write $H_{\mathrm{loc}}(\nabla,\Omega^{\mathrm{e}})$ instead of $H^1_{\mathrm{loc}}(\Omega^{\mathrm{e}})$. In the same sense, we introduce

$$\begin{aligned}\boldsymbol{H}_{\mathrm{loc}}(\operatorname{div},\Omega^{\mathrm{e}}) &:= \{\boldsymbol{v}^{\mathrm{e}} \in \boldsymbol{L}^2_{\mathrm{loc}}(\Omega^{\mathrm{e}}) : \operatorname{div}\boldsymbol{v}^{\mathrm{e}} \in L^2_{\mathrm{loc}}(\Omega^{\mathrm{e}})\},\\ \boldsymbol{H}_{\mathrm{loc}}(\mathbf{curl},\Omega^{\mathrm{e}}) &:= \{\boldsymbol{v}^{\mathrm{e}} \in \boldsymbol{L}^2_{\mathrm{loc}}(\Omega^{\mathrm{e}}) : \mathbf{curl}\,\boldsymbol{v}^{\mathrm{e}} \in \boldsymbol{L}^2_{\mathrm{loc}}(\Omega^{\mathrm{e}})\},\\ H_{\mathrm{loc}}(\Delta,\Omega^{\mathrm{e}}) &:= \{v^{\mathrm{e}} \in L^2_{\mathrm{loc}}(\Omega^{\mathrm{e}}) : \Delta v^{\mathrm{e}} \in L^2_{\mathrm{loc}}(\Omega^{\mathrm{e}})\},\\ \boldsymbol{H}_{\mathrm{loc}}(\mathbf{curl}\ \mathbf{curl},\Omega^{\mathrm{e}}) &:= \{\boldsymbol{v}^{\mathrm{e}} \in \boldsymbol{L}^2_{\mathrm{loc}}(\Omega^{\mathrm{e}}) : \mathbf{curl}\,\mathbf{curl}\,\boldsymbol{v}^{\mathrm{e}} \in \boldsymbol{L}^2_{\mathrm{loc}}(\Omega^{\mathrm{e}})\},\end{aligned}$$

which are Hilbert spaces that inherit the structure of the corresponding $L^2_{\mathrm{loc}}(\Omega^{\mathrm{e}})$ or $\boldsymbol{L}^2_{\mathrm{loc}}(\Omega^{\mathrm{e}})$ space. For convenience, we also give the notation of Bochner spaces that take instantaneous values in energy spaces. They are defined equivalently to (2.14), i.e.,

$$L^2(\partial_t,T;\,H(\nabla,\Omega)) := \{v \in L^2(T;\,H(\nabla,\Omega)) : \partial_t v \in L^2(T;\,H(\nabla,\Omega))\}, \tag{2.53a}$$

$$\boldsymbol{L}^2(\partial_t,T;\,\boldsymbol{H}(\mathbf{curl},\Omega)) := \{\boldsymbol{v} \in \boldsymbol{L}^2(T;\,\boldsymbol{H}(\mathbf{curl},\Omega)) : \partial_t \boldsymbol{v} \in \boldsymbol{L}^2(T;\,\boldsymbol{H}(\mathbf{curl},\Omega))\}, \tag{2.53b}$$

$$\boldsymbol{L}^2(\partial_t,T;\,\boldsymbol{H}(\operatorname{div},\Omega)) := \{\boldsymbol{v} \in \boldsymbol{L}^2(T;\,\boldsymbol{H}(\operatorname{div},\Omega)) : \partial_t \boldsymbol{v} \in \boldsymbol{L}^2(T;\,\boldsymbol{H}(\operatorname{div},\Omega))\}, \tag{2.53c}$$

where $T=[0,t_{\mathrm{max}}]$, $t_{\mathrm{max}}>0$ is again a specific time interval. Furthermore, the Bochner spaces associated to $H(\Delta,\Omega)$ and $\boldsymbol{H}(\mathbf{curl}\ \mathbf{curl},\Omega)$ can be defined in complete analogy. We denote them by $L^2(\partial_t,T;\,H(\Delta,\Omega))$, $\boldsymbol{L}^2(\partial_t,T;\,\boldsymbol{H}(\mathbf{curl}\ \mathbf{curl},\Omega))$, respectively. In addition, Bochner spaces that take values in quotient spaces are defined by

$$L^2(\partial_t,T;\,[H(\nabla,\Omega)]) := \{v \in L^2(T;\,[H(\nabla,\Omega)]) : \partial_t v \in L^2(T;\,[H(\nabla,\Omega)])\}, \tag{2.54a}$$

$$\boldsymbol{L}^2(\partial_t,T;\,[\boldsymbol{H}(\mathbf{curl},\Omega)]) := \{\boldsymbol{v} \in \boldsymbol{L}^2(T;\,[\boldsymbol{H}(\mathbf{curl},\Omega)]) : \partial_t \boldsymbol{v} \in \boldsymbol{L}^2(T;\,[\boldsymbol{H}(\mathbf{curl},\Omega)])\}, \tag{2.54b}$$

$$\boldsymbol{L}^2(\partial_t,T;\,[\boldsymbol{H}(\operatorname{div},\Omega)]) := \{\boldsymbol{v} \in \boldsymbol{L}^2(T;\,[\boldsymbol{H}(\operatorname{div},\Omega)]) : \partial_t \boldsymbol{v} \in \boldsymbol{L}^2(T;\,[\boldsymbol{H}(\operatorname{div},\Omega)])\}. \tag{2.54c}$$

Eventually, boundary conditions are incorporated in the spaces with a similar notation as in (2.30) and (2.31).

In the next section we focus on the formulation of the problem on the boundary, and introduce the setting that will lead to BIEs. For instance, suitable trace spaces have to be characterized. The latter arise by application of the trace operators from Definition 2.14 to energy spaces. For this, specifying the ranges of the trace operators such that we obtain continuous and surjective operators is necessary. Moreover, a de Rham complex that relates energy spaces to their traces summarizes the setting.

2.3 Trace spaces

In the Maxwell framework presented in Section 1.1, we saw for instance that boundary conditions are formulated in terms of tangential and normal components of the fields. Hence, a straightforward application of Gauß's divergence theorem, cf. (2.27), to an interface problem suggests that an appropriate trace space should satisfy weak normal continuity on the boundary. Similarly, the Stokes theorem, cf. [88, Corollary 3.21], points out the need of spaces that guarantee tangential continuity. Before introducing such spaces, we motivate briefly our requirement that Γ, which is the boundary of a domain Ω, should be Lipschitz. First of all, this choice is general enough to cover most technical geometries. Second, Lebesgue integrals make sense for Lipschitz boundaries, and we know from the Rademacher theorem [103, Theorem 2.7.1] that normal vectors (outward pointing) exist a.e. on Γ, and are bounded. Last, the theory of Sobolev spaces on the boundary is well-established, see, e.g., [87, 103, 109]. Even though finding trace spaces for $\boldsymbol{H}(\mathbf{curl}, \Omega)$ defined over Lipschitz domains was a missing piece in the theory, it no longer poses a restriction thanks to the results provided by Buffa, Costabel, and Sheen [20].

Following the procedure of the last section, we first define tangential differential operators. First, let $\varphi \in H^1(\Gamma)$. We denote by $\widetilde{\varphi} \in \mathcal{D}(\overline{\Omega})$ an extension of φ into the domain Ω such that

$$\varphi = \gamma_0 \widetilde{\varphi}.$$

Then, the surface gradient operator ∇_Γ, and the vectorial surface **curl**-operator can be defined as traces of the gradient ∇ as follows

$$\nabla_\Gamma \varphi = \boldsymbol{\gamma}_{\mathrm{D}}(\nabla \widetilde{\varphi}), \tag{2.55a}$$
$$\mathbf{curl}_\Gamma\, \varphi = \boldsymbol{\gamma}_{\times}(\nabla \widetilde{\varphi}). \tag{2.55b}$$

Their adjoint operators are called surface divergence and scalar surface curl-operator. They are denoted by div_Γ and curl_Γ, respectively. Formally, they are computed by duality

$$\langle \mathrm{div}_\Gamma\, \boldsymbol{\varphi}, \varphi \rangle_\Gamma = -\langle \boldsymbol{\varphi}, \nabla_\Gamma \varphi \rangle_\Gamma, \tag{2.56a}$$
$$\langle \mathrm{curl}_\Gamma\, \boldsymbol{\varphi}, \varphi \rangle_\Gamma = \langle \boldsymbol{\varphi}, \mathbf{curl}_\Gamma\, \varphi \rangle_\Gamma, \tag{2.56b}$$

where $\boldsymbol{\varphi} \in \boldsymbol{L}^2_{\mathrm{t}}(\Gamma)$. We refer to [20, Section 3] for a intrinsic construction of the above mentioned tangential differential operators for Lipschitz domains. Beside the Sobolev space $H^{\frac{1}{2}}(\Gamma)$ and its dual $H^{-\frac{1}{2}}(\Gamma)$, we require traces for $\boldsymbol{H}(\mathbf{curl}, \Omega)$. A characterization for Lipschitz domains is furnished in [20, Section 4]. In the following, we present some related results for convenience, and refer the reader to the cited paper, and e.g., [22], for more details.

Let $\boldsymbol{\gamma}_0 : \boldsymbol{H}^1(\Omega) \to \boldsymbol{H}^{\frac{1}{2}}(\Gamma)$ be the vector restriction trace [20, Section 2]. Similarly to the derivation of tangential differential operators, applying the traces $\boldsymbol{\gamma}_\times$ and $\boldsymbol{\gamma}_{\mathrm{D}}$ to $\boldsymbol{H}^1(\Omega)$ yields the Hilbert spaces $\boldsymbol{H}_\times^{\frac{1}{2}}(\Gamma) := \boldsymbol{\gamma}_\times(\boldsymbol{H}^1(\Omega))$ and $\boldsymbol{H}_{\mathrm{D}}^{\frac{1}{2}}(\Gamma) := \boldsymbol{\gamma}_{\mathrm{D}}(\boldsymbol{H}^1(\Omega))$. For convenience, let $\widetilde{\boldsymbol{\xi}} \in \boldsymbol{H}^1(\Omega)$ be defined such that $\boldsymbol{\gamma}_0\widetilde{\boldsymbol{\xi}} = \boldsymbol{\xi}$. Then, we equip $\boldsymbol{H}_\times^{\frac{1}{2}}(\Gamma)$ and $\boldsymbol{H}_{\mathrm{D}}^{\frac{1}{2}}(\Gamma)$ with the norms

$$\|\boldsymbol{\psi}\|_{\boldsymbol{H}_\times^{\frac{1}{2}}(\Gamma)} := \inf_{\boldsymbol{\xi}\in\boldsymbol{H}^{\frac{1}{2}}(\Gamma)} \{\|\boldsymbol{\xi}\|_{\boldsymbol{H}^{\frac{1}{2}}(\Gamma)} \text{ with } \boldsymbol{\gamma}_\times \widetilde{\boldsymbol{\xi}} = \boldsymbol{\psi}\},$$
$$\|\boldsymbol{\psi}\|_{\boldsymbol{H}_{\mathrm{D}}^{\frac{1}{2}}(\Gamma)} := \inf_{\boldsymbol{\xi}\in\boldsymbol{H}^{\frac{1}{2}}(\Gamma)} \{\|\boldsymbol{\xi}\|_{\boldsymbol{H}^{\frac{1}{2}}(\Gamma)} \text{ with } \boldsymbol{\gamma}_{\mathrm{D}} \widetilde{\boldsymbol{\xi}} = \boldsymbol{\psi}\},$$

which assure the continuity of the operators $\boldsymbol{\gamma}_\times$ and $\boldsymbol{\gamma}_{\mathrm{D}}$, see [20, Definition 2.2]. In other words, along an edge, a function in $\boldsymbol{H}_{\mathrm{D}}^{\frac{1}{2}}(\Gamma)$ exhibits a weak tangential continuity, whereas the normal component of a function in $\boldsymbol{H}_\times^{\frac{1}{2}}(\Gamma)$ is continuous in a weak sense. Moreover, we designate by $\boldsymbol{H}_\times^{-\frac{1}{2}}(\Gamma)$ and $\boldsymbol{H}_{\mathrm{D}}^{-\frac{1}{2}}(\Gamma)$ the dual spaces of $\boldsymbol{H}_\times^{\frac{1}{2}}(\Gamma)$ and $\boldsymbol{H}_{\mathrm{D}}^{\frac{1}{2}}(\Gamma)$, respectively.

Remark 2.28. *For a smooth Γ, the spaces $\boldsymbol{H}_\times^{\frac{1}{2}}(\Gamma)$ and $\boldsymbol{H}_{\mathrm{D}}^{\frac{1}{2}}(\Gamma)$ coincide, and they can be identified with the space of tangential vector fields of regularity $\frac{1}{2}$, namely,*

$$\boldsymbol{H}_{\mathrm{t}}^{\frac{1}{2}}(\Gamma) := \{\boldsymbol{\psi} \in \boldsymbol{H}^{\frac{1}{2}}(\Gamma) : \boldsymbol{\psi}\cdot\boldsymbol{n} = 0\}.$$

Similarly, $\boldsymbol{H}_\times^{-\frac{1}{2}}(\Gamma) = \boldsymbol{H}_{\mathrm{D}}^{-\frac{1}{2}}(\Gamma) = \boldsymbol{H}_{\mathrm{t}}^{-\frac{1}{2}}(\Gamma)$, where $\boldsymbol{H}_{\mathrm{t}}^{-\frac{1}{2}}(\Gamma)$ denotes the dual space of $\boldsymbol{H}_{\mathrm{t}}^{\frac{1}{2}}(\Gamma)$, see [20, Section 2].

Altogether, the trace spaces of $\boldsymbol{H}(\mathbf{curl},\Omega)$ for Lipschitz domains are specified as

$$\boldsymbol{H}^{-\frac{1}{2}}(\mathrm{div}_\Gamma,\Gamma) := \{\boldsymbol{\psi} \in \boldsymbol{H}_\times^{-\frac{1}{2}}(\Gamma) : \mathrm{div}_\Gamma\,\boldsymbol{\psi} \in H^{-\frac{1}{2}}(\Gamma)\},$$
$$\boldsymbol{H}^{-\frac{1}{2}}(\mathrm{curl}_\Gamma,\Gamma) := \{\boldsymbol{\psi} \in \boldsymbol{H}_{\mathrm{D}}^{-\frac{1}{2}}(\Gamma) : \mathrm{curl}_\Gamma\,\boldsymbol{\psi} \in H^{-\frac{1}{2}}(\Gamma)\}.$$

They are endowed with the graph norms

$$\boldsymbol{\psi} \in \boldsymbol{H}^{-\frac{1}{2}}(\mathrm{div}_\Gamma,\Gamma), \qquad \|\boldsymbol{\psi}\|_{\boldsymbol{H}^{-\frac{1}{2}}(\mathrm{div}_\Gamma,\Gamma)} := \sqrt{\|\boldsymbol{\psi}\|^2_{\boldsymbol{H}_\times^{-\frac{1}{2}}(\Gamma)} + \|\mathrm{div}_\Gamma\,\boldsymbol{\psi}\|^2_{H^{-\frac{1}{2}}(\Gamma)}}, \tag{2.57a}$$
$$\boldsymbol{\psi} \in \boldsymbol{H}^{-\frac{1}{2}}(\mathrm{curl}_\Gamma,\Gamma), \qquad \|\boldsymbol{\psi}\|_{\boldsymbol{H}^{-\frac{1}{2}}(\mathrm{curl}_\Gamma,\Gamma)} := \sqrt{\|\boldsymbol{\psi}\|^2_{\boldsymbol{H}_{\mathrm{D}}^{-\frac{1}{2}}(\Gamma)} + \|\mathrm{curl}_\Gamma\,\boldsymbol{\psi}\|^2_{H^{-\frac{1}{2}}(\Gamma)}}. \tag{2.57b}$$

The next result concerns the mapping properties of the trace operators that are employed to map the energy spaces to their traces, building up to a de Rham sequence on the boundary, which we depict in Figure 2.6, and will discuss subsequently.

Theorem 2.29 (Mapping properties of trace operators)**.** *The following trace operators can be extended to linear, continuous, and surjective operators:*

- *The standard trace is uniquely extended to $\gamma_0 : H(\nabla,\Omega) \to H^{\frac{1}{2}}(\Gamma)$, and there exists $C_0 > 0$ such that*

$$\|\gamma_0 v\|_{H^{\frac{1}{2}}(\Gamma)} \le C_0\|v\|_{H(\nabla,\Omega)} \qquad \forall v \in H(\nabla,\Omega). \tag{2.58}$$

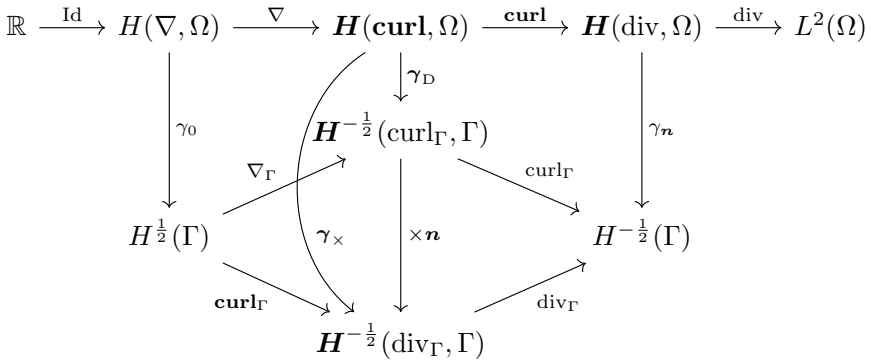

Figure 2.6: Commutative de Rham complex relating energy spaces to their traces.

- *The tangential trace is uniquely extended to* $\boldsymbol{\gamma}_\times : \boldsymbol{H}(\mathbf{curl},\Omega) \to \boldsymbol{H}^{-\frac{1}{2}}(\mathrm{div}_\Gamma,\Gamma)$*, and there exists* $C_\times > 0$ *such that*
$$\left\|\boldsymbol{\gamma}_\times \boldsymbol{v}\right\|_{\boldsymbol{H}^{-\frac{1}{2}}(\mathrm{div}_\Gamma,\Gamma)} \leq C_\times \|\boldsymbol{v}\|_{\boldsymbol{H}(\mathbf{curl},\Omega)} \qquad \forall \boldsymbol{v} \in \boldsymbol{H}(\mathbf{curl},\Omega). \tag{2.59}$$

- *The Dirichlet trace is uniquely extended to* $\boldsymbol{\gamma}_{\mathrm{D}} : \boldsymbol{H}(\mathbf{curl},\Omega) \to \boldsymbol{H}^{-\frac{1}{2}}(\mathrm{curl}_\Gamma,\Gamma)$*, and there exists* $C_{\mathrm{D}} > 0$ *such that*
$$\|\boldsymbol{\gamma}_{\mathrm{D}} \boldsymbol{v}\|_{\boldsymbol{H}^{-\frac{1}{2}}(\mathrm{curl}_\Gamma,\Gamma)} \leq C_{\mathrm{D}} \|\boldsymbol{v}\|_{\boldsymbol{H}(\mathbf{curl},\Omega)} \qquad \forall \boldsymbol{v} \in \boldsymbol{H}(\mathbf{curl},\Omega). \tag{2.60}$$

- *The normal trace is uniquely extended to* $\gamma_{\boldsymbol{n}} : \boldsymbol{H}(\mathrm{div},\Omega) \to H^{-\frac{1}{2}}(\Gamma)$*, and there exists* $C_{\boldsymbol{n}} > 0$ *such that*
$$\|\gamma_{\boldsymbol{n}} \boldsymbol{v}\|_{H^{-\frac{1}{2}}(\Gamma)} \leq C_{\boldsymbol{n}} \|\boldsymbol{v}\|_{\boldsymbol{H}(\mathrm{div},\Omega)} \qquad \forall \boldsymbol{v} \in \boldsymbol{H}(\mathrm{div},\Omega). \tag{2.61}$$

Moreover, γ_0*,* $\boldsymbol{\gamma}_\times$*,* $\boldsymbol{\gamma}_{\mathrm{D}}$*, and* $\gamma_{\boldsymbol{n}}$ *are surjective with continuous right inverses.*

Proof. The assertions are obtained by density arguments. For instance, the extension and properties of γ_0 and $\gamma_{\boldsymbol{n}}$ are provided in [87, Theorem 3.37] and [88, Theorem 3.24], respectively. For the results of $\boldsymbol{\gamma}_\times$ and $\boldsymbol{\gamma}_{\mathrm{D}}$, we further refer to [20, Theorem 4.1]. □

By recalling the expressions of $\boldsymbol{\gamma}_\times$ and $\boldsymbol{\gamma}_{\mathrm{D}}$ in Definition 2.14, we notice that they are connected geometrically by means of the rotation operator $\times\boldsymbol{n} : \boldsymbol{L}^2_{\mathrm{t}} \to \boldsymbol{L}^2_{\mathrm{t}}$ (or its adjoint $\boldsymbol{n}\times$). As stated in the next theorem, this yields a definition of a duality pairing for $\boldsymbol{H}^{-\frac{1}{2}}(\mathrm{div}_\Gamma,\Gamma)$ and $\boldsymbol{H}^{-\frac{1}{2}}(\mathrm{curl}_\Gamma,\Gamma)$ with $\boldsymbol{L}^2_{\mathrm{t}}(\Gamma)$ as a pivot space.

Theorem 2.30 (Extrinsic relation of $\boldsymbol{H}^{-\frac{1}{2}}(\mathrm{div}_\Gamma,\Gamma)$ and $\boldsymbol{H}^{-\frac{1}{2}}(\mathrm{curl}_\Gamma,\Gamma)$)**.** *The rotation operator* $\times\boldsymbol{n}$ *and its adjoint* $\boldsymbol{n}\times$ *can be extended to linear and continuous isomorphisms:*

- *The operator* $\times\boldsymbol{n}$ *is uniquely extended to* $\times\boldsymbol{n} : \boldsymbol{H}^{-\frac{1}{2}}(\mathrm{curl}_\Gamma,\Gamma) \to \boldsymbol{H}^{-\frac{1}{2}}(\mathrm{div}_\Gamma,\Gamma)$*, such that*
$$\boldsymbol{\psi} \in \boldsymbol{H}^{-\frac{1}{2}}(\mathrm{curl}_\Gamma,\Gamma),\ \exists!\boldsymbol{\xi} \in \boldsymbol{H}^{-\frac{1}{2}}(\mathrm{div}_\Gamma,\Gamma) : \quad \langle \boldsymbol{\psi}\times\boldsymbol{n}, \boldsymbol{\varphi}\rangle_\Gamma = \langle \boldsymbol{\xi}, \boldsymbol{\varphi}\rangle_\Gamma \quad \forall \boldsymbol{\varphi} \in \boldsymbol{H}^{-\frac{1}{2}}(\mathrm{curl}_\Gamma,\Gamma).$$

- *The operator $\boldsymbol{n}\times$ is uniquely extended to $\boldsymbol{n}\times : \boldsymbol{H}^{-\frac{1}{2}}(\mathrm{div}_\Gamma, \Gamma) \to \boldsymbol{H}^{-\frac{1}{2}}(\mathrm{curl}_\Gamma, \Gamma)$, such that*

$$\boldsymbol{\psi} \in \boldsymbol{H}^{-\frac{1}{2}}(\mathrm{div}_\Gamma, \Gamma),\ \exists! \boldsymbol{\xi} \in \boldsymbol{H}^{-\frac{1}{2}}(\mathrm{curl}_\Gamma, \Gamma) : \quad \langle \boldsymbol{\varphi}, \boldsymbol{n} \times \boldsymbol{\psi} \rangle_\Gamma = \langle \boldsymbol{\varphi}, \boldsymbol{\xi} \rangle_\Gamma \quad \forall \boldsymbol{\varphi} \in \boldsymbol{H}^{-\frac{1}{2}}(\mathrm{div}_\Gamma, \Gamma).$$

Proof. The essence of the result is demonstrated in [20, Section 2], and phrased in [116, Theorem 2.5.4], for instance. □

Corollary 2.31. *The conormal derivative γ_1 and the Neumann trace $\boldsymbol{\gamma}_\mathrm{N}$, with $\mathcal{U} = \mathrm{Id}$, can be extended accordingly such that*

$$\gamma_1 : H(\Delta, \Omega) \to H^{-\frac{1}{2}}(\Gamma), \tag{2.62}$$

$$\boldsymbol{\gamma}_\mathrm{N} : \boldsymbol{H}(\mathbf{curl}\ \mathbf{curl}, \Omega) \to \boldsymbol{H}^{-\frac{1}{2}}(\mathrm{div}_\Gamma, \Gamma) \tag{2.63}$$

are linear, continuous, and surjective. Therefore, there exists $C_1 > 0$, $C_\mathrm{N} > 0$ such that

$$\|\gamma_1 w\|_{H^{-\frac{1}{2}}(\Gamma)} \leq C_1 \|v\|_{H(\Delta,\Omega)} \qquad \forall w \in H(\Delta, \Omega),$$

$$\|\boldsymbol{\gamma}_\mathrm{N} \boldsymbol{w}\|_{\boldsymbol{H}^{-\frac{1}{2}}(\mathrm{div}_\Gamma,\Gamma)} \leq C_\mathrm{N} \|\boldsymbol{v}\|_{\boldsymbol{H}(\mathbf{curl}\ \mathbf{curl},\Omega)} \qquad \forall \boldsymbol{w} \in \boldsymbol{H}(\mathbf{curl}\ \mathbf{curl}, \Omega).$$

Proof. The extensions follow from Theorem 2.29, in particular from the properties of $\gamma_{\boldsymbol{n}}$ and $\boldsymbol{\gamma}_\times$, respectively. Namely, the assertions arise by choosing $\boldsymbol{v} = \nabla w$, with $w \in H(\Delta, \Omega)$, in (2.61), and by setting $\boldsymbol{v} = \mathbf{curl}\, \boldsymbol{w}$ in (2.59). □

With the aid of Figure 2.6, the tangential differential operators ∇_Γ, $\mathbf{curl}_\Gamma$ as well as their adjoint operators, i.e., div_Γ and curl_Γ, respectively, can be extended to linear and continuous operators such that the de Rham complex commutes. For instance, the following mapping properties are proposed in [20, Proposition 3.6]

$$\begin{aligned}
\nabla_\Gamma :\ & H^{\frac{1}{2}}(\Gamma) \longrightarrow \boldsymbol{H}_\times^{-\frac{1}{2}}(\Gamma), \\
\mathbf{curl}_\Gamma :\ & H^{\frac{1}{2}}(\Gamma) \longrightarrow \boldsymbol{H}_\mathrm{D}^{-\frac{1}{2}}(\Gamma), \\
\mathrm{div}_\Gamma :\ & \boldsymbol{H}_\times^{\frac{1}{2}}(\Gamma) \longrightarrow H^{-\frac{1}{2}}(\Gamma), \\
\mathrm{curl}_\Gamma :\ & \boldsymbol{H}_\mathrm{D}^{\frac{1}{2}}(\Gamma) \longrightarrow H^{-\frac{1}{2}}(\Gamma).
\end{aligned}$$

Similarly to Figure 2.2 and Figure 2.3 the structure of the de Rham sequence on the boundary depends as well on the topological properties of Ω and Γ. Hence, we write

$$\mathbb{R} \subseteq \ker(\nabla_\Gamma), \tag{2.64a}$$

$$\mathbb{R} \subseteq \ker(\mathbf{curl}_\Gamma), \tag{2.64b}$$

$$\mathrm{Im}(\nabla_\Gamma) \subseteq \ker(\mathrm{curl}_\Gamma) \cap \boldsymbol{H}_\times^{-\frac{1}{2}}(\Gamma), \tag{2.64c}$$

$$\mathrm{Im}(\mathbf{curl}_\Gamma) \subseteq \ker(\mathrm{div}_\Gamma) \cap \boldsymbol{H}_\mathrm{D}^{-\frac{1}{2}}(\Gamma), \tag{2.64d}$$

and define the null-spaces by

$$\ker(\mathrm{curl}_\Gamma) := \boldsymbol{H}^{-\frac{1}{2}}(\mathrm{curl}_\Gamma\, 0, \Gamma) = \{\boldsymbol{\psi} \in \boldsymbol{H}^{-\frac{1}{2}}(\mathrm{curl}_\Gamma, \Gamma) : \mathrm{curl}_\Gamma\, \boldsymbol{\psi} = 0\},$$

$$\ker(\operatorname{div}_\Gamma) := \boldsymbol{H}^{-\frac{1}{2}}(\operatorname{div}_\Gamma 0,\Gamma) = \{\boldsymbol{\psi} \in \boldsymbol{H}^{-\frac{1}{2}}(\operatorname{div}_\Gamma,\Gamma) : \operatorname{div}_\Gamma \boldsymbol{\psi} = 0\}.$$

The subspace $\boldsymbol{H}^{-\frac{1}{2}}(\operatorname{div}_\Gamma 0,\Gamma)$ will be of particular interest in the formulation of the 3D problem in the exterior domain. Similarly to the de Rham complex for energy spaces, the inclusions in (2.64) might be strict for general topologies. This is due to the fact that harmonic fields contribute also to the kernel. Such fields live in the following space, which is isomorphic to the first surface cohomology space, namely,

$$\mathbb{H}_1(\Gamma) = \{\boldsymbol{\psi} \in \boldsymbol{L}^2_{\mathrm{t}}(\Gamma) : \operatorname{curl}_\Gamma \boldsymbol{\psi} = 0,\ \operatorname{div}_\Gamma \boldsymbol{\psi} = 0\}.$$

Hence, the dimension of $\mathbb{H}_1(\Gamma)$ is determined by means of the first Betti number associated to the boundary Γ. Note that $\mathbb{H}_1(\Gamma)$ consists of the direct sum of tangential traces of the cohomology spaces associated to Ω and Ω^{e}, see [23, Remark 3.5] and [15, Corollary 1] for more details. Hence, the dimension of $\mathbb{H}_1(\Gamma)$ given by $\beta_1(\Gamma)$ can be determined as follows

$$\beta_1(\Gamma) = \beta_1(\Omega) + \beta_1(\Omega^{\mathrm{e}}).$$

With this, we can further characterize the null-space $\boldsymbol{H}^{-\frac{1}{2}}(\operatorname{div}_\Gamma 0,\Gamma)$ via a direct orthogonal decomposition into the space of surface stream functions and $\mathbb{H}_1(\Gamma)$, which contains surface cohomology vector fields.

Theorem 2.32 (Direct decomposition for $\boldsymbol{H}^{-\frac{1}{2}}(\operatorname{div}_\Gamma 0,\Gamma)$, [23, Equation 3.3])**.** *Let Γ be a Lipschitz boundary of some domain Ω. Then, the space $\boldsymbol{H}^{-\frac{1}{2}}(\operatorname{div}_\Gamma 0,\Gamma)$ admits an orthogonal decomposition*

$$\boldsymbol{H}^{-\frac{1}{2}}(\operatorname{div}_\Gamma 0,\Gamma) = \mathbf{curl}_\Gamma\, H^{\frac{1}{2}}(\Gamma) \oplus \mathbb{H}_1(\Gamma)$$

with $\dim \mathbb{H}_1(\Gamma) = \beta_1(\Gamma)$.

Remark 2.33. *For a simply-connected Γ, the non-strict inclusions $\subseteq$ in* (2.64) *turn into equalities. For a proof, we refer to [20, Corollary 3.7, Theorem 5.1, Corollary 5.3]. In particular, it clearly follows that*

$$\boldsymbol{H}^{-\frac{1}{2}}(\operatorname{div}_\Gamma 0,\Gamma) = \mathbf{curl}_\Gamma\, H^{\frac{1}{2}}(\Gamma),$$

since $\beta_1(\Gamma) = 0$.

With this, we present a fundamental result that delivers a characterization of $\boldsymbol{H}^{-\frac{1}{2}}(\operatorname{div}_\Gamma,\Gamma)$. Indeed, it can be perceived as the boundary counterpart of Helmholtz decompositions of Theorem 2.26 and Remark 2.27.

Theorem 2.34 (Hodge decomposition, [18, Theorem 5.5])**.** *Let Γ be a Lipschitz boundary of some domain Ω, and let*

$$H(\Delta_\Gamma,\Gamma) := \{\varphi \in H^1(\Gamma) :\ \Delta_\Gamma\varphi \in H^{-\frac{1}{2}}(\Gamma)\}$$

denote the boundary counterpart of $H(\Delta,\Omega)$, where $\Delta_\Gamma = \operatorname{div}_\Gamma \nabla_\Gamma = -\operatorname{curl}_\Gamma \mathbf{curl}_\Gamma$ is known as the Laplace-Beltrami operator. Then, the following direct decomposition holds

$$\boldsymbol{H}^{-\frac{1}{2}}(\operatorname{div}_\Gamma,\Gamma) = \nabla_\Gamma H(\Delta_\Gamma,\Gamma) \oplus \boldsymbol{H}^{-\frac{1}{2}}(\operatorname{div}_\Gamma 0,\Gamma),$$

where $\boldsymbol{H}^{-\frac{1}{2}}(\operatorname{div}_\Gamma 0,\Gamma)$ admits the decomposition of Theorem 2.32.

Note that the same type of decomposition holds also for $\boldsymbol{H}^{-\frac{1}{2}}(\mathrm{curl}_\Gamma, \Gamma)$, see e.g., [15, Theorem 3], where the decomposition of $\boldsymbol{H}^{-\frac{1}{2}}(\mathrm{curl}_\Gamma, \Gamma)$ is valid for Lipschitz polyhedra. An extension to Lipschitz domains can be conducted as in [20, Theorem 5.5].
The following theorem is a continuation of Corollary 2.17. In particular, it showcases besides the de facto duality of $H^{\frac{1}{2}}(\Gamma)$ and $H^{-\frac{1}{2}}(\Gamma)$, the correspondence

$$\boldsymbol{H}^{-\frac{1}{2}}(\mathrm{div}_\Gamma, \Gamma)' = \boldsymbol{H}^{-\frac{1}{2}}(\mathrm{curl}_\Gamma, \Gamma), \qquad \boldsymbol{H}^{-\frac{1}{2}}(\mathrm{curl}_\Gamma, \Gamma)' = \boldsymbol{H}^{-\frac{1}{2}}(\mathrm{div}_\Gamma, \Gamma).$$

Moreover, the integration by parts introduced therein, which we also call first Green's identities, plays a central role in the derivation of our variational formulations in interior domains.

Theorem 2.35 (First Green's identities)**.** *Let Ω, Γ, and $\mathcal{U}$ be defined as in Corollary 2.17. The following integration by parts formulae can be stated.*

- *For $w \in H(\Delta, \Omega)$, it holds*

$$(\mathrm{div}\,\mathcal{U}\nabla w, v)_\Omega + (\mathcal{U}\nabla w, \nabla v)_\Omega = \left\langle \gamma_1^{\mathcal{U}}\, w, \gamma_0 v \right\rangle_\Gamma \quad \forall v \in H(\nabla, \Omega). \tag{2.65}$$

- *For $\boldsymbol{w} \in \boldsymbol{H}(\mathbf{curl}\ \mathbf{curl}, \Omega)$, it holds*

$$(\mathcal{U}\,\mathbf{curl}\,\boldsymbol{w}, \mathbf{curl}\,\boldsymbol{v})_\Omega - (\mathbf{curl}\,\mathcal{U}\,\mathbf{curl}\,\boldsymbol{w}, \boldsymbol{v})_\Omega = \left\langle \boldsymbol{\gamma}_{\mathrm{N}}^{\mathcal{U}}\, \boldsymbol{w}, \boldsymbol{\gamma}_{\mathrm{D}}\, \boldsymbol{v} \right\rangle_\Gamma \quad \forall \boldsymbol{v} \in \boldsymbol{H}(\mathbf{curl}, \Omega). \tag{2.66}$$

Proof. The extension of (2.26a) to

$$(\boldsymbol{w}, \mathbf{curl}\,\boldsymbol{v})_\Omega - (\mathbf{curl}\,\boldsymbol{w}, \boldsymbol{v})_\Omega = \left\langle \boldsymbol{\gamma}_\times\, \boldsymbol{w}, \boldsymbol{\gamma}_{\mathrm{D}}\, \boldsymbol{v} \right\rangle_\Gamma \tag{2.67}$$

for all $\boldsymbol{w}$, $\boldsymbol{v} \in \boldsymbol{H}(\mathbf{curl}, \Omega)$ is demonstrated in [17]. With this, the proof follows from Corollary 2.17. The same holds true for (2.65) by using [109, Equation 4.3]. □

As in the previous section, we introduce according to Definition 2.3 some relevant quotient spaces on the boundary by

$$[H^{\frac{1}{2}}(\Gamma)] := H^{\frac{1}{2}}(\Gamma)/\mathbb{R}, \tag{2.68a}$$

$$[\boldsymbol{H}^{-\frac{1}{2}}(\mathrm{curl}_\Gamma, \Gamma)] := \boldsymbol{H}^{-\frac{1}{2}}(\mathrm{curl}_\Gamma, \Gamma)/\boldsymbol{H}^{-\frac{1}{2}}(\mathrm{curl}_\Gamma\, 0, \Gamma) \cap \boldsymbol{H}_\times^{-\frac{1}{2}}(\Gamma). \tag{2.68b}$$

In addition, as an analogon[4] to $\boldsymbol{H}^{-\frac{1}{2}}(\mathrm{div}_\Gamma\, 0, \Gamma)$ for the scalar setting, we define the following subspace of $H^{-\frac{1}{2}}(\Gamma)$

$$H_\star^{-\frac{1}{2}}(\Gamma) = \{\psi \in H^{-\frac{1}{2}}(\Gamma) : \langle \psi, 1 \rangle_\Gamma = 0\}. \tag{2.69}$$

In this setting, we can prove in complete analogy to [20, Corollary 5.4] that the restrictions

$$\nabla_\Gamma : [H^{\frac{1}{2}}(\Gamma)] \longrightarrow \boldsymbol{H}_\times^{-\frac{1}{2}}(\Gamma),$$
$$\mathbf{curl}_\Gamma : [H^{\frac{1}{2}}(\Gamma)] \longrightarrow \boldsymbol{H}_{\mathrm{D}}^{-\frac{1}{2}}(\Gamma)$$

[4] The condition $\mathrm{div}_\Gamma\, \boldsymbol{\psi} = 0$, which holds for all $\boldsymbol{\psi} \in \boldsymbol{H}^{-\frac{1}{2}}(\mathrm{div}_\Gamma\, 0, \Gamma)$, leads also to $\langle \boldsymbol{\psi}, \nabla_\Gamma \psi \rangle_\Gamma = 0$ for all $\psi \in H^{\frac{1}{2}}(\Gamma)$. Hence, $\boldsymbol{H}^{-\frac{1}{2}}(\mathrm{div}_\Gamma\, 0, \Gamma)$ contains vector fields that are orthogonal to the gradient fields. In complete analogy, the scalar counterpart should satisfy orthogonality with respect to the constants.

yield continuous and normally solvable ∇_Γ and $\mathbf{curl}_\Gamma$. Consequently, their adjoint operators div_Γ and curl_Γ are continuous and surjective with respect to the mappings

$$\mathrm{div}_\Gamma : \boldsymbol{H}_{\times}^{\frac{1}{2}}(\Gamma) \longrightarrow H_\star^{-\frac{1}{2}}(\Gamma),$$
$$\mathrm{curl}_\Gamma : \boldsymbol{H}_{\mathrm{D}}^{\frac{1}{2}}(\Gamma) \longrightarrow H_\star^{-\frac{1}{2}}(\Gamma),$$

see [19].

Starting from the eddy-current approximation (1.2), and by using the mathematical framework of this section, we introduce in the next chapter the considered model problems, and the tools needed for a coupling of the Finite Element Method (FEM) with Boundary Element Methods (BEMs).

3 Modelling and discrete setting

> Physics is mathematical not because we know so much about the physical world, but because we know so little; it is only its mathematical properties that we can discover.
>
> B. Russell

This chapter is devoted to pave the way to the concrete model problems that will be addressed in the next chapter, and which are aimed to be solved by using non-symmetric couplings of the Finite Element Method (FEM) and the direct Boundary Element Method (BEM) in an isogeometric context. First, we derive the necessary equations for a vector potential formulation in bounded domains starting from the eddy-current approximation discussed in Section 1.1. In addition, the linear and static cases for both bounded and unbounded domains are addressed. We recall that non-linear Partial Differential Equations (PDEs) are exclusively intended to be handled with FEM, whereas BEM is considered for model problems that are formulated in a static regime and in domains that are filled with linear materials (either bounded or unbounded). In order to use BEM, additional tools such as Boundary Layer Potentials (BLPs) and Boundary Integral Operators (BIOs) are required. Their definitions and properties are furnished in Subsection 3.2.1 along with the involved Boundary Integral Equations (BIEs) and Steklov-Poincaré operators both for the scalar and vectorial case. In particular, we present contractivity estimates for the double-layer operators by means of the corresponding interior Steklov-Poincaré operator. In the last section of this chapter, we introduce the tools of the isogeometric framework, i.e., we define the B-Spline and Non-Uniform Rational B-Splines (NURBS) basis functions that are employed in the design step [65, 94] in most Computer Aided Design (CAD) software. Additionally, they are used as the building blocks for the discretization of the de Rham sequence and its traces. Thereby, we refer mostly to [21, 33, 119]. If not stated otherwise, the operators and equations in this chapter are understood in a weak sense.

3.1 Vector potential formulations

Throughout this section, the domain Ω is assumed to be bounded, Lipschitz and connected. Hence, it may have holes, and its boundary Γ consists in general of N_Γ connected components, i.e., we assume $\Gamma = \bigcup_{k=0}^{N_\Gamma - 1} \Gamma_k$.

Let us first recall the governing equations of the eddy-current approximation as introduced in Section 1.1: For $\boldsymbol{x} \in \Omega$ and $t \in T := [0, t_{\text{max}}]$, $t_{\text{max}} > 0$, we have

$$\mathbf{curl}\, \boldsymbol{e}(\boldsymbol{x}, t) = -\frac{\partial}{\partial t} \boldsymbol{b}(\boldsymbol{x}, t), \tag{3.1a}$$

$$\mathbf{curl}\, \boldsymbol{h}(\boldsymbol{x},t) = \boldsymbol{j}(\boldsymbol{x},t), \tag{3.1b}$$
$$\operatorname{div} \boldsymbol{b}(\boldsymbol{x},t) = 0, \tag{3.1c}$$
$$\boldsymbol{h}(\boldsymbol{x},t) = \nu(|\boldsymbol{b}(\boldsymbol{x},t)|)\boldsymbol{b}(\boldsymbol{x},t), \tag{3.1d}$$
$$\boldsymbol{j}(\boldsymbol{x},t) = \kappa \boldsymbol{e}(\boldsymbol{x},t) + \boldsymbol{j}_{\mathrm{s}}(\boldsymbol{x},t). \tag{3.1e}$$

Thereby, $\kappa > 0$ is a constant in the whole domain Ω. Note that the constitutive law (3.1d) is defined for soft magnetic materials but can merely be replaced by (1.3) and (1.4) for linear and hard magnetic materials, respectively.
In the presence of an interface Γ_{k} between two domains Ω_1 and Ω_2, i.e., $\Gamma_{\mathrm{k}} = \overline{\Omega}_1 \cap \overline{\Omega}_2$, the following jump conditions have to be satisfied by the vector fields on Γ_{k},

$$(\boldsymbol{b}_1(\boldsymbol{x},t) - \boldsymbol{b}_2(\boldsymbol{x},t)) \cdot \boldsymbol{n}(\boldsymbol{x}) = 0, \tag{3.2a}$$
$$(\boldsymbol{j}_1(\boldsymbol{x},t) - \boldsymbol{j}_2(\boldsymbol{x},t)) \cdot \boldsymbol{n}(\boldsymbol{x}) = 0, \tag{3.2b}$$
$$(\boldsymbol{h}_1(\boldsymbol{x},t) - \boldsymbol{h}_2(\boldsymbol{x},t)) \times \boldsymbol{n}(\boldsymbol{x}) = \boldsymbol{k}(\boldsymbol{x},t), \tag{3.2c}$$
$$(\boldsymbol{e}_1(\boldsymbol{x},t) - \boldsymbol{e}_2(\boldsymbol{x},t)) \times \boldsymbol{n}(\boldsymbol{x}) = \boldsymbol{0}, \tag{3.2d}$$

where the subscripts $\cdot_1$ and $\cdot_2$ indicate a corresponding field defined on Ω_1 and Ω_2, respectively, and $\boldsymbol{n}$ is a normal vector on Γ_k directed from Ω_1 to Ω_2. Obviously, if there are no surface currents on Γ_k, $\boldsymbol{k}(\boldsymbol{x},t)$ in (3.2c) should be set to zero.

To solve the eddy-current model (3.1), the equations have to be supplemented by suitable Boundary Conditions (BCs), which may naturally arise for some concrete physical problem from (3.2). For instance, by assuming that Ω_1 is a Perfect Electric Conductor (PEC), it is usual to set $\boldsymbol{e}_2(\boldsymbol{x},t)\times\boldsymbol{n}(\boldsymbol{x}) = \boldsymbol{0}$ and $\boldsymbol{b}_2(\boldsymbol{x},t)\cdot\boldsymbol{n}(\boldsymbol{x}) = 0$ on the interface. Hence, (3.2a) reduces to $\boldsymbol{b}(\boldsymbol{x},t)\cdot\boldsymbol{n}(\boldsymbol{x}) = 0$ and $\boldsymbol{e}(\boldsymbol{x},t)\times\boldsymbol{n}(\boldsymbol{x}) = \boldsymbol{0}$ with $\boldsymbol{b}(\boldsymbol{x},t) := \boldsymbol{b}_1(\boldsymbol{x},t)$ and $\boldsymbol{e}(\boldsymbol{x},t) := \boldsymbol{e}_1(\boldsymbol{x},t)$. Typically, the derivation of the corresponding vector potential formulation involves the assumption that the periods of $\boldsymbol{b}$ and of $\boldsymbol{e}+\partial_t\boldsymbol{a}$ vanish, which is (topologically) stronger than local Maxwell's equations. These assumptions have a physical background, namely, they mean that the flux through any closed surface vanishes (absence of magnetic monopoles) and that except for magnetic induction, no loop voltage exists that could drive a current through a closed conducting loop (energy conservation).

In the following, we rather propose a mathematical approach using the framework of Section 2.2 to derive vector potential formulations from the above equations. Concretely, we consider two cases, which are known in the physical literature as electric wall (or PEC) and magnetic wall (or Perfect Magnetic Conductor (PMC)) cases. Both derivations are completely analogous but yield as expected different vector potentials. Hence, we present here only the latter, and refer to Appendix B for the former.

In the sequel, to simplify the notation, we omit to specify the function's arguments whenever they are clear from the context, i.e., a function or vector field in a Bochner space depends on $\boldsymbol{x}$ and t, whereas an element of a Hilbert space depends only on $\boldsymbol{x}$.

For every $t \in T$, (3.1c) and (3.2a) suggest that $\boldsymbol{b} \in \boldsymbol{H}(\operatorname{div} 0, \Omega)$. As illustrated in Figure 2.4, the decomposition

$$\boldsymbol{b} = \boldsymbol{b}_\Gamma + \boldsymbol{\eta}_2$$

with $\boldsymbol{b}_\Gamma \in \boldsymbol{H}^\Gamma(\operatorname{div} 0, \Omega)$ and $\boldsymbol{\eta}_2 \in \mathbb{H}_2(\Omega)$ is readily obtained. By using Corollary 2.25, there exists a unique

vector potential $\boldsymbol{a} \in \boldsymbol{H}(\mathbf{curl}, \Omega) \cap \boldsymbol{H}_0^{\mathsf{C}}(\operatorname{div} 0, \Omega)$, such that

$$\boldsymbol{b} = \mathbf{curl}\, \boldsymbol{a} + \boldsymbol{\eta}_2. \tag{3.3}$$

In addition, the vector fields involved in (3.1) are time dependent. In particular, we have a first order time derivative in (3.1a). Then it is natural to set $\boldsymbol{a} \in \boldsymbol{L}^2(\partial_t, T;\, \boldsymbol{H}(\mathbf{curl}, \Omega) \cap \boldsymbol{H}_0^{\mathsf{C}}(\operatorname{div} 0, \Omega))$, which is for convenience defined in (2.54b).
Now, from Faraday's law (3.1a), and the jump condition (3.2d), we infer that the electric field $\boldsymbol{e}$ is an element of $\boldsymbol{L}^2(T;\, \boldsymbol{H}(\mathbf{curl}, \Omega))$. Inserting (3.3) in (3.1a) yields

$$\mathbf{curl}(\boldsymbol{e} + \partial_t \boldsymbol{a}) = -\partial_t \boldsymbol{\eta}_2 = \mathbf{0}. \tag{3.4}$$

This can be explained as follows: for every $t \in T$, we know that $\mathbf{curl}(\boldsymbol{e} + \partial_t \boldsymbol{a}) \in \boldsymbol{H}^{\Gamma}(\operatorname{div} 0, \Omega)$. Moreover, $\boldsymbol{H}^{\Gamma}(\operatorname{div} 0, \Omega)$ is orthogonal to $\mathbb{H}_2(\Omega)$, i.e., $\boldsymbol{H}^{\Gamma}(\operatorname{div} 0, \Omega) \cap \mathbb{H}_2(\Omega) = \{\mathbf{0}\}$. Therefore, $\partial_t \boldsymbol{\eta}_2 = \mathbf{0}$.
As a consequence of (3.4), for all $t \in T$, it follows that $(\boldsymbol{e} + \partial_t \boldsymbol{a}) \in \boldsymbol{H}(\mathbf{curl}\, \mathbf{0}, \Omega)$. Then, by the decomposition (2.42a) together with (2.43a), there exists a unique scalar potential $\varphi \in L^2(T;\, H(\nabla, \Omega))$ (up to a constant) and $\boldsymbol{\eta}_1 \in \boldsymbol{L}^2(T;\, \mathbb{H}_1(\Omega))$, such that

$$\boldsymbol{e} + \partial_t \boldsymbol{a} = -\nabla \varphi + \boldsymbol{\eta}_1. \tag{3.5}$$

Note that the minus sign on the right-hand side is motivated by the physical interpretation of $-\nabla\varphi$, namely, an electric field. In this case, it is a convention to introduce the gradient of the scalar potential with a negative sign. By inserting $\boldsymbol{e}$ from (3.5) into (3.1e), we arrive at

$$\boldsymbol{j} = \boldsymbol{j}_{\mathrm{s}} + \kappa(-\partial_t \boldsymbol{a} + \boldsymbol{\eta}_1 - \nabla \varphi), \tag{3.6}$$

which gives us a representation of the right-hand side of Ampère's law (3.1b). Moreover, with $\operatorname{div} \boldsymbol{\eta}_1 = 0$ we obtain a continuity condition

$$\operatorname{div}(\boldsymbol{j}_{\mathrm{s}} - \kappa \nabla \varphi) = \operatorname{div}(\kappa \partial_t \boldsymbol{a}) = 0.$$

In this magnetic wall case, in addition to Ampère's law, we prescribe zero tangential magnetic field, thus, we have that $\boldsymbol{h} \in \boldsymbol{L}^2(T;\, \boldsymbol{H}_{\mathbf{0}}(\mathbf{curl}, \Omega))$. With this, we see from Ampère's law (3.1b) that $\boldsymbol{j} \in \boldsymbol{H}_0^{\mathsf{C}}(\operatorname{div} 0, \Omega)$, see Figure 2.4. Note that $\boldsymbol{j}$ is in the same constrained divergence space as the one of $\boldsymbol{a}$, which yields consistency. Using the constitutive law (3.1d), which relates the magnetic field strength $\boldsymbol{h}$ to the magnetic flux density $\boldsymbol{b}$ leads with $\mathbf{curl}\, \boldsymbol{\eta}_2 = \mathbf{0}$ to

$$\mathbf{curl}\, \nu(|\mathbf{curl}\, \boldsymbol{a} + \boldsymbol{\eta}_2|)\, \mathbf{curl}\, \boldsymbol{a} + \kappa \partial_t \boldsymbol{a} - \kappa \boldsymbol{\eta}_1 = -\kappa \nabla \varphi + \boldsymbol{j}_{\mathrm{s}}. \tag{3.7}$$

Thereby, we have the vector potential $\boldsymbol{a} \in \boldsymbol{L}^2(\partial_t, T;\, [\boldsymbol{H}(\mathbf{curl}, \Omega)])$, a scalar potential $\varphi \in L^2(T;\, H(\nabla, \Omega))$, and cohomology vector fields $\boldsymbol{\eta}_1 \in \boldsymbol{L}^2(T;\, \mathbb{H}_1(\Omega))$ and $\boldsymbol{\eta}_2 \in \boldsymbol{L}^2(T;\, \mathbb{H}_2(\Omega))$. Moreover, we used (2.52a), i.e., the identification $\boldsymbol{H}(\mathbf{curl}, \Omega) \cap \boldsymbol{H}_0^{\mathsf{C}}(\operatorname{div} 0, \Omega) \cong [\boldsymbol{H}(\mathbf{curl}, \Omega)]$.
By assuming that $\nabla\varphi$ is known, e.g., computed a priori with suitable boundary conditions, then it can be considered as an additional source term. Thus, we may define $\boldsymbol{j}_{\mathrm{in}} = -\kappa \nabla \varphi + \boldsymbol{j}_{\mathrm{s}} \in \boldsymbol{L}^2(T;\, \boldsymbol{H}_0^{\mathsf{C}}(\operatorname{div} 0, \Omega))$.

Remark 3.1. *The topological terms η_1 and η_2 are linked in the setting of* (3.7) *to the electric field $\boldsymbol{e}$ and to the magnetic flux density $\boldsymbol{b}$, respectively. To eliminate the topological effects of the domain on the vector potential formulation, suitable additional boundary conditions can be prescribed. Indeed, it can be shown by following and adapting the steps from the derivation of* (3.7) *that this can be achieved by restricting $(\boldsymbol{b}, \boldsymbol{e})$ to $\boldsymbol{L}^2(T;\, \boldsymbol{H}^{\Gamma}(\operatorname{div} 0, \Omega)) \times \boldsymbol{L}^2(\partial_t, T;\, [\boldsymbol{H}(\mathbf{curl}, \Omega)])$. Physically, these spaces correspond to the assumptions that there is no flux through closed surfaces and that no loop voltage exists that could drive a current through a closed conducting loop.*

Keeping the aimed numerical methods in mind, namely, couplings of FEM and BEMs, we may need mixed boundary conditions. For simplicity of notation, we prescribe the same boundary condition to all connected parts of $\Gamma_{\text{FEM}} = \bigcup_{k=1}^{N_{\text{FEM}}} \Gamma_{\text{FEM},k}$ with N_{FEM} denoting the number of all interior boundaries, and similarly to $\Gamma_{\text{BEM}} = \bigcup_{k=1}^{N_{\text{BEM}}} \Gamma_{\text{BEM},k}$, where $N_{\text{BEM}} = N_\Gamma - N_{\text{FEM}}$ are the interfaces that separate a FEM and a BEM domain. Note that N_Γ is again the total number of boundary components, as introduced in the beginning of the section. For instance, with respect to Figure 2.1a, we may set $\Gamma_{\text{FEM}} = \Gamma_1 \cup \Gamma_2$ and $\Gamma_{\text{BEM}} = \Gamma_0$. For convenience, we refer the reader to (2.31) for the definition of energy spaces that are endowed with BCs assigned only on a boundary part.
An extension of the presented theory to mixed and non-homogeneous boundary conditions is furnished in the magnetostatic regime in [50, Section 3.1]. An adaptation to the eddy-current model is straightforward. Then, we can arrive at a vector potential formulation of the eddy-current problem (electric wall case) in a bounded domain Ω that reads:

Find $\boldsymbol{a} \in \boldsymbol{L}^2(\partial_t, T;\, \boldsymbol{H}_{\boldsymbol{0}}(\mathbf{curl}, \Omega, \Gamma_{\text{FEM}}) \cap \boldsymbol{H}^{\Gamma}(\operatorname{div} 0, \Omega)) \cong \boldsymbol{L}^2(\partial_t, T;\, [\boldsymbol{H}_{\boldsymbol{0}}(\mathbf{curl}, \Omega, \Gamma_{\text{FEM}})])$ such that

$$\mathbf{curl}\, \nu(|\mathbf{curl}\, \boldsymbol{a}|)\, \mathbf{curl}\, \boldsymbol{a} + \kappa \partial_t \boldsymbol{a} = \boldsymbol{j}_{\text{in}} \qquad \text{in } \Omega \times T\backslash\{0\}, \tag{3.8a}$$

$$\boldsymbol{\gamma}_{\text{N}}^{\mathcal{U}}\, \boldsymbol{a} = \boldsymbol{\phi}_0 \qquad \text{on } \Gamma_{\text{BEM}} \times T\backslash\{0\}, \tag{3.8b}$$

$$\boldsymbol{\gamma}_{\times}\, \boldsymbol{a} = \boldsymbol{u}_0 \qquad \text{on } \Gamma_{\text{BEM}} \times T\backslash\{0\}, \tag{3.8c}$$

$$\boldsymbol{a} = \boldsymbol{0} \qquad \text{in } \Omega \times \{0\} \tag{3.8d}$$

with $\boldsymbol{j}_{\text{in}} \in \boldsymbol{L}^2(T;\, \boldsymbol{H}^{\Gamma}(\operatorname{div} 0, \Omega))$, $\boldsymbol{\phi}_0 \in \boldsymbol{L}^2(T;\, \boldsymbol{H}^{-\frac{1}{2}}(\operatorname{div}_\Gamma, \Gamma))$, and $\boldsymbol{u}_0 \in \boldsymbol{L}^2(T;\, \boldsymbol{H}^{-\frac{1}{2}}(\operatorname{div}_\Gamma, \Gamma))$.

Thereby, $\mathcal{U}$ should be adapted depending on the magnetic properties of the material, i.e., $\mathcal{U}\boldsymbol{u} := \nu(|\boldsymbol{u}|)\boldsymbol{u}$ for soft magnetic materials, and $\mathcal{U}\boldsymbol{u} := \nu\boldsymbol{u}$ if the dependence is linear, see Section 1.1. Moreover, note that Equations (3.8b) and (3.8c) stem from the jump conditions (3.2c) and (3.2a), respectively, when the value of the field coming from the other side of the boundary is supposed to be known. More details on $\boldsymbol{\phi}_0$ and $\boldsymbol{u}_0$ will be given in Section 3.2. Furthermore, the initial condition (3.8d) is necessary to determine the solution at the initial step, here supposed to be $t = 0$, see Remark 2.8. For convenience, we restrict ourselves to the special case of zero initial field.
Note that for the magnetic wall case, a similar initial Boundary Value Problem (BVP) follows with $\boldsymbol{a} \in \boldsymbol{L}^2(\partial_t, T;\, [\boldsymbol{H}(\mathbf{curl}, \Omega, \Gamma_{\text{FEM}})])$ and $\boldsymbol{j}_{\text{in}} \in \boldsymbol{L}^2(T;\, \boldsymbol{H}_0^{\text{C}}(\operatorname{div} 0, \Omega))$.

Remark 3.2. *For a FEM only approach, assuming $\boldsymbol{\gamma}_{\times}\, \boldsymbol{a} \neq \boldsymbol{0}$ on the boundary of the virtual computational domain would be in practice difficult to build from $\gamma_{\boldsymbol{n}}\boldsymbol{b} \neq 0$, cf. [50, Section 3.1]. Therefore, the restriction $\boldsymbol{\gamma}_{\times}\, \boldsymbol{a} = \boldsymbol{0}$ is a convenient modelling choice, which also agrees with the physical laws, in particular with the divergence-free property of the magnetic flux density. In our case, the FEM and BEM domains are coupled via the boundary data, and particularly, via their jump relation across the interface. Hence, it is more suitable to assume non-homogeneous boundary conditions, as will be made clear in the next subsection.*
The condition $\boldsymbol{\gamma}_{\text{N}}^{\nu}\boldsymbol{a} \neq \boldsymbol{0}$ makes sense from a physical perspective, even in the FEM only approach. It would suggest the existence of surface currents on the considered boundary, because it is directly related to (3.2c).

In addition to vector potential formulations for eddy-currents in three dimensions, some other particular cases are also relevant to our study. Independently of the additional BCs prescribed for $\boldsymbol{b}$ and $\boldsymbol{e}$, see Remarks 3.1

and B.1, if Ω is filled with an insulator, i.e., a non-conducting material with $\kappa = 0$, the topological term that is related to κ in (3.6) and (B.3), i.e., either $\boldsymbol{\eta}_1$ or $\boldsymbol{\eta}_2$ (depending on the magnetic or electric BCs) vanishes, as well as the scalar potential gradient and the non-stationary term of $\boldsymbol{a}$. This gives rise with the restriction on either $\boldsymbol{b}$ or $\boldsymbol{e}$ as in Remarks 3.1 and B.1 to the equations of magnetostatics:

Find $\boldsymbol{a} \in [\boldsymbol{H}_{\mathbf{0}}(\mathbf{curl}, \Omega, \Gamma_{\text{FEM}})]$ (or $\boldsymbol{a} \in [\boldsymbol{H}(\mathbf{curl}, \Omega, \Gamma_{\text{FEM}})]$) such that

$$\mathbf{curl}\, \nu(|\mathbf{curl}\, \boldsymbol{a}|)\, \mathbf{curl}\, \boldsymbol{a} = \boldsymbol{j}_{\text{s}} \quad \text{in } \Omega, \tag{3.9a}$$
$$\boldsymbol{\gamma}_{\text{N}}^{\nu} \boldsymbol{a} = \boldsymbol{\phi}_0 \quad \text{on } \Gamma_{\text{BEM}}, \tag{3.9b}$$
$$\boldsymbol{\gamma}_{\times}\, \boldsymbol{a} = \boldsymbol{u}_0 \quad \text{on } \Gamma_{\text{BEM}} \tag{3.9c}$$

with $\boldsymbol{j}_{\text{s}} \in \boldsymbol{H}^{\Gamma}(\operatorname{div} 0, \Omega)$ (or $\boldsymbol{j}_{\text{s}} \in \boldsymbol{H}_0^{\text{C}}(\operatorname{div} 0, \Omega)$), $\boldsymbol{\phi}_0 \in \boldsymbol{H}^{-\frac{1}{2}}(\operatorname{div}_\Gamma, \Gamma)$, and $\boldsymbol{u}_0 \in [\boldsymbol{H}^{-\frac{1}{2}}(\operatorname{curl}_\Gamma, \Gamma)]$.

As motivated by Figure 1.4, we are also interested in the two-dimensional (2D) case. Let $\Omega \subset \mathbb{R}^3$ be represented in a local Cartesian coordinate system (x_1, x_2, x_3). There, the vector potential reads $\boldsymbol{a} = (a_1, a_2, a_3)$. Considering a symmetry along the x_3-axis reduces the problem to find a_3 in the x_1-x_2 hyperplane. Then, it can be shown that a de Rham complex with similar structure as Figure 2.6 (the boundary part) arises, i.e., we can define two **curl**-operators. The first one takes a scalar as input and can be defined as a rotated gradient in the x_1-x_2 hyperplane, i.e., $\widetilde{\mathbf{curl}} = \widetilde{\mathrm{Id}}(\nabla \times \boldsymbol{n})$, with $\widetilde{\mathrm{Id}} : \mathbb{R}^3 \to \mathbb{R}^2$ is the augmented identity matrix $\widetilde{\mathrm{Id}} = (\mathrm{Id}|\mathbf{0})$, and $\boldsymbol{n} = (0, 0, 1)^\top$. Formally, we write $\widetilde{\mathbf{curl}}\, a = (\partial_{x_2} a, -\partial_{x_1} a)$. The second one takes a planar vector from the x_1-x_2 hyperplane as input. It can be computed for $\boldsymbol{u} = (u_1, u_2)$ by $\operatorname{curl} \boldsymbol{u} := (\mathbf{curl}\, \widetilde{\boldsymbol{u}}) \cdot \boldsymbol{n} = \partial_{x_1} u_2 - \partial_{x_2} u_1$, where $\widetilde{\boldsymbol{u}} = (u_1, u_2, \alpha)$ and α is an arbitrary differentiable scalar function, see [113, Section 1.4], for instance. It can be shown, e.g., by a direct computation of $\operatorname{curl} \widetilde{\mathbf{curl}}$ that the **curl curl**-operator in three dimensions turns into a Laplace operator (with negative sign) in the 2D case. Similarly, $\operatorname{curl} \mathcal{U} \widetilde{\mathbf{curl}}$ transforms to $\operatorname{div} \mathcal{U} \nabla$, cf. [113, Chapter 3]. Moreover, we can also verify that $\left| \widetilde{\mathbf{curl}}\, a \right| = |\nabla a|$. With this, we state equivalent problems to (3.8) and (3.9) for $\Omega \subset \mathbb{R}^2$. In the magnetoquasistationary regime, we obtain:

Find $a \in L^2(\partial_t, T;\, H_0(\nabla, \Omega, \Gamma_{\text{FEM}}))$ such that

$$-\operatorname{div} \nu(|\nabla a|) \nabla a + \kappa \partial_t a = j \quad \text{in } \Omega \times T \backslash \{0\}, \tag{3.10a}$$
$$\gamma_1^{\nu} a = \phi_0 \quad \text{on } \Gamma_{\text{BEM}} \times T \backslash \{0\}, \tag{3.10b}$$
$$\gamma_0 a = u_0 \quad \text{on } \Gamma_{\text{BEM}} \times T \backslash \{0\}, \tag{3.10c}$$
$$a = 0 \quad \text{in } \Omega \times \{0\} \tag{3.10d}$$

with $j \in L^2(T;\, H(\nabla, \Omega)')$, $\phi_0 \in L^2(T;\, H^{-\frac{1}{2}}(\Gamma))$, and $u_0 \in L^2(T;\, H^{\frac{1}{2}}(\Gamma))$.

In the magnetostatic case, the problem above reduces to:

Find $a \in H_0(\nabla, \Omega, \Gamma_{\text{FEM}})$ such that

$$-\operatorname{div} \nu(|\nabla a|) \nabla a = j \quad \text{in } \Omega, \tag{3.11a}$$
$$\gamma_1^{\nu} a = \phi_0 \quad \text{on } \Gamma_{\text{BEM}}, \tag{3.11b}$$
$$\gamma_0 a = u_0 \quad \text{on } \Gamma_{\text{BEM}} \tag{3.11c}$$

with $j \in H(\nabla, \Omega)'$, $\phi_0 \in H^{-\frac{1}{2}}(\Gamma)$, and $u_0 \in H^{\frac{1}{2}}(\Gamma)$.

The boundary conditions can easily be derived from [113, Equation 3.10]. Note that we did not require a special gauging in the above formulation. The kernel of the gradient operator contains the set of real numbers, by ruling them out, e.g., by prescribing suitable boundary conditions to fix the constant, the interior problem can be uniquely solved.

In the next section, we consider the exterior problem, and introduce the needed tools for a boundary integral formulation.

3.2 Boundary integral equations and Steklov-Poincaré operators

Let us first clarify our interpretation of some terms. Under boundary data we understand functions or vector fields that are defined over the boundary. In particular, we call Cauchy data the set of boundary data that are obtained via an application of appropriate trace operators, and which render the solution of the corresponding BVP or Initial Value Problem (IVP) unique, or at least ensure its existence. For instance, the sets of Cauchy data that we will encounter in this work are either $\left(\gamma_0 v,\, \gamma_1^{\mathcal{U}}\, v\right)$ for scalar BVPs, or $\left(\boldsymbol{\gamma}_{\mathrm{D}}\, \boldsymbol{v},\, \boldsymbol{\gamma}_{\mathrm{N}}^{\mathcal{U}}\, \boldsymbol{v}\,(,\gamma_{\boldsymbol{n}} \boldsymbol{v})\right)$ for vectorial ones. They correspond to Dirichlet and Neumann boundary conditions. At this point, we also have to distinguish between traces that approach the boundary from the interior and from the exterior side of the domain that it encloses. Instead of Ω in Definition 2.14, considering Ω^{e} yields the exterior trace operators, which we differentiate from the interior ones by a superscript $\cdot^{\mathrm{e}}$. In particular, because in our context exterior domains are only filled with linear materials, e.g., $\mathcal{U} = \mathrm{Id}$, the exterior counterparts of $\gamma_1^{\mathcal{U}}$ and $\boldsymbol{\gamma}_{\mathrm{N}}^{\mathcal{U}}$ are denoted by γ_1^{e} and $\boldsymbol{\gamma}_{\mathrm{N}}^{\mathrm{e}}$, respectively. Moreover, the extension results hold accordingly for the exterior traces with self-evident notational adaptations; for example, Ω^{e} instead of Ω and $H_{\mathrm{loc}}(\Omega^{\mathrm{e}})$ instead of $H(\Omega^{\mathrm{e}})$ for a generic space $H(\Omega^{\mathrm{e}})$, if Ω^{e} is unbounded. A last remark is due, an exterior domain is not necessarily unbounded in this work, we rather mean a domain, where BEM is applied. Hence, we may use the terms exterior domain and BEM-domain interchangeably.

3.2.1 Boundary integral equations

The model problems for the exterior domain derive from the magnetostatic case with linear reluctivity. In particular, we assume $\nu = \mathrm{Id}$ for simplicity throughout this work. Note that this can be achieved by a suitable normalization from $\nu = \nu_0 \mathrm{Id}$, with ν_0 being the vacuum reluctivity. Moreover, no source current is supported in the exterior domain. Hence, the corresponding equations are homogeneous. Therefore, the topological terms are clearly eliminated from the explicit equations independently of the considered BCs on $\boldsymbol{b}$ and $\boldsymbol{e}$. This can be seen by setting to zero the term of (3.6) in (3.7) and a linear ν.
If Ω^{e} is unbounded, we additionally require a decay condition that describes the behavior of the field or function at infinity. For the vector potential, this follows from the decay condition of the magnetic field (1.12). However, it does not hold in general for 2D problems. Therefore, we first assume a logarithmic decay, which is a standard choice for unbounded Laplacian interface problems [87, Theorem 8.9]. This choice will be addressed again later.

We start with the following problems (in a weak sense): Let $\boldsymbol{a}^{\mathrm{e}} \in \boldsymbol{H}_{\mathrm{loc}}(\mathbf{curl}, \Omega^{\mathrm{e}}) \cap \boldsymbol{H}_{\mathrm{loc}}(\mathrm{div}, \Omega^{\mathrm{e}})$ and $a^{\mathrm{e}} \in H_{\mathrm{loc}}(\nabla, \Omega^{\mathrm{e}})$. In three-dimensional (3D), we have a **curl curl**-equation

$$\mathbf{curl}\,\mathbf{curl}\,\boldsymbol{a}^{\mathrm{e}} = \mathbf{0} \qquad \text{in } \Omega^{\mathrm{e}}, \tag{3.12a}$$

$$\operatorname{div} \boldsymbol{a}^{\mathrm{e}} = 0 \qquad \text{in } \Omega^{\mathrm{e}}, \tag{3.12b}$$
$$\boldsymbol{a}^{\mathrm{e}} = \mathcal{O}\left(|\boldsymbol{x}|^{-1}\right) \qquad \text{for } |\boldsymbol{x}| \to \infty, \tag{3.12c}$$

and in 2D a Laplace equation

$$-\Delta a^{\mathrm{e}} = 0 \qquad \text{in } \Omega^{\mathrm{e}}, \tag{3.13a}$$
$$a^{\mathrm{e}} = C_\infty \log(|\boldsymbol{x}|) + \mathcal{O}\left(|\boldsymbol{x}|^{-1}\right) \qquad \text{for } |\boldsymbol{x}| \to \infty. \tag{3.13b}$$

For now, we leave C_∞ unspecified. For convenience, it is a constant in the static regime and a time-dependent function in the quasistationary one, which can be computed from the solution. Furthermore, if Ω^{e} is bounded, there is no need to prescribe a decay condition, and the local behavior of the spaces may be dropped.

The core of boundary integral formulations is based on linear operators, known as potential operators, that map boundary data to smooth functions off the boundary. For this, an operator equation should possess a fundamental solution. We refer to [48, Section 6] for a rigorous introduction, and more details about the subject. For instance, the fundamental solution of the Laplace equation reads for $\boldsymbol{x}, \boldsymbol{y} \in \mathbb{R}^d$ and $\boldsymbol{x} \neq \boldsymbol{y}$

$$u^*(\boldsymbol{x}, \boldsymbol{y}) = \begin{cases} \frac{-1}{2\pi} \log\left(|\boldsymbol{x} - \boldsymbol{y}|\right), & d = 2, \\ \frac{1}{4\pi} \frac{1}{|\boldsymbol{x}-\boldsymbol{y}|}, & d = 3, \end{cases} \tag{3.14}$$

see e.g. [109, Section 5.1] for a detailed computation. We consider in this work two types of potential operators that can be associated to Dirichlet and Neumann BCs, which we call single-layer and double-layer potentials, respectively. Moreover, for each type we distinguish between potentials that take scalar functions and vector fields as input. This gives rise to the subsequent four potentials.

Definition 3.3 (Potentials)**.** *Let Γ be a Lipschitz boundary of $\Omega \subset \mathbb{R}^d$, $d = 2, 3$. For $\boldsymbol{x} \in \mathbb{R}^d \backslash \Gamma$, and for smooth enough inputs, we define the following potentials:*

- *The scalar Single-Layer Potential (SLP)*

$$\Psi_{\mathrm{SL}}(\varphi)(\boldsymbol{x}) = \int_\Gamma u^*(\boldsymbol{x}, \boldsymbol{y}) \varphi(\boldsymbol{y}) \, \mathrm{d}\sigma_{\boldsymbol{y}}. \tag{3.15}$$

- *The vectorial SLP ($d = 3$)*

$$\boldsymbol{\Psi}_{\mathrm{SL}}(\boldsymbol{\varphi})(\boldsymbol{x}) = \int_\Gamma u^*(\boldsymbol{x}, \boldsymbol{y}) \boldsymbol{\varphi}(\boldsymbol{y}) \, \mathrm{d}\sigma_{\boldsymbol{y}}. \tag{3.16}$$

- *The scalar Double-Layer Potential (DLP)*

$$\Psi_{\mathrm{DL}}(v)(\boldsymbol{x}) = \int_\Gamma \left(\nabla_{\boldsymbol{y}} u^*(\boldsymbol{x}, \boldsymbol{y}) \cdot \boldsymbol{n}(\boldsymbol{y})\right) v(\boldsymbol{y}) \, \mathrm{d}\sigma_{\boldsymbol{y}}. \tag{3.17}$$

- *The vectorial DLP, also known as Maxwell DLP ($d = 3$)*

$$\boldsymbol{\Psi}_{\mathrm{DL}}(\boldsymbol{v})(\boldsymbol{x}) = \mathbf{curl}_{\boldsymbol{x}} \, \boldsymbol{\Psi}_{\mathrm{SL}}\left(\boldsymbol{v} \times \boldsymbol{n}\right)(\boldsymbol{x}) = \mathbf{curl}_{\boldsymbol{x}} \int_\Gamma u^*(\boldsymbol{x}, \boldsymbol{y}) \left(\boldsymbol{v}(\boldsymbol{y}) \times \boldsymbol{n}(\boldsymbol{y})\right) \, \mathrm{d}\sigma_{\boldsymbol{y}}. \tag{3.18}$$

The above potentials can be extended to continuous mappings as follows.

Lemma 3.4 (Boundary Layer Potentials)**.** *Let $d = 2, 3$. The potentials of Definition 3.3 can be uniquely extended to linear operators such that*

$$\begin{aligned}
&\Psi_{\mathrm{SL}} : H^{-\frac{1}{2}}(\Gamma) \to H_{\mathrm{loc}}(\nabla,\, \mathbb{R}^d),\\
&\boldsymbol{\Psi}_{\mathrm{SL}} : \boldsymbol{H}^{-\frac{1}{2}}(\mathrm{div}_\Gamma, \Gamma) \to \boldsymbol{H}_{\mathrm{loc}}(\mathbf{curl},\, \mathbb{R}^3),\\
&\Psi_{\mathrm{DL}} : H^{\frac{1}{2}}(\Gamma) \to H_{\mathrm{loc}}(\nabla,\, \mathbb{R}^d\backslash\Gamma),\\
&\boldsymbol{\Psi}_{\mathrm{DL}} : \boldsymbol{H}^{-\frac{1}{2}}(\mathrm{curl}_\Gamma, \Gamma) \to \boldsymbol{H}_{\mathrm{loc}}(\mathbf{curl},\, \mathbb{R}^3\backslash\Gamma) \cap \boldsymbol{H}_{\mathrm{loc}}(\mathrm{div}\,\mathbf{0},\, \mathbb{R}^3\backslash\Gamma)
\end{aligned}$$

are bounded.

Proof. We refer to [31, Theorem 1] for the scalar potentials, and to [61, Section 5] for the vectorial ones. □

With this, representation formulae can be derived, which allow the computation of a scalar function or a vector field evaluated in Ω or Ω^{e} solely through the corresponding Cauchy data.

Theorem 3.5 (Representation formulae)**.** *Scalar functions $a \in H(\nabla, \Omega)$ and $a^{\mathrm{e}} \in H_{\mathrm{loc}}(\nabla, \Omega^{\mathrm{e}})$ that solve* (3.13) *in a weak sense in the interior and exterior domain, respectively, can be represented as*

$$a(\boldsymbol{x}) = \Psi_{\mathrm{SL}}(\gamma_1\, a)(\boldsymbol{x}) - \Psi_{\mathrm{DL}}(\gamma_0 a)(\boldsymbol{x}) \qquad \text{for } \boldsymbol{x} \in \Omega, \tag{3.19a}$$

$$a^{\mathrm{e}}(\boldsymbol{x}) = \Psi_{\mathrm{DL}}(\gamma_0^{\mathrm{e}} a^{\mathrm{e}})(\boldsymbol{x}) - \Psi_{\mathrm{SL}}(\gamma_1^{\mathrm{e}}\, a^{\mathrm{e}})(\boldsymbol{x}) \qquad \text{for } \boldsymbol{x} \in \Omega^{\mathrm{e}}. \tag{3.19b}$$

Moreover, vector fields $\boldsymbol{a} \in \boldsymbol{H}(\mathbf{curl}, \Omega)$ and $\boldsymbol{a}^{\mathrm{e}} \in \boldsymbol{H}_{\mathrm{loc}}(\mathbf{curl}, \Omega^{\mathrm{e}})$ that solve (3.12) *in a weak sense in the interior and exterior domain, respectively, can be represented as*

$$\boldsymbol{a}(\boldsymbol{x}) = \boldsymbol{\Psi}_{\mathrm{SL}}(\boldsymbol{\gamma}_{\mathrm{N}}\, \boldsymbol{a})(\boldsymbol{x}) + \boldsymbol{\Psi}_{\mathrm{DL}}(\boldsymbol{\gamma}_{\mathrm{D}}\, \boldsymbol{a})(\boldsymbol{x}) + \nabla\Psi_{\mathrm{SL}}(\gamma_{\boldsymbol{n}}\boldsymbol{a})(\boldsymbol{x}) \qquad \text{for } \boldsymbol{x} \in \Omega, \tag{3.20a}$$

$$\boldsymbol{a}^{\mathrm{e}}(\boldsymbol{x}) = -\boldsymbol{\Psi}_{\mathrm{SL}}(\boldsymbol{\gamma}_{\mathrm{N}}^{\mathrm{e}}\, \boldsymbol{a}^{\mathrm{e}})(\boldsymbol{x}) - \boldsymbol{\Psi}_{\mathrm{DL}}(\boldsymbol{\gamma}_{\mathrm{D}}^{\mathrm{e}}\, \boldsymbol{a}^{\mathrm{e}})(\boldsymbol{x}) - \nabla\Psi_{\mathrm{SL}}(\gamma_{\boldsymbol{n}}^{\mathrm{e}}\boldsymbol{a}^{\mathrm{e}})(\boldsymbol{x}) \qquad \text{for } \boldsymbol{x} \in \Omega^{\mathrm{e}}. \tag{3.20b}$$

Proof. The representation formulae for the scalar case follow from [87, Theorems 7.12 & 7.15]. The result for our vector fields is given in [62, Section 3], for instance. □

The next step is to introduce the corresponding BIOs. They arise by taking the traces of the BLPs. Note that the potentials are not necessarily continuous across the boundary. Hence, possible discontinuities should be taken into account. This motivates the definition of BIOs as averages of the corresponding potential traces.

Definition 3.6. *Let $\{\gamma\} := \frac{1}{2}(\gamma^{\mathrm{e}} + \gamma)$ denote the average of some exterior and interior trace operator γ. We define the following BIOs:*

- *single-layer:* $\mathcal{V}_0 := \{\gamma_0\} \circ \Psi_{\mathrm{SL}}$,
- *double-layer:* $\mathcal{K}_0 := \{\gamma_0\} \circ \Psi_{\mathrm{DL}}$,
- *adjoint double-layer:* $\mathcal{K}_0' := \{\gamma_1\} \circ \Psi_{\mathrm{SL}}$,
- *hyper-singular:* $\mathcal{W}_0 := \{\gamma_1\} \circ \Psi_{\mathrm{DL}}$

as well as:

- *vectorial single-layer:* $\boldsymbol{\mathcal{A}}_0 := \{\boldsymbol{\gamma}_{\mathrm{D}}\} \circ \boldsymbol{\Psi}_{\mathrm{SL}}$,
- *Maxwell double-layer:* $\boldsymbol{\mathcal{C}}_0 := \{\boldsymbol{\gamma}_{\mathrm{D}}\} \circ \boldsymbol{\Psi}_{\mathrm{DL}}$,
- *adjoint Maxwell double-layer:* $\boldsymbol{\mathcal{B}}_0 := \{\boldsymbol{\gamma}_{\mathrm{N}}\} \circ \boldsymbol{\Psi}_{\mathrm{SL}}$,
- *vectorial hyper-singular:* $\boldsymbol{\mathcal{N}}_0 := \{\boldsymbol{\gamma}_{\mathrm{N}}\} \circ \boldsymbol{\Psi}_{\mathrm{DL}}$.

Concretely, the jump relations of the potential operators are specified below.

Theorem 3.7 (Jump relations)**.** *Let $[\![\gamma\Psi]\!]_\Gamma := \gamma\Psi - \gamma^{\mathrm{e}}\Psi$ denote the jump of some function Ψ across a boundary Γ. The BLPs involved in the representation formulae of Theorem 3.5 satisfy the following jump relations:*

$$\begin{aligned} [\![\gamma_0 \Psi_{\mathrm{SL}}]\!]_\Gamma &= 0, & [\![\boldsymbol{\gamma}_{\mathrm{D}}\, \boldsymbol{\Psi}_{\mathrm{SL}}]\!]_\Gamma &= 0, \\ [\![\gamma_0 \Psi_{\mathrm{DL}}]\!]_\Gamma &= -\mathrm{Id}, & [\![\boldsymbol{\gamma}_{\mathrm{D}}\, \boldsymbol{\Psi}_{\mathrm{DL}}]\!]_\Gamma &= -\mathrm{Id}, \\ [\![\gamma_1\, \Psi_{\mathrm{SL}}]\!]_\Gamma &= \mathrm{Id}, & [\![\boldsymbol{\gamma}_{\mathrm{N}}\, \boldsymbol{\Psi}_{\mathrm{SL}}]\!]_\Gamma &= -\mathrm{Id}, \\ [\![\gamma_1\, \Psi_{\mathrm{DL}}]\!]_\Gamma &= 0, & [\![\boldsymbol{\gamma}_{\mathrm{N}}\, \boldsymbol{\Psi}_{\mathrm{DL}}]\!]_\Gamma &= 0. \end{aligned}$$

Proof. We refer, e.g., to [87, Theorem 6.11] for the jump relations of the scalar potentials Ψ_{SL}, Ψ_{DL}, and to [61, Section 5] and [62, Theorem 3.4] for those of $\boldsymbol{\Psi}_{\mathrm{SL}}$, $\boldsymbol{\Psi}_{\mathrm{DL}}$. □

Then, we give some properties of the newly introduced BIOs.

Theorem 3.8 (Mapping properties of BIOs)**.** *The boundary integral operators*

$$\begin{aligned} \mathcal{V}_0 &: H^{-\frac{1}{2}}(\Gamma) \to H^{\frac{1}{2}}(\Gamma), & \mathcal{K}_0 &: H^{\frac{1}{2}}(\Gamma) \to H^{\frac{1}{2}}(\Gamma), \\ \mathcal{K}_0' &: H^{-\frac{1}{2}}(\Gamma) \to H^{-\frac{1}{2}}(\Gamma), & \mathcal{W}_0 &: H^{\frac{1}{2}}(\Gamma) \to H^{-\frac{1}{2}}(\Gamma) \end{aligned}$$

as well as

$$\begin{aligned} \boldsymbol{\mathcal{A}}_0 &: \boldsymbol{H}^{-\frac{1}{2}}(\mathrm{div}_\Gamma, \Gamma) \to \boldsymbol{H}^{-\frac{1}{2}}(\mathrm{curl}_\Gamma, \Gamma), & \boldsymbol{\mathcal{C}}_0 &: \boldsymbol{H}^{-\frac{1}{2}}(\mathrm{curl}_\Gamma, \Gamma) \to \boldsymbol{H}^{-\frac{1}{2}}(\mathrm{curl}_\Gamma, \Gamma), \\ \boldsymbol{\mathcal{B}}_0 &: \boldsymbol{H}^{-\frac{1}{2}}(\mathrm{div}_\Gamma, \Gamma) \to \boldsymbol{H}^{-\frac{1}{2}}(\mathrm{div}_\Gamma, \Gamma), & \boldsymbol{\mathcal{N}}_0 &: \boldsymbol{H}^{-\frac{1}{2}}(\mathrm{curl}_\Gamma, \Gamma) \to \boldsymbol{H}^{-\frac{1}{2}}(\mathrm{div}_\Gamma, \Gamma) \end{aligned}$$

define continuous and linear mappings.

Proof. See [87, Theorem 6.11] and [61, Section 5]. □

Theorem 3.9 (Properties of $\mathcal{V}_0$ and $\mathcal{W}_0$)**.** *The BIOs $\mathcal{V}_0$ and $\mathcal{W}_0$ are symmetric, i.e., for all $\varphi,\, \psi \in H^{-\frac{1}{2}}(\Gamma)$ and $u,\, v \in H^{\frac{1}{2}}(\Gamma)$ we have*

$$\langle \psi, \mathcal{V}_0 \varphi \rangle_\Gamma = \langle \varphi, \mathcal{V}_0 \psi \rangle_\Gamma, \quad \langle \mathcal{W}_0 u, v \rangle_\Gamma = \langle \mathcal{W}_0 v, u \rangle_\Gamma. \tag{3.21}$$

Moreover, let $\Omega \subset \mathbb{R}^d$. The single-layer operator $\mathcal{V}_0$ is $H^{-\frac{1}{2}}(\Gamma)$-elliptic (but under a condition on Ω when $d = 2$), i.e., there exists $C_{\mathcal{V}_0} = C_{\mathcal{V}_0}(\Gamma) > 0$ such that

$$\langle \varphi, \mathcal{V}_0 \varphi \rangle_\Gamma \geq C_{\mathcal{V}_0} \|\varphi\|^2_{H^{-\frac{1}{2}}(\Gamma)} \qquad \text{for } d = 3, \tag{3.22}$$

$$\langle \varphi, \mathcal{V}_0 \varphi \rangle_\Gamma \geq C_{\mathcal{V}_0} \|\varphi\|^2_{H^{-\frac{1}{2}}(\Gamma)} \qquad \text{for } d = 2, \text{ if } \operatorname{diam} \Omega < 1. \tag{3.23}$$

The hyper-singular operator $\mathcal{W}_0$ is positive definite on $H^{\frac{1}{2}}(\Gamma)$ and elliptic on $[H^{\frac{1}{2}}(\Gamma)]$, i.e., there exists $C_{\mathcal{W}_0} = C_{\mathcal{W}_0}(\Gamma) > 0$ such that

$$\langle \mathcal{W}_0 u, u \rangle_\Gamma \geq 0 \qquad \text{for all } u \in H^{\frac{1}{2}}(\Gamma), \tag{3.24}$$

$$\langle \mathcal{W}_0 u, u \rangle_\Gamma \geq C_{\mathcal{W}_0} \|u\|^2_{H^{\frac{1}{2}}(\Gamma)} \qquad \text{for all } u \in [H^{\frac{1}{2}}(\Gamma)]. \tag{3.25}$$

Proof. The symmetry is provided, e.g., in [87, Chapter 7]. For the ellipticity results we refer to [109, Theorem 22 & 23] for the single-layer operator, and to [109, Theorem 24] for the hyper-singular operator, for instance. Obviously, the latter proof is also valid in the quotient space formulation because of Corollary 2.4. □

Remark 3.10. *Note that the requirement* $\operatorname{diam} \Omega < 1$ *to ensure a $H^{-\frac{1}{2}}(\Gamma)$-elliptic single-layer operator is in practice not restrictive. Indeed, it can be merely achieved by scaling the domain or the fundamental solution.*

Analogously, we find similar results for the vectorial single-layer and hyper-singular operators.

Theorem 3.11 (Properties of $\boldsymbol{\mathcal{A}}_0$ and $\boldsymbol{\mathcal{N}}_0$)**.** *The Boundary Integral Operators (BIOs) $\boldsymbol{\mathcal{A}}_0$ and $\boldsymbol{\mathcal{N}}_0$ are symmetric, i.e., for all $\boldsymbol{\varphi}$, $\boldsymbol{\psi} \in \boldsymbol{H}^{-\frac{1}{2}}(\operatorname{div}_\Gamma, \Gamma)$ and $\boldsymbol{u}$, $\boldsymbol{v} \in \boldsymbol{H}^{-\frac{1}{2}}(\operatorname{curl}_\Gamma, \Gamma)$ we have*

$$\langle \boldsymbol{\psi}, \boldsymbol{\mathcal{A}}_0 \boldsymbol{\varphi} \rangle_\Gamma = \langle \boldsymbol{\varphi}, \boldsymbol{\mathcal{A}}_0 \boldsymbol{\psi} \rangle_\Gamma, \quad \langle \boldsymbol{\mathcal{N}}_0 \boldsymbol{u}, \boldsymbol{v} \rangle_\Gamma = \langle \boldsymbol{\mathcal{N}}_0 \boldsymbol{v}, \boldsymbol{u} \rangle_\Gamma. \tag{3.26}$$

The vectorial single-layer operator $\boldsymbol{\mathcal{A}}_0$ is $\boldsymbol{H}^{-\frac{1}{2}}(\operatorname{div}_\Gamma 0, \Gamma)$-elliptic[1], i.e., there exists $C_{\boldsymbol{\mathcal{A}}_0} = C_{\boldsymbol{\mathcal{A}}_0}(\Gamma) > 0$ such that

$$\langle \boldsymbol{\varphi}, \boldsymbol{\mathcal{A}}_0 \boldsymbol{\varphi} \rangle_\Gamma \geq C_{\boldsymbol{\mathcal{A}}_0} \|\boldsymbol{\varphi}\|^2_{\boldsymbol{H}^{-\frac{1}{2}}(\operatorname{div}_\Gamma, \Gamma)} \qquad \text{for all } \boldsymbol{\varphi} \in \boldsymbol{H}^{-\frac{1}{2}}(\operatorname{div}_\Gamma 0, \Gamma). \tag{3.27}$$

The vectorial hyper-singular operator $\boldsymbol{\mathcal{N}}_0$ is positive definite on $\boldsymbol{H}^{-\frac{1}{2}}(\operatorname{curl}_\Gamma, \Gamma)$ and elliptic on $[\boldsymbol{H}^{-\frac{1}{2}}(\operatorname{curl}_\Gamma, \Gamma)]$, i.e., there exists $C_{\boldsymbol{\mathcal{N}}_0} = C_{\boldsymbol{\mathcal{N}}_0}(\Gamma) > 0$ such that

$$\langle \boldsymbol{\mathcal{N}}_0 \boldsymbol{u}, \boldsymbol{u} \rangle_\Gamma \geq 0 \qquad \text{for all } \boldsymbol{u} \in \boldsymbol{H}^{-\frac{1}{2}}(\operatorname{curl}_\Gamma, \Gamma), \tag{3.28}$$

$$\langle \boldsymbol{\mathcal{N}}_0 \boldsymbol{u}, \boldsymbol{u} \rangle_\Gamma \geq C_{\boldsymbol{\mathcal{N}}_0} \|\boldsymbol{u}\|^2_{\boldsymbol{H}^{-\frac{1}{2}}(\operatorname{curl}_\Gamma, \Gamma)} \qquad \text{for all } \boldsymbol{u} \in [\boldsymbol{H}^{-\frac{1}{2}}(\operatorname{curl}_\Gamma, \Gamma)]. \tag{3.29}$$

Proof. The symmetry and $\boldsymbol{H}^{-\frac{1}{2}}(\operatorname{div}_\Gamma 0, \Gamma)$-ellipticity of $\boldsymbol{\mathcal{A}}_0$ follows from [62, Theorem 4.4 with $\kappa = 0$]. For the hyper-singular operator, an alternative representation, which can be found in [44, Remark 4.26 with $\kappa = 0$], for instance, makes the proof of the related assertions straightforward, namely,

$$\langle \boldsymbol{\mathcal{N}}_0 \boldsymbol{u}, \boldsymbol{u} \rangle_\Gamma = \langle \operatorname{curl}_\Gamma \boldsymbol{u}, \mathcal{V}_0 \operatorname{curl}_\Gamma \boldsymbol{u} \rangle_\Gamma \quad \text{for all } \boldsymbol{u} \in \boldsymbol{H}^{-\frac{1}{2}}(\operatorname{curl}_\Gamma, \Gamma). \tag{3.30}$$

Then, by using (3.22), namely, the $H^{-\frac{1}{2}}(\Gamma)$-ellipticity of $\mathcal{V}_0$, and the inclusion (2.64c), we obtain

$$\langle \boldsymbol{\mathcal{N}}_0 \boldsymbol{u}, \boldsymbol{u} \rangle_\Gamma = \langle \operatorname{curl}_\Gamma \boldsymbol{u}, \mathcal{V}_0 \operatorname{curl}_\Gamma \boldsymbol{u} \rangle_\Gamma \geq 0 \quad \text{for all } \boldsymbol{u} \in \boldsymbol{H}^{-\frac{1}{2}}(\operatorname{curl}_\Gamma, \Gamma). \tag{3.31}$$

[1] Note that $\boldsymbol{\mathcal{A}}_0$ is even elliptic on the whole space $\boldsymbol{H}^{-\frac{1}{2}}(\operatorname{div}_\Gamma, \Gamma)$, see [19, 31].

However, by using the same argument for representatives in $[\boldsymbol{H}^{-\frac{1}{2}}(\mathrm{curl}_\Gamma, \Gamma)]$, we establish the ellipticity of $\boldsymbol{\mathcal{N}}_0$, i.e., there exists $C_{\boldsymbol{\mathcal{N}}_0} > 0$ such that

$$\langle \boldsymbol{\mathcal{N}}_0 \boldsymbol{u}, \boldsymbol{u} \rangle_\Gamma \geq C_{\boldsymbol{\mathcal{N}}_0} \|\boldsymbol{u}\|^2_{\boldsymbol{H}^{-\frac{1}{2}}(\mathrm{curl}_\Gamma, \Gamma)} \tag{3.32}$$

for all $\boldsymbol{u} \in [\boldsymbol{H}^{-\frac{1}{2}}(\mathrm{curl}_\Gamma, \Gamma)]$. □

Moreover, the Maxwell double-layer $\boldsymbol{\mathcal{C}}_0$ and the adjoint Maxwell double-layer $\boldsymbol{\mathcal{B}}_0$ are related in the following sense: for $\boldsymbol{\varphi} \in \boldsymbol{H}^{-\frac{1}{2}}(\mathrm{div}_\Gamma, \Gamma)$ and $\boldsymbol{u} \in \boldsymbol{H}^{-\frac{1}{2}}(\mathrm{curl}_\Gamma, \Gamma)$ it holds that

$$\langle \boldsymbol{\varphi}, \boldsymbol{\mathcal{C}}_0 \boldsymbol{u} \rangle_\Gamma = -\langle \boldsymbol{\mathcal{B}}_0 \boldsymbol{\varphi}, \boldsymbol{u} \rangle_\Gamma, \tag{3.33}$$

cf. [61, Theorem 3.9 with $\kappa = 0$].

Corollary 3.12 (Equivalent norms)**.** *For $\psi \in H^{-\frac{1}{2}}(\Gamma)$ and $\boldsymbol{\psi} \in \boldsymbol{H}^{-\frac{1}{2}}(\mathrm{div}_\Gamma 0, \Gamma)$, the following norm equivalences*

$$\|\psi\|_{\mathcal{V}_0} := \sqrt{\langle \psi, \mathcal{V}_0 \psi \rangle_\Gamma} \cong \|\psi\|_{H^{-\frac{1}{2}}(\Gamma)}, \tag{3.34}$$

$$\|\boldsymbol{\psi}\|_{\boldsymbol{\mathcal{A}}_0} := \sqrt{\langle \boldsymbol{\psi}, \boldsymbol{\mathcal{A}}_0 \boldsymbol{\psi} \rangle_\Gamma} \cong \|\psi\|_{\boldsymbol{H}^{-\frac{1}{2}}(\mathrm{div}_\Gamma, \Gamma)} \tag{3.35}$$

hold.

Proof. The assertions follow merely from the properties of $\mathcal{V}_0$ and $\boldsymbol{\mathcal{A}}_0$, in particular, from the $H^{-\frac{1}{2}}(\Gamma)$-ellipticity of $\mathcal{V}_0$, and the $\boldsymbol{H}^{-\frac{1}{2}}(\mathrm{div}_\Gamma 0, \Gamma)$-ellipticity of $\boldsymbol{\mathcal{A}}_0$, see (3.23) and (3.27), respectively. □

For implementation, a concrete representation of the BIOs is necessary. Indeed, provided the inputs are smooth enough, they admit an integral representation. Subsequently, we only state those that are relevant for actual implementation.

Lemma 3.13 (Integral representations)**.** *The following representations hold:*

$$\begin{aligned}
\varphi \in L^\infty(\Gamma), \quad \langle \varphi, \mathcal{V}_0 \psi \rangle_\Gamma &= \int_\Gamma \int_\Gamma u^*(\boldsymbol{x}, \boldsymbol{y}) \varphi(\boldsymbol{x}) \psi(\boldsymbol{y}) \, \mathrm{d}\sigma_{\boldsymbol{y}} \, \mathrm{d}\sigma_{\boldsymbol{x}} && \forall \psi \in L^\infty(\Gamma), \\
v \in L^\infty(\Gamma), \quad \langle v, \mathcal{K}_0 w \rangle_\Gamma &= \int_\Gamma \int_\Gamma \nabla_{\boldsymbol{y}} u^*(\boldsymbol{x}, \boldsymbol{y}) \cdot \boldsymbol{n}(\boldsymbol{y}) v(\boldsymbol{x}) w(\boldsymbol{y}) \, \mathrm{d}\sigma_{\boldsymbol{y}} \, \mathrm{d}\sigma_{\boldsymbol{x}} && \forall w \in L^\infty(\Gamma), \\
\boldsymbol{\varphi} \in \boldsymbol{L}^\infty(\Gamma), \quad \langle \boldsymbol{\varphi}, \boldsymbol{\mathcal{A}}_0 \boldsymbol{\psi} \rangle_\Gamma &= \int_\Gamma \int_\Gamma u^*(\boldsymbol{x}, \boldsymbol{y}) \boldsymbol{\varphi}(\boldsymbol{x}) \cdot \boldsymbol{\psi}(\boldsymbol{y}) \, \mathrm{d}\sigma_{\boldsymbol{y}} \, \mathrm{d}\sigma_{\boldsymbol{x}} && \forall \boldsymbol{\psi} \in \boldsymbol{L}^\infty(\Gamma), \\
\boldsymbol{v} \in \boldsymbol{L}^\infty(\Gamma), \quad \langle \boldsymbol{v}, \boldsymbol{\mathcal{C}}_0 \boldsymbol{w} \rangle_\Gamma &= \int_\Gamma \int_\Gamma \nabla_{\boldsymbol{y}} u^*(\boldsymbol{x}, \boldsymbol{y}) (\boldsymbol{v}(\boldsymbol{x}) \times \boldsymbol{w}(\boldsymbol{y})) \, \mathrm{d}\sigma_{\boldsymbol{y}} \, \mathrm{d}\sigma_{\boldsymbol{x}} && \forall \boldsymbol{w} \in \boldsymbol{L}^\infty(\Gamma).
\end{aligned}$$

Proof. cf. [109, Section 6] and [22, Section 5]. □

Remark 3.14. *Note that the integrals above are singular when $\boldsymbol{x} \to \boldsymbol{y}$. Hence, they have to be understood as improper integrals, if the corresponding kernel is weakly singular ($\mathcal{O}(|\boldsymbol{x} - \boldsymbol{y}|^{-1})$), and as a Cauchy principal value if it is strongly singular ($\mathcal{O}(|\boldsymbol{x} - \boldsymbol{y}|^{-2})$).*

By taking the corresponding traces of the representation formulae of Theorem 3.5, and by considering the jump relations of Theorem 3.7, we obtain two BIEs per representation formula. On one hand, we arrive for the scalar case at

$$\gamma_0 a = (\frac{1}{2} - \mathcal{K}_0)\gamma_0 a + \mathcal{V}_0\,\gamma_1\,a, \qquad \gamma_1\,a = \mathcal{W}_0\gamma_0 a + (\frac{1}{2} + \mathcal{K}_0')\,\gamma_1\,a, \tag{3.37a}$$

$$\gamma_0^{\mathrm{e}} a^{\mathrm{e}} = (\frac{1}{2} + \mathcal{K}_0)\gamma_0^{\mathrm{e}} a^{\mathrm{e}} - \mathcal{V}_0\,\gamma_1^{\mathrm{e}}\,a^{\mathrm{e}}, \qquad \gamma_1^{\mathrm{e}}\,a^{\mathrm{e}} = -\,\mathcal{W}_0\gamma_0^{\mathrm{e}} a^{\mathrm{e}} + (\frac{1}{2} - \mathcal{K}_0')\,\gamma_1^{\mathrm{e}}\,a^{\mathrm{e}}, \tag{3.37b}$$

which for convenience can be rewritten as

$$\begin{pmatrix}\gamma_0 a\\ \gamma_1\,a\end{pmatrix} = \left(\frac{1}{2}\mathrm{Id} + \mathcal{P}_{\mathrm{s}}\right)\begin{pmatrix}\gamma_0 a\\ \gamma_1\,a\end{pmatrix}, \quad \begin{pmatrix}\gamma_0^{\mathrm{e}} a^{\mathrm{e}}\\ \gamma_1^{\mathrm{e}}\,a^{\mathrm{e}}\end{pmatrix} = \left(\frac{1}{2}\mathrm{Id} - \mathcal{P}_{\mathrm{s}}\right)\begin{pmatrix}\gamma_0^{\mathrm{e}} a^{\mathrm{e}}\\ \gamma_1^{\mathrm{e}}\,a^{\mathrm{e}}\end{pmatrix} \quad \text{with } \mathcal{P}_{\mathrm{s}} = \begin{pmatrix}-\mathcal{K}_0 & \mathcal{V}_0\\ \mathcal{W}_0 & \mathcal{K}_0'\end{pmatrix}.$$

The operators $\frac{1}{2}\mathrm{Id} \pm \mathcal{P}_{\mathrm{s}}$ are known as interior and exterior Calderón projectors, respectively, see [109, Section 6.6], for instance. However, the arising BIEs for the vectorial case are

$$\boldsymbol{\gamma}_{\mathrm{D}}\,\boldsymbol{a} = \boldsymbol{\mathcal{A}}_0\,\boldsymbol{\gamma}_{\mathrm{N}}\,\boldsymbol{a} + (\frac{1}{2} + \boldsymbol{\mathcal{C}}_0)\,\boldsymbol{\gamma}_{\mathrm{D}}\,\boldsymbol{a} + \nabla_\Gamma \mathcal{V}_0(\gamma_{\boldsymbol{n}}\boldsymbol{a}), \tag{3.38a}$$

$$\boldsymbol{\gamma}_{\mathrm{N}}\,\boldsymbol{a} = (\frac{1}{2} + \boldsymbol{\mathcal{B}}_0)\,\boldsymbol{\gamma}_{\mathrm{N}}\,\boldsymbol{a} + \boldsymbol{\mathcal{N}}_0\,\boldsymbol{\gamma}_{\mathrm{D}}\,\boldsymbol{a} \tag{3.38b}$$

for the interior problem, and

$$\boldsymbol{\gamma}_{\mathrm{D}}^{\mathrm{e}}\,\boldsymbol{a}^{\mathrm{e}} = -\boldsymbol{\mathcal{A}}_0\,\boldsymbol{\gamma}_{\mathrm{N}}^{\mathrm{e}}\,\boldsymbol{a}^{\mathrm{e}} + (\frac{1}{2} - \boldsymbol{\mathcal{C}}_0)\,\boldsymbol{\gamma}_{\mathrm{D}}^{\mathrm{e}}\,\boldsymbol{a}^{\mathrm{e}} - \nabla_\Gamma \mathcal{V}_0(\gamma_{\boldsymbol{n}}^{\mathrm{e}}\boldsymbol{a}^{\mathrm{e}}), \tag{3.39a}$$

$$\boldsymbol{\gamma}_{\mathrm{N}}^{\mathrm{e}}\,\boldsymbol{a}^{\mathrm{e}} = (\frac{1}{2} - \boldsymbol{\mathcal{B}}_0)\,\boldsymbol{\gamma}_{\mathrm{N}}^{\mathrm{e}}\,\boldsymbol{a}^{\mathrm{e}} - \boldsymbol{\mathcal{N}}_0\,\boldsymbol{\gamma}_{\mathrm{D}}^{\mathrm{e}}\,\boldsymbol{a}^{\mathrm{e}} \tag{3.39b}$$

for the exterior one. Hence, an analogous extraction of Calderón projectors is not possible in this case due the presence of the terms including the normal trace. Getting rid of this term is also convenient for the definition of Steklov-Poincaré operators, which are crucial for our analysis of the coupled problem. We introduce them below in Subsection 3.2.2. Therefore, in accordance to the vector potential formulation in the interior domain, cf. Section 3.1, and similarly to [43], we project (3.38a) and (3.39a) onto $[\boldsymbol{H}^{-\frac{1}{2}}(\mathrm{curl}_\Gamma, \Gamma)]$. Moreover, by taking the commutativity of the de Rham complex into account, see Figure 2.6, the identity

$$\mathrm{div}_\Gamma\,\boldsymbol{\gamma}_\times\,\boldsymbol{w} = \gamma_{\boldsymbol{n}}\,\mathbf{curl}\,\boldsymbol{w}$$

holds for all $\boldsymbol{w} \in \boldsymbol{H}(\mathbf{curl}, \Omega)$ (or $\boldsymbol{w} \in \boldsymbol{H}_{\mathrm{loc}}(\mathbf{curl}, \Omega^{\mathrm{e}})$). In particular, if we choose $\boldsymbol{w} = \mathbf{curl}\,\boldsymbol{v} \in \boldsymbol{H}(\mathbf{curl}\;\mathbf{curl}, \Omega)$ (or $\boldsymbol{w} = \mathbf{curl}\,\boldsymbol{v} \in \boldsymbol{H}_{\mathrm{loc}}(\mathbf{curl}\;\mathbf{curl}, \Omega^{\mathrm{e}})$) such that the $\mathbf{curl}\,\mathbf{curl}$-equation (3.12a) is satisfied, we obtain

$$\mathrm{div}_\Gamma\,\boldsymbol{\gamma}_{\mathrm{N}}\,\boldsymbol{v} = \gamma_{\boldsymbol{n}}\,\mathbf{curl}\,\mathbf{curl}\,\boldsymbol{v} = 0.$$

Therefore, (3.38b) and (3.39b) have to be set in $\boldsymbol{H}^{-\frac{1}{2}}(\mathrm{div}_\Gamma\,0, \Gamma)$. In the following, we show that the duality pairing defined by $\boldsymbol{H}^{-\frac{1}{2}}(\mathrm{curl}_\Gamma, \Gamma)$ and $\boldsymbol{H}^{-\frac{1}{2}}(\mathrm{div}_\Gamma, \Gamma)$ transfers to the quotient space $[\boldsymbol{H}^{-\frac{1}{2}}(\mathrm{curl}_\Gamma, \Gamma)]$ and the subspace $\boldsymbol{H}^{-\frac{1}{2}}(\mathrm{div}_\Gamma\,0, \Gamma)$. The proof follows the same idea as for the duality of $\boldsymbol{H}^{-\frac{1}{2}}(\mathrm{curl}_\Gamma, \Gamma)$ and $\boldsymbol{H}^{-\frac{1}{2}}(\mathrm{div}_\Gamma, \Gamma)$, which can be found in [20, Lemma 5.6] for simply-connected boundaries. An alternative proof is furnished in [43, Proposition 3.2].

Lemma 3.15. *Let Γ be simply- or multiply-connected. The quotient space $[\boldsymbol{H}^{-\frac{1}{2}}(\mathrm{curl}_\Gamma, \Gamma)]$ and the subspace $\boldsymbol{H}^{-\frac{1}{2}}(\mathrm{div}_\Gamma\,0, \Gamma)$ define a duality pairing with $\boldsymbol{L}_{\mathrm{t}}^2(\Gamma)$ as pivot space.*

Proof. Let $\boldsymbol{u} \in \boldsymbol{H}^{-\frac{1}{2}}(\operatorname{div}_\Gamma 0, \Gamma)$ and $\boldsymbol{v} \in [\boldsymbol{H}^{-\frac{1}{2}}(\operatorname{curl}_\Gamma, \Gamma)]$. By Theorem 2.32, we know that there exists unique $\beta \in H^{\frac{1}{2}}(\Gamma)$ and $\boldsymbol{\eta} \in \mathbb{H}_1(\Gamma)$, such that $\boldsymbol{u} = \mathbf{curl}_\Gamma \beta + \boldsymbol{\eta}$. Moreover, using Corollary 2.4 and [20, Theorem 5.5], there exists a unique $\alpha \in H(\Delta_\Gamma, \Gamma)$ such that $\boldsymbol{v} = \mathbf{curl}_\Gamma \alpha$. Note that the latter representation is independent of the topology. Now, let $\{\beta_n\}_{n\in\mathbb{N}_0} \subseteq H^1(\Gamma)$ such that $\beta_n \to \beta$. Then, for $\boldsymbol{u}_n = \mathbf{curl}_\Gamma \beta_n + \boldsymbol{\eta} \in \boldsymbol{L}^2_{\mathrm{t}}(\Gamma)$ and $\boldsymbol{v} \in \boldsymbol{L}^2_{\mathrm{t}}(\Gamma)$ we have

$$\langle \boldsymbol{u}_n, \boldsymbol{v} \rangle = -\langle \Delta_\Gamma \alpha, \beta_n \rangle,$$

where we used (2.56b), $\operatorname{curl}_\Gamma \boldsymbol{\eta} = 0$, and $\operatorname{curl}_\Gamma \mathbf{curl}_\Gamma \alpha = -\Delta_\Gamma$. By taking the limiting case $n \to \infty$, we arrive at a well-defined duality pairing in the sense of $[\boldsymbol{H}^{-\frac{1}{2}}(\operatorname{curl}_\Gamma, \Gamma)]$ and $\boldsymbol{H}^{-\frac{1}{2}}(\operatorname{div}_\Gamma 0, \Gamma)$ with $\boldsymbol{L}^2_{\mathrm{t}}(\Gamma)$ as a pivot space. □

3.2.2 Steklov-Poincaré operators and contractivity results

In the following, we introduce Dirichlet-to-Neumann maps, which are given by Steklov-Poincaré operators. Let us first focus on the scalar case. By rearranging the first BIEs of (3.37a) and (3.37b), and by using the $H^{-\frac{1}{2}}(\Gamma)$-ellipticity of $\mathcal{V}_0$, we arrive at

$$\gamma_1 a = \mathcal{V}_0{}^{-1}(\frac{1}{2} + \mathcal{K}_0)\gamma_0 a, \tag{3.40a}$$

$$\gamma_1^{\mathrm{e}} a^{\mathrm{e}} = -\mathcal{V}_0{}^{-1}(\frac{1}{2} - \mathcal{K}_0)\gamma_0^{\mathrm{e}} a^{\mathrm{e}}, \tag{3.40b}$$

and define the interior and exterior Steklov-Poincaré operators $\mathcal{S}^{\mathrm{int}}$, $\mathcal{S}^{\mathrm{ext}} : H^{\frac{1}{2}}(\Gamma) \to H^{-\frac{1}{2}}(\Gamma)$ with

$$\mathcal{S}^{\mathrm{int}} = \mathcal{V}_0{}^{-1}(\frac{1}{2} + \mathcal{K}_0), \tag{3.41a}$$

$$\mathcal{S}^{\mathrm{ext}} = \mathcal{V}_0{}^{-1}(\frac{1}{2} - \mathcal{K}_0). \tag{3.41b}$$

Moreover, inserting the Dirichlet-to-Neumann maps defined above in the second equations of (3.37a) and (3.37b) yields an equivalent representation of the Steklov-Poincaré operators,

$$\mathcal{S}^{\mathrm{int}} = \mathcal{W}_0 + (\frac{1}{2} + \mathcal{K}_0')\mathcal{V}_0{}^{-1}(\frac{1}{2} + \mathcal{K}_0), \tag{3.42a}$$

$$\mathcal{S}^{\mathrm{ext}} = \mathcal{W}_0 + (\frac{1}{2} - \mathcal{K}_0')\mathcal{V}_0{}^{-1}(\frac{1}{2} - \mathcal{K}_0). \tag{3.42b}$$

Obviously, the representation above is symmetric because of the symmetry of $\mathcal{V}_0$ and $\mathcal{W}_0$. Moreover, we can also see that the ellipticity of Steklov-Poincaré operators is inherited from the ellipticity of $\mathcal{W}_0$. In particular, it follows that $\mathcal{S}^{\mathrm{int}}$ and $\mathcal{S}^{\mathrm{ext}}$ are $[H^{\frac{1}{2}}(\Gamma)]$-elliptic[2], see (3.25). For further reading, we refer to [31, 109], for instance.

Our analysis requires the ellipticity of the Steklov-Poincaré operators, which is with respect to $\mathcal{S}^{\mathrm{int}}$ only guaranteed for Dirichlet data that are in $[H^{\frac{1}{2}}(\Gamma)]$, as we saw above. Now the question that arises in this case is where do the corresponding Neumann data live? In other words, the dual space of $[H^{\frac{1}{2}}(\Gamma)]$ needs to be specified.

[2]Note that $\mathcal{S}^{\mathrm{ext}}$ is even elliptic on the whole space $H^{\frac{1}{2}}(\Gamma)$, see [26].

Lemma 3.16. *The dual space of* $[H^{\frac{1}{2}}(\Gamma)]$ *can be identified with* $H_\star^{-\frac{1}{2}}(\Gamma)$.

Proof. Let $a \in H(\nabla, \Omega)$ satisfy $\Delta a = 0$ in Ω. Then, with $\gamma_0 a \in H^{\frac{1}{2}}(\Gamma)$, $\gamma_1 a \in H^{-\frac{1}{2}}(\Gamma)$, and ${\mathcal{V}_0}^{-1}\mathcal{K}_0 = \mathcal{K}_0'{\mathcal{V}_0}^{-1}$, see [109, Corollary 6.19], we note that

$$\begin{aligned}\langle \gamma_1 a, 1\rangle_\Gamma = \left\langle \mathcal{V}_0\gamma_1 a, {\mathcal{V}_0}^{-1}1\right\rangle_\Gamma = \left\langle (\frac{1}{2}+\mathcal{K}_0)\gamma_0 a, {\mathcal{V}_0}^{-1}1\right\rangle_\Gamma &= \left\langle \gamma_0 a, (\frac{1}{2}+\mathcal{K}_0')\mathcal{V}_0^{-1}1\right\rangle_\Gamma \\ &= \left\langle \gamma_0 a, \mathcal{V}_0^{-1}(\frac{1}{2}+\mathcal{K}_0)1\right\rangle_\Gamma = 0.\end{aligned}$$

Hence, $\gamma_1 a \in H_\star^{-\frac{1}{2}}(\Gamma)$ with $H_\star^{-\frac{1}{2}}(\Gamma)$ being the subspace of $H^{-\frac{1}{2}}(\Gamma)$ with zero average elements, see (2.69). With this, and by the duality of $H^{\frac{1}{2}}(\Gamma)$ and $H^{-\frac{1}{2}}(\Gamma)$, we obtain a well-defined duality pairing $\langle u, v\rangle_\Gamma$ with $u \in [H^{\frac{1}{2}}(\Gamma)]$ and $v \in H_\star^{-\frac{1}{2}}(\Gamma)$. □

Similar operators can be defined for the vectorial case in our new setting, namely, $[\boldsymbol{H}^{-\frac{1}{2}}(\mathrm{curl}_\Gamma, \Gamma)]$ and $\boldsymbol{H}^{-\frac{1}{2}}(\mathrm{div}_\Gamma\, 0, \Gamma)$ instead of the whole trace spaces. Before proceeding to their introduction, some remarks are due:

Remark 3.17. *By using integration by parts and the definitions of the trace operators* $\boldsymbol{\gamma}_\mathrm{D}$ *and* $\boldsymbol{\gamma}_\mathrm{N}$*, we can verify that their mapping properties transfer to the setting given by* $[\boldsymbol{H}^{-\frac{1}{2}}(\mathrm{curl}_\Gamma, \Gamma)]$ *and* $\boldsymbol{H}^{-\frac{1}{2}}(\mathrm{div}_\Gamma\, 0, \Gamma)$ *with self-evident adaptation. In addition, together with Definition 3.3 and Lemma 3.4 it follows that the BIOs obtained by Definition 3.6 inherit the properties and relations that were established in the previous subsection.*

By using the $\boldsymbol{H}^{-\frac{1}{2}}(\mathrm{div}_\Gamma\, 0, \Gamma)$-ellipticity of $\boldsymbol{\mathcal{A}}_0$, we define analogously the interior and exterior vectorial Steklov-Poincaré operators $\boldsymbol{\mathcal{S}}^{\mathrm{int}}$, $\boldsymbol{\mathcal{S}}^{\mathrm{ext}} : \boldsymbol{H}^{-\frac{1}{2}}(\mathrm{curl}_\Gamma, \Gamma) \to \boldsymbol{H}^{-\frac{1}{2}}(\mathrm{div}_\Gamma\, 0, \Gamma)$ from (3.38a) and (3.39a) by

$$\boldsymbol{\gamma}_\mathrm{N}\, \boldsymbol{u} = {\boldsymbol{\mathcal{A}}_0}^{-1}(\frac{1}{2} - \boldsymbol{\mathcal{C}}_0)\, \boldsymbol{\gamma}_\mathrm{D}\, \boldsymbol{u} := \boldsymbol{\mathcal{S}}^{\mathrm{int}}\, \boldsymbol{\gamma}_\mathrm{D}\, \boldsymbol{u}, \tag{3.43a}$$

$$\boldsymbol{\gamma}_\mathrm{N}^\mathrm{e}\, \boldsymbol{u}^\mathrm{e} := -{\boldsymbol{\mathcal{A}}_0}^{-1}(\frac{1}{2} + \boldsymbol{\mathcal{C}}_0)\, \boldsymbol{\gamma}_\mathrm{D}^\mathrm{e}\, \boldsymbol{u}^\mathrm{e} := -\boldsymbol{\mathcal{S}}^{\mathrm{ext}}\, \boldsymbol{\gamma}_\mathrm{D}^\mathrm{e}\, \boldsymbol{u}^\mathrm{e}. \tag{3.43b}$$

Furthermore, inserting the above definitions of $\boldsymbol{\mathcal{S}}^{\mathrm{int}}$ and $\boldsymbol{\mathcal{S}}^{\mathrm{ext}}$ in (3.38b) and (3.39b) leads to a symmetric representation of the Steklov-Poincaré operators:

$$\boldsymbol{\mathcal{S}}^{\mathrm{int}} = \left(\frac{1}{2} + \boldsymbol{\mathcal{B}}_0\right) {\boldsymbol{\mathcal{A}}_0}^{-1} \left(\frac{1}{2} - \boldsymbol{\mathcal{C}}_0\right) + \boldsymbol{\mathcal{N}}_0, \tag{3.44a}$$

$$\boldsymbol{\mathcal{S}}^{\mathrm{ext}} = \left(\frac{1}{2} - \boldsymbol{\mathcal{B}}_0\right) {\boldsymbol{\mathcal{A}}_0}^{-1} \left(\frac{1}{2} + \boldsymbol{\mathcal{C}}_0\right) + \boldsymbol{\mathcal{N}}_0. \tag{3.44b}$$

An analogous observation as in the scalar case allows us to establish the symmetry of $\boldsymbol{\mathcal{S}}^{\mathrm{int}}$ and $\boldsymbol{\mathcal{S}}^{\mathrm{ext}}$, and to relate the properties of the vectorial Steklov-Poincaré operators to those of the vectorial hyper-singular operator $\boldsymbol{\mathcal{N}}_0$. In particular, we notice that $\boldsymbol{\mathcal{S}}^{\mathrm{int}}$, $\boldsymbol{\mathcal{S}}^{\mathrm{ext}}$ are only positive semi-definite if we consider the entire space $\boldsymbol{H}^{-\frac{1}{2}}(\mathrm{curl}_\Gamma, \Gamma)$, but elliptic in the quotient space $[\boldsymbol{H}^{-\frac{1}{2}}(\mathrm{curl}_\Gamma, \Gamma)]$, see (3.32).

For analysis purposes, the subsequent contractivity results for the double-layer operators play an important role.

Lemma 3.18 (Contractivity of $\mathcal{K}_0$, [110]). *Let $\mathcal{S}^{\text{int}} : H^{\frac{1}{2}}(\Gamma) \to H^{-\frac{1}{2}}(\Gamma)$ be the scalar interior Steklov-Poincaré operator as defined in* (3.41a). *There exists a contraction constant $C_{\mathcal{K}_0} := \frac{1}{2} + \sqrt{\frac{1}{4} - C_{\mathcal{V}_0} C_{\mathcal{W}_0}} \in [\frac{1}{2}, 1)$ such that*

$$\left\| \left(\frac{1}{2} + \mathcal{K}_0 \right) \psi \right\|^2_{\mathcal{V}_0{}^{-1}} \leq C_{\mathcal{K}_0} \left\langle \mathcal{S}^{\text{int}} \psi, \psi \right\rangle_\Gamma, \quad \psi \in H^{\frac{1}{2}}(\Gamma).$$

Thereby, $C_{\mathcal{V}_0}$ and $C_{\mathcal{W}_0}$ are the ellipticity constants given in Theorem 3.9, and $\|\cdot\|_{\mathcal{V}_0{}^{-1}} = \langle \mathcal{V}_0{}^{-1} \cdot, \cdot \rangle_\Gamma^{\frac{1}{2}}$.

In the 3D vectorial case, we prove the existence of a similar result.

Lemma 3.19 (Contractivity of $\boldsymbol{\mathcal{C}}_0$, [43]). *Let $\boldsymbol{\mathcal{S}}^{\text{int}} : [\boldsymbol{H}^{-\frac{1}{2}}(\text{curl}_\Gamma, \Gamma)] \to \boldsymbol{H}^{-\frac{1}{2}}(\text{div}_\Gamma 0, \Gamma)$ be the vectorial interior Steklov-Poincaré operator as defined in* (3.43a). *There exists a contraction constant $C_{\boldsymbol{\mathcal{C}}_0} := \frac{1}{2} + \sqrt{\frac{1}{4} - C_{\boldsymbol{\mathcal{A}}_0} C_{\boldsymbol{\mathcal{N}}_0}} \in [\frac{1}{2}, 1)$ such that*

$$(1 - C_{\boldsymbol{\mathcal{C}}_0}) \|\boldsymbol{\psi}\|_{\boldsymbol{\mathcal{A}}_0{}^{-1}} \leq \left\| \left(\frac{1}{2} - \boldsymbol{\mathcal{C}}_0 \right) \boldsymbol{\psi} \right\|_{\boldsymbol{\mathcal{A}}_0{}^{-1}} \leq C_{\boldsymbol{\mathcal{C}}_0} \|\boldsymbol{\psi}\|_{\boldsymbol{\mathcal{A}}_0{}^{-1}}, \quad \boldsymbol{\psi} \in [\boldsymbol{H}^{-\frac{1}{2}}(\text{curl}_\Gamma, \Gamma)],$$

and

$$\left\| \left(\frac{1}{2} - \boldsymbol{\mathcal{C}}_0 \right) \boldsymbol{\psi} \right\|^2_{\boldsymbol{\mathcal{A}}_0{}^{-1}} \leq C_{\boldsymbol{\mathcal{C}}_0} \left\langle \boldsymbol{\mathcal{S}}^{\text{int}} \boldsymbol{\psi}, \boldsymbol{\psi} \right\rangle_\Gamma, \quad \boldsymbol{\psi} \in [\boldsymbol{H}^{-\frac{1}{2}}(\text{curl}_\Gamma, \Gamma)].$$

Thereby, $C_{\boldsymbol{\mathcal{A}}_0}$ and $C_{\boldsymbol{\mathcal{N}}_0}$ are the ellipticity constants given in Theorem 3.11, and $\|\cdot\|_{\boldsymbol{\mathcal{A}}_0{}^{-1}} = \langle \boldsymbol{\mathcal{A}}_0{}^{-1} \cdot, \cdot \rangle_\Gamma^{\frac{1}{2}}$.

Proof. The first assertion follows analogously to the scalar case in [110]. Using the symmetric representation of the interior Steklov-Poincaré operator, given in (3.44a), together with the $\boldsymbol{H}^{-\frac{1}{2}}(\text{div}_\Gamma 0, \Gamma)$-ellipticity of $\boldsymbol{\mathcal{A}}_0$, it holds

$$\begin{aligned} \left\| \left(\frac{1}{2} - \boldsymbol{\mathcal{C}}_0 \right) \boldsymbol{\psi} \right\|^2_{\boldsymbol{\mathcal{A}}_0{}^{-1}} &= \left\langle \boldsymbol{\mathcal{A}}_0{}^{-1} \left(\frac{1}{2} - \boldsymbol{\mathcal{C}}_0 \right) \boldsymbol{\psi}, \left(\frac{1}{2} - \boldsymbol{\mathcal{C}}_0 \right) \boldsymbol{\psi} \right\rangle_\Gamma \\ &= \left\langle \boldsymbol{\mathcal{S}}^{\text{int}} \boldsymbol{\psi}, \boldsymbol{\psi} \right\rangle_\Gamma - \langle \boldsymbol{\mathcal{N}}_0 \boldsymbol{\psi}, \boldsymbol{\psi} \rangle_\Gamma. \end{aligned} \tag{3.45}$$

Using the same argumentation as in [110, Proposition 5.4], we rely on [100, Theorem 12.33], which states that there exists a self-adjoint square root $\boldsymbol{\mathcal{A}}_0{}^{\frac{1}{2}}$ of $\boldsymbol{\mathcal{A}}_0$, which is also invertible, since $\boldsymbol{\mathcal{A}}_0$ is a self-adjoint, and invertible operator in $\boldsymbol{H}^{-\frac{1}{2}}(\text{div}_\Gamma 0, \Gamma)$. We denote the inverse of the square root operator by $\boldsymbol{\mathcal{A}}_0{}^{-\frac{1}{2}}$. As a consequence, it follows that $\boldsymbol{\mathcal{A}}_0{}^{-\frac{1}{2}} = \boldsymbol{\mathcal{A}}_0{}^{\frac{1}{2}} \boldsymbol{\mathcal{A}}_0{}^{-1}$ and $\left\| \boldsymbol{\mathcal{A}}_0{}^{-\frac{1}{2}} \boldsymbol{v} \right\|_{\boldsymbol{L}^2(\Gamma)} = \|\boldsymbol{v}\|_{\boldsymbol{\mathcal{A}}_0{}^{-1}}$. With this, and following the steps of [110, Theorem 5.1], we get for the first term of the right-hand side of (3.45)

$$\begin{aligned} \left\langle \boldsymbol{\mathcal{S}}^{\text{int}} \boldsymbol{\psi}, \boldsymbol{\psi} \right\rangle_\Gamma &= \left\langle \boldsymbol{\mathcal{A}}_0{}^{-\frac{1}{2}} \boldsymbol{\mathcal{A}}_0 \boldsymbol{\mathcal{S}}^{\text{int}} \boldsymbol{\psi}, \boldsymbol{\mathcal{A}}_0{}^{-\frac{1}{2}} \boldsymbol{\psi} \right\rangle_\Gamma \\ &\leq \left\| \left(\frac{1}{2} - \boldsymbol{\mathcal{C}}_0 \right) \boldsymbol{\psi} \right\|_{\boldsymbol{\mathcal{A}}_0{}^{-1}} \|\boldsymbol{\psi}\|_{\boldsymbol{\mathcal{A}}_0{}^{-1}}, \end{aligned} \tag{3.46}$$

where we used the first identity of $\boldsymbol{\mathcal{S}}^{\text{int}}$ given in (3.43a). For the second term, we need the following result

$$C_{\boldsymbol{\mathcal{A}}_0} \langle \boldsymbol{\mathcal{A}}_0{}^{-1} \boldsymbol{\psi}, \boldsymbol{\psi} \rangle_\Gamma \leq \|\boldsymbol{\psi}\|^2_{\boldsymbol{H}^{-\frac{1}{2}}(\text{curl}_\Gamma, \Gamma)},$$

which can be derived as in [110, Proposition 5.2] by a duality argument, and by making use of the bijectivity of $\boldsymbol{\mathcal{A}}_0$ in $\boldsymbol{H}^{-\frac{1}{2}}(\mathrm{div}_\Gamma\, 0, \Gamma)$. Then, it follows from the $[\boldsymbol{H}^{-\frac{1}{2}}(\mathrm{curl}_\Gamma, \Gamma)]$-ellipticity of $\boldsymbol{\mathcal{N}}_0$ (3.32) that

$$\begin{aligned}\langle \boldsymbol{\mathcal{N}}_0 \boldsymbol{\psi}, \boldsymbol{\psi} \rangle_\Gamma &\geq C_{\boldsymbol{\mathcal{N}}_0} C_{\boldsymbol{\mathcal{A}}_0} \langle {\boldsymbol{\mathcal{A}}_0}^{-1} \boldsymbol{\psi}, \boldsymbol{\psi} \rangle_\Gamma \\ &= C_{\boldsymbol{\mathcal{N}}_0} C_{\boldsymbol{\mathcal{A}}_0} \|\boldsymbol{\psi}\|^2_{{\boldsymbol{\mathcal{A}}_0}^{-1}}.\end{aligned} \tag{3.47}$$

Inserting (3.46) and (3.47) in (3.45), yields

$$\left\| \left(\frac{1}{2} - \boldsymbol{\mathcal{C}}_0 \right) \boldsymbol{\psi} \right\|^2_{{\boldsymbol{\mathcal{A}}_0}^{-1}} \leq \left\| \left(\frac{1}{2} - \boldsymbol{\mathcal{C}}_0 \right) \boldsymbol{\psi} \right\|_{{\boldsymbol{\mathcal{A}}_0}^{-1}} \|\boldsymbol{\psi}\|_{{\boldsymbol{\mathcal{A}}_0}^{-1}} - C_{\boldsymbol{\mathcal{N}}_0} C_{\boldsymbol{\mathcal{A}}_0} \|\boldsymbol{\psi}\|^2_{{\boldsymbol{\mathcal{A}}_0}^{-1}}.$$

Therefore, solving the second order inequality leads to the assertion

$$(1 - C_{\boldsymbol{\mathcal{C}}_0}) \|\boldsymbol{\psi}\|_{{\boldsymbol{\mathcal{A}}_0}^{-1}} \leq \left\| \left(\frac{1}{2} - \boldsymbol{\mathcal{C}}_0 \right) \boldsymbol{\psi} \right\|_{{\boldsymbol{\mathcal{A}}_0}^{-1}} \leq C_{\boldsymbol{\mathcal{C}}_0} \|\boldsymbol{\psi}\|_{{\boldsymbol{\mathcal{A}}_0}^{-1}}$$

with $C_{\boldsymbol{\mathcal{C}}_0} := \frac{1}{2} + \sqrt{\frac{1}{4} - C_{\boldsymbol{\mathcal{A}}_0} C_{\boldsymbol{\mathcal{N}}_0}}$. Moreover, it follows clearly that $C_{\boldsymbol{\mathcal{C}}_0}$ lies in $[\frac{1}{2}, 1)$.
The second assertion follows similarly to [90, Lemma 2.1]. Equation (3.45) reads

$$\left\langle \boldsymbol{\mathcal{S}}^{\mathrm{int}} \boldsymbol{\psi}, \boldsymbol{\psi} \right\rangle_\Gamma = \left\| \left(\frac{1}{2} - \boldsymbol{\mathcal{C}}_0 \right) \boldsymbol{\psi} \right\|^2_{{\boldsymbol{\mathcal{A}}_0}^{-1}} + \langle \boldsymbol{\mathcal{N}}_0 \boldsymbol{\psi}, \boldsymbol{\psi} \rangle_\Gamma. \tag{3.48}$$

The second term of the right-hand side can be estimated by (3.47) and the first assertion. Hence

$$\langle \boldsymbol{\mathcal{N}}_0 \boldsymbol{\psi}, \boldsymbol{\psi} \rangle_\Gamma \geq \frac{C_{\boldsymbol{\mathcal{A}}_0} C_{\boldsymbol{\mathcal{N}}_0}}{C^2_{\boldsymbol{\mathcal{C}}_0}} \left\| \left(\frac{1}{2} - \boldsymbol{\mathcal{C}}_0 \right) \boldsymbol{\psi} \right\|^2_{{\boldsymbol{\mathcal{A}}_0}^{-1}}.$$

By observing that $C_{\boldsymbol{\mathcal{A}}_0} C_{\boldsymbol{\mathcal{N}}_0} = C_{\boldsymbol{\mathcal{C}}_0}(1 - C_{\boldsymbol{\mathcal{C}}_0})$, the assertion follows merely. □

Until now, we introduced the targeted types of model problems that we aim to consider in the interior (Section 3.1) as well as in the exterior domain. The coupling, variational formulations, and analysis of the coupled system is postponed to the next chapters. In the next section, we give an overview on the framework of the discrete setting.

3.3 The isogeometric framework

The goal of this section is providing a discrete counterpart for the energy and trace spaces that are involved in the de Rham complex given in Figure 2.6. For this, we use the framework of Isogeometric Analysis (IGA), which allows the linkage of design to numerical analysis, such that simulations are conducted on the exact geometry, see [32, 65]. Obviously, this avoids meshing errors. In particular, the geometry is not altered by h-refinements, as it can occur for standard finite elements. Moreover, the definition of the basis functions in IGA offers a straightforward way to perform p-refinements, which stands for a refinement with respect to the basis functions' degree. Usually, these basis functions are represented by B-Splines or some of their extensions, such as NURBS, T-Splines etc. In this thesis, we use B-Splines for discretization purposes, and NURBS for geometrical modelling. We refer to [94] for a more extensive introduction to B-Splines, and to [21, 33, 119] for the mathematical analysis and approximation properties of B-Spline spaces that are involved in the

discretization of the de Rham complex.

B-Splines of a specific degree are defined over a parametric domain. In contrast to classical finite elements, the parametric domain is intrinsic to the definition. Hence, refinements and evaluations are performed in there, then mapped to the physical domain. In one dimension, parametric domains can be characterized by a so called knot vector, which is a collection of knots $\Xi := \{\xi_0, \dots, \xi_m\}$ for a certain $m \in \mathbb{N}$ giving rise to a non-decreasing sequence of numbers. In the following, we define a specific type of knot vectors.

Definition 3.20 (p-open knot vector, [33, Section 2])**.** *Let $p \in \mathbb{N}$ be the aimed at degree of the B-Splines. Given $m \geq 2p+1$, the knot vector $\Xi := \{\xi_0, \dots, \xi_m\}$ is said to be p-open if*

$$0 = \xi_0 = \ldots = \xi_p < \xi_{p+1} \leq \ldots \leq \xi_{m-p-1} < \xi_{m-p} = \ldots = \xi_m = 1.$$

Throughout this thesis, we assume that all knot vectors are p-open.
With this, we define B-Splines in one-dimensional (1D) parametric domains.

Definition 3.21 (B-Splines, [33, Section 2])**.** *Given a knot vector $\Xi := \{\xi_0, \dots, \xi_m\}$, let $k := m - p$, with m and p defined as above. Then, the corresponding B-Splines can be computed recursively using the Cox-de-Boor formula, which starts for $p = 0$ with a piecewise constant function*

$$b_i^0(x) = \begin{cases} 1 & \text{if } \xi_i \leq x \leq \xi_{i+1} \\ 0 & \text{otherwise} \end{cases},$$

and proceeds for $p \geq 1$ by

$$b_i^p(x) = \frac{x - \xi_i}{\xi_{i+p} - \xi_i} b_i^{p-1}(x) + \frac{\xi_{i+p+1} - x}{\xi_{i+p+1} - \xi_{i+1}} b_{i+1}^{p-1}(x)$$

for all $i = 0 \dots k-1$. Moreover, note that $k := m - p$, which gives the number of B-Splines, can also be readily obtained from the corresponding knot vector.

Some further remarks are due:

- Let $0 \leq i \leq m$ and let m_i denote the multiplicity of a knot ξ_i. The regularity r_i of the B-Splines at ξ_i is readily obtained from the corresponding multiplicity m_i, and the degree p, namely, $r_i = p - m_i$. Hence, as the name suggests, a p-open knot vector gives rise to B-Splines with $r_i = -1$ at the extremities ξ_0 and ξ_m, i.e., discontinuous. Therefore, by assuming a p-open knot vector, the basis function's degree can be merely determined from the multiplicity of ξ_0 or ξ_m.
- In the context of IGA, one h-refinement step can be in general interpreted as the insertion of a distinct knot in the knot vector Ξ, whereas p-refinement can be reached by elevating the multiplicity of ξ_0 or ξ_m by one. This is showcased for $p = 1$ and $p = 2$ in Figures 3.1a and 3.1c at an h-refinement's level $\ell = 0$, and in Figures 3.1b and 3.1d at $\ell = 1$.

The Definition 3.21 of 1D B-Splines can be merely extended to a d-dimensional domain, in particular to $d = 2, 3$. For this, let $\boldsymbol{\Xi} = \Xi_1 \times \cdots \times \Xi_d$ denote a multidimensional knot vector, which is given by a Cartesian product of p-open knot vectors. Analogously to the 1D case, $\boldsymbol{\Xi}$ induces a vector $\boldsymbol{p} \in \mathbb{N}^d$ that contains the degrees $\{p_i\}_{i=1\dots d}$ in every parametric direction, and a vector $\boldsymbol{k} \in \mathbb{N}^d$ with the corresponding dimensions $\{k_i\}_{i=1\dots d}$ of the space.

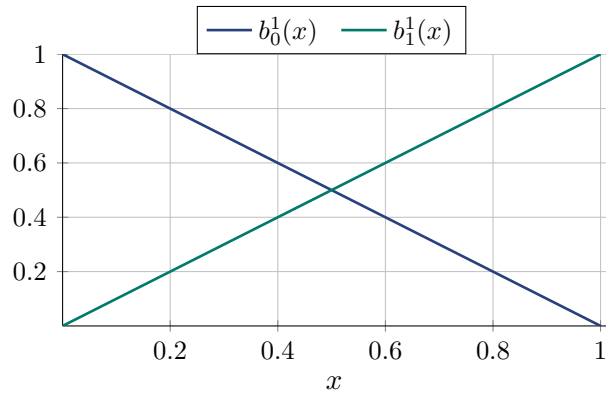

(a) Knot vector $\Xi = (0, 0, 1, 1)$, $p = 1$, $\ell = 0$

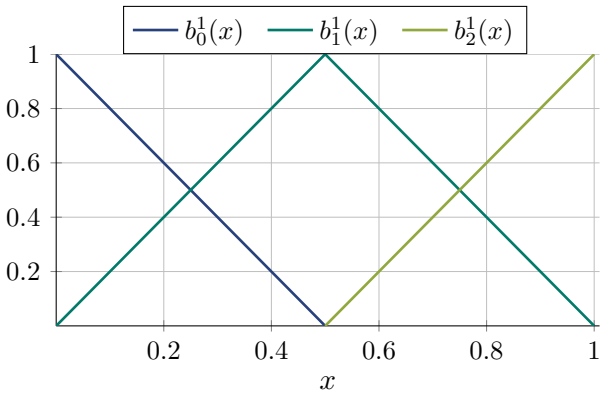

(b) Refined knot vector $\Xi = (0, 0, \frac{1}{2}, 1, 1)$, $p = 1$, $\ell = 1$

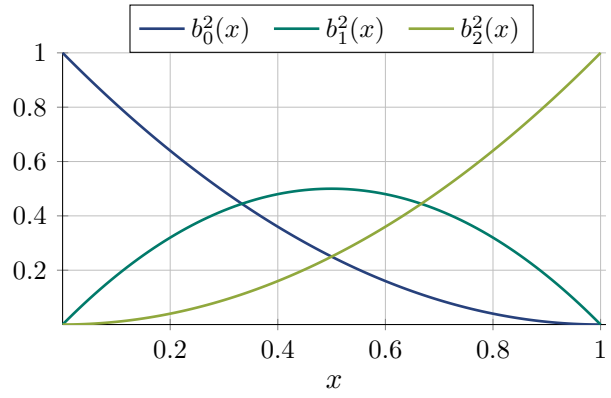

(c) Knot vector $\Xi = (0, 0, 0, 1, 1, 1)$, $p = 2$, $\ell = 0$

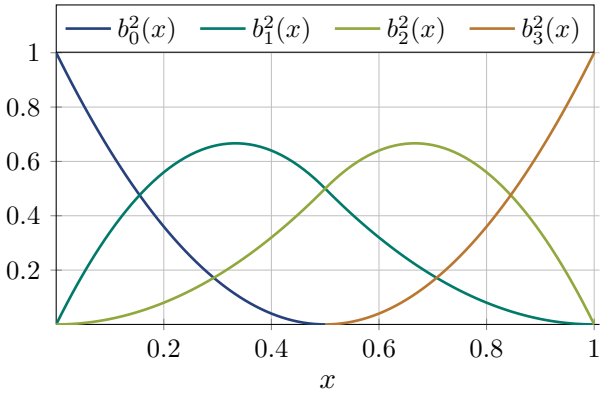

(d) Refined knot vector $\Xi = (0, 0, 0, \frac{1}{2}, 1, 1, 1)$, $p = 2$, $\ell = 1$

Figure 3.1: Examples of B-Splines in a 1D parametric domain with degrees $p = 1$ and $p = 2$, respectively. Thereby, $\ell = 0$ and $\ell = 1$ denote the corresponding refinement level.

Definition 3.22 (B-Spline space in the parametric domain)**.** *A B-Spline space on a d-dimensional parametric domain can be defined as*

$$\mathbb{S}_{\boldsymbol{p}}(\boldsymbol{\Xi}) = \text{span}\,\{b_{\boldsymbol{i}}^{\boldsymbol{p}}\},$$

where $b_{\boldsymbol{i}}^{\boldsymbol{p}} := \prod_{j=1}^{d} \{b_{i_j}^{p_j}\}_{i_j=0\ldots k_j-1}$.

To shorten the notation, we associate to $\boldsymbol{\Xi} = \Xi_1 \times \cdots \times \Xi_d$, $\boldsymbol{p} = \{p_i\}_{i=1\ldots d}$, and $\boldsymbol{k} = \{k_i\}_{i=1\ldots d}$ a multi-index $\boldsymbol{i} \in \boldsymbol{\mathcal{I}} := \{\boldsymbol{i} = (i_1, \ldots, i_d) : i_j = 0, \ldots, k_j - 1 \text{ with } j = 1, \ldots, d\}$, which is interpreted in the sense of Definition 3.22. With this we define NURBS basis functions as follows

$$r_{\boldsymbol{i}}^{\boldsymbol{p}}(\boldsymbol{x}) := \frac{w_{\boldsymbol{i}} b_{\boldsymbol{i}}^{\boldsymbol{p}}(\boldsymbol{x})}{\sum_{\boldsymbol{j}\in\boldsymbol{\mathcal{I}}} w_{\boldsymbol{j}} b_{\boldsymbol{j}}^{\boldsymbol{p}}(\boldsymbol{x})}, \tag{3.49}$$

where $\boldsymbol{i} \in \boldsymbol{\mathcal{I}}$, and $w_{\boldsymbol{i}}$ is a set of weighting functions. For more details about NURBS, we refer to [32, 94]. In this thesis, NURBS are only utilized for design purposes. The reason behind this choice will be explained below.

Next, we introduce the derivative of a B-Spline space. Let $\boldsymbol{x} = \{x_i\}_{i=1,\dots,d} \in \mathbb{R}^d$. We know from [33, Section 5.2] that the derivative of $\mathbb{S}_{\boldsymbol{p}}(\boldsymbol{\Xi})$ with respect to x_i consists of B-Splines with a reduced knot vector in the i-th component in the following sense,

$$\frac{\partial}{\partial x_i}\mathbb{S}_{\boldsymbol{p}}(\boldsymbol{\Xi}) = \frac{\partial}{\partial x_i}\mathbb{S}_{(p_1,\dots,p_i,\dots,p_d)}(\Xi_1,\dots,\Xi_i,\dots,\Xi_d) = \mathbb{S}_{(p_1,\dots,p_i-1,\dots,p_d)}(\Xi_1,\dots,\Xi_i',\dots,\Xi_d),$$

where $\Xi_i' = \{\xi_1,\dots,\xi_{m-1}\}$. Let $\boldsymbol{\Xi}$ represent a 3D parametric domain. Again from [33, Section 5.2], we know that the following B-Spline spaces

$$\begin{aligned}
\mathbb{S}^0_{\boldsymbol{p}}(\boldsymbol{\Xi}) &= \mathbb{S}_{(p_1,p_2,p_3)}(\Xi_1,\Xi_2,\Xi_3),\\
\mathbb{S}^1_{\boldsymbol{p}}(\boldsymbol{\Xi}) &= \mathbb{S}_{(p_1-1,p_2,p_3)}(\Xi_1',\Xi_2,\Xi_3)\times\mathbb{S}_{(p_1,p_2-1,p_3)}(\Xi_1,\Xi_2',\Xi_3)\times\mathbb{S}_{(p_1,p_2,p_3-1)}(\Xi_1,\Xi_2,\Xi_3'),\\
\mathbb{S}^2_{\boldsymbol{p}}(\boldsymbol{\Xi}) &= \mathbb{S}_{(p_1,p_2-1,p_3-1)}(\Xi_1,\Xi_2',\Xi_3')\times\mathbb{S}_{(p_1-1,p_2,p_3-1)}(\Xi_1',\Xi_2,\Xi_3')\times\mathbb{S}_{(p_1-1,p_2-1,p_3)}(\Xi_1',\Xi_2',\Xi_3),\\
\mathbb{S}^3_{\boldsymbol{p}}(\boldsymbol{\Xi}) &= \mathbb{S}_{(p_1-1,p_2-1,p_3-1)}(\Xi_1',\Xi_2',\Xi_3')
\end{aligned} \tag{3.50}$$

form a sequence with respect to the differential operators ∇, **curl**, and div, which is analogous to the continuous case, namely,

$$\mathbb{S}^0_{\boldsymbol{p}}(\boldsymbol{\Xi}) \xrightarrow{\nabla} \mathbb{S}^1_{\boldsymbol{p}}(\boldsymbol{\Xi}) \xrightarrow{\textbf{curl}} \mathbb{S}^2_{\boldsymbol{p}}(\boldsymbol{\Xi}) \xrightarrow{\text{div}} \mathbb{S}^3_{\boldsymbol{p}}(\boldsymbol{\Xi}). \tag{3.51}$$

For the spaces to be relevant for numerical methods, it is necessary to find suitable invertible mappings that permit the transfer of the basis functions from the parameter to the physical domain, and vice versa. These are known as pull-backs and push-forwards. Before we get to a concrete characterization, let us first specify the representation in the physical space. We focus on the 3D case, and note that an analogous representation holds for 2D problems with self-evident adaptations.

Definition 3.23 (Multipatch domain)**.** *Let K be a compact, orientable manifold of dimension $d = 1, 2, 3$, which is embedded in a 3D Euclidean space. Moreover, let us assume that there exists a regular tessellation*

$$K = \bigcup_{l=0}^{N_\kappa-1} \overline{\kappa}_l$$

with κ_l open, such that for all $l_1, l_2 = 0,\dots,N_\kappa-1$, $l_1 \neq l_2$, $\kappa_{l_1} \cap \kappa_{l_2}$ is empty, and that $\{\kappa_l\}_{l=0,\dots,N_\kappa-1}$ is given by a family of diffeomorphisms $\{\boldsymbol{f}_l : [0,1]^d \to \kappa_l\}_{l=0,\dots,N_\kappa-1}$. In this case, we call κ_l a patch. Furthermore, at all patch interfaces, i.e., for all $l_1 \neq l_2$ with $\partial\kappa_{l_1} \cap \partial\kappa_{l_2} \neq \emptyset$, we require the corresponding parametrizations to coincide (up to orientation). This yields $\boldsymbol{p}$ and $\boldsymbol{\Xi}$ to coincide on every patch interface, which either consists of a common surface or edge, or reduces to a single common point. Under these considerations, K is called a multipatch domain.

Definition 3.24 (Elements and mesh size)**.** *Let $\Xi = \{\xi_0,\dots,\xi_m\}$ be a p-open knot vector. A patch element in the parameter domain is defined as $[\xi_i, \xi_{i+1}]$ for some $0 \le i < m$ that satisfies $\xi_i \neq \xi_{i+1}$. The local mesh size is defined as the length of an element, i.e., $h_i = \xi_{i+1} - \xi_i$. Furthermore, we denote by $h_{\mathrm{p}} = \max_{0\le i<m} h_i$ the global mesh size of a single patch. Equivalently, h denotes the largest local mesh size of all patches for a multipatch domain.*

Assumption 3.25. *Henceforth, we assume the following:*

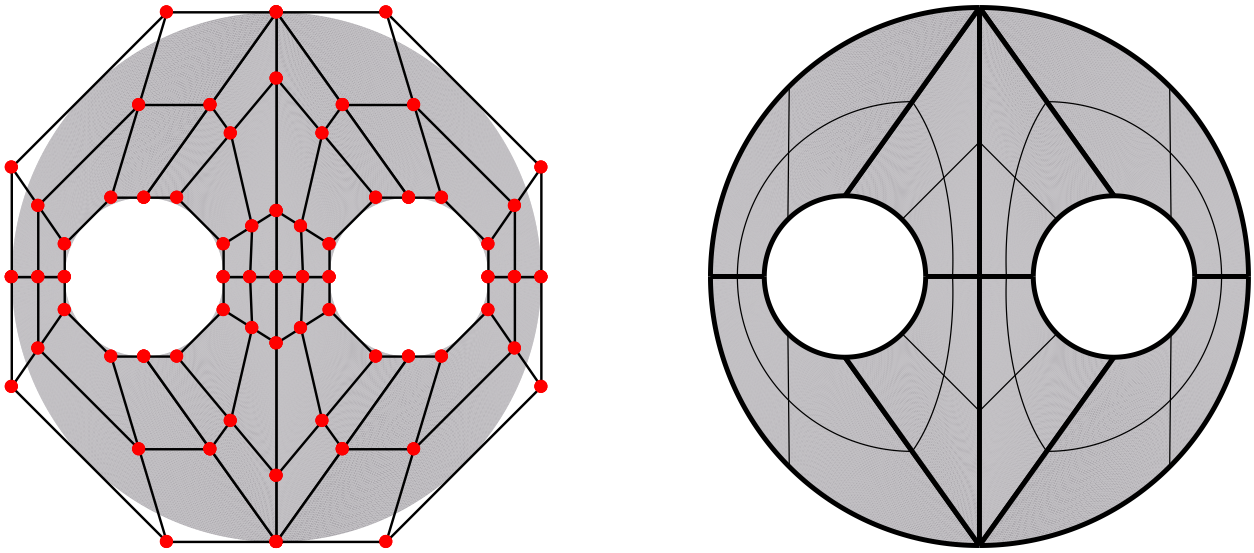

(a) Control polygon (black lines) linking the control points (red dots).

(b) The patches and the elements in each patch are delimited by the bold and thin lines, respectively.

Figure 3.2: An example of a 2D multipatch NURBS representation of a geometry using eight patches, each described by the knot vector $\boldsymbol{\Xi} = \{0,0,0,\frac{1}{2},1,1,1\} \times \{0,0,0,\frac{1}{2},1,1,1\}$.

- *All knot vectors are locally quasi-uniform, i.e., for all non-empty elements* $[\xi_{i_1}, \xi_{i_1+1}]$ *and* $[\xi_{i_2}, \xi_{i_2+1}]$*, there exists* $C_\theta \geq 1$*, such that*
$$C_\theta^{-1} \leq h_{i_1} h_{i_2}^{-1} \leq C_\theta.$$
- *The multipatch geometry of* Ω *is generated by a family of regular, smooth parameterizations.*

In the context of IGA, the parametrizations $\{\boldsymbol{f}_l\}_{l=0,\dots,N_\kappa-1}$ from the previous definition are given in terms of B-Spline basis functions (or an extension of B-Splines, e.g., NURBS). For instance, we formally have

$$\boldsymbol{f}_l(\boldsymbol{x}) = \sum_{\boldsymbol{i} \in \boldsymbol{\mathcal{I}}_l} \boldsymbol{c_i} b_{\boldsymbol{i}}^{\boldsymbol{p}}(\boldsymbol{x}), \tag{3.52}$$

where $\boldsymbol{\mathcal{I}}_l$ denotes the set of multi-indices corresponding to the patch with index l, and $\boldsymbol{c_i} \in \mathbb{R}^3$ are elements of a set of control points, which have to be specified by the user to obtain a certain form, see [94] for more details about the concrete computation of the suitable control points. That is, changing the position of a control point affects the shape of the geometry locally. Nevertheless, conic sections cannot be represented exactly when using B-Splines as basis functions. A remedy to this is provided, e.g., by NURBS [94]. Formally, to obtain a NURBS parametrization, we replace $b_{\boldsymbol{i}}^{\boldsymbol{p}}(\boldsymbol{x})$ in (3.52) by $r_{\boldsymbol{i}}^{\boldsymbol{p}}(\boldsymbol{x})$. As an example, let us consider Figure 3.2. To reach the represented geometry, we chose a set of control points, which form a control polygon, as depicted in Figure 3.2a. In addition, we employed NURBS basis functions of degree $\boldsymbol{p} = \{2,2\}$ at a level of refinement $\ell = 1$, i.e., with $\boldsymbol{\Xi} = \{0,0,0,\frac{1}{2},1,1,1\} \times \{0,0,0,\frac{1}{2},1,1,1\}$ in each of the eight patches visualized in Figure 3.2b by the bold lines. Besides the control points, a NURBS parametrization allows more control on the local shape than a parametrization with B-Splines due to the additional degrees of freedom consisting in the weighting functions. For this reason, NURBS parametrizations are widely considered in common CAD softwares for the modelling of free-form and sculptured surfaces; in short, most technical geometries. In the underlined

example, the weighting functions in each patch read $w_{\boldsymbol{j}} = \{1, \frac{1}{4}(2+\sqrt{2}), \frac{1}{4}(2+\sqrt{2}), 1\} \times \{1, \frac{1}{4}(2+\sqrt{2}), \frac{1}{4}(2+\sqrt{2}), 1\}$. However, because of these weighting functions in the denominator $\sum_{\boldsymbol{j}\in\boldsymbol{\mathcal{I}}} w_{\boldsymbol{j}} b_{\boldsymbol{j}}^{\boldsymbol{p}}(\boldsymbol{x})$, multivariate NURBS spaces cannot be simply constructed by means of tensor products, which is a central property used for the definition of our ansatz spaces. This explains the motivation behind resorting to B-Spline spaces for the discretization of the de Rham complex.

Remark 3.26. *Using B-Splines for discretization and NURBS for design violates one of main claims of IGA, which consists in using the same basis functions in both steps. Nevertheless, by observing the definition of NURBS* (3.49)*, we see that B-Splines can be interpreted as NURBS, which are defined on the hyperplane corresponding to* $(w_i)_{i=0,\dots,k-1} = 1$*. This can be seen from the fact that B-Splines form a partition of unity, see [94]. Therefore, we choose to keep labeling the presented couplings isogeometric.*

The required parametric mappings are given by the following push-forwards

$$\iota_0^{-1}(\boldsymbol{f}_l)(v) := v \circ \boldsymbol{f}_l^{-1}, \tag{3.53a}$$
$$\iota_1^{-1}(\boldsymbol{f}_l)(\boldsymbol{v}) := (\,\mathrm{d}\boldsymbol{f}_l^{\top})^{-1}(\boldsymbol{v} \circ \boldsymbol{f}_l^{-1}), \tag{3.53b}$$
$$\iota_2^{-1}(\boldsymbol{f}_l)(\boldsymbol{v}) := \frac{(\,\mathrm{d}\boldsymbol{f}_l)(\boldsymbol{v} \circ \boldsymbol{f}_l^{-1})}{\det(\,\mathrm{d}\boldsymbol{f}_l)}, \tag{3.53c}$$
$$\iota_3^{-1}(\boldsymbol{f}_l)(v) := \frac{v \circ \boldsymbol{f}_l^{-1}}{\det(\,\mathrm{d}\boldsymbol{f}_l)}, \tag{3.53d}$$

where $\mathrm{d}\boldsymbol{f}_l$ denotes the Jacobian of $\boldsymbol{f}_l$, and ι_j, $j = 0, 1, 2, 3$, are the corresponding inverse mappings, called pull-backs. Indeed, the application of ι_0, ι_1, and ι_2 preserves the differential operators ∇, **curl**, and div, respectively, see [33, Section 5.1]. With this, the equivalent B-Spline spaces on a particular patch Ω_l can be merely defined by,

$$\mathbb{S}^0_{\boldsymbol{p}}(\Omega_l) = \{v : v = \iota_0^{-1}(\boldsymbol{f}_l)(u), u \in \mathbb{S}^0_{\boldsymbol{p}}(\boldsymbol{\Xi})\}, \tag{3.54a}$$
$$\mathbb{S}^1_{\boldsymbol{p}}(\Omega_l) = \{\boldsymbol{v} : \boldsymbol{v} = \iota_1^{-1}(\boldsymbol{f}_l)(\boldsymbol{u}), \boldsymbol{u} \in \mathbb{S}^1_{\boldsymbol{p}}(\boldsymbol{\Xi})\}, \tag{3.54b}$$
$$\mathbb{S}^2_{\boldsymbol{p}}(\Omega_l) = \{\boldsymbol{v} : \boldsymbol{v} = \iota_2^{-1}(\boldsymbol{f}_l)(\boldsymbol{u}), \boldsymbol{u} \in \mathbb{S}^2_{\boldsymbol{p}}(\boldsymbol{\Xi})\}, \tag{3.54c}$$
$$\mathbb{S}^3_{\boldsymbol{p}}(\Omega_l) = \{v : v = \iota_3^{-1}(\boldsymbol{f}_l)(u), u \in \mathbb{S}^3_{\boldsymbol{p}}(\boldsymbol{\Xi})\}. \tag{3.54d}$$

Due to the properties of the pull-backs, we obtain a commutative diagram relating the B-Spline spaces in the parametric domains to the ones above with respect to the pull-backs, see [60, Section 2.2].
Then, we address the above discrete spaces in a multipatch setting. In accordance to Definition 3.23, we define the following global B-Spline spaces in a physical domain $K = \Omega \subset \mathbb{R}^3$ by

$$\begin{aligned}
\mathbb{S}^0_{\boldsymbol{p}}(\Omega) &= \{v \in H(\nabla, \Omega) : v_{|\kappa_l} \in \mathbb{S}^0_{\boldsymbol{p}}(\kappa_l),\ \forall\, 0 \le l < N_\kappa\},\\
\mathbb{S}^1_{\boldsymbol{p}}(\Omega) &= \{\boldsymbol{v} \in \boldsymbol{H}(\mathbf{curl}, \Omega) : \boldsymbol{v}_{|\kappa_l} \in \mathbb{S}^1_{\boldsymbol{p}}(\kappa_l),\ \forall\, 0 \le l < N_\kappa\},\\
\mathbb{S}^2_{\boldsymbol{p}}(\Omega) &= \{\boldsymbol{v} \in \boldsymbol{H}(\mathrm{div}, \Omega) : \boldsymbol{v}_{|\kappa_l} \in \mathbb{S}^2_{\boldsymbol{p}}(\kappa_l),\ \forall\, 0 \le l < N_\kappa\},\\
\mathbb{S}^3_{\boldsymbol{p}}(\Omega) &= \{v \in L^2(\Omega) : v_{|\kappa_l} \in \mathbb{S}^3_{\boldsymbol{p}}(\kappa_l),\ \forall\, 0 \le l < N_\kappa\},
\end{aligned} \tag{3.55}$$

where Ω_l denotes a patch, and N_κ the number of patches. With this definition, the sequence (3.51) holds.

If we consider $K = \partial\Omega := \Gamma$ to be a 2D manifold, which is constructed according to Definition 3.23, a first possibility to obtain the corresponding global B-Spline spaces can be reached by squeezing the third

dimension in (3.50), i.e., by removing Ξ_3 and the corresponding dimension p_3, together with the third terms in $\mathbb{S}^1_{\boldsymbol{p}}(\boldsymbol{\Xi})$ and $\mathbb{S}^2_{\boldsymbol{p}}(\boldsymbol{\Xi})$. Henceforth, we denote by $\widetilde{\boldsymbol{p}}$ and $\widetilde{\boldsymbol{\Xi}}$ the reduced vector of degrees and the reduced knot vector, respectively. This way, we obtain

$$\begin{aligned}
\mathbb{S}^0_{\widetilde{\boldsymbol{p}}}(\widetilde{\boldsymbol{\Xi}}) &= \mathbb{S}_{(p_1,p_2)}(\Xi_1,\Xi_2),\\
\mathbb{S}^{1,\parallel}_{\widetilde{\boldsymbol{p}}}(\widetilde{\boldsymbol{\Xi}}) &= \mathbb{S}_{(p_1-1,p_2)}(\Xi'_1,\Xi_2)\times\mathbb{S}_{(p_1,p_2-1)}(\Xi_1,\Xi'_2),\\
\mathbb{S}^{1,\perp}_{\widetilde{\boldsymbol{p}}}(\widetilde{\boldsymbol{\Xi}}) &= \mathbb{S}_{(p_1,p_2-1)}(\Xi_1,\Xi'_2)\times\mathbb{S}_{(p_1-1,p_2)}(\Xi'_1,\Xi_2),\\
\mathbb{S}^2_{\widetilde{\boldsymbol{p}}}(\widetilde{\boldsymbol{\Xi}}) &= \mathbb{S}_{(p_1-1,p_2-1)}(\Xi'_1,\Xi'_2).
\end{aligned} \tag{3.56}$$

For some boundary patch $\kappa_l \subset \Gamma$, applying the corresponding push-forwards (3.53) to (3.56) yields $\mathbb{S}^0_{\widetilde{\boldsymbol{p}}}(\kappa_l)$, $\mathbb{S}^{1,\parallel}_{\widetilde{\boldsymbol{p}}}(\kappa_l)$, $\mathbb{S}^{1,\perp}_{\widetilde{\boldsymbol{p}}}(\kappa_l)$, and $\mathbb{S}^2_{\widetilde{\boldsymbol{p}}}(\kappa_l)$ equivalently to (3.54). In a multipatch setting in the sense of Definition 3.23, we define with $K=\Gamma$

$$\begin{aligned}
\mathbb{S}^0_{\widetilde{\boldsymbol{p}}}(\Gamma) &= \{\psi\in H^{\frac{1}{2}}(\Gamma) : \psi_{|\kappa_l}\in\mathbb{S}^0_{\widetilde{\boldsymbol{p}}}(\kappa_l),\ \forall\, 0\le l<N_\kappa\},\\
\mathbb{S}^{1,\parallel}_{\widetilde{\boldsymbol{p}}}(\Gamma) &= \{\boldsymbol{\psi}\in\boldsymbol{H}^{-\frac{1}{2}}(\mathrm{curl}_\Gamma,\Gamma) : \boldsymbol{\psi}_{|\kappa_l}\in\mathbb{S}^{1,\parallel}_{\widetilde{\boldsymbol{p}}}(\kappa_l),\ \forall\, 0\le l<N_\kappa\},\\
\mathbb{S}^{1,\perp}_{\widetilde{\boldsymbol{p}}}(\Gamma) &= \{\boldsymbol{\psi}\in\boldsymbol{H}^{-\frac{1}{2}}(\mathrm{div}_\Gamma,\Gamma) : \boldsymbol{\psi}_{|\kappa_l}\in\mathbb{S}^{1,\perp}_{\widetilde{\boldsymbol{p}}}(\kappa_l),\ \forall\, 0\le l<N_\kappa\},\\
\mathbb{S}^2_{\widetilde{\boldsymbol{p}}}(\Gamma) &= \{\psi\in H^{-\frac{1}{2}}(\Gamma) : \psi_{|\kappa_l}\in\mathbb{S}^2_{\widetilde{\boldsymbol{p}}}(\kappa_l),\ \forall\, 0\le l<N_\kappa\},
\end{aligned} \tag{3.57}$$

see [21, 119].

Remark 3.27. *An alternative definition can be obtained via the application of the appropriate trace operators to* (3.55)*, namely,* $\gamma_0 : H(\nabla,\Omega)\to H^{\frac{1}{2}}(\Gamma)$*,* $\boldsymbol{\gamma}_{\mathrm{D}} : \boldsymbol{H}(\mathbf{curl},\Omega)\to\boldsymbol{H}^{-\frac{1}{2}}(\mathrm{curl}_\Gamma,\Gamma)$*,* $\boldsymbol{\gamma}_\times : \boldsymbol{H}(\mathbf{curl},\Omega)\to\boldsymbol{H}^{-\frac{1}{2}}(\mathrm{div}_\Gamma,\Gamma)$*, and* $\gamma_{\boldsymbol{n}} : \boldsymbol{H}(\mathrm{div},\Omega)\to H^{-\frac{1}{2}}(\Gamma)$*, which we defined in Section 2.3. We note that both cases yield equivalent spaces [21, 119].*

Thereby, note that $\mathbb{S}^{1,\parallel}_{\widetilde{\boldsymbol{p}}}(\Gamma)$ and $\mathbb{S}^{1,\perp}_{\widetilde{\boldsymbol{p}}}(\Gamma)$ are both trace spaces of $\mathbb{S}^1_{\boldsymbol{p}}(\Omega)$. This follows from the fact that the trace operators $\boldsymbol{\gamma}_\times$ and $\boldsymbol{\gamma}_{\mathrm{D}}$ act both on vector fields in $\boldsymbol{H}(\mathbf{curl},\Omega)$. It is shown in [21, 119] that the B-Spline spaces given above are also related with respect to the surface differential operators and form a sequence, which is understood similarly to the continuous case, illustrated with Figure 2.6. Altogether, a full discretization of the de Rham complex using conforming B-Spline spaces is depicted in Figure 3.3. Of particular interest is the definition of a discrete counterpart of $\boldsymbol{H}^{-\frac{1}{2}}(\mathrm{div}_\Gamma\, 0,\Gamma)$. Let $\mathbb{S}^{1,\perp}_{\widetilde{\boldsymbol{p}},0}(\Gamma)$ be the subspace of $\mathbb{S}^{1,\perp}_{\widetilde{\boldsymbol{p}}}(\Gamma)$ that contains solenoidal surface divergence conforming B-Splines, i.e.,

$$\mathbb{S}^{1,\perp}_{\widetilde{\boldsymbol{p}},0}(\Gamma) = \{\boldsymbol{\psi}\in\mathbb{S}^{1,\perp}_{\widetilde{\boldsymbol{p}}}(\Gamma) : \mathrm{div}_\Gamma\,\boldsymbol{\psi}=0\}.$$

Similarly to [61] and in complete analogy to the continuous setting, see Theorem 2.32, this subspace can be characterized by exploiting the properties of the discrete de Rham complex. This yields the following orthogonal decomposition

$$\mathbb{S}^{1,\perp}_{\widetilde{\boldsymbol{p}},0}(\Gamma) = \mathbf{curl}_\Gamma\,\mathbb{S}^0_{\widetilde{\boldsymbol{p}}}(\Gamma) + \mathbb{H}_{1,\ell}(\Gamma),\quad \dim\mathbb{H}_{1,\ell}=\beta_1(\Gamma), \tag{3.58}$$

where $\mathbb{H}_{1,\ell}(\Gamma)$ is the discrete first surface cohomology space, whose dimension $\beta_1(\Gamma)$ corresponds to the first Betti number of Γ, and $\ell\ge 0$ is the refinement level. We refer the reader to [63] for a concrete construction of the needed bases for $\mathbb{H}_{1,\ell}(\Gamma)$.

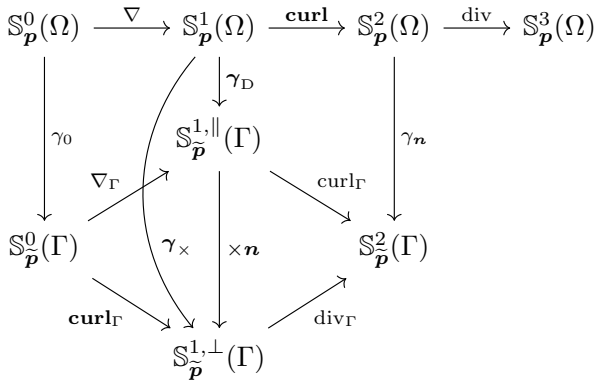

Figure 3.3: Conforming discretization of the de Rham complex of Figure 2.6 using B-Spline spaces.

Remark 3.28. *In the case of a trivial topology, the characterization* (3.58) *reduces to* $\mathbb{S}^{1,\perp}_{\widetilde{\boldsymbol{p}},0}(\Gamma) = \mathbf{curl}_\Gamma\, \mathbb{S}^0_{\widetilde{\boldsymbol{p}}}(\Gamma)$.

Analogously, a similar complex as in Figure 3.3 starting from a 2D domain can be derived. We refer the interested reader, e.g., to [21, 119] and the literature cited therein. In this thesis, we need only a discretization of $H(\nabla,\Omega)$ and $H^{-\frac{1}{2}}(\Gamma)$ in 2D problems. For convenience, they read

$$\mathbb{S}^0_{\boldsymbol{p}}(\Omega) = \{v \in H(\nabla,\Omega) : v_{|\kappa_l} \in \mathbb{S}^0_{\boldsymbol{p}}(\kappa_l),\, \forall\, 0 \leq l < N_\kappa\}, \tag{3.59a}$$

$$\mathbb{S}^2_{\widetilde{p}}(\Gamma) = \{\psi \in H^{-\frac{1}{2}}(\Gamma) : \psi_{|\kappa_l} \in \mathbb{S}^2_{\widetilde{p}}(\kappa_l),\, \forall\, 0 \leq l < N_\kappa\}. \tag{3.59b}$$

Thereby, and in accordance to the 3D case, $\widetilde{p} = p - 1$. Moreover, note that κ refers to a domain patch in (3.59a), and to a boundary patch in (3.59b), i.e., with K from Definition 3.23 corresponding to Ω and Γ, respectively.

With this, we close the section as well as the chapter. In the next one, we proceed to the derivation and analysis of the Johnson-Nédélec coupling for some relevant model problems in the continuous and discrete Galerkin setting in the isogeometric context.

4 The direct non-symmetric couplings

> The only way to learn mathematics is to do mathematics.
>
> P. Halmos

Starting from the equations given in Chapter 3, we can readily derive several interface problems. As mentioned throughout this thesis, we consider a coupling of the Finite Element Method (FEM) with a Boundary Element Method (BEM). The weak formulations with respect to the interior domains, which are associated to possibly non-linear Partial Differential Equations (PDEs) are obtained in a standard way by testing the equation, integrating, and applying a suitable Green's identity. For exterior domains, which are exclusively filled with linear materials, the corresponding equations in the domain are transferred onto the interface and represented via some Boundary Integral Equations (BIEs), according to Subsection 3.2.1. The choice of the BIEs depends on the specific coupling strategy. On one hand, we differentiate between symmetric and non-symmetric couplings. The former utilize both BIEs, whereas the latter employ only one. On the other hand, we have direct and indirect approaches. The unknowns in the direct formulation correspond to the Cauchy data, thus, they have a physical interpretation and can be used directly to compute derived quantities. However, indirect approaches rely on a potential ansatz, which requires the resolution of an additional system to obtain physically meaningful quantities. We refer to [9, 30, 69] for the original papers, and for instance to [6] for an overview on the mentioned coupling techniques and a historical development of their mathematical background. For completeness, we also refer the reader to [45] for an additional strategy, known as the three field coupling. In this thesis, we opt for a direct non-symmetric coupling, which is also named after the authors of [69] the Johnson-Nédélec coupling. In contrast to (direct) symmetric couplings, the approach of Johnson and Nédélec uses only one BIE, which involves two Boundary Integral Operators (BIOs) versus four when both BIEs are considered. Moreover, by keeping in mind the application's field of our method, namely, a multi-physics problem, which is coupled to a mechanical subsystem via forces or torques, it is more reasonable to favor a direct method over indirect ones. Note that a complete mathematical analysis on Lipschitz domains for the Johnson-Nédélec coupling has only been known for about ten years, starting with the seminal work of Sayas [104].

In this chapter, we study some relevant and standard model problems. A good starting point is the Laplacian interface problem. In Section 4.1, we show the well-posedness by extending the results of [46] to non-linear operators. In particular, we consider the framework of Lipschitz continuous and strongly monotone operators, as employed in [6]. The theory behind this framework is provided extensively in [122]. Moreover, we provide a stability result for a specific practice-oriented type of non-linear materials, see Definition 1.1. The problem is discretized by means of suitable B-Spline spaces with a conforming Galerkin method, such that well-posedness can be transmitted to the discrete setting, and that a Céa-type quasi-optimality can be merely stated. Based on this, we derive a priori error estimates with respect to h-refinements. Thereby, we use the approximation results for B-Spline spaces and their traces that are furnished in [21, 33]. The content of this section is already published in [42]. These results facilitate an extension of the analysis to the parabolic

case. In the linear case, a complete analysis of the non-symmetric FEM-BEM coupling is provided in [41]. To adapt these results to our non-linear case, we consider the framework of monotone equations, see [122]. This is the subject of Section 4.2. As a more concrete model problem for the simulation of electric machines, see Figure 1.4, for instance, we derive in Section 4.3 an adapted variational formulation for this purpose, and analyze the direct non-symmetric coupling by using similar tools. Furthermore, we study the behavior of the solution in the BEM domain, and notice an amelioration of the convergence rates, which may double under certain circumstances. This behavior is known as super-convergence, and it is indeed advantageous considering the fact that forces and torques are evaluated in this domain. This has also been published in [42]. As a last model problem, we address the three-dimensional (3D) case in Section 4.4. In particular, we restrict ourselves to the magnetostatic regime for convenience. Note however that an extension to the parabolic case or to a similar Boundary Value Problem (BVP) for the simulation of electric machines can be conducted similarly to Section 4.2 and Section 4.3, respectively. We formulate the 3D problem in suitable quotient spaces to rule out the difficulty caused by the infinite dimensional kernel of the **curl** operator, then proceed analogously to the two-dimensional (2D) case. This is made possible by the contractivity result of Lemma 3.19, and a Friedrichs' inequality, which provides an equivalent norm in $\boldsymbol{H}(\mathbf{curl}, \Omega)$. The latter can be found in [88], for instance, in a slightly different form, which is however easily adapted to the quotient space formulation. The results of Section 4.4 are already published in [43].

4.1 The two-dimensional (2D) elliptic-elliptic interface problem

Let $\Omega \subset \mathbb{R}^2$ be a bounded domain with Lipschitz boundary $\Gamma = \partial\Omega$, and let $\Omega^{\mathrm{e}} := \mathbb{R}^2 \backslash \overline{\Omega}$ be the corresponding exterior domain. Furthermore, motivated by Theorem 3.9, we assume that $\operatorname{diam}(\Omega) < 1$ to ensure the $H^{-\frac{1}{2}}(\Gamma)$-ellipticity of the boundary integral operator $\mathcal{V}_0$. A suitable model problem can be obtained by coupling the corresponding equations of the interior and exterior problems, which are given by (3.11) and (3.13), respectively. As pointed out in Chapter 3, the coupling is performed via the jump conditions of the Cauchy data $(\llbracket \gamma_0 u \rrbracket_\Gamma, \llbracket \gamma_1^{\mathcal{U}} u \rrbracket_\Gamma)$.

We consider the following interface problem (in a weak sense):

Problem 4.1 (Classical problem)**.** *Find* $(u, u^{\mathrm{e}}) \in H(\nabla, \Omega) \times H_{\mathrm{loc}}(\nabla, \Omega^{\mathrm{e}})$ *such that*

$$
\begin{aligned}
-\operatorname{div}(\mathcal{U}\nabla u) &= f && \text{in } \Omega, && (4.1a)\\
-\Delta u^{\mathrm{e}} &= 0 && \text{in } \Omega^{\mathrm{e}}, && (4.1b)\\
\llbracket \gamma_0 u \rrbracket_\Gamma := \gamma_0 u - \gamma_0^{\mathrm{e}} u^{\mathrm{e}} &= \widehat{u} && \text{on } \Gamma, && (4.1c)\\
\llbracket \gamma_1^{\mathcal{U}} u \rrbracket_\Gamma := \gamma_1^{\mathcal{U}} u - \gamma_1^{\mathrm{e}} u^{\mathrm{e}} &= \widehat{\phi} && \text{on } \Gamma, && (4.1d)\\
u^{\mathrm{e}} &= C_\infty \log|\boldsymbol{x}| + \mathcal{O}\left(|\boldsymbol{x}|^{-1}\right) && \text{for } |\boldsymbol{x}| \to \infty && (4.1e)
\end{aligned}
$$

with $(f, \widehat{u}, \widehat{\phi}) \in H(\nabla, \Omega)' \times H^{\frac{1}{2}}(\Gamma) \times H^{-\frac{1}{2}}(\Gamma)$.

Furthermore, the following remarks are due:

- For the sake of a more general analysis, we allow both $\widehat{u} \neq 0$ and $\widehat{\phi} \neq 0$. Moreover, if not stated otherwise, the non-linear operator $\mathcal{U}$ is assumed to be strongly monotone and Lipschitz continuous according to Assumption 2.13 .

- In contrast to (3.11), we seek for $u \in H(\nabla, \Omega)$ instead of the subspace $H_0(\nabla, \Omega)$. There, we recall that the homogeneous boundary condition was needed to fix the constants, which correspond to the kernel of the gradient operator. However, in this case, this role is taken over by the exterior problem (3.13), in particular, by the decay condition (4.1e).
- The constant C_∞ in (4.1e) follows from the corresponding representation formula. It reads $C_\infty := \frac{1}{2\pi}\langle \gamma_1^{\mathrm{e}} u^{\mathrm{e}}, 1\rangle_\Gamma$. From the weak formulation below, we find the equivalent representation

$$C_\infty := -\frac{1}{2\pi}\left(\langle f, 1\rangle_\Omega + \left\langle \widehat{\phi}, 1\right\rangle_\Gamma\right).$$

  Hence, (4.1e) can be replaced by

$$u^{\mathrm{e}} = \mathcal{O}\left(|\boldsymbol{x}|^{-1}\right) \quad \text{for } |\boldsymbol{x}| \to \infty$$

  with a further compatibility condition on the data

$$\langle f, 1\rangle_\Omega + \left\langle \widehat{\phi}, 1\right\rangle_\Gamma = 0.$$

4.1.1 Well-posedness and stability

The derivation of a variational formulation for the non-symmetric coupling follows a standard procedure: For the interior part, we test (4.1a) with $v \in H(\nabla, \Omega)$, apply the integration by parts (2.65), then use the jump condition (4.1d) to introduce $\gamma_1^{\mathrm{e}} u^{\mathrm{e}}$ in the weak form of the interior problem. For the exterior part, the weak formulation follows similarly by testing the first BIE in (3.37b) with $\psi \in H^{-\frac{1}{2}}(\Gamma)$, and inserting the jump condition (4.1c), such that the exterior problem is coupled with the interior one via $\gamma_0 u$.
Formally, by writing $\phi = \gamma_1^{\mathrm{e}} u^{\mathrm{e}}$, the weak formulation of the non-symmetric coupling of Problem 4.1 reads:

$$\text{Find } \mathbf{u} := (u, \phi) \in H(\nabla, \Omega) \times H^{-\frac{1}{2}}(\Gamma) \text{ such that}$$

$$(\mathcal{U}\nabla u, \nabla v)_\Omega - \langle \phi, \gamma_0 v\rangle_\Gamma = \langle f, v\rangle_\Omega + \left\langle \widehat{\phi}, \gamma_0 v\right\rangle_\Gamma,$$

$$\left\langle \psi, \left(\frac{1}{2} - \mathcal{K}_0\right)\gamma_0 u\right\rangle_\Gamma + \langle \psi, \mathcal{V}_0\phi\rangle_\Gamma = \left\langle \psi, \left(\frac{1}{2} - \mathcal{K}_0\right)\widehat{u}\right\rangle_\Gamma$$

$$\text{hold } \forall \mathbf{v} := (v, \psi) \in H(\nabla, \Omega) \times H^{-\frac{1}{2}}(\Gamma).$$

For convenience, we write the variational form above in a compact form. For this, we introduce the product space $\boldsymbol{\mathcal{H}} := H(\nabla, \Omega) \times H^{-\frac{1}{2}}(\Gamma)$, and endow it with the norm

$$\|\mathbf{v}\|_{\boldsymbol{\mathcal{H}}} := \sqrt{\|v\|^2_{H(\nabla,\Omega)} + \|\psi\|^2_{H^{-\frac{1}{2}}(\Gamma)}} \qquad \text{for } \mathbf{v} = (v, \psi) \in \boldsymbol{\mathcal{H}}. \tag{4.2}$$

Problem 4.2 (Compact form)**.** *Find* $\mathbf{u} \in \boldsymbol{\mathcal{H}} := H(\nabla, \Omega) \times H^{-\frac{1}{2}}(\Gamma)$ *such that* $a(\mathbf{u}, \mathbf{v}) = \ell(\mathbf{v})$ *holds* $\forall \mathbf{v} \in \boldsymbol{\mathcal{H}}$ *with the linear form (linear in the second argument)* $a : \boldsymbol{\mathcal{H}} \times \boldsymbol{\mathcal{H}} \to \mathbb{R}$

$$a(\mathbf{u}, \mathbf{v}) := (\mathcal{U}\nabla u, \nabla v)_\Omega - \langle \phi, \gamma_0 v\rangle_\Gamma + \left\langle \psi, \left(\frac{1}{2} - \mathcal{K}_0\right)\gamma_0 u\right\rangle_\Gamma + \langle \psi, \mathcal{V}_0\phi\rangle_\Gamma, \tag{4.3}$$

and the linear functional ℓ on $\boldsymbol{\mathcal{H}}$,

$$\ell(\mathbf{v}) := \langle f, v\rangle_\Omega + \left\langle \widehat{\phi}, \gamma_0 v \right\rangle_\Gamma + \left\langle \psi, \left(\frac{1}{2} - \mathcal{K}_0\right) \widehat{u} \right\rangle_\Gamma . \tag{4.4}$$

It is easy to find a counterexample to show that $a(\mathbf{v}, \mathbf{v})$ is not elliptic, we mention $\mathbf{v} = (1, 0)$, for instance. To prove well-posedness of Problem 4.2, we proceed as in [6] by considering an equivalent stabilized problem that is amenable to analysis. We mean by equivalent that a solution of the original problem is also a solution of the stabilized one and vice versa. Provided this is the case, this approach is called implicit stabilization. The proposed stabilized problem reads:

Problem 4.3 (Stabilized problem, [6])**.** *Find $\mathbf{u} \in \boldsymbol{\mathcal{H}}$ such that $\widetilde{a}(\mathbf{u}, \mathbf{v}) = \widetilde{\ell}(\mathbf{v})$ holds $\forall \mathbf{v} := (v, \psi) \in \boldsymbol{\mathcal{H}}$, where we define with*

$$s(\mathbf{v}) := \left\langle 1, \left(\frac{1}{2} - \mathcal{K}_0\right) \gamma_0 v \right\rangle_\Gamma + \langle 1, \mathcal{V}_0 \psi\rangle_\Gamma$$

the stabilized linear form

$$\widetilde{a}(\mathbf{u}, \mathbf{v}) := a(\mathbf{u}, \mathbf{v}) + s(\mathbf{u}) s(\mathbf{v}),$$

and the functional

$$\widetilde{\ell}(\mathbf{v}) := \ell(\mathbf{v}) + \left\langle 1, \left(\frac{1}{2} - \mathcal{K}_0\right) \widehat{u} \right\rangle_\Gamma s(\mathbf{v}).$$

The equivalence is stated in the following.

Lemma 4.4 (Equivalence of the formulations, [6])**.** *The original and the stabilized formulations are equivalent, i.e., $\mathbf{u} \in \boldsymbol{\mathcal{H}}$ solves Problem 4.2 if and only if it solves Problem 4.3, and vice versa.*

Therefore, the analysis can be performed with the aid of the stabilized form. In particular, Lemma 4.4 implies that well-posedness of the stabilized problem transfers to the original one. However, for implementation purposes, we still use the original one for simplicity.

According to Theorem 2.5, well-posedness follows, provided the considered operator is Lipschitz continuous and strongly monotone. First, let $\boldsymbol{\mathcal{H}}'$ denote the dual space of $\boldsymbol{\mathcal{H}}$. Then, we define the induced non-linear operator $\widetilde{\mathcal{A}} : \boldsymbol{\mathcal{H}} \to \boldsymbol{\mathcal{H}}'$ by

$$\left\langle \widetilde{\mathcal{A}}(\mathbf{u}), \mathbf{v} \right\rangle := \widetilde{a}(\mathbf{u}, \mathbf{v}) \qquad \forall\, \mathbf{u}, \mathbf{v} \in \boldsymbol{\mathcal{H}}. \tag{4.5}$$

The following result establishes the needed properties of $\widetilde{\mathcal{A}}$.

Theorem 4.5 (Lipschitz continuity and strong monotonicity)**.** *Let us consider the non-linear operator $\widetilde{\mathcal{A}} : \boldsymbol{\mathcal{H}} \to \boldsymbol{\mathcal{H}}'$ defined in* (4.5) *with $\boldsymbol{\mathcal{H}} = H(\nabla, \Omega) \times H^{-\frac{1}{2}}(\Gamma)$. We state the following three assertions.*

1. *$\widetilde{\mathcal{A}}$ is Lipschitz continuous, i.e., there exists $C_{\mathrm{L}} > 0$ such that*

$$\left\| \widetilde{\mathcal{A}}(\mathbf{u}) - \widetilde{\mathcal{A}}(\mathbf{v}) \right\|_{\boldsymbol{\mathcal{H}}'} \leq C_{\mathrm{L}} \|\mathbf{u} - \mathbf{v}\|_{\boldsymbol{\mathcal{H}}}$$

   for all $\mathbf{u}, \mathbf{v} \in \boldsymbol{\mathcal{H}}$.

2. *If* $C_{\mathrm{M}}^{\mathcal{U}} > \frac{1}{4}$ *then*

$$\left\langle \widetilde{\mathcal{A}}(\mathbf{u}) - \widetilde{\mathcal{A}}(\mathbf{v}), \mathbf{u} - \mathbf{v} \right\rangle \geq C_{\mathrm{stab}} \left(\|\nabla u - \nabla v\|_{L^2(\Omega)}^2 + \|\phi - \psi\|_{\mathcal{V}_0}^2 + s(\mathbf{u} - \mathbf{v})^2 \right) \tag{4.6}$$

for all $\mathbf{u} = (u, \phi) \in \boldsymbol{\mathcal{H}}$, $\mathbf{v} = (v, \psi) \in \boldsymbol{\mathcal{H}}$ *with the norm* $\|\psi\|_{\mathcal{V}_0}^2 := \langle \psi, \mathcal{V}_0 \psi \rangle_\Gamma$ *and with*

$$C_{\mathrm{stab}} = \min \left\{ 1, \frac{1}{2} \left(1 + C_{\mathrm{M}}^{\mathcal{U}} - \sqrt{\left(C_{\mathrm{M}}^{\mathcal{U}} - 1 \right)^2 + 1} \right) \right\}.$$

3. *If* $C_{\mathrm{M}}^{\mathcal{U}} > \frac{1}{4}$ *then* $\widetilde{\mathcal{A}}$ *is strongly monotone, i.e., there exists* $C_{\mathrm{M}} > 0$ *such that*

$$\left\langle \widetilde{\mathcal{A}}(\mathbf{u}) - \widetilde{\mathcal{A}}(\mathbf{v}), \mathbf{u} - \mathbf{v} \right\rangle \geq C_{\mathrm{M}} \|\mathbf{u} - \mathbf{v}\|_{\boldsymbol{\mathcal{H}}}^2$$

for all $\mathbf{u}, \mathbf{v} \in \boldsymbol{\mathcal{H}}$.

Proof. The Lipschitz continuity of $\widetilde{\mathcal{A}}$ follows from the Lipschitz continuity of $\mathcal{U}$, and the continuity of the integral operators.
The proof of the second assertion follows the lines of [46, Theorem 1] for $\beta = 1$. We replace the coercivity estimate of the bilinear form $(\mathcal{U}\nabla u, \nabla v)_\Omega$ considered in [46] for a linear $\mathcal{U}$ by the strong monotonicity property of $\mathcal{U}$, i.e,

$$(\mathcal{U}\nabla u - \mathcal{U}\nabla v, \nabla u - \nabla v)_\Omega \geq C_{\mathrm{M}}^{\mathcal{U}} \|\nabla u - \nabla v\|_{L^2(\Omega)}^2.$$

The restriction $C_{\mathrm{M}}^{\mathcal{U}} > \frac{1}{4}$ is a direct result of the use of the contractivity result for the double-layer operator $\mathcal{K}_0$ of Lemma 3.18, where we use the worst case of $C_{\mathcal{K}_0} = 1$ in the statement, see also [89, Lemma 2.1].
For the last assertion we note the norm equivalence (3.34), and by a Rellich compactness argument it can be shown [6, Lemma 10] that

$$|||\mathbf{v}|||^2 := \|\nabla v\|_{L^2(\Omega)}^2 + \|\psi\|_{\mathcal{V}_0}^2 + s(\mathbf{v})^2$$

defines an equivalent norm in $\boldsymbol{\mathcal{H}}$ for all $\mathbf{v} := (v, \psi) \in \boldsymbol{\mathcal{H}}$. Together with (4.6) this leads to the last assertion with $C_{\mathrm{M}}^{\mathcal{U}} > \frac{1}{4}$, which is required for (4.6). □

Remark 4.6. *The constants* C_{L} *and* C_{M} *in Theorem 4.5 depend on various other constants, namely, the continuity constants of the boundary integral operators* $\mathcal{V}_0$ *and* $\mathcal{K}_0$*, the ellipticity constant of* $\mathcal{V}_0$*,* $C_{\mathrm{L}}^{\mathcal{U}}$*,* $C_{\mathrm{M}}^{\mathcal{U}}$ *and* C_0*, in particular on* Ω *and* Γ*. Thereby,* $C_0 > 0$ *is the constant from the trace inequality* (2.58) .

With this, we state the main result of this section.

Theorem 4.7 (Well-posedness)**.** *Provided that* $C_{\mathrm{M}}^{\mathcal{U}} > \frac{1}{4}$*, there exists a unique solution* $\mathbf{u} := (u, \phi) \in \boldsymbol{\mathcal{H}}$ *of the variational Problem 4.2 for any* $(f, \widehat{u}, \widehat{\phi}) \in H(\nabla, \Omega)' \times H^{\frac{1}{2}}(\Gamma) \times H^{-\frac{1}{2}}(\Gamma)$.

Proof. From Theorem 4.5, it follows that the induced operator $\widetilde{\mathcal{A}}$ of $\widetilde{a}(\cdot, \cdot)$ is strongly monotone and Lipschitz continuous for $C_{\mathrm{M}}^{\mathcal{U}} > \frac{1}{4}$. Hence, by using Theorem 2.5, there exists a unique solution $\mathbf{u} := (u, \phi) \in \boldsymbol{\mathcal{H}}$ of the variational Problem 4.3 for any $(f, \widehat{u}, \widehat{\phi}) \in H(\nabla, \Omega)' \times H^{\frac{1}{2}}(\Gamma) \times H^{-\frac{1}{2}}(\Gamma)$. Thanks to the equivalence stated in Lemma 4.4, this is also the unique solution of Problem 4.2. □

In the context of electromechanical energy converters, it is usual to consider $\mathcal{U}\nabla u := \nu(|\nabla u|)\nabla u$ in the sense of Definition 1.1. For this particular type of non-linearity, we can establish the following stability result.

Lemma 4.8. *Let $C_{\mathrm{M}}^{\mathcal{U}} > \frac{1}{4}$ and let the non-linear operator $\mathcal{U}$ be of the form $\mathcal{U}\nabla u := \nu(|\nabla u|)\nabla u$ with a non-linear function $\nu : \mathbb{R} \to \mathbb{R}$ induced by an admissible B-H curve according to Definition 1.1. Then, for the solution $\mathbf{u} := (u, \phi) \in \boldsymbol{\mathcal{H}}$ of Problem 4.2, we have the stability result*

$$\|\mathbf{u}\|_{\boldsymbol{\mathcal{H}}} \leq C \left(\|f\|_{H(\nabla,\Omega)'} + \|\widehat{u}\|_{H^{\frac{1}{2}}(\Gamma)} + \left\|\widehat{\phi}\right\|_{H^{-\frac{1}{2}}(\Gamma)} \right) \qquad \text{with } C > 0.$$

Proof. Let $\mathbf{v} \in \boldsymbol{\mathcal{H}}$ be arbitrary. We know from the strong monotonicity of $\widetilde{\mathcal{A}}$ that

$$C_{\mathrm{M}} \|\mathbf{u} - \mathbf{v}\|_{\boldsymbol{\mathcal{H}}}^2 \leq \left\langle \widetilde{\mathcal{A}}(\mathbf{u}) - \widetilde{\mathcal{A}}(\mathbf{v}), \mathbf{u} - \mathbf{v} \right\rangle.$$

Without loss of generality, we choose $\mathbf{v} := (0, 0)$ and note that $\mathcal{U}\nabla v = 0$. Thanks to Lemma 4.4 $\mathbf{u} := (u, \phi)$ is also the unique solution of the Problem 4.3. Thus, we conclude that

$$\begin{aligned} C_{\mathrm{M}} \|\mathbf{u}\|_{\boldsymbol{\mathcal{H}}}^2 &\leq \left\langle \widetilde{\mathcal{A}}(\mathbf{u}), \mathbf{u} \right\rangle = \widetilde{\ell}(\mathbf{u}), \\ &= \langle f, u \rangle_{\Omega} + \left\langle \widehat{\phi}, \gamma_0 u \right\rangle_{\Gamma} + \left\langle \phi, \left(\frac{1}{2} - \mathcal{K}_0 \right) \widehat{u} \right\rangle_{\Gamma} + \left\langle 1, \left(\frac{1}{2} - \mathcal{K}_0 \right) \widehat{u} \right\rangle_{\Gamma} s(\mathbf{u}) \end{aligned}$$

with $s(\mathbf{u}) := \left\langle 1, \left(\frac{1}{2} - \mathcal{K}_0 \right) \gamma_0 u \right\rangle_{\Gamma} + \langle 1, \mathcal{V}_0 \phi \rangle_{\Gamma}$. Next, we use the Cauchy-Schwarz inequality along with the boundedness of $\mathcal{K}_0$ and $\mathcal{V}_0$, and the trace inequality Equation (2.58). Then, rearranging the terms yields

$$\begin{aligned} C_{\mathrm{M}} \|\mathbf{u}\|_{\boldsymbol{\mathcal{H}}}^2 \leq &\left(\|f\|_{H(\nabla,\Omega)'} + C_0 \left\|\widehat{\phi}\right\|_{H^{-\frac{1}{2}}(\Gamma)} + \|1\|_{H^{-\frac{1}{2}}(\Gamma)} \left(\frac{1}{2} + C^{\mathcal{K}_0} \right)^2 C_0 \|\widehat{u}\|_{H^{\frac{1}{2}}(\Gamma)} \right) \|u\|_{H(\nabla,\Omega)} \\ &+ \|1\|_{H^{-\frac{1}{2}}(\Gamma)} \left(\left(\frac{1}{2} + C^{\mathcal{K}_0} \right) \left(1 + C^{\mathcal{V}_0} \right) \|\widehat{u}\|_{H^{\frac{1}{2}}(\Gamma)} \right) \|\phi\|_{H^{-\frac{1}{2}}(\Gamma)}, \end{aligned}$$

where $C^{\mathcal{K}_0}$, $C^{\mathcal{V}_0} > 0$ are continuity constants of the boundary integral operators $\mathcal{K}_0$ and $\mathcal{V}_0$, respectively, which arise from Theorem 3.8. From this follows the assertion with a constant $C > 0$ that depends on $C^{\mathcal{K}_0}$, $C^{\mathcal{V}_0}$, C_0, C_{M} and Γ. □

The next subsection is dedicated to the discretization of the original Problem 4.2 via a Galerkin approximation. Recall that this allowed by the equivalence stated in Lemma 4.4.

4.1.2 Galerkin discretization

Let $V_\ell \subset H(\nabla, \Omega)$ and $X_\ell \subset H^{-\frac{1}{2}}(\Gamma)$ be some finite dimensional subspaces, where the index ℓ expresses a refinement level, see Section 3.3. In order to be able to transfer the implicit stabilization to the discrete problem, we need to make the following assumption.

Assumption 4.9. *The discrete space X_ℓ contains the constants, i.e.,*

$$\exists \xi \in \bigcap_{\ell \in \mathbb{N}_0} X_\ell \text{ such that } \langle \xi, 1 \rangle_\Gamma \neq 0.$$

The discrete problem is then obtained by replacing the spaces $H(\nabla, \Omega)$ and $H^{-\frac{1}{2}}(\Gamma)$ in Problem 4.2 with V_ℓ and X_ℓ, respectively. We consider a conforming Galerkin discretization of the Problem 4.2. By denoting the discrete product space by $\boldsymbol{\mathcal{H}}_\ell := V_\ell \times X_\ell$, the discrete problem can be written in a compact form.

Problem 4.10 (Discrete problem)**.** *Find $\mathbf{u}_\ell = (u_\ell, \phi_\ell) \in \boldsymbol{\mathcal{H}}_\ell = V_\ell \times X_\ell$ such that $a(\mathbf{u}_\ell, \mathbf{v}_\ell) = \ell(\mathbf{v}_\ell)$ holds $\forall \mathbf{v}_\ell = (v_\ell, \psi_\ell) \in \boldsymbol{\mathcal{H}}_\ell$. The linear form $a(\cdot, \cdot)$ and the linear functional ℓ are defined in* (4.3) *and* (4.4)*, respectively.*

Note that we consider a conforming Galerkin discretization. Provided that Assumption 4.9 is satisfied, the analysis for Problem 4.10 is done analogously to the continuous Problem 4.2 since the discrete spaces are conforming. In other words, all the above results including the introduction of a stabilized form and Lemma 4.4 also apply for the subspaces.

Corollary 4.11 (Well-posedness)**.** *Let $\mathbf{u} \in \boldsymbol{\mathcal{H}}$ be the solution of Problem 4.2. The solution $\mathbf{u}_\ell \in \boldsymbol{\mathcal{H}}_\ell$ of Problem 4.10 exists, converges to $\mathbf{u}$ such that $\lim_{\ell \to \infty} \mathbf{u}_\ell = \mathbf{u}$, and is unique.*

Proof. The assertion follows with Theorem 4.7, and by taking into account the conforming Galerkin discretization, see [122, Corollary 25.7]. □

In the same context, we can establish a quasi-optimality result in the sense of a Céa-type lemma. This is a central result for a priori error estimates of the non-symmetric coupling, as will be addressed in the next subsection.

Theorem 4.12 (Quasi-optimality)**.** *Let Assumption 4.9 hold, and $C_{\mathrm{M}}^{\mathcal{U}} > \frac{1}{4}$. Moreover, let $\mathbf{u} := (u, \phi) \in \boldsymbol{\mathcal{H}}$ be the unique solution of Problem 4.2, and $\mathbf{u}_\ell := (u_\ell, \phi_\ell) \in \boldsymbol{\mathcal{H}}_\ell$ the solution of its discrete counterpart Problem 4.10. Then*

$$\|u - u_\ell\|_{H(\nabla,\Omega)} + \|\phi - \phi_\ell\|_{H^{-\frac{1}{2}}(\Gamma)} \leq C_{\text{Céa}} \min_{v_\ell \in V_\ell, \psi_\ell \in X_\ell} \left(\|u - v_\ell\|_{H(\nabla,\Omega)} + \|\phi - \psi_\ell\|_{H^{-\frac{1}{2}}(\Gamma)} \right)$$

with $C_{\text{Céa}} = \frac{C_{\mathrm{L}}}{C_{\mathrm{M}}}$.

Proof. The assertion follows as a result of the main theorem on strongly monotone operators, Theorem 2.5. That means with $\mathbf{v}_\ell = (v_\ell, \psi_\ell)$, as a consequence to Lemma 4.4, the strong monotonicity, Galerkin orthogonality, Cauchy-Schwarz inequality, and the Lipschitz continuity we get

$$\begin{aligned} C_{\mathrm{M}} \|\mathbf{u} - \mathbf{u}_\ell\|_{\boldsymbol{\mathcal{H}}}^2 &\leq \left\langle \widetilde{\mathcal{A}}(\mathbf{u}) - \widetilde{\mathcal{A}}(\mathbf{u}_\ell), \mathbf{u} - \mathbf{u}_\ell \right\rangle = \left\langle \widetilde{\mathcal{A}}(\mathbf{u}) - \widetilde{\mathcal{A}}(\mathbf{u}_\ell), \mathbf{u} - \mathbf{v}_\ell \right\rangle \leq \left\| \widetilde{\mathcal{A}}(\mathbf{u}) - \widetilde{\mathcal{A}}(\mathbf{u}_\ell) \right\|_{\boldsymbol{\mathcal{H}}'} \|\mathbf{u} - \mathbf{v}_\ell\|_{\boldsymbol{\mathcal{H}}} \\ &\leq C_{\mathrm{L}} \|\mathbf{u} - \mathbf{u}_\ell\|_{\boldsymbol{\mathcal{H}}} \|\mathbf{u} - \mathbf{v}_\ell\|_{\boldsymbol{\mathcal{H}}}, \end{aligned}$$

where the assertion follows directly. □

4.1.3 A priori error estimates

Let the assumptions of Section 4.1 on Ω hold. We consider the discrete Problem 4.10 with $V_\ell = \mathbb{S}^0_{\boldsymbol{p}}(\Omega)$ and $X_\ell = \mathbb{S}^2_{\widetilde{p}}(\Gamma)$, with $\boldsymbol{p} = (p,p)$ and $\widetilde{p} = p-1$, cf. (3.59), and let $\boldsymbol{\mathcal{H}}_\ell := \mathbb{S}^0_{\boldsymbol{p}}(\Omega) \times \mathbb{S}^2_{\widetilde{p}}(\Gamma)$. Note that with this particular choice the degrees of the B-Spline spaces are solely fixed by one parameter $p > 0$. Hence, we say that $\boldsymbol{\mathcal{H}}_\ell$ is of degree p.

In the following, we need to define regularity in a patchwise sense.

Definition 4.13. *Let $K \in \{\Omega, \Gamma\}$ be a multipatch domain with N_κ patches. For some $s \in \mathbb{R}$, we define the space of patchwise regularity by*

$$H^s_{\mathrm{pw}}(K) = \{u \in L^2(K) : \|u\|_{H^s_{\mathrm{pw}}(K)} < \infty\},$$

where

$$\|u\|^2_{H^s_{\mathrm{pw}}(K)} = \sum_{0 \le l < N_\kappa} \left\|u_{|\kappa_l}\right\|^2_{H^s(K)}. \tag{4.7}$$

For an a priori error estimate for the non-symmetric isogeometric FEM-BEM coupling, we first recall a result on the approximation properties of the considered B-Spline spaces in $H(\nabla,\Omega)$ and $H^{-\frac{1}{2}}(\Gamma)$.

Lemma 4.14 (Approximation properties)**.** *Let $u \in H(\nabla,\Omega) \cap H^{1+s}_{\mathrm{pw}}(\Omega)$ and $\phi \in H^{-\frac{1}{2}}(\Gamma) \cap H^{-\frac{1}{2}+s}_{\mathrm{pw}}(\Gamma)$. Consider $\mathbb{S}^0_{\boldsymbol{p}}(\Omega)$ and $\mathbb{S}^2_{\widetilde{p}}(\Gamma)$ as given above. There exists C_1, $C_2 > 0$ depending only on p and C_θ from Assumption 3.25 such that*

$$\inf_{u_\ell \in \mathbb{S}^0_{\boldsymbol{p}}(\Omega)} \|u - u_\ell\|_{H(\nabla,\Omega)} \le C_1\, h^s \|u\|_{H^{1+s}_{\mathrm{pw}}(\Omega)}, \qquad 0 \le s \le p,$$

$$\inf_{\phi_\ell \in \mathbb{S}^2_{\widetilde{p}}(\Gamma)} \|\phi - \phi_\ell\|_{H^{-\frac{1}{2}}(\Gamma)} \le C_2\, h^s \|\phi\|_{H^{-\frac{1}{2}+s}_{\mathrm{pw}}(\Gamma)}, \qquad \frac{1}{2} \le s \le p + \frac{1}{2}.$$

Proof. The first estimate is given in [21, Corollary 2], and the second one follows from [21, Corollary 4]. □

With this, we state the following result.

Theorem 4.15 (A priori estimate)**.** *We assume $C^{\mathcal{U}}_{\mathrm{M}} > \frac{1}{4}$. Let $(u,\phi) \in \boldsymbol{\mathcal{H}}$ be the solution of Problem 4.2 and let $(u_\ell,\phi_\ell) \in \boldsymbol{\mathcal{H}}_\ell = \mathbb{S}^0_{\boldsymbol{p}}(\Omega) \times \mathbb{S}^2_{\widetilde{p}}(\Gamma)$ be the solution of the discrete Problem 4.10. Then, for $0 \le s \le \frac{1}{2}$, $u \in H(\nabla,\Omega) \cap H^{1+s}_{\mathrm{pw}}(\Omega)$, and $\phi \in H^{-\frac{1}{2}}(\Gamma) \cap H^0_{\mathrm{pw}}(\Gamma)$*

$$\|u - u_\ell\|_{H(\nabla,\Omega)} + \|\phi - \phi_\ell\|_{H^{-\frac{1}{2}}(\Gamma)} \le C\, h^s \left(\|u\|_{H^{1+s}_{\mathrm{pw}}(\Omega)} + \|\phi\|_{H^0_{\mathrm{pw}}(\Gamma)}\right).$$

For $\frac{1}{2} \le s \le p$, $u \in H(\nabla,\Omega) \cap H^{1+s}_{\mathrm{pw}}(\Omega)$, and $\phi \in H^{-\frac{1}{2}}(\Gamma) \cap H^{-\frac{1}{2}+s}_{\mathrm{pw}}(\Gamma)$ we have

$$\|u - u_\ell\|_{H(\nabla,\Omega)} + \|\phi - \phi_\ell\|_{H^{-\frac{1}{2}}(\Gamma)} \le C\, h^s \left(\|u\|_{H^{1+s}_{\mathrm{pw}}(\Omega)} + \|\phi\|_{H^{-\frac{1}{2}+s}_{\mathrm{pw}}(\Gamma)}\right)$$

with a constant $C = C(C_{\mathrm{Céa}}, p, C_\theta) > 0$, which is in particular independent of h.

Proof. From [21] we know that $\mathbb{S}^0_{\boldsymbol{p}}(\Omega)$ and $\mathbb{S}^2_{\widetilde{p}}(\Gamma)$ are closed subspaces of $H(\nabla,\Omega)$ and $H^{-\frac{1}{2}}(\Gamma)$, respectively. Moreover, Assumption 4.9 is fulfilled per construction of the B-Spline spaces. Hence, the usual analysis for a conforming Galerkin discretization of a non-symmetric FEM-BEM coupling can also be considered in the isogeometric context. Now, using Lemma 4.14 and the quasi-optimality stated in Theorem 4.12 yields the assertion. □

Remark 4.16. *Throughout this section, we required for the analysis that $C_{\mathrm{M}}^{\mathcal{U}} > \frac{1}{4}$. However, this assumption is sufficient for the solvability of the Johnson-Nédélec coupling, but not necessary. See also [6] and [46, Remark 10], where numerical experiments still converge although the condition is violated.*

4.2 The two-dimensional (2D) parabolic-elliptic interface problem

Let us consider the same configuration as in the previous section, namely, an interface problem with a bounded domain $\Omega \subset \mathbb{R}^2$ with Lipschitz boundary $\Gamma = \partial\Omega$. The unbounded exterior domain is denoted by $\Omega^{\mathrm{e}} := \mathbb{R}^2 \backslash \overline{\Omega}$. For the same reason as previously, we assume that $\operatorname{diam}(\Omega) < 1$. In this section, we study a non-linear evolution problem of first order. The model problem stems, e.g., from the 2D magnetoquasistationary case, and can be obtained by coupling (3.10) (instead of (3.11)) with (3.13).

The following Initial Value Problem (IVP) has to be understood in a weak sense:

Problem 4.17 (Classical problem)**.** *Find $(u, u^{\mathrm{e}}) \in L^2(\partial_t, T;\, H(\nabla,\Omega)) \times L^2(T;\, H_{\mathrm{loc}}(\nabla,\Omega^{\mathrm{e}}))$ such that*

$$
\begin{aligned}
-\operatorname{div}(\mathcal{U}\nabla u) + \kappa\,\partial_t u &= f && \text{in } \Omega \times T\backslash\{0\}, && \text{(4.8a)}\\
-\Delta u^{\mathrm{e}} &= 0 && \text{in } \Omega^{\mathrm{e}} \times T\backslash\{0\}, && \text{(4.8b)}\\
[\![\gamma_0 u]\!]_\Gamma &= \widehat{u} && \text{on } \Gamma \times T\backslash\{0\}, && \text{(4.8c)}\\
[\![\gamma_1^{\mathcal{U}} u]\!]_\Gamma &= \widehat{\phi} && \text{on } \Gamma \times T\backslash\{0\}, && \text{(4.8d)}\\
u &= 0 && \text{in } \Omega \times \{0\}, && \text{(4.8e)}\\
u^{\mathrm{e}} &= C_\infty \log|\boldsymbol{x}| + \mathcal{O}\left(|\boldsymbol{x}|^{-1}\right) && \text{for } |\boldsymbol{x}| \to \infty \text{ and } T\backslash\{0\} && \text{(4.8f)}
\end{aligned}
$$

with $(f, \widehat{u}, \widehat{\phi}) \in L^2(T;\, H(\nabla,\Omega)') \times L^2(T;\, H^{\frac{1}{2}}(\Gamma)) \times L^2(T;\, H^{-\frac{1}{2}}(\Gamma))$, $T = [0, t_{\max}]$, and $\kappa > 0$.

Similar arguments and remarks to the ones that led to Problem 4.1 can be employed here with the following adaptation:

- In addition to Assumption 2.13, we require the non-linear operator $\mathcal{U} := \mathcal{U}(t)$ to be hemicontinuous.
- Note that the term C_∞ in (4.8f) reads $C_\infty(t) := \frac{1}{2\pi}\langle \gamma_1^{\mathrm{e}}\, u^{\mathrm{e}}(t), 1\rangle_\Gamma$.

In complete analogy with the previous section, we derive a variational formulation for the non-symmetric coupling. With $\phi := \gamma_1^{\mathrm{e}}\, u^{\mathrm{e}}$ we obtain:

$$
\text{Find } \mathbf{u} := (u, \phi) \in L^2(\partial_t, T;\, H(\nabla,\Omega)) \times L^2(T;\, H^{-\frac{1}{2}}(\Gamma)) \text{ such that } u(0) = 0 \text{ and}
$$

$$
(\mathcal{U}\nabla u, \nabla v)_\Omega + \kappa\,(\partial_t u, v)_\Omega - \langle \phi, \gamma_0 v\rangle_\Gamma = \langle f, v\rangle_\Omega + \left\langle \widehat{\phi}, \gamma_0 v \right\rangle_\Gamma,
$$

$$\left\langle \psi, \left(\frac{1}{2} - \mathcal{K}_0\right)\gamma_0 u \right\rangle_\Gamma + \langle \psi, \mathcal{V}_0\phi\rangle_\Gamma = \left\langle \psi, \left(\frac{1}{2} - \mathcal{K}_0\right)\widehat{u} \right\rangle_\Gamma$$

hold $\forall \mathbf{v} := (v,\psi) \in \boldsymbol{\mathcal{H}} := H(\nabla,\Omega) \times H^{-\frac{1}{2}}(\Gamma)$ and almost everywhere (a.e.) on $\mathring{T} := (0, t_{\max})$.

We denote by $\boldsymbol{\mathcal{H}}_{\mathrm{T}} := L^2(\partial_t, T;\, H(\nabla,\Omega)) \times L^2(T;\, H^{-\frac{1}{2}}(\Gamma))$ the Bochner product space, and endow it with the norm

$$\begin{aligned}\|\mathbf{v}\|^2_{\boldsymbol{\mathcal{H}}_{\mathrm{T}}} :=& \|v\|^2_{L^2(\partial_t,T;\,H(\nabla,\Omega))} + \|\psi\|^2_{L^2(T;\,H^{-\frac{1}{2}}(\Gamma))} \\ =& \|v\|^2_{L^2(T;\,H(\nabla,\Omega))} + \|\partial_t v\|^2_{L^2(T;\,H(\nabla,\Omega)')} + \|\psi\|^2_{L^2(T;\,H^{-\frac{1}{2}}(\Gamma))},\end{aligned}$$

where $\mathbf{v} := (v,\psi)$. Thereby, we used the definition of $\|\cdot\|_{L^2(\partial_t,T;\,H(\nabla,\Omega))}$ according to (2.15). For convenience, we also recall that $\|\cdot\|_{L^2(T;\,H)}$ is defined for some generic space H in (2.13).

With this, the variational formulation above can be written in compact form.

Problem 4.18 (Compact form)**.** *Find* $\mathbf{u} := (u,\phi) \in \boldsymbol{\mathcal{H}}_{\mathrm{T}}$ *such that* $a_{\mathrm{T}}(\mathbf{u},\mathbf{v}) = \ell(\mathbf{v})$ *holds* $\forall \mathbf{v} := (v,\psi) \in \boldsymbol{\mathcal{H}}$ *with the linear form (linear in the second argument)* $a_{\mathrm{T}} : \boldsymbol{\mathcal{H}}_{\mathrm{T}} \times \boldsymbol{\mathcal{H}} \to \mathbb{R}$*,*

$$a_{\mathrm{T}}(\mathbf{u},\mathbf{v}) := \kappa\,(\partial_t u, v)_\Omega + a(\mathbf{u},\mathbf{v}). \tag{4.9}$$

Thereby, $a(\cdot,\cdot)$ *and the linear functional* $\ell(\cdot)$ *are defined in Problem 4.2.*

To analyze the problem above, we proceed similarly to [41, Remark 10] by considering an implicit stabilization in order to profit from the results of Section 4.1.

Remark 4.19. *Note that [41] proposes in the first place a more general approach based on energy estimates without resorting to a stabilized problem. That is, the analysis of [41] could also be adapted for our problem independently of the non-linearity in the interior domain.*

Problem 4.20 (Stabilized problem)**.** *Find* $\mathbf{u} := (u,\phi) \in \boldsymbol{\mathcal{H}}_{\mathrm{T}}$ *such that* $\widetilde{a}_{\mathrm{T}}(\mathbf{u},\mathbf{v}) = \widetilde{\ell}(\mathbf{v})$ *holds* $\forall \mathbf{v} := (v,\psi) \in \boldsymbol{\mathcal{H}}$ *with the linear form (linear in the second argument)* $\widetilde{a}_{\mathrm{T}} : \boldsymbol{\mathcal{H}}_{\mathrm{T}} \times \boldsymbol{\mathcal{H}} \to \mathbb{R}$*,*

$$\widetilde{a}_{\mathrm{T}}(\mathbf{u},\mathbf{v}) := \kappa\,(\partial_t u, v)_\Omega + \widetilde{a}(\mathbf{u},\mathbf{v}). \tag{4.10}$$

Thereby, $\widetilde{a}(\cdot,\cdot)$ *and the linear functional* $\widetilde{\ell}(\cdot)$ *are defined in Problem 4.3.*

Lemma 4.21 (Equivalence of the formulations)**.** *The original and the stabilized problems are equivalent, i.e.,* $\mathbf{u} \in \boldsymbol{\mathcal{H}}_{\mathrm{T}}$ *solves Problem 4.18 if and only if it solves Problem 4.20, and vice versa.*

Proof. The equivalence carries out verbatim from the linear case in [41], since the argument used therein is based on the choice of a test function, such that $\widetilde{a}_{\mathrm{T}}(\mathbf{u},\mathbf{v})$ is expressed only in boundary terms. □

Let $\widetilde{\mathcal{A}}(t) : \boldsymbol{\mathcal{H}} \to \boldsymbol{\mathcal{H}}'$ be as in (4.5). The following result establishes the needed properties of $\widetilde{\mathcal{A}}(t)$.

Lemma 4.22 (Properties of $\widetilde{\mathcal{A}}(t)$)**.** *Let us consider the non-linear operator $\widetilde{\mathcal{A}}(t) : \boldsymbol{\mathcal{H}} \to \boldsymbol{\mathcal{H}}'$ with $\boldsymbol{\mathcal{H}} = H(\nabla,\Omega)\times H^{-\frac{1}{2}}(\Gamma)$. We state the following assertions.*

1. *$\widetilde{\mathcal{A}}(t)$ is Lipschitz continuous.*
2. *If $C_{\mathrm{M}}^{\mathcal{U}} > \frac{1}{4}$ then $\widetilde{\mathcal{A}}(t)$ is strongly monotone.*
3. *$\widetilde{\mathcal{A}}(t)$ is hemicontinuous.*

Proof. The first and second assertions are proved in Theorem 4.5. Recall that for $\mathbf{u}(t), \mathbf{v}(t) \in \boldsymbol{\mathcal{H}}$

$$\left\langle \widetilde{\mathcal{A}}(t)(\mathbf{u}(t)), \mathbf{v}(t) \right\rangle = (\mathcal{U}\nabla u(t), \nabla v(t))_\Omega - \langle \phi(t), \gamma_0 v(t)\rangle_\Gamma + \left\langle \psi(t), \left(\frac{1}{2} - \mathcal{K}_0\right)\gamma_0 u(t)\right\rangle_\Gamma + \langle \psi(t), \mathcal{V}_0\phi(t)\rangle_\Gamma + s(\mathbf{u}(t))s(\mathbf{v}(t))$$

with $s(\cdot)$ as defined in Problem 4.3. The hemicontinuity of $\widetilde{\mathcal{A}}(t)$ is clearly inherited from the properties of $(\mathcal{U}\nabla u(t), \nabla v(t))_\Omega$, because the second term is bilinear and bounded, and all other boundary terms are continuous due to the continuity of BIOs, see Subsection 3.2.1. The hemicontinuity of $\widetilde{\mathcal{A}}(t)$ is a result of the hemicontinuity of $\mathcal{U}(t)$, and [73, Theorem 2.1.6]. □

By using the main theorem on monotone operators, we establish well-posedness of Problem 4.18.

Theorem 4.23 (Well-posedness)**.** *Provided that $C_{\mathrm{M}}^{\mathcal{U}} > \frac{1}{4}$, there exists a unique solution $\mathbf{u} \in \boldsymbol{\mathcal{H}}_{\mathrm{T}}$ of the variational Problem 4.18, for any $(f, \widehat{u}, \widehat{\phi}) \in L^2(T;\, H(\nabla,\Omega)') \times L^2(T;\, H^{\frac{1}{2}}(\Gamma)) \times L^2(T;\, H^{-\frac{1}{2}}(\Gamma))$.*

Proof. The assertion results from Lemma 4.22, Theorem 2.7, Lemma 2.9, and the equivalence of the stabilized problem with the original one, which follows from Lemma 4.21. □

Similarly to the previous section, if we consider $\mathcal{U}(t)\nabla u(t) := \nu(|\nabla u(t)|)\nabla u(t)$ to be defined in the sense of Definition 1.1, the following stability result can be established.

Lemma 4.24. *Let $C_{\mathrm{M}}^{\mathcal{U}} > \frac{1}{4}$ and let the non-linear operator $\mathcal{U}$ be of the form $\mathcal{U}(t)\nabla u(t) := \nu(|\nabla u(t)|)\nabla u(t)$ with $\nu : \mathbb{R} \to \mathbb{R}$ being a non-linear reluctivity $\nu : \mathbb{R} \to \mathbb{R}$ induced by an admissible B-H curve according to Definition 1.1. Then, for the solution $\mathbf{u} := (u, \phi) \in \boldsymbol{\mathcal{H}}_{\mathrm{T}}$ of Problem 4.18, we have the stability result*

$$\|\mathbf{u}\|_{\boldsymbol{\mathcal{H}}_{\mathrm{T}}} \leq C\left(\|f\|_{L^2(T;\, H(\nabla,\Omega)')} + \|\widehat{u}\|_{L^2(T;\, H^{\frac{1}{2}}(\Gamma))} + \left\|\widehat{\phi}\right\|_{L^2(T;\, H^{-\frac{1}{2}}(\Gamma))}\right), \quad C > 0.$$

Proof. By profiting from the linearity of the integral, the $\boldsymbol{\mathcal{H}}_{\mathrm{T}}$-norm Section 4.2 can be written as

$$\|\mathbf{u}\|_{\boldsymbol{\mathcal{H}}_{\mathrm{T}}}^2 = \int_0^{t_{\max}} \|\mathbf{u}(t)\|_{\boldsymbol{\mathcal{H}}}^2 + \|\partial_t u(t)\|_{H(\nabla,\Omega)'}^2 \,\mathrm{d}t,$$

where $\|\cdot\|_{\boldsymbol{\mathcal{H}}}$ is defined as in (4.2). First, the approximation for $\|\mathbf{u}(t)\|^2_{\boldsymbol{\mathcal{H}}}$ is given in Lemma 4.8. Second, the estimate for $\|\partial_t u(t)\|^2_{H(\nabla,\Omega)'}$ is provided in several works and manuscripts, e.g., [48, Part II. Section 7.1.2]. In [41, Lemma 11] an estimate with the aid of the dual norm leads to

$$\|\partial_t u(t)\|_{H(\nabla,\Omega)'} \leq C_{\mathrm{t}} \left(\|f(t)\|_{H(\nabla,\Omega)'} + \|\mathbf{u}(t)\|_{\boldsymbol{\mathcal{H}}} + \left\| \widehat{\phi}(t) \right\|_{H^{-\frac{1}{2}}(\Gamma)} \right), \quad C_{\mathrm{t}} > 0.$$

Therefore, combining both results, integrating over the time interval T, and taking into account that $u(0) = 0$ yields the assertion with a constant $C_{\mathrm{t}} > 0$, which has the same dependence as C in Lemma 4.8. □

In a semi-discrete setting, namely, by using a Galerkin approach as in Subsection 4.1.2, existence and uniqueness of a discrete solution are direct consequences of [122, Theorem 30.A]. Moreover, we can show quasi-optimality in the sense of a Céa-type lemma by adapting the proof of [41, Theorem 12].

Remark 4.25. *In this thesis, we do not address a concrete time discretization, and refer to [41] for the analysis of the fully discretized problem, where no duality argument is used (which is in general not available for non-symmetric systems). Furthermore, a variant of a classical implicit Euler scheme is considered for the time discretization with the advantage of avoiding time regularity assumptions. The classical implicit Euler, which is the scheme that we will consider for simplicity in our related numerical experiments, arises therefrom as a special case. By introducing a regular subdivision of the time interval T, we arrive at an ordinary differential equation with implicit components in the algebraic part, and a stiff differential part. This explains the choice of an implicit approach, since it avoids the numerical stability problems that arise for explicit schemes.*
In addition, note that higher order time discretizations are without doubt expected to be more advantageous for our isogeometric approach. For the analysis of a full discretization with a higher order time discretization, a Taylor expansion technique as demonstrated in [47] can be adapted with the drawback of the usual higher regularity assumptions in the time component. An investigation in this respect in future works would be beneficial.

4.3 A possible extension for the simulation of electric machines

In this section, we go back to the static case of Section 4.1 for convenience, but extend the geometrical configuration such that the arrangement of domains mimics a typical type of electrical machines, such as the one visualized in Figure 1.4.

Let $\Omega_1, \Omega^{\mathrm{e}}, \Omega_2 \subset \mathbb{R}^2$ be bounded Lipschitz domains with $\operatorname{diam}(\Omega^{\mathrm{e}}) < 1$, see Figure 4.1, and let $\Omega \subset \Omega_1$ be a Lipschitz inclusion with boundary $\Gamma_{0,1}$. We denote by $\Gamma^{\mathrm{e}} = \Gamma_1 \cup \Gamma_2$ the boundary of Ω^{e} and associate $\Gamma_{0,1}$ and $\Gamma_{0,2}$, which correspond to the "interior" and "exterior" boundary of Ω_1 and Ω_2, respectively, with homogeneous Dirichlet BCs.

For the sake of clarity, we use throughout this section a different notation for the Cauchy data of some $w \in H(\nabla, \Omega_k, \Gamma_k)$: We write $w_{|\Gamma_k}$ to denote the standard interior trace of w on the boundary part Γ_k of Ω_k, and $\mathcal{U}_k \nabla w_{|\Gamma_k} \cdot \boldsymbol{n}_k$ for the corresponding interior conormal trace. Thereby, $\boldsymbol{n}_k$ is as usual the outer normal vector of Ω_k on Γ_k. Note that a formal definition can be made by adapting Definition 2.14. The exterior traces follow similarly. For convenience, we refer to (2.31a) for the definition of spaces with BCs.

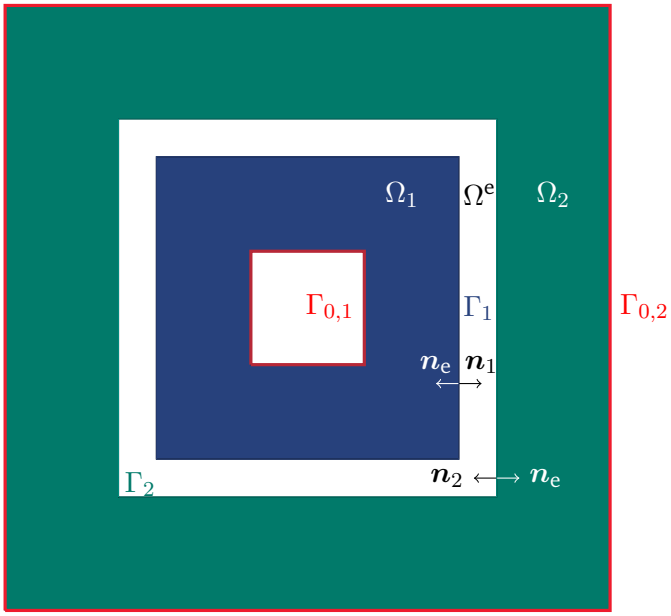

Figure 4.1: A possible multi-domain arrangement that is, e.g., topologically equivalent to Figure 1.4. Ω_1 and Ω_2 are filled with possibly non-linear materials, whereas Ω^e contains air. $\Gamma_{0,1}$ and $\Gamma_{0,2}$ are associated with homogeneous Boundary Conditions (BCs).

We consider the following boundary value problem (in a weak sense):

Problem 4.26 (Classical problem)**.** *Find* $(u_1, u_2, u^e) \in H_0(\nabla, \Omega_1, \Gamma_{0,1}) \times H_0(\nabla, \Omega_2, \Gamma_{0,2}) \times H(\nabla, \Omega^e)$ *such that*

$$
\begin{aligned}
-\operatorname{div}(\mathcal{U}_i \nabla u_i) &= f_i && \text{in } \Omega_i, \quad i = 1,2, && \text{(4.11a)}\\
-\Delta u^e &= 0 && \text{in } \Omega^e, && \text{(4.11b)}\\
u^e{}_{|\Gamma_i} - u_{i|\Gamma_i} &= \widehat{u}_i && \text{on } \Gamma_i, \quad i = 1,2, && \text{(4.11c)}\\
\mathcal{U}_i \nabla u_{i|\Gamma_i} \cdot \boldsymbol{n}_i + \nabla u^e{}_{|\Gamma_i} \cdot \boldsymbol{n}_e &= \widehat{\phi}_i && \text{on } \Gamma_i, \quad i = 1,2, && \text{(4.11d)}\\
u_{i|\Gamma_{0,i}} &= 0 && \text{on } \Gamma_{0,i}, \quad i = 1,2 && \text{(4.11e)}
\end{aligned}
$$

with $(f_i, \widehat{u}_i, \widehat{\phi}_i) \in H_0(\nabla, \Omega_i)' \times H^{\frac{1}{2}}(\Gamma_i) \times H^{-\frac{1}{2}}(\Gamma_i)$ *for* $i = 1, 2$*, and* $\boldsymbol{n}_e$ *being the outer normal vector with respect to* Ω^e *on* Γ^e.

The non-linear operators $\mathcal{U}_i$ are assumed to be strongly monotone and Lipschitz continuous. Note here that the exterior domain Ω^e is bounded. Therefore, we replaced the decay condition with the homogeneous BCs. A similar analysis follows merely with non-zero constant BCs.

4.3.1 Well-posedness and stability

To derive a weak formulation for Equation (4.11), we first derive a weak formulation in Ω_1 and Ω_2. For this, we multiply (4.11a) with test functions v_i and apply the first Green's identity (2.65) in each part to get

$$(\mathcal{U}_i \nabla u_i, \nabla v_i)_{\Omega_i} - \left\langle \mathcal{U}_i \nabla u_{i|\Gamma_i} \cdot \boldsymbol{n}_i, v_{i|\Gamma_i} \right\rangle_{\Gamma_i} = \langle f_i, v_i \rangle_{\Omega_i} \tag{4.12}$$

for $i = 1, 2$. We used thereby the BCs $u_i = 0$ on $\Gamma_{0,i}$ with $i = 1, 2$. In Ω^{e} the Laplace equation is represented by the interior BIE (3.37a)

$$\mathcal{V}_0 \phi = \left(\frac{1}{2} + \mathcal{K}_0 \right) u^{\mathrm{e}}{}_{|\Gamma^{\mathrm{e}}} \tag{4.13}$$

with $\phi := \nabla u^{\mathrm{e}}{}_{|\Gamma^{\mathrm{e}}} \cdot \boldsymbol{n}_{\mathrm{e}}$. From Lemma 3.16, we choose the Neumann data with $\phi \in H_\star^{-\frac{1}{2}}(\Gamma^{\mathrm{e}})$. Consequently, we set $\widehat{\phi}_i \in H_\star^{-\frac{1}{2}}(\Gamma_i)$, $i = 1, 2$. The choice of the corresponding space for Dirichlet data will be discussed below.

Furthermore, similarly to Section 4.1 we introduce the product space

$$\boldsymbol{\mathcal{H}}_0 := H_0(\nabla, \Omega_1, \Gamma_{0,1}) \times H_0(\nabla, \Omega_2, \Gamma_{0,2}) \times H_\star^{-\frac{1}{2}}(\Gamma^{\mathrm{e}}), \tag{4.14}$$

and endow it with the norm

$$\|\mathbf{v}\|_{\boldsymbol{\mathcal{H}}_0} := \sqrt{\|v_1\|^2_{H(\nabla,\Omega_1)} + \|v_2\|^2_{H(\nabla,\Omega_2)} + \|\psi\|^2_{H^{-\frac{1}{2}}(\Gamma^{\mathrm{e}})}} \qquad \text{for } \mathbf{v} = (v_1, v_2, \psi) \in \boldsymbol{\mathcal{H}}_0.$$

Using $\Gamma^{\mathrm{e}} = \Gamma_1 \cup \Gamma_2$ and inserting the corresponding jump conditions (4.11c) and (4.11d) in (4.13) and (4.12), respectively, yields the following weak formulation for Problem 4.26:

Find $\mathbf{u} := (u_1, u_2, \phi) \in \boldsymbol{\mathcal{H}}_0 := H_0(\nabla, \Omega_1, \Gamma_{0,1}) \times H_0(\nabla, \Omega_2, \Gamma_{0,2}) \times H_\star^{-\frac{1}{2}}(\Gamma^{\mathrm{e}})$ such that

$$\begin{aligned}
(\mathcal{U}_1 \nabla u_1, \nabla v_1)_{\Omega_1} + \left\langle \phi_{|\Gamma_1}, v_{1|\Gamma_1} \right\rangle_{\Gamma_1} &= \langle f_1, v_1 \rangle_{\Omega_1} + \left\langle \widehat{\phi}_1, v_{1|\Gamma_1} \right\rangle_{\Gamma_1}, \\
(\mathcal{U}_2 \nabla u_2, \nabla v_2)_{\Omega_2} + \left\langle \phi_{|\Gamma_2}, v_{2|\Gamma_2} \right\rangle_{\Gamma_2} &= \langle f_2, v_2 \rangle_{\Omega_2} + \left\langle \widehat{\phi}_2, v_{2|\Gamma_2} \right\rangle_{\Gamma_2}, \\
\langle \psi, \mathcal{V}_0 \phi \rangle_{\Gamma^{\mathrm{e}}} - \sum_{i=1}^{2} \left\langle \psi, \left(\frac{1}{2} + \mathcal{K}_0 \right) u_{i|\Gamma_i} \right\rangle_{\Gamma^{\mathrm{e}}} &= \sum_{i=1}^{2} \left\langle \psi, \left(\frac{1}{2} + \mathcal{K}_0 \right) \widehat{u}_i \right\rangle_{\Gamma^{\mathrm{e}}}
\end{aligned}$$

hold $\forall \mathbf{v} := (v_1, v_2, \psi) \in \boldsymbol{\mathcal{H}}_0$.

Because of $\left(\frac{1}{2} + \mathcal{K}_0\right) 1_{\Gamma_i} = 0$ with $i = 1, 2$, the Dirichlet data $\widehat{u}_i$ can be considered in the corresponding whole space $H^{\frac{1}{2}}(\Gamma_i)$ instead of $[H^{\frac{1}{2}}(\Gamma_i)]$. With this, we first write the problem in a compact form.

Problem 4.27. *Find* $\mathbf{u} := (u_1, u_2, \phi) \in \boldsymbol{\mathcal{H}}_0$ *such that* $b(\mathbf{u}, \mathbf{v}) = \iota(\mathbf{v})$ *holds* $\forall \mathbf{v} := (v_1, v_2, \psi) \in \boldsymbol{\mathcal{H}}_0$.

Thereby,

$$b(\mathbf{u}, \mathbf{v}) := \sum_{i=1}^{2} \left((\mathcal{U}_i \nabla u_i, \nabla v_i)_{\Omega_i} + \left\langle \phi_{|\Gamma_i}, v_{i|\Gamma_i} \right\rangle_{\Gamma_i} - \left\langle \psi, \left(\frac{1}{2} + \mathcal{K}_0 \right) u_{i|\Gamma_i} \right\rangle_{\Gamma^{\mathrm{e}}} \right) + \langle \psi, \mathcal{V}_0 \phi \rangle_{\Gamma^{\mathrm{e}}},$$

and

$$\iota(\mathbf{v}) := \sum_{i=1}^{2} \left(\langle f_i, v_i \rangle_{\Omega_i} + \left\langle \widehat{\phi}_i, v_{i|\Gamma_i} \right\rangle_{\Gamma_i} + \left\langle \psi, \left(\frac{1}{2} + \mathcal{K}_0 \right) \widehat{u}_i \right\rangle_{\Gamma^{\mathrm{e}}} \right).$$

In this case no stabilization is needed, because the Dirichlet BCs clearly allow the application of the Friedrichs' inequality, which establishes a norm in interior domains. Therefore, we prove directly the strong monotonicity of $b(\cdot,\cdot)$. Analogously to (4.5), the form $b(\cdot,\cdot)$ induces a non-linear operator $\mathcal{B} : \boldsymbol{\mathcal{H}}_0 \to \boldsymbol{\mathcal{H}}_0'$ with

$$\langle \mathcal{B}(\mathbf{u}), \mathbf{v}\rangle := b(\mathbf{u},\mathbf{v}) \quad \forall \mathbf{u},\mathbf{v} \in \boldsymbol{\mathcal{H}}_0. \tag{4.15}$$

The next theorem establishes the strong monotonicity of the method for the extended BVP. It is based on the idea used for a stability estimate for an interior Dirichlet BVP of a diffusion equation with a hard inclusion, see [90]. The key idea therein is to estimate the energy of the bounded finite element domains with the energy of some related problem in the exterior domain. Let $\lambda > 0$ be the minimal eigenvalue of the related exterior problem. If both corresponding Steklov-Poincaré operators are $H^{\frac{1}{2}}(\Gamma)$-elliptic, then we have that

$$\lambda\left\langle \mathcal{S}^{\text{ext}} v, v\right\rangle \leq \left\langle \mathcal{S}^{\text{int}} v, v\right\rangle, \text{ for all } v \in H^{\frac{1}{2}}(\Gamma), \tag{4.16}$$

where $\mathcal{S}^{\text{ext}}$ and $\mathcal{S}^{\text{int}}$ are the Steklov-Poincaré operators of the exterior and the interior domain, respectively, cf. [90]. The constants in the following theorem have similar dependencies as described in Remark 4.6.

Theorem 4.28. *Let us consider the non-linear operator $\mathcal{B} : \boldsymbol{\mathcal{H}}_0 \to \boldsymbol{\mathcal{H}}_0'$ defined in* (4.15) *with $\boldsymbol{\mathcal{H}}_0$ being the product space introduced in* (4.14)*. Furthermore, $\lambda_1, \lambda_2 > 0$ are the eigenvalues in* (4.16) *with respect to the domains Ω_1 and Ω_2. We state the following three assertions:*

1. *$\mathcal{B}$ is Lipschitz continuous, i.e., there exists $C_{\text{L}} > 0$ such that*

$$\|\mathcal{B}(\mathbf{u}) - \mathcal{B}(\mathbf{v})\|_{\boldsymbol{\mathcal{H}}_0'} \leq C_{\text{L}} \|\mathbf{u}-\mathbf{v}\|_{\boldsymbol{\mathcal{H}}_0} \tag{4.17}$$

   for all $\mathbf{u},\mathbf{v} \in \boldsymbol{\mathcal{H}}_0$.

2. *If $C_{\text{M}}^{\mathcal{U}_i} > \frac{1}{4\lambda_i}$ for $i = 1, 2$, then*

$$\langle \mathcal{B}(\mathbf{u}) - \mathcal{B}(\mathbf{v}), \mathbf{u}-\mathbf{v}\rangle \geq C_{\text{stab}} \left(\|\nabla u_1 - \nabla v_1\|^2_{L^2(\Omega_1)} + \|\nabla u_2 - \nabla v_2\|^2_{L^2(\Omega_2)} + \|\phi - \psi\|^2_{\mathcal{V}_0} \right) \tag{4.18}$$

   for all $\mathbf{u} := (u_1, u_2, \phi) \in \boldsymbol{\mathcal{H}}_0$, $\mathbf{v} := (v_1, v_2, \psi) \in \boldsymbol{\mathcal{H}}_0$ with

$$C_{\text{stab}} = \min\left\{ 1, \frac{1}{2}\left(1 + C_{\text{M}}^{\mathcal{U}_1} - \sqrt{\left(C_{\text{M}}^{\mathcal{U}_1} - 1\right)^2 + \frac{1}{\lambda_1}}\right), \frac{1}{2}\left(1 + C_{\text{M}}^{\mathcal{U}_2} - \sqrt{\left(C_{\text{M}}^{\mathcal{U}_2} - 1\right)^2 + \frac{1}{\lambda_2}}\right)\right\}.$$

3. *If $C_{\text{M}}^{\mathcal{U}_i} > \frac{1}{4\lambda_i}$ for $i = 1, 2$, then $\mathcal{B}$ is strongly monotone, i.e., there exists $C_{\text{M}} > 0$ such that*

$$\langle \mathcal{B}(\mathbf{u}) - \mathcal{B}(\mathbf{v}), \mathbf{u}-\mathbf{v}\rangle \geq C_{\text{M}} \|\mathbf{u}-\mathbf{v}\|^2_{\boldsymbol{\mathcal{H}}_0} \tag{4.19}$$

   for all $\mathbf{u},\mathbf{v} \in \boldsymbol{\mathcal{H}}_0$.

Proof. The Lipschitz continuity follows merely from the Lipschitz continuity of $\mathcal{U}_1$ and $\mathcal{U}_2$ and the continuity of the boundary integral operators.
The stability estimate follows strongly the steps of the proofs of [90, Theorem 2.2.ii.] and [90, Section 5.1]. Since we are dealing with a different BVP and non-linear material tensors, we sketch the main steps of the

proof, for convenience.
For ease of notation, let $\mathbf{w} := (w_1, w_2, \xi) = \mathbf{u} - \mathbf{v} = (u_1 - v_1, u_2 - v_2, \phi - \psi) \in \boldsymbol{\mathcal{H}}_0$. From (4.15), we get

$$\langle \mathcal{B}(\mathbf{u}) - \mathcal{B}(\mathbf{v}), \mathbf{w} \rangle := \sum_{i=1}^{2} \left((\mathcal{U}_i \nabla u_i - \mathcal{U}_i \nabla v_i, \nabla w_i)_{\Omega_i} + \left\langle \xi, \left(\frac{1}{2} - \mathcal{K}_0 \right) w_{i|\Gamma_i} \right\rangle_{\Gamma^e} \right) + \langle \xi, \mathcal{V}_0 \xi \rangle_{\Gamma^e} . \tag{4.20}$$

First, we start with the domain parts. Provided $\mathcal{U}_i$ with $i = 1, 2$ are strongly monotone, then it holds

$$(\mathcal{U}_i \nabla u_i - \mathcal{U}_i \nabla v_i, \nabla w_i)_{\Omega_i} \geq C_{\mathrm{M}}^{\mathcal{U}_i} \, \|\nabla w_i\|^2_{L^2(\Omega_i)}.$$

For $w_i \in H_0(\nabla, \Omega_i, \Gamma_{0,i})$, we now consider the splitting $w_i = \overline{w}_i + w_{0,i}$, where $\overline{w}_i$ is the harmonic extension of $w_{i|\Gamma_i}$ and $w_{0,i} \in H_0(\nabla, \Omega_i, \partial\Omega_i)$; see, e.g., [46]. From this follows

$$\|\nabla w_i\|^2_{L^2(\Omega_i)} = \|\nabla w_{0,i}\|^2_{L^2(\Omega_i)} + \left\langle \mathcal{S}_i^{\mathrm{int}} w_{i|\Gamma_i}, w_{i|\Gamma_i} \right\rangle_{\Gamma_i},$$

where $\mathcal{S}_i^{\mathrm{int}}$ with $i = 1, 2$ denote the interior Steklov-Poincaré operators of the bounded domains Ω_1 and Ω_2, respectively. Hence,

$$(\mathcal{U}_i \nabla u_i - \mathcal{U}_i \nabla v_i, \nabla w_i)_{\Omega_i} \geq C_{\mathrm{M}}^{\mathcal{U}_i} \left(\|\nabla w_{0,i}\|^2_{L^2(\Omega_i)} + \left\langle \mathcal{S}_i^{\mathrm{int}} w_{i|\Gamma_i}, w_{i|\Gamma_i} \right\rangle_{\Gamma_i} \right). \tag{4.21}$$

Next, by using a contractivity-based result for $\mathcal{K}_0$ with respect to $\mathcal{S}_i^{\mathrm{ext}}$, as given in [90, Lemma 2.1], as well as the invertibility of $\mathcal{V}_0$, we obtain

$$\left\langle \xi, \left(\frac{1}{2} - \mathcal{K}_0 \right) w_{i|\Gamma_i} \right\rangle_{\Gamma^e} \leq \|\xi\|_{\mathcal{V}_0} \sqrt{\langle \mathcal{S}_i^{\mathrm{ext}} w_{i|\Gamma_i}, w_{i|\Gamma_i} \rangle_{\Gamma^e}}, \quad i = 1, 2,$$

where $\mathcal{S}_i^{\mathrm{ext}} : H^{\frac{1}{2}}(\Gamma^e) \to H^{-\frac{1}{2}}(\Gamma^e)$ are the Steklov-Poincaré operators associated to the corresponding exterior eigenvalue problem, see [90, Section 2.2]. Note that we considered in the above estimate the worst case $C_{\mathcal{K}_0} = 1$ with the same constant as in Lemma 3.18. Similarly, we assume the following spectral equivalence

$$\langle \mathcal{S}_i^{\mathrm{ext}} w_{i|\Gamma_i}, w_{i|\Gamma_i} \rangle_{\Gamma_i} \leq \frac{1}{\lambda_i} \left\langle \mathcal{S}_i^{\mathrm{int}} w_{i|\Gamma_i}, w_{i|\Gamma_i} \right\rangle_{\Gamma_i} \quad \text{for all } w_i \in H_0(\nabla, \Omega_i, \Gamma_{0,i}),$$

where λ_i, $i = 1, 2$ are characterized as minimal eigenvalues of the related problem, respectively. Thus,

$$\left\langle \xi, \left(\frac{1}{2} - \mathcal{K}_0 \right) w_{i|\Gamma_i} \right\rangle_{\Gamma^e} \leq \|\xi\|_{\mathcal{V}_0} \sqrt{\frac{1}{\lambda_i} \langle \mathcal{S}_i^{\mathrm{int}} w_{i|\Gamma_i}, w_{i|\Gamma_i} \rangle_{\Gamma_i}}, \quad i = 1, 2. \tag{4.22}$$

Inserting (4.21) and (4.22) in (4.20) leads with $\langle \xi, \mathcal{V}_0 \xi \rangle_{\Gamma^e} = \|\xi\|^2_{\mathcal{V}_0}$ and some manipulations as in the proof of [46, Theorem 1] to the assertion.
To prove the last claim we consider $\mathbf{v} := (v_1, v_2, \psi) \in \boldsymbol{\mathcal{H}}_0$. Note that $v_1 = 0$ on $\Gamma_{0,1}$ and $v_2 = 0$ on $\Gamma_{0,2}$ with $|\Gamma_{0,1}|, |\Gamma_{0,2}| > 0$. Due to Friedrichs' inequality and (3.34) it follows that $\|\nabla v_1\|^2_{L^2(\Omega_1)} + \|\nabla v_2\|^2_{L^2(\Omega_2)} + \|\psi\|^2_{\mathcal{V}_0}$ is an equivalent norm on $\boldsymbol{\mathcal{H}}_0$. Thus, (4.19) follows directly from (4.18). □

With this follows well-posedness of the extended problem.

Theorem 4.29 (Well-posedness)**.** *Provided that $C_{\mathrm{M}}^{\mathcal{U}} > \frac{1}{4}$, there exists a unique solution $\mathbf{u} := (u_1, u_2, \phi) \in \boldsymbol{\mathcal{H}}_0 :=$*

$H_0(\nabla,\Omega_1,\Gamma_{0,1})\times H_0(\nabla,\Omega_2,\Gamma_{0,2})\times H_\star^{-\frac{1}{2}}(\Gamma^{\mathrm{e}})$ *of Problem 4.27 for any* $\left(f_i,\widehat{u}_i,\widehat{\phi}_i\right)\in H_0(\nabla,\Omega_i)'\times H^{\frac{1}{2}}(\Gamma_i)\times\widehat{\phi}_i\in H_\star^{-\frac{1}{2}}(\Gamma_i)$ *with* $i=1,2$.

Proof. The assertion is an immediate consequence of Theorem 4.28 and Theorem 2.5. □

The non-linear operators $\mathcal{U}_i$, $i=1,2$ are now considered to have the form $\mathcal{U}_i\nabla u:=\nu_i(|\nabla u|)\nabla u$ with non-linear functions $\nu_i:\mathbb{R}\to\mathbb{R}$ that are admissible in the sense of Definition 1.1. Similarly to the interface problem, we state the following stability result.

Lemma 4.30. *Let* $C_{\mathrm{M}}^{\mathcal{U}_i}>\frac{1}{4\lambda_i}$, $i=1,2$, *with* λ_i *as in Theorem 4.28. Furthermore, the non-linear operators* $\mathcal{U}_i$, $i=1,2$, *shall have the form* $\mathcal{U}_i\nabla u:=\nu_i(|\nabla u|)\nabla u$ *with admissible non-linear functions* $\nu_i:\mathbb{R}\to\mathbb{R}$ *in the sense of Definition 1.1. Moreover, let* $\mathbf{u}\in\boldsymbol{\mathcal{H}}_0$ *be the unique solution of Problem 4.27 and* $\left(f_i,\widehat{u}_i,\widehat{\phi}_i\right)\in H_0(\nabla,\Omega_i)'\times H^{\frac{1}{2}}(\Gamma_i)\times H^{-\frac{1}{2}}(\Gamma_i)$ *with* $i=1,2$, *being some inputs. Then, there exists* $C>0$ *such that*

$$\|\mathbf{u}\|_{\boldsymbol{\mathcal{H}}_0}\leq C\sum_{i=1}^{2}\left(\|f_i\|_{H(\nabla,\Omega_i)'}+\|u_{i,0}\|_{H^{\frac{1}{2}}(\Gamma_i)}+\|\phi_{i,0}\|_{H^{-\frac{1}{2}}(\Gamma_i)}\right).$$

Proof. We know from the strong monotonicity of $\mathcal{B}$ that

$$C_{\mathrm{M}}\|\mathbf{u}-\mathbf{v}\|_{\boldsymbol{\mathcal{H}}_0}^2\leq\langle\mathcal{B}(\mathbf{u})-\mathcal{B}(\mathbf{v}),\mathbf{u}-\mathbf{v}\rangle$$

holds for all $\mathbf{u},\mathbf{v}\in\boldsymbol{\mathcal{H}}_0$. Without loss of generality, we choose $\mathbf{v}=(0,0,0)$ and note that $\mathcal{U}_i\nabla v_i=0$, $i=1,2$, for our specific non-linearity. Since $\mathbf{u}:=(u_1,u_2,\phi)$ is the unique solution of the problem, we conclude that

$$\begin{aligned}C_{\mathrm{M}}\|\mathbf{u}\|_{\boldsymbol{\mathcal{H}}_0}^2&\leq\langle\mathcal{B}(\mathbf{u}),\mathbf{u}\rangle=\iota(\mathbf{u})\\&=\sum_{i=1}^{2}\left(\langle f_i,u_i\rangle_{\Omega_i}+\left\langle\widehat{\phi}_i,u_{i|\Gamma_i}\right\rangle_{\Gamma_i}+\left\langle\phi,\left(\frac{1}{2}+\mathcal{K}_0\right)\widehat{u}_i\right\rangle_{\Gamma^{\mathrm{e}}}\right).\end{aligned}$$

Using the trace inequality (2.58), along with the boundedness of $\mathcal{K}_0$ and $\mathcal{V}_0$, and rearranging the terms provides the assertion. □

4.3.2 A priori error estimates and super-convergence

Let us consider the same conforming isogeometric Galerkin discretization as in Section 4.1. Namely, the discrete problem is obtained by replacing $\mathbf{u}:=(u_1,u_2,\phi)\in\boldsymbol{\mathcal{H}}_0:=H_0(\nabla,\Omega_1,\Gamma_{0,1})\times H_0(\nabla,\Omega_2,\Gamma_{0,2})\times H_\star^{-\frac{1}{2}}(\Gamma^{\mathrm{e}})$ in Problem 4.27 with $\mathbf{u}_\ell:=(u_{1,\ell},u_{2,\ell},\phi_\ell)\in\boldsymbol{\mathcal{H}}_{0,\ell}:=\mathbb{S}^0_{\boldsymbol{p}}(\Omega_1,\Gamma_{0,1})\times\mathbb{S}^0_{\boldsymbol{p}}(\Omega_2,\Gamma_{0,2})\times\mathbb{S}^2_{\widetilde{p}}(\Gamma^{\mathrm{e}})$. Note that accordingly to the notation in the continuous setting, $\mathbb{S}^0_{\boldsymbol{p}}(\Omega,\Gamma)$ denotes the B-Spline space $\mathbb{S}^0_{\boldsymbol{p}}(\Omega)$ of order p with a Dirichlet BC on $\Gamma\subseteq\partial\Omega$, and $\mathbb{S}^2_{\widetilde{p}}(\Gamma^{\mathrm{e}})$ is of order $\widetilde{p}=p-1$, see Subsection 4.1.3.

Problem 4.31 (Discrete problem)**.** *Find* $\mathbf{u}_\ell:=(u_{1,\ell},u_{2,\ell},\phi_\ell)\in\boldsymbol{\mathcal{H}}_{0,\ell}:=\mathbb{S}^0_{\boldsymbol{p}}(\Omega_1,\Gamma_{0,1})\times\mathbb{S}^0_{\boldsymbol{p}}(\Omega_2,\Gamma_{0,2})\times\mathbb{S}^2_{\widetilde{p}}(\Gamma^{\mathrm{e}})$ *such that* $b(\mathbf{u}_\ell,\mathbf{v}_\ell)=\iota(\mathbf{v}_\ell)$ *holds for all* $\mathbf{v}_\ell:=(v_{1,\ell},v_{2,\ell},\psi_\ell)\in\boldsymbol{\mathcal{H}}_{0,\ell}$.

In complete analogy to the interface problem, we state in the following theorem the quasi-optimality in the sense of a Céa-type lemma of the discrete Problem, as well as an a priori error estimate for the introduced B-Spline discretization. For convenience, let us introduce a piecewise defined product space $s \geq 0$ with

$$\boldsymbol{\mathcal{H}}^s_{\text{pw}} := \big(H(\nabla,\Omega_1) \cap H^{1+s}_{\text{pw}}(\Omega_1)\big) \times \big(H(\nabla,\Omega_2) \cap H^{1+s}_{\text{pw}}(\Omega_2)\big) \times \big(H_\star^{-\frac{1}{2}}(\Gamma^{\text{e}}) \cap H_{\text{pw}}^{-\frac{1}{2}+s}(\Gamma^{\text{e}})\big), \tag{4.23}$$

and equip it with the norm $\|\cdot\|_{\boldsymbol{\mathcal{H}}^s_{\text{pw}}}$, which is defined as in (4.7). Then, we can establish the following results.

Theorem 4.32. *For $i = 1, 2$, let $C_{\text{M}}^{\mathcal{U}_i} > \frac{1}{4\lambda_i}$, with λ_i as in Theorem 4.28. Moreover, let $\mathbf{u} \in \boldsymbol{\mathcal{H}}_0$ be the solution of Problem 4.27 and $\mathbf{u}_\ell \in \boldsymbol{\mathcal{H}}_{0,\ell}$ be the discrete solution of Problem 4.31. Then we have the following results:*

- *Quasi-optimality:*

$$\|\mathbf{u} - \mathbf{u}_\ell\|_{\boldsymbol{\mathcal{H}}_0} \leq C_{\text{Céa}} \min_{\mathbf{v}_\ell \in \boldsymbol{\mathcal{H}}_{0,\ell}} \|\mathbf{u} - \mathbf{v}_\ell\|_{\boldsymbol{\mathcal{H}}_0}, \tag{4.24}$$

  where $C_{\text{Céa}} = \frac{C_{\text{L}}}{C_{\text{M}}}$.

- *A priori estimate: For $\frac{1}{2} \leq s \leq p$ and $\mathbf{u} \in \boldsymbol{\mathcal{H}}^s_{\text{pw}}$,*

$$\|\mathbf{u} - \mathbf{u}_\ell\|_{\boldsymbol{\mathcal{H}}_0} \leq C\, h^s \|\mathbf{u}\|_{\boldsymbol{\mathcal{H}}^s_{\text{pw}}}$$

  with a constant $C = C(C_{\text{Céa}}, p, C_\theta) > 0$, which is independent of h. For $0 \leq s \leq \frac{1}{2}$, we get a similar result as stated in Theorem 4.15 with $\phi \in H_\star^{-\frac{1}{2}}(\Gamma^{\text{e}}) \cap H^0_{\text{pw}}(\Gamma^{\text{e}})$.

Proof. Quasi-optimality follows from the strong monotonicity and Lipschitz continuity stated in Theorem 4.28, by following the lines of Theorem 4.12. The a priori estimate follows from the quasi-optimality and Lemma 4.14, as is done in Theorem 4.15 for the interface problem. □

In many practical applications, we might not be directly interested in the solution (u_1, u_2, ϕ) of Problem 4.27 rather than in some derived physical entities, which are, for example, evaluated in the exterior/air gap domain. As it can be observed for standalone BEM applications, estimating the error in functionals of the solution may lead to so called super-convergence, i.e., linear functionals of the solution may converge better than the solution in the energy norm, see [103, Section 4.2.5]. With enough regularity the convergence rate doubles.
In the following, this behavior is also shown for the coupled problem. For this, we use the following Aubin-Nitsche argument, similar to [103, Theorem 4.2.14].

Theorem 4.33. *Let $\mathfrak{F} \in \boldsymbol{\mathcal{H}}_0'$ be a continuous and linear functional. Moreover, let $\mathbf{u} := (u_1, u_2, \phi) \in \boldsymbol{\mathcal{H}}_0 := H_0(\nabla,\Omega_1,\Gamma_{0,1}) \times H_0(\nabla,\Omega_2,\Gamma_{0,2}) \times H_\star^{-\frac{1}{2}}(\Gamma^{\text{e}})$ be the solution of Problem 4.27 and $\mathbf{u}_\ell := (u_{1,\ell}, u_{2,\ell}, \phi_\ell) \in \boldsymbol{\mathcal{H}}_{0,\ell}$ be the discrete solution of Problem 4.31. By assuming that $\mathbf{w} \in \boldsymbol{\mathcal{H}}_0$ is the unique solution of the dual problem*

$$b(\mathbf{v}, \mathbf{w}) = \mathfrak{F}(\mathbf{v}) \tag{4.25}$$

for all $\mathbf{v} \in \boldsymbol{\mathcal{H}}_0$, there exists a constant $C_1 = C_1(C_{\text{L}}) > 0$ such that

$$|\mathfrak{F}(\mathbf{u}) - \mathfrak{F}(\mathbf{u}_\ell)| \leq C_1 \, \|\mathbf{u} - \mathbf{v}_\ell\|_{\boldsymbol{\mathcal{H}}_0} \|\mathbf{w} - \mathbf{z}_\ell\|_{\boldsymbol{\mathcal{H}}_0} \tag{4.26}$$

for arbitrary $\mathbf{v}_\ell \in \boldsymbol{\mathcal{H}}_{0,\ell}$, $\mathbf{z}_\ell \in \boldsymbol{\mathcal{H}}_{0,\ell}$. *Furthermore, let* $\frac{1}{2} \leq s,t \leq p$ *and recall the product space defined in* (4.23). *Provided* $\mathbf{u}$ *and* $\mathbf{w}$ *are additionally in* $\boldsymbol{\mathcal{H}}^s_{\mathrm{pw}}$ *and* $\boldsymbol{\mathcal{H}}^t_{\mathrm{pw}}$, *respectively, there exists a constant* $C_2 = C_2(C_{\mathrm{L}}, p, C_\theta) > 0$ *such that*

$$|\mathfrak{F}(\mathbf{u}) - \mathfrak{F}(\mathbf{u}_\ell)| \leq C_2\, h^{s+t} \|\mathbf{u}\|_{\boldsymbol{\mathcal{H}}^s_{\mathrm{pw}}} \|\mathbf{w}\|_{\boldsymbol{\mathcal{H}}^t_{\mathrm{pw}}}. \tag{4.27}$$

Proof. The proof follows strongly the lines in [103, Theorem 4.2.14]. Since we allow non-linearities, we give a brief sketch. First of all, we note that Theorem 4.28 holds for arbitrary vector fields in $\boldsymbol{\mathcal{H}}_0$. Thus, well-posedness, and hence the existence of a unique solution can be established for the dual problem (4.25) as well. Furthermore, the dual problem (4.25), the Galerkin orthogonality $b(\mathbf{u} - \mathbf{u}_\ell, \mathbf{z}_\ell) = 0$ for all $\mathbf{z}_\ell \in \boldsymbol{\mathcal{H}}_{0,\ell}$, and the Lipschitz continuity of the form $b(\cdot,\cdot)$ provide

$$|\mathfrak{F}(\mathbf{u}) - \mathfrak{F}(\mathbf{u}_\ell)| = |\mathfrak{F}(\mathbf{u} - \mathbf{u}_\ell)| = |b(\mathbf{u} - \mathbf{u}_\ell, \mathbf{w} - \mathbf{z}_\ell)| \leq C_1 \|\mathbf{u} - \mathbf{u}_\ell\|_{\boldsymbol{\mathcal{H}}_0} \|\mathbf{w} - \mathbf{z}_\ell\|_{\boldsymbol{\mathcal{H}}_0}$$

for arbitrary $\mathbf{z}_\ell = (z_{1,\ell}, z_{2,\ell}, \varphi_\ell) \in \boldsymbol{\mathcal{H}}_{0,\ell}$.

With (4.24) we get the claim (4.26). Since Lemma 4.14 holds for arbitrary $\mathbf{u}$, (4.27) follows from (4.26). □

Remark 4.34. *In practice the functional of Theorem 4.33 may be, e.g., the representation formula of the exterior BEM part* Ω^{e}, *see* (3.19b), *i.e., for* $\mathbf{u} = (u_1, u_2, \phi) \in \boldsymbol{\mathcal{H}}_0$

$$u^{\mathrm{e}}(\boldsymbol{x}) = \mathfrak{F}(\mathbf{u}) := \sum_{i=1}^{2} \Big(\int_{\Gamma_i} u^*(\boldsymbol{x},\boldsymbol{y}) \phi_{|\Gamma_i}(\boldsymbol{y})\, \mathrm{d}\sigma_{\boldsymbol{y}} - \int_{\Gamma_i} \nabla_{\boldsymbol{y}} u^*(\boldsymbol{x},\boldsymbol{y}) \cdot \boldsymbol{n}(\boldsymbol{y}) (u_{i|\Gamma_i} + \widehat{u}_i)(\boldsymbol{y})\, \mathrm{d}\sigma_{\boldsymbol{y}} \Big).$$

Next, let us assume the regularity $\mathbf{u} \in \boldsymbol{\mathcal{H}}^p_{\mathrm{pw}}$ *for the solution of Problem 4.27 and* $\mathbf{w} \in \boldsymbol{\mathcal{H}}^p_{\mathrm{pw}}$ *of its dual problem* (4.25), *where the spaces are defined in* (4.23). *Then, with the discrete solution* $\mathbf{u}_\ell \in \boldsymbol{\mathcal{H}}_{0,\ell}$ *of Problem 4.31 and* (4.27) *we calculate the pointwise error in* Ω^{e} *as*

$$|u^{\mathrm{e}}(\boldsymbol{x}) - u^{\mathrm{e}}_\ell(\boldsymbol{x})| = |\mathfrak{F}(\mathbf{u})(\boldsymbol{x}) - \mathfrak{F}(\mathbf{u}_\ell)(\boldsymbol{x})| \leq C h^{2p}, \tag{4.28}$$

which is the maximal possible super-convergence. Since the constant C *depends on* $\|\mathbf{u}\|_{\boldsymbol{\mathcal{H}}^p_{\mathrm{pw}}}$ *and* $\|\mathbf{w}\|_{\boldsymbol{\mathcal{H}}^p_{\mathrm{pw}}}$, *a possible estimate of these norms would probably involve their right-hand sides. The right-hand side of the dual problem* (4.25) *is the functional* $\mathfrak{F}(\mathbf{u})$. *Thus, the constant* C *might include a factor like*

$$\sum_{i=1}^{2} \Big(\|u^*(\boldsymbol{x},\cdot)\|_{H^{\frac{1}{2}+p}(\Gamma_i)} + \|\nabla u^*(\boldsymbol{x},\cdot) \cdot \boldsymbol{n}(\cdot)\|_{H^{-\frac{1}{2}+p}(\Gamma_i)} \Big). \tag{4.29}$$

Note that this term is finite for all $\boldsymbol{x} \in \mathbb{R}^2 \backslash \Gamma^{\mathrm{e}}$ *and* $p \geq 0$. *However, because of the singularity of the kernels,* (4.29) *tends to infinity when approaching the boundaries. Thus, also* C *from* (4.28) *might tend to infinity. It should be noted however that this effect can be avoided or reduced by employing suitable integration techniques. This will be discussed and illustrated numerically in Subsection 5.1.1. Finally, we mention that the regularity assumptions might hold only for smooth surfaces.*

Remark 4.35. *As stated in* (1.19), *the computation of forces and torques requires the knowledge of the magnetic flux density* $\boldsymbol{b}^{\mathrm{e}}$. *If we interpret* u^{e} *as the magnetic vector potential, we know that for* $\boldsymbol{x} = (x_1, x_2)$, *we have*

$\boldsymbol{b}^{\mathrm{e}}(\boldsymbol{x}) = \widetilde{\mathbf{curl}}\, u^{\mathrm{e}}(\boldsymbol{x})$*, see Section 3.1. Then, the functional* $\mathfrak{F}$ *on* $\mathbf{u}$ *can be chosen such that*

$$\boldsymbol{b}^{\mathrm{e}}(\boldsymbol{x}) = \mathfrak{F}(\mathbf{u}) := \sum_{i=1}^{2} \begin{pmatrix} \int_{\Gamma_i} \partial_{x_2} u^*(\boldsymbol{x},\boldsymbol{y}) \phi_{|\Gamma_i}(\boldsymbol{y}) \,\mathrm{d}\sigma_{\boldsymbol{y}} - \int_{\Gamma_i} \partial_{x_2} (\nabla_{\boldsymbol{y}} u^*(\boldsymbol{x},\boldsymbol{y}) \cdot \boldsymbol{n}(\boldsymbol{y}))(u_{i|\Gamma_i} + \widehat{u}_i)(\boldsymbol{y}) \,\mathrm{d}\sigma_{\boldsymbol{y}} \\ - \int_{\Gamma_i} \partial_{x_1} u^*(\boldsymbol{x},\boldsymbol{y}) \phi_{|\Gamma_i}(\boldsymbol{y}) \,\mathrm{d}\sigma_{\boldsymbol{y}} + \int_{\Gamma_i} \partial_{x_1} (\nabla_{\boldsymbol{y}} u^*(\boldsymbol{x},\boldsymbol{y}) \cdot \boldsymbol{n}(\boldsymbol{y}))(u_{i|\Gamma_i} + \widehat{u}_i)(\boldsymbol{y}) \,\mathrm{d}\sigma_{\boldsymbol{y}} \end{pmatrix}.$$

We can easily check analogously to the previous remark that the constant C*, which arises in this case depends on a higher degree of singularity because of the additional derivatives. Hence, it might tend more rapidly towards infinity, when approaching the boundaries.*

Remark 4.36. *In the linear case, the dual problem to Problem 4.2 or Problem 4.27 is the corresponding Bielak-MacCamy coupling [6]. Hence, the same approximation properties hold for the dual problem, see [6].*

Remark 4.37. *Note that similar results as in Theorem 4.33 and in Remark 4.34 for the extended Problem 4.27 can be gained for the interface Problem 4.2 and analogously for the parabolic Problem 4.18.*

4.4 The three-dimensional (3D) magnetostatic case

Let $\Omega \subset \mathbb{R}^3$ be a Lipschitz bounded domain with a boundary $\Gamma = \Gamma_{\mathrm{FEM}} \cup \Gamma_{\mathrm{BEM}}$ as defined in Section 3.1, and let $\Omega^{\mathrm{e}} := \mathbb{R}^3 \backslash \overline{\Omega}$ denote the exterior domain. In this section, we study the equations of magnetostatics as given in Chapter 3 in the 3D case. Thereby, we observed that the model problem depends on the topology and on the specific BCs. We derived for instance two types of vector potentials. In the interior domain, the first one lies in $[\boldsymbol{H}_{\mathbf{0}}(\mathbf{curl}, \Omega, \Gamma_{\mathrm{FEM}})]$ (electric wall) and the second in $[\boldsymbol{H}(\mathbf{curl}, \Omega, \Gamma_{\mathrm{FEM}})]$ (magnetic wall). In this respect, the right-hand side is either in $\boldsymbol{H}^{\Gamma}(\operatorname{div} 0, \Omega)$ or $\boldsymbol{H}_0^{\mathsf{C}}(\operatorname{div} 0, \Omega)$. Basically, the subsequent analysis works for both cases with self-evident modifications. The crucial point for the interior part is the existence of a Friedrichs' inequality, which can indeed be derived for both types of spaces, cf. [88, Corollary 3.51]. Therefore, we conduct the analysis with the latter mentioned spaces, namely the couple $[\boldsymbol{H}(\mathbf{curl}, \Omega, \Gamma_{\mathrm{FEM}})]$ and $\boldsymbol{H}_0^{\mathsf{C}}(\operatorname{div} 0, \Omega)$. With a slight abuse of notation, we drop the explicit mention of Γ_{FEM} in the definition of the energy spaces, and write Γ as an argument of the trace spaces but mean Γ_{BEM} instead.

The concrete interface problem derives from the coupling of (3.9) and (3.12) via the jump conditions. In a weak sense, it reads:

Problem 4.38 (Classical problem)**.** *Find* $\boldsymbol{u} \in [\boldsymbol{H}(\mathbf{curl}, \Omega)]$ *and* $\boldsymbol{u}^{\mathrm{e}} \in \boldsymbol{H}_{\mathrm{loc}}(\mathbf{curl}, \Omega^{\mathrm{e}}) \cap \boldsymbol{H}_{\mathrm{loc}}(\operatorname{div}, \Omega^{\mathrm{e}})$ *such that*

$$\mathbf{curl}\,(\mathcal{U}\,\mathbf{curl}\,\boldsymbol{u}) = \boldsymbol{f} \qquad \text{in } \Omega, \tag{4.30a}$$

$$\mathbf{curl}\,\mathbf{curl}\,\boldsymbol{u}^{\mathrm{e}} = \mathbf{0} \qquad \text{in } \Omega^{\mathrm{e}}, \tag{4.30b}$$

$$\operatorname{div} \boldsymbol{u}^{\mathrm{e}} = 0 \qquad \text{in } \Omega^{\mathrm{e}}, \tag{4.30c}$$

$$\gamma_{\mathrm{D}}\,\boldsymbol{u} - \gamma_{\mathrm{D}}^{\mathrm{e}}\,\boldsymbol{u}^{\mathrm{e}} = \widehat{\boldsymbol{u}} \qquad \text{on } \Gamma, \tag{4.30d}$$

$$\gamma_{\mathrm{N}}^{\mathcal{U}}\,\boldsymbol{u} - \gamma_{\mathrm{N}}^{\mathrm{e}}\,\boldsymbol{u}^{\mathrm{e}} = \widehat{\boldsymbol{\phi}} \qquad \text{on } \Gamma, \tag{4.30e}$$

$$\boldsymbol{u}^{\mathrm{e}} = \mathcal{O}\left(|\boldsymbol{x}^{-1}|\right) \qquad \text{for } |\boldsymbol{x}| \to \infty \tag{4.30f}$$

with $(\boldsymbol{f}, \widehat{\boldsymbol{u}}, \widehat{\boldsymbol{\phi}}) \in \left(\boldsymbol{H}_0^{\mathsf{C}}(\operatorname{div} 0, \Omega), [\boldsymbol{H}^{-\frac{1}{2}}(\operatorname{curl}_\Gamma, \Gamma)], \boldsymbol{H}^{-\frac{1}{2}}(\operatorname{div}_\Gamma 0, \Gamma)\right)$.

4.4.1 Well-posedness and stability

Let us consider Problem 4.38. Testing (4.30a) with $\boldsymbol{v} \in [\boldsymbol{H}(\mathbf{curl}, \Omega)]$, applying the Green's identity (2.66), and inserting (4.30e) leads to

$$(\mathcal{U}\,\mathbf{curl}\,\boldsymbol{u}, \mathbf{curl}\,\boldsymbol{v})_\Omega - \langle \gamma_{\mathrm{N}}^{\mathrm{e}}\,\boldsymbol{u}^{\mathrm{e}}, \gamma_{\mathrm{D}}\,\boldsymbol{v}\rangle_\Gamma = (\boldsymbol{f}, \boldsymbol{v})_\Omega + \left\langle \widehat{\boldsymbol{\phi}}, \gamma_{\mathrm{D}}\,\boldsymbol{v}\right\rangle_\Gamma. \tag{4.31}$$

The equations of the exterior domain are modeled by the BIE (3.39). By taking into account that $\gamma_{\mathrm{N}}^{\mathrm{e}}\,\boldsymbol{u}^{\mathrm{e}} \in \boldsymbol{H}^{-\frac{1}{2}}(\mathrm{div}_\Gamma\, 0, \Gamma)$, see Subsection 3.2.1, inserting (4.30d) in (3.39) yields together with (4.31) to the following variational formulation:

$$\text{Find } \mathbf{u} := (\boldsymbol{u}, \boldsymbol{\phi} := \gamma_{\mathrm{N}}^{\mathrm{e}}\,\boldsymbol{u}^{\mathrm{e}}) \in \boldsymbol{\mathcal{H}}_{\mathrm{v}} := [\boldsymbol{H}(\mathbf{curl}, \Omega)] \times \boldsymbol{H}^{-\frac{1}{2}}(\mathrm{div}_\Gamma\, 0, \Gamma) \text{ such that}$$

$$\begin{aligned}(\mathcal{U}\,\mathbf{curl}\,\boldsymbol{u}, \mathbf{curl}\,\boldsymbol{v})_\Omega - \langle \boldsymbol{\phi}, \gamma_{\mathrm{D}}\,\boldsymbol{v}\rangle_\Gamma &= (\boldsymbol{f}, \boldsymbol{v})_\Omega + \left\langle \widehat{\boldsymbol{\phi}}, \gamma_{\mathrm{D}}\,\boldsymbol{v}\right\rangle_\Gamma,\\ \langle \boldsymbol{\psi}, \boldsymbol{\mathcal{A}}_0\boldsymbol{\phi}\rangle_\Gamma + \left\langle \boldsymbol{\psi}, (\frac{1}{2} + \boldsymbol{\mathcal{C}}_0)\,\gamma_{\mathrm{D}}\,\boldsymbol{u}\right\rangle_\Gamma &= \left\langle \boldsymbol{\psi}, (\frac{1}{2} + \boldsymbol{\mathcal{C}}_0)\widehat{\boldsymbol{u}}\right\rangle_\Gamma\end{aligned}$$

$$\text{for all } \mathbf{v} := (\boldsymbol{v}, \boldsymbol{\psi}) \in \boldsymbol{\mathcal{H}}_{\mathrm{v}}, \text{ and } \left(\boldsymbol{f}, \widehat{\boldsymbol{u}}, \widehat{\boldsymbol{\phi}}\right) \in \left(\boldsymbol{H}_0^{\mathrm{C}}(\mathrm{div}\, 0, \Omega) \times [\boldsymbol{H}^{-\frac{1}{2}}(\mathrm{curl}_\Gamma, \Gamma)] \times \boldsymbol{H}^{-\frac{1}{2}}(\mathrm{div}_\Gamma\, 0, \Gamma)\right).$$

For convenience, we equip the product space $\boldsymbol{\mathcal{H}}_{\mathrm{v}} := [\boldsymbol{H}(\mathbf{curl}, \Omega)] \times \boldsymbol{H}^{-\frac{1}{2}}(\mathrm{div}_\Gamma\, 0, \Gamma)$ with the following norm

$$\|\mathbf{v}\|_{\boldsymbol{\mathcal{H}}_{\mathrm{v}}} := \sqrt{\|\boldsymbol{v}\|^2_{\boldsymbol{H}(\mathbf{curl},\Omega)} + \|\boldsymbol{\psi}\|^2_{\boldsymbol{H}^{-\frac{1}{2}}(\mathrm{div}_\Gamma,\Gamma)}} \qquad \text{for } \mathbf{v} := (\boldsymbol{v}, \boldsymbol{\psi}) \in \boldsymbol{\mathcal{H}}_{\mathrm{v}}, \tag{4.32}$$

and write the variational formulation derived above in a compact form:

Problem 4.39 (Compact form)**.** *Find* $\mathbf{u} := (\boldsymbol{u}, \boldsymbol{\phi}) \in \boldsymbol{\mathcal{H}}_{\mathrm{v}}$ *such that* $\boldsymbol{b}(\mathbf{u}, \mathbf{v}) = \boldsymbol{\ell}(\mathbf{v})$ *for all* $\mathbf{v} := (\boldsymbol{v}, \boldsymbol{\psi}) \in \boldsymbol{\mathcal{H}}_{\mathrm{v}}$*. Thereby,*

$$\boldsymbol{b}(\mathbf{u}, \mathbf{v}) := (\mathcal{U}\,\mathbf{curl}\,\boldsymbol{u}, \mathbf{curl}\,\boldsymbol{v})_\Omega - \langle \boldsymbol{\phi}, \gamma_{\mathrm{D}}\,\boldsymbol{v}\rangle_\Gamma + \langle \boldsymbol{\psi}, \boldsymbol{\mathcal{A}}_0\boldsymbol{\phi}\rangle_\Gamma + \left\langle \boldsymbol{\psi}, (\frac{1}{2} + \boldsymbol{\mathcal{C}}_0)\,\gamma_{\mathrm{D}}\,\boldsymbol{u}\right\rangle_\Gamma$$

is a linear form (linear in the second argument), and

$$\boldsymbol{\ell}(\mathbf{v}) := (\boldsymbol{f}, \boldsymbol{v})_\Omega + \left\langle \widehat{\boldsymbol{\phi}}, \gamma_{\mathrm{D}}\,\boldsymbol{v}\right\rangle_\Gamma + \left\langle \boldsymbol{\psi}, (\frac{1}{2} + \boldsymbol{\mathcal{C}}_0)\widehat{\boldsymbol{u}}\right\rangle_\Gamma$$

is a linear functional.

In the subsequent analysis, we employ similar arguments as in the previous sections. This can be done with Lemma 3.19. Let $\boldsymbol{\mathcal{H}}_{\mathrm{v}}'$ denote the dual space of $\boldsymbol{\mathcal{H}}_{\mathrm{v}}$ and let $\widetilde{\mathcal{B}} : \boldsymbol{\mathcal{H}}_{\mathrm{v}} \to \boldsymbol{\mathcal{H}}_{\mathrm{v}}'$ be the induced non-linear operator

$$\left\langle \widetilde{\mathcal{B}}(\mathbf{u}), \mathbf{v}\right\rangle = \boldsymbol{b}(\mathbf{u}, \mathbf{v}) \qquad \forall \mathbf{u}, \mathbf{v} \in \boldsymbol{\mathcal{H}}_{\mathrm{v}}. \tag{4.33}$$

Then, we establish Lipschitz continuity and strong monotonicity of the non-linear operator $\widetilde{\mathcal{B}}$.

Theorem 4.40 (Lipschitz continuity and strong monotonicity)**.** *Let* $\widetilde{\mathcal{B}} : \boldsymbol{\mathcal{H}}_{\mathrm{v}} \to \boldsymbol{\mathcal{H}}_{\mathrm{v}}'$ *be defined as in* (4.33) *with* $\boldsymbol{\mathcal{H}}_{\mathrm{v}} := [\boldsymbol{H}(\mathbf{curl}, \Omega)] \times \boldsymbol{H}^{-\frac{1}{2}}(\mathrm{div}_\Gamma\, 0, \Gamma)$*. Then, it holds for all* $\mathbf{u}, \mathbf{v} \in \boldsymbol{\mathcal{H}}_{\mathrm{v}}$ *that:*

- *$\widetilde{\mathcal{B}}$ is Lipschitz continuous, i.e., there exists a constant $C_{\mathrm{L}} > 0$ such that*

$$\left\| \widetilde{\mathcal{B}}(\mathbf{u}) - \widetilde{\mathcal{B}}(\mathbf{v}) \right\|_{\boldsymbol{\mathcal{H}}_{\mathrm{v}'}} \leq C_{\mathrm{L}} \|\mathbf{u} - \mathbf{v}\|_{\boldsymbol{\mathcal{H}}_{\mathrm{v}}}.$$

- *If $C_{\mathrm{M}}^{\mathcal{U}} > \frac{1}{4} C_{\boldsymbol{\mathcal{C}}_0}$, then $\widetilde{\mathcal{B}}$ is strongly monotone, i.e., there exists a constant $C_{\mathrm{M}} > 0$ such that*

$$\left\langle \widetilde{\mathcal{B}}(\mathbf{u}) - \widetilde{\mathcal{B}}(\mathbf{v}), \mathbf{u} - \mathbf{v} \right\rangle \geq C_{\mathrm{M}} \|\mathbf{u} - \mathbf{v}\|^2_{\boldsymbol{\mathcal{H}}_{\mathrm{v}}}.$$

Proof. The Lipschitz continuity of $\widetilde{\mathcal{B}}$ follows from the Lipschitz continuity of the operator $\mathcal{U}$, and the continuity of the boundary integral operators.
The second assertion follows the same approach as in the scalar case. Let $\mathbf{w} = (\boldsymbol{w}, \boldsymbol{\xi}) := \mathbf{u} - \mathbf{v} \in \boldsymbol{\mathcal{H}}_{\mathrm{v}}$. Then,

$$\left\langle \widetilde{\mathcal{B}}(\mathbf{u}) - \widetilde{\mathcal{B}}(\mathbf{v}), \mathbf{w} \right\rangle = \underbrace{(\mathcal{U}\,\mathbf{curl}\,\boldsymbol{u} - \mathcal{U}\,\mathbf{curl}\,\boldsymbol{v}, \boldsymbol{w})_{\Omega}}_{(I)} - \underbrace{\left\langle \boldsymbol{\xi}, (\frac{1}{2} - \boldsymbol{\mathcal{C}}_0)\,\boldsymbol{\gamma}_{\mathrm{D}}\,\boldsymbol{w} \right\rangle_{\Gamma}}_{(II)} + \langle \boldsymbol{\xi}, \boldsymbol{\mathcal{A}}_0 \boldsymbol{\xi} \rangle_{\Gamma}.$$

First, the strong monotonicity of $\mathcal{U}$ yields the estimate

$$(\mathcal{U}\,\mathbf{curl}\,\boldsymbol{u} - \mathcal{U}\,\mathbf{curl}\,\boldsymbol{v}, \boldsymbol{w})_{\Omega} \geq C_M^{\mathcal{U}} \|\mathbf{curl}\,\boldsymbol{w}\|^2_{\boldsymbol{L}^2(\Omega)},$$

which holds for all $\boldsymbol{u}, \boldsymbol{v} \in \boldsymbol{H}(\mathbf{curl}, \Omega)$. Hence, it remains true for any representatives in $[\boldsymbol{H}(\mathbf{curl}, \Omega)]$. Next, we consider for a representative $\boldsymbol{w} \in [\boldsymbol{H}(\mathbf{curl}, \Omega)]$ the splitting $\boldsymbol{w} = \boldsymbol{w}_\Gamma + \widetilde{\boldsymbol{w}}$ with $\widetilde{\boldsymbol{w}} \in [\boldsymbol{H}_{\mathbf{0}}(\mathbf{curl}, \Omega)]$, and $\boldsymbol{w}_\Gamma$ being the solution of the following BVP

$$\begin{aligned} \mathbf{curl}\,\mathbf{curl}\,\boldsymbol{w}_\Gamma &= \mathbf{0} && \text{in } \Omega, \\ \boldsymbol{\gamma}_{\mathrm{D}}\,\boldsymbol{w}_\Gamma &= \boldsymbol{\gamma}_{\mathrm{D}}\,\boldsymbol{w} && \text{on } \Gamma. \end{aligned}$$

Applying (2.66) (with $\mathcal{U} = \mathrm{Id}$) to the BVP leads to

$$(\mathbf{curl}\,\boldsymbol{w}_\Gamma, \mathbf{curl}\,\boldsymbol{w}_\Gamma)_{\Omega} = \langle \boldsymbol{\gamma}_{\mathrm{N}}\,\boldsymbol{w}_\Gamma, \boldsymbol{\gamma}_{\mathrm{D}}\,\boldsymbol{w}_\Gamma \rangle_{\Gamma} = \left\langle \boldsymbol{\mathcal{S}}^{\mathrm{int}}\,\boldsymbol{\gamma}_{\mathrm{D}}\,\boldsymbol{w}_\Gamma, \boldsymbol{\gamma}_{\mathrm{D}}\,\boldsymbol{w}_\Gamma \right\rangle_{\Gamma},$$

where $\boldsymbol{\mathcal{S}}^{\mathrm{int}}$ is the interior Steklov-Poincaré operator. Since by construction $(\mathbf{curl}\,\boldsymbol{w}_\Gamma, \mathbf{curl}\,\widetilde{\boldsymbol{w}})_{\Omega} = 0$ for all $\widetilde{\boldsymbol{w}} \in [\boldsymbol{H}_0(\mathbf{curl}, \Omega)]$, we have

$$\begin{aligned} \|\mathbf{curl}\,\boldsymbol{w}\|^2_{\boldsymbol{L}^2(\Omega)} &= \|\mathbf{curl}\,\widetilde{\boldsymbol{w}}\|^2_{\boldsymbol{L}^2(\Omega)} + \|\mathbf{curl}\,\boldsymbol{w}_\Gamma\|^2_{\boldsymbol{L}^2(\Omega)} \\ &= \|\mathbf{curl}\,\widetilde{\boldsymbol{w}}\|^2_{\boldsymbol{L}^2(\Omega)} + \left\langle \boldsymbol{\mathcal{S}}^{\mathrm{int}}\,\boldsymbol{\gamma}_{\mathrm{D}}\,\boldsymbol{w}_\Gamma, \boldsymbol{\gamma}_{\mathrm{D}}\,\boldsymbol{w}_\Gamma \right\rangle_{\Gamma}. \end{aligned} \tag{4.34}$$

Hence, (I) can be estimated by

$$(\mathcal{U}\,\mathbf{curl}\,\boldsymbol{u} - \mathcal{U}\,\mathbf{curl}\,\boldsymbol{v}, \boldsymbol{w})_{\Omega} \geq C_M^{\mathcal{U}} \|\mathbf{curl}\,\widetilde{\boldsymbol{w}}\|^2_{\boldsymbol{L}^2(\Omega)} + C_M^{\mathcal{U}} \left\langle \boldsymbol{\mathcal{S}}^{\mathrm{int}}\,\boldsymbol{\gamma}_{\mathrm{D}}\,\boldsymbol{w}_\Gamma, \boldsymbol{\gamma}_{\mathrm{D}}\,\boldsymbol{w}_\Gamma \right\rangle_{\Gamma}.$$

To estimate (II) we have that

$$\left\langle \boldsymbol{\xi}, (\frac{1}{2} - \boldsymbol{\mathcal{C}}_0)\,\boldsymbol{\gamma}_{\mathrm{D}}\,\boldsymbol{w} \right\rangle_{\Gamma} = \left\langle \boldsymbol{\mathcal{A}}_0 \boldsymbol{\xi}, \boldsymbol{\mathcal{A}}_0{}^{-1} (\frac{1}{2} - \boldsymbol{\mathcal{C}}_0)\,\boldsymbol{\gamma}_{\mathrm{D}}\,\boldsymbol{w} \right\rangle_{\Gamma}$$

$$\leq \|\boldsymbol{\xi}\|_{\boldsymbol{\mathcal{A}}_0} \left\| (\frac{1}{2} - \boldsymbol{\mathcal{C}}_0)\, \gamma_{\mathrm{D}}\, \boldsymbol{w} \right\|_{\boldsymbol{\mathcal{A}}_0{}^{-1}}$$
$$\leq \|\boldsymbol{\xi}\|_{\boldsymbol{\mathcal{A}}_0} \sqrt{C_{\boldsymbol{\mathcal{C}}_0} \langle \boldsymbol{\mathcal{S}}^{\mathrm{int}}\, \gamma_{\mathrm{D}}\, \boldsymbol{w}_\Gamma, \gamma_{\mathrm{D}}\, \boldsymbol{w}_\Gamma \rangle_\Gamma},$$

where we used Lemma 3.19 in the last step. Altogether,

$$\left\langle \widetilde{\mathcal{B}}(\mathbf{u}) - \widetilde{\mathcal{B}}(\mathbf{v}), \boldsymbol{w} \right\rangle \geq C_M^{\mathcal{U}} \|\mathbf{curl}\, \widetilde{\boldsymbol{w}}\|^2_{\boldsymbol{L}^2(\Omega)} + C_M^{\mathcal{U}} \left\langle \boldsymbol{\mathcal{S}}^{\mathrm{int}}\, \gamma_{\mathrm{D}}\, \boldsymbol{w}_\Gamma, \gamma_{\mathrm{D}}\, \boldsymbol{w}_\Gamma \right\rangle_\Gamma$$
$$- \|\boldsymbol{\xi}\|_{\boldsymbol{\mathcal{A}}_0} \sqrt{C_{\boldsymbol{\mathcal{C}}_0} \langle \boldsymbol{\mathcal{S}}^{\mathrm{int}}\, \gamma_{\mathrm{D}}\, \boldsymbol{w}_\Gamma, \gamma_{\mathrm{D}}\, \boldsymbol{w}_\Gamma \rangle_\Gamma} + \|\boldsymbol{\xi}\|^2_{\boldsymbol{\mathcal{A}}_0},$$

which can be written in quadratic form as

$$\left\langle \widetilde{\mathcal{B}}(\mathbf{u}) - \widetilde{\mathcal{B}}(\mathbf{v}), \boldsymbol{w} \right\rangle \geq C_{\mathrm{M}}^{\mathcal{U}} \|\mathbf{curl}\, \widetilde{\boldsymbol{w}}\|^2_{\boldsymbol{L}^2(\Omega)} + \left\langle \begin{pmatrix} C_{\mathrm{M}}^{\mathcal{U}} & -\frac{1}{2}\sqrt{C_{\boldsymbol{\mathcal{C}}_0}} \\ -\frac{1}{2}\sqrt{C_{\boldsymbol{\mathcal{C}}_0}} & 1 \end{pmatrix} \mathbf{x}, \mathbf{x} \right\rangle$$

with $\mathbf{x} = \left(\sqrt{\langle \boldsymbol{\mathcal{S}}^{\mathrm{int}}\, \gamma_{\mathrm{D}}\, \boldsymbol{w}_\Gamma, \gamma_{\mathrm{D}}\, \boldsymbol{w}_\Gamma \rangle_\Gamma}, \|\boldsymbol{\xi}\|_{\boldsymbol{\mathcal{A}}_0} \right)^\top$. We see that positive definiteness of the quadratic form is guaranteed, if $C_{\mathrm{M}}^{\mathcal{U}} > \frac{1}{4} C_{\boldsymbol{\mathcal{C}}_0}$ holds. By using the smallest eigenvalue of the matrix, we reach with $C_{\mathrm{stab}} = \min \left\{ C_{\mathrm{M}}^{\mathcal{U}}, \frac{1}{2} \left(C_{\mathrm{M}}^{\mathcal{U}} + 1 - \sqrt{\left(C_{\mathrm{M}}^{\mathcal{U}} - 1\right)^2 + C_{\boldsymbol{\mathcal{C}}_0}} \right) \right\}$ the estimate

$$\begin{aligned} \left\langle \widetilde{\mathcal{B}}(\mathbf{u}) - \widetilde{\mathcal{B}}(\mathbf{v}), \boldsymbol{w} \right\rangle &\geq C_{\mathrm{stab}} \left(\|\mathbf{curl}\, \widetilde{\boldsymbol{w}}\|^2_{\boldsymbol{L}^2(\Omega)} + \left\langle \boldsymbol{\mathcal{S}}^{\mathrm{int}}\, \gamma_{\mathrm{D}}\, \boldsymbol{w}_\Gamma, \gamma_{\mathrm{D}}\, \boldsymbol{w}_\Gamma \right\rangle_\Gamma + \|\boldsymbol{\xi}\|^2_{\boldsymbol{\mathcal{A}}_0} \right) \\ &\overset{(4.34)}{=} C_{\mathrm{stab}} \left(\|\mathbf{curl}\, \boldsymbol{w}\|^2_{\boldsymbol{L}^2(\Omega)} + \|\boldsymbol{\xi}\|^2_{\boldsymbol{\mathcal{A}}_0} \right). \end{aligned} \tag{4.35}$$

The remaining step consists in showing that $\sqrt{\|\mathbf{curl}\, \boldsymbol{w}\|^2_{\boldsymbol{L}^2(\Omega)} + \|\boldsymbol{\xi}\|^2_{\boldsymbol{\mathcal{A}}_0}}$ defines an equivalent norm to $\|\mathbf{w}\|_{\boldsymbol{\mathcal{H}}_{\mathrm{v}}}$. From Corollary 3.12, we know that $\|\boldsymbol{\xi}\|_{\boldsymbol{\mathcal{A}}_0}$ defines an equivalent norm of $\|\boldsymbol{\xi}\|_{\boldsymbol{H}^{-\frac{1}{2}}(\mathrm{div}_\Gamma, \Gamma)}$ for $\boldsymbol{\xi} \in \boldsymbol{H}^{-\frac{1}{2}}(\mathrm{div}_\Gamma\, 0, \Gamma)$. This reduces the problem to the proof that $\|\mathbf{curl}\, \boldsymbol{w}\|_{\boldsymbol{L}^2(\Omega)}$ is an equivalent norm to $\|\boldsymbol{w}\|_{\boldsymbol{H}(\mathbf{curl}, \Omega)}$ for the representatives in $[\boldsymbol{H}(\mathbf{curl}, \Omega)]$. From the definition of $[\boldsymbol{H}(\mathbf{curl}, \Omega)]$, we can show the validity of the Friedrichs' inequality [88, Corollary 3.51]. Whence, by using $\gamma_{\boldsymbol{n}} \boldsymbol{v} = 0$ on Γ, there exists $C_{\mathrm{F}} > 0$ such that

$$\|\boldsymbol{v}\|_{\boldsymbol{L}^2(\Omega)} \leq C_{\mathrm{F}} \|\mathbf{curl}\, \boldsymbol{v}\|_{\boldsymbol{L}^2(\Omega)}.$$

Therefore, inserting

$$\|\boldsymbol{w}\|_{\boldsymbol{H}(\mathbf{curl}, \Omega)} \leq (1 + C_{\mathrm{F}}) \|\mathbf{curl}\, \boldsymbol{w}\|_{\boldsymbol{L}^2(\Omega)} \qquad \text{with } \boldsymbol{w} \in [\boldsymbol{H}(\mathbf{curl}, \Omega)]$$

in the estimate (4.35) establishes together with the norm equivalence of $\|\boldsymbol{\xi}\|_{\boldsymbol{\mathcal{A}}_0}$ and $\|\boldsymbol{\xi}\|_{\boldsymbol{H}^{-\frac{1}{2}}(\mathrm{div}_\Gamma, \Gamma)}$ for $\boldsymbol{\xi} \in \boldsymbol{H}^{-\frac{1}{2}}(\mathrm{div}_\Gamma\, 0, \Gamma)$, the strong monotonicity of the non-linear operator $\widetilde{\mathcal{B}}$. □

Finally, we state the main result of this section.

Theorem 4.41 (Well-posedness)**.** *Let $\widetilde{\mathcal{B}} : \boldsymbol{\mathcal{H}}_{\mathrm{v}} \to \boldsymbol{\mathcal{H}}_{\mathrm{v}}{}'$ be as defined in* (4.33)*, and let $C_{\mathrm{M}}^{\mathcal{U}} > \frac{1}{4} C_{\boldsymbol{\mathcal{C}}_0}$. Then, for $\widetilde{\mathcal{B}}$ Lipschitz continuous and strongly monotone, Problem 4.39 admits a unique solution, for any $(\boldsymbol{f}, \widehat{\boldsymbol{u}}, \widehat{\boldsymbol{\phi}}) \in \boldsymbol{H}_0^{\mathrm{C}}(\mathrm{div}\, 0, \Omega) \times [\boldsymbol{H}^{-\frac{1}{2}}(\mathrm{curl}_\Gamma, \Gamma)] \times \boldsymbol{H}^{-\frac{1}{2}}(\mathrm{div}_\Gamma\, 0, \Gamma)$.*

Proof. The result is a consequence of the main theorem on strongly monotone operator equations, see Theorem 2.5, together with the assertions of Theorem 4.40. □

In complete analogy with the previous sections, we arrive at a stability result for non-linear operators $\mathcal{U}$ that take the form $\mathcal{U}\boldsymbol{w} := \nu(|\boldsymbol{w}|)\boldsymbol{w}$ with $\nu : \mathbb{R} \to \mathbb{R}$ defined in the sense of Definition 1.1. In this special case, a stability result can further be obtained.

Lemma 4.42. *Let the non-linear operator $\mathcal{U}$ be of the form $\mathcal{U}\boldsymbol{w} := \nu(|\boldsymbol{w}|)\boldsymbol{w}$ with $\nu : \mathbb{R} \to \mathbb{R}$ being a non-linear reluctivity, which is induced by an admissible B-H curve according to Definition 1.1. Moreover, we assume that $C_{\mathrm{M}}^{\mathcal{U}} > \frac{1}{4} C_{\boldsymbol{\mathcal{C}}_0}$. Then, for the solution $\mathbf{u} \in \boldsymbol{\mathcal{H}}_{\mathrm{v}}$ of Problem 4.39, and the right-hand sides $(\boldsymbol{f}, \widehat{\boldsymbol{u}}, \widehat{\boldsymbol{\phi}}) \in \boldsymbol{H}_0^{\mathrm{C}}(\operatorname{div} 0, \Omega) \times [\boldsymbol{H}^{-\frac{1}{2}}(\operatorname{curl}_\Gamma, \Gamma)] \times \boldsymbol{H}^{-\frac{1}{2}}(\operatorname{div}_\Gamma 0, \Gamma)$, there exists $C > 0$ such that*

$$\|\mathbf{u}\|_{\boldsymbol{\mathcal{H}}_{\mathrm{v}}} \leq C \left(\|\boldsymbol{f}\|_{[\boldsymbol{H}(\mathbf{curl},\Omega)]'} + \|\widehat{\boldsymbol{u}}\|_{\boldsymbol{H}^{-\frac{1}{2}}(\operatorname{curl}_\Gamma,\Gamma)} + \left\|\widehat{\boldsymbol{\phi}}\right\|_{\boldsymbol{H}^{-\frac{1}{2}}(\operatorname{div}_\Gamma,\Gamma)} \right).$$

Proof. Theorem 4.40 states that $\widetilde{\mathcal{B}}$ is strongly monotone for $C_{\mathrm{M}}^{\mathcal{U}} > \frac{1}{4} C_{\boldsymbol{\mathcal{C}}_0}$. Moreover, the boundary integral operator $\boldsymbol{\mathcal{C}}_0 : [\boldsymbol{H}^{-\frac{1}{2}}(\operatorname{curl}_\Gamma, \Gamma)] \to [\boldsymbol{H}^{-\frac{1}{2}}(\operatorname{curl}_\Gamma, \Gamma)]$ is a continuous operator, see Theorem 3.8. Hence, there exists $C^{\boldsymbol{\mathcal{C}}_0} > 0$, such that $\|\boldsymbol{\mathcal{C}}_0 \boldsymbol{\psi}\|_{\boldsymbol{H}^{-\frac{1}{2}}(\operatorname{curl}_\Gamma,\Gamma)} \leq C^{\boldsymbol{\mathcal{C}}_0} \|\boldsymbol{\psi}\|_{\boldsymbol{H}^{-\frac{1}{2}}(\operatorname{curl}_\Gamma,\Gamma)}$, $\boldsymbol{\psi} \in [\boldsymbol{H}^{-\frac{1}{2}}(\operatorname{curl}_\Gamma, \Gamma)]$. By Theorem 2.29, there exists a $C_{\mathrm{D}} > 0$, such that $\|\boldsymbol{\gamma}_{\mathrm{D}} \boldsymbol{v}\|_{\boldsymbol{H}^{-\frac{1}{2}}(\operatorname{curl}_\Gamma,\Gamma)} \leq C_{\mathrm{D}} \|\boldsymbol{v}\|_{\boldsymbol{H}(\mathbf{curl},\Omega)}$ holds for all $\boldsymbol{v} \in \boldsymbol{H}(\mathbf{curl}, \Omega)$. Therefore, it holds also for representatives in $\boldsymbol{v} \in [\boldsymbol{H}(\mathbf{curl}, \Omega)]$. With this, the proof can be done analogously to Lemma 4.8, when removing the stabilization term. □

The next section is devoted to the discretization framework intended to the approximation of the variational formulation given in Problem 4.39.

4.4.2 Galerkin discretization

Similarly to the previous sections, we also consider here a conforming discretization, such that the results of the continuous setting can be transferred to the discrete one.

Let $\boldsymbol{V}_\ell \subset \boldsymbol{H}(\mathbf{curl}, \Omega)$, and $\boldsymbol{X}_\ell \subset \boldsymbol{H}^{-\frac{1}{2}}(\operatorname{div}_\Gamma, \Gamma)$ be some finite dimensional subspaces with refinement level ℓ, and let

$$\begin{aligned} \boldsymbol{V}_{0,\ell} &:= \{\boldsymbol{v}_\ell \in \boldsymbol{V}_\ell : \mathbf{curl}\, \boldsymbol{v}_\ell = \mathbf{0}\}, \\ \boldsymbol{X}_{0,\ell} &:= \{\boldsymbol{\psi}_\ell \in \boldsymbol{X}_\ell : \operatorname{div} \boldsymbol{\psi}_\ell = 0\} \end{aligned}$$

be the discrete counterparts of the subspaces $\boldsymbol{H}(\mathbf{curl}\, \mathbf{0}, \Omega)$ and $\boldsymbol{H}^{-\frac{1}{2}}(\operatorname{div}_\Gamma 0, \Gamma)$, respectively. Equivalently to the continuous setting, we define the discrete quotient space $[\boldsymbol{V}_\ell] := \boldsymbol{V}_\ell / \boldsymbol{V}_{0,\ell}$. Note that by considering an orthogonal projection $\mathsf{P}_\ell : \boldsymbol{V}_\ell \to \boldsymbol{V}_{0,\ell}^\perp$, where $\boldsymbol{V}_{0,\ell}^\perp$ denotes the orthogonal complement of $\boldsymbol{V}_{0,\ell}$ in $\boldsymbol{V}_\ell$, representatives can be chosen from $\boldsymbol{V}_{0,\ell}^\perp$.

Replacing $\boldsymbol{\mathcal{H}}_{\mathrm{v}} := [\boldsymbol{H}(\mathbf{curl}, \Omega)] \times \boldsymbol{H}^{-\frac{1}{2}}(\operatorname{div}_\Gamma 0, \Gamma)$ by $\boldsymbol{\mathcal{H}}_{\mathrm{v},\ell} := [\boldsymbol{V}_\ell] \times \boldsymbol{X}_{0,\ell}$ in Problem 4.39 yields a discrete variational formulation.

Problem 4.43 (Discrete problem)**.** *Find* $\mathbf{u}_\ell := (\boldsymbol{u}_\ell, \boldsymbol{\phi}_\ell) \in \boldsymbol{\mathcal{H}}_{\mathrm{v},\ell}$ *such that*

$$(\mathcal{U}\,\mathbf{curl}\,\boldsymbol{u}_\ell, \mathbf{curl}\,\boldsymbol{v}_\ell)_\Omega - \langle \boldsymbol{\phi}_\ell, \gamma_{\mathrm{D}}\,\boldsymbol{v}_\ell\rangle_\Gamma = (\boldsymbol{f}, \boldsymbol{v}_\ell)_\Omega + \left\langle \widehat{\boldsymbol{\phi}}, \gamma_{\mathrm{D}}\,\boldsymbol{v}_\ell \right\rangle_\Gamma,$$
$$\langle \boldsymbol{\psi}_\ell, \boldsymbol{\mathcal{A}}_0\boldsymbol{\phi}_\ell\rangle_\Gamma + \left\langle \boldsymbol{\psi}_\ell, (\frac{1}{2} + \boldsymbol{\mathcal{C}}_0)\,\gamma_{\mathrm{D}}\,\boldsymbol{u}_\ell \right\rangle_\Gamma = \left\langle \boldsymbol{\psi}_\ell, (\frac{1}{2} + \boldsymbol{\mathcal{C}}_0)\widehat{\boldsymbol{u}} \right\rangle_\Gamma$$

for all $\mathbf{v}_\ell := (\boldsymbol{v}_\ell, \boldsymbol{\psi}_\ell) \in \boldsymbol{\mathcal{H}}_{\mathrm{v},\ell}$.

Due to the conforming discretization, Theorem 4.41 applies. Consequently, there exists a unique $\mathbf{u}_\ell := (\boldsymbol{u}_\ell, \boldsymbol{\phi}_\ell) \in \boldsymbol{\mathcal{H}}_{\mathrm{v},\ell} := [\boldsymbol{V}_\ell] \times \boldsymbol{X}_{0,\ell}$ that solves Problem 4.43 under the same conditions, namely, Lipschitz continuity and strong monotonicity of $\mathcal{U}$ with $C_{\mathrm{M}}^{\mathcal{U}} > \frac{1}{4} C_{\boldsymbol{\mathcal{C}}_0}$, see Corollary 4.11.

Theorem 4.44 (Quasi-optimality)**.** *Let Assumption 4.9 hold, and* $C_{\mathrm{M}}^{\mathcal{U}} > \frac{1}{4}$*. Moreover, let* $\mathbf{u} = (\boldsymbol{u}, \boldsymbol{\phi}) \in \boldsymbol{\mathcal{H}}_{\mathrm{v}}$ *be the unique solution of Problem 4.39, and* $\mathbf{u}_\ell := (\boldsymbol{u}_\ell, \boldsymbol{\phi}_\ell) \in \boldsymbol{\mathcal{H}}_{\mathrm{v},\ell}$ *the solution of its discrete counterpart Problem 4.43. Then, there exists* $C_{\text{Céa}} = \frac{C_L}{C_M}$ *such that*

$$\begin{aligned}\|\boldsymbol{u} - \boldsymbol{u}_\ell\|_{\boldsymbol{H}(\mathbf{curl},\Omega)} + \|\boldsymbol{\phi} - \boldsymbol{\phi}_\ell\|_{\boldsymbol{H}^{-\frac{1}{2}}(\mathrm{div}_\Gamma,\Gamma)} \leq C_{\text{Céa}} \min_{\boldsymbol{v}_\ell \in \boldsymbol{V}_\ell, \boldsymbol{\psi}_\ell \in \boldsymbol{X}_{0,\ell}} \Big(&\|\boldsymbol{u} - \boldsymbol{v}_\ell\|_{\boldsymbol{H}(\mathbf{curl},\Omega)} \\ &+ \|\boldsymbol{\phi} - \boldsymbol{\psi}_\ell\|_{\boldsymbol{H}^{-\frac{1}{2}}(\mathrm{div}_\Gamma,\Gamma)} \Big).\end{aligned} \tag{4.36}$$

Proof. The assertion follows analogously to Theorem 4.12. □

4.4.3 A priori error estimates and super-convergence

Now we set $\boldsymbol{V}_\ell = \mathbb{S}^1_{\boldsymbol{p}}(\Omega)$ and $\boldsymbol{X}_\ell = \mathbb{S}^{1,\perp}_{\widetilde{\boldsymbol{p}}}(\Gamma)$. We refer to Section 3.3 for the definition of the B-Spline spaces. Moreover, we set $\boldsymbol{X}_{0,\ell} = \mathbb{S}^{1,\perp}_{\widetilde{\boldsymbol{p}},0}(\Gamma)$ as a suitable discrete space for the Neumann data. We refer to (3.58) and Remark 3.28 for its definition.

In addition, let us define the kernel of the **curl** operator in $\mathbb{S}^1_{\boldsymbol{p}}(\Omega)$ by

$$\mathbb{S}^1_{\boldsymbol{p}}(\mathbf{curl}\,\mathbf{0}, \Omega) = \{\boldsymbol{v}_\ell \in \mathbb{S}^1_{\boldsymbol{p}}(\Omega) : \mathbf{curl}\,\boldsymbol{v}_\ell = \mathbf{0}\}.$$

As for the scalar case, we need to define spaces of patchwise regularity.

Definition 4.45. *Let* $K \in \{\Omega, \Gamma\}$ *be a multipatch domain with* N_κ *patches, and let* $\mathbf{d}$ *be some differential operator. For some* $s \in \mathbb{R}$*, we define the space of patchwise regularity endowed with the norm*

$$\|\boldsymbol{u}\|^2_{\boldsymbol{H}^s_{\mathrm{pw}}(\mathbf{d},K)} = \sum_{0 \leq l < N_\kappa} \left\|\boldsymbol{u}_{|\kappa_l}\right\|^2_{\boldsymbol{H}^s(\mathbf{d},K)}$$

by

$$\boldsymbol{H}^s_{\mathrm{pw}}(\mathbf{d}, K) = \{\boldsymbol{u} \in \boldsymbol{L}^2(K) : \|\boldsymbol{u}\|_{\boldsymbol{H}^s_{\mathrm{pw}}(\mathbf{d},K)} < \infty\}.$$

Thereby, $\boldsymbol{H}^s(\mathbf{d}, K)$ *denotes an energy space of regularity* s*, formally,*

$$\boldsymbol{H}^s(\mathbf{d}, K) := \{\boldsymbol{v} \in \boldsymbol{H}^s(K) : \mathbf{d}\boldsymbol{v} \in \boldsymbol{H}^s(K)\}.$$

The approximation properties of B-Spline spaces and their trace spaces for the discretization of the de Rham complex in Figure 2.6, see Figure 3.3, are provided in [33] and [21] for multipatch domains, respectively. In particular, for $\mathbb{S}^1_{\boldsymbol{p}}(\Omega)$ and $\mathbb{S}^{1,\perp}_{\widetilde{\boldsymbol{p}}}(\Gamma)$, we state the following results.

Lemma 4.46. *Let $\boldsymbol{u} \in \boldsymbol{H}(\mathbf{curl},\Omega) \cap \boldsymbol{H}^s_{\mathrm{pw}}(\mathbf{curl},\Omega)$ and $\boldsymbol{\phi} \in \boldsymbol{H}^{-\frac{1}{2}}(\mathrm{div}_\Gamma,\Gamma) \cap \boldsymbol{H}^s_{\mathrm{pw}}(\mathrm{div}_\Gamma,\Gamma)$. There exists C_0, $C_{1,1}$, $C_{1,2} > 0$ such that*

$$\inf_{\boldsymbol{u}_\ell \in \mathbb{S}^1_{\boldsymbol{p}}(\Omega)} \|\boldsymbol{u}-\boldsymbol{u}_\ell\|_{\boldsymbol{H}(\mathbf{curl},\Omega)} \leq C_0\, h^s \|\boldsymbol{u}\|_{\boldsymbol{H}^s_{\mathrm{pw}}(\mathbf{curl},\Omega)} \qquad 2 < s \leq p, \tag{4.37a}$$

$$\inf_{\boldsymbol{\phi}_\ell \in \mathbb{S}^{1,\perp}_{\widetilde{\boldsymbol{p}}}(\Gamma)} \|\boldsymbol{\phi}-\boldsymbol{\phi}_\ell\|_{\boldsymbol{H}^{-\frac{1}{2}}(\mathrm{div}_\Gamma,\Gamma)} \leq C_{1,1}\, h^s \|\boldsymbol{\phi}\|_{\boldsymbol{H}^{-\frac{1}{2}+s}(\mathrm{div}_\Gamma,\Gamma)} \qquad 0 \leq s \leq \frac{1}{2}, \tag{4.37b}$$

$$\inf_{\boldsymbol{\phi}_\ell \in \mathbb{S}^{1,\perp}_{\widetilde{\boldsymbol{p}}}(\Gamma)} \|\boldsymbol{\phi}-\boldsymbol{\phi}_\ell\|_{\boldsymbol{H}^{-\frac{1}{2}}(\mathrm{div}_\Gamma,\Gamma)} \leq C_{1,2}\, h^s \|\boldsymbol{\phi}\|_{\boldsymbol{H}^{-\frac{1}{2}+s}_{\mathrm{pw}}(\mathrm{div}_\Gamma,\Gamma)} \qquad \frac{1}{2} \leq s \leq p+\frac{1}{2}. \tag{4.37c}$$

Proof. The first estimate in $\boldsymbol{H}(\mathbf{curl},\Omega)$ is given in [21, Corollary 5]. The $\boldsymbol{H}^{-\frac{1}{2}}(\mathrm{div}_\Gamma,\Gamma)$ estimates are proved in [21, Theorem 3]. □

Theorem 4.47 (A priori estimate)**.** *Let $C^{\mathcal{U}}_{\mathrm{E}} > \frac{1}{4} C_{\boldsymbol{\mathcal{C}}_0}$. Moreover, let $(\boldsymbol{u},\boldsymbol{\phi}) \in \boldsymbol{\mathcal{H}}_{\mathrm{v}}$ be the solution of Problem 4.39 and let $(\boldsymbol{u}_\ell,\boldsymbol{\phi}_\ell) \in \boldsymbol{\mathcal{H}}_{\mathrm{v},\ell} = \mathbb{S}^1_{\boldsymbol{p}}(\Omega) \times \mathbb{S}^{1,\perp}_{\widetilde{\boldsymbol{p}},0}(\Gamma)$ be the solution of Problem 4.43. Then, for $0 \leq s \leq \frac{1}{2}$, there holds with $\boldsymbol{u} \in \boldsymbol{H}(\mathbf{curl},\Omega) \cap \boldsymbol{H}^2_{\mathrm{pw}}(\mathbf{curl},\Omega)$ and $\boldsymbol{\phi} \in \boldsymbol{H}^{-\frac{1}{2}}(\mathrm{div}_\Gamma,\Gamma) \cap \boldsymbol{H}^{-\frac{1}{2}+s}(\mathrm{div}_\Gamma,\Gamma)$*

$$\|\boldsymbol{u}-\boldsymbol{u}_\ell\|_{\boldsymbol{H}(\mathbf{curl},\Omega)} + \|\boldsymbol{\phi}-\boldsymbol{\phi}_\ell\|_{\boldsymbol{H}^{-\frac{1}{2}}(\mathrm{div}_\Gamma,\Gamma)} \leq C h^s \left(\|\boldsymbol{u}\|_{\boldsymbol{H}^2_{\mathrm{pw}}(\mathbf{curl},\Omega)} + \|\boldsymbol{\phi}\|_{\boldsymbol{H}^{-\frac{1}{2}+s}(\mathrm{div}_\Gamma,\Gamma)} \right).$$

For $\frac{1}{2} \leq s \leq 2$, there holds with $\boldsymbol{u} \in \boldsymbol{H}(\mathbf{curl},\Omega) \cap \boldsymbol{H}^2_{\mathrm{pw}}(\mathbf{curl},\Omega)$ and $\boldsymbol{\phi} \in \boldsymbol{H}^{-\frac{1}{2}}(\mathrm{div}_\Gamma,\Gamma) \cap \boldsymbol{H}^{-\frac{1}{2}+s}_{\mathrm{pw}}(\mathrm{div}_\Gamma,\Gamma)$

$$\|\boldsymbol{u}-\boldsymbol{u}_\ell\|_{\boldsymbol{H}(\mathbf{curl},\Omega)} + \|\boldsymbol{\phi}-\boldsymbol{\phi}_\ell\|_{\boldsymbol{H}^{-\frac{1}{2}}(\mathrm{div}_\Gamma,\Gamma)} \leq C h^s \left(\|\boldsymbol{u}\|_{\boldsymbol{H}^2_{\mathrm{pw}}(\mathbf{curl},\Omega)} + \|\boldsymbol{\phi}\|_{\boldsymbol{H}^{-\frac{1}{2}+s}_{\mathrm{pw}}(\mathrm{div}_\Gamma,\Gamma)} \right).$$

For $2 < s \leq p$, there holds with $\boldsymbol{u} \in \boldsymbol{H}(\mathbf{curl},\Omega) \cap \boldsymbol{H}^s_{\mathrm{pw}}(\mathbf{curl},\Omega)$ and $\boldsymbol{\phi} \in \boldsymbol{H}^{-\frac{1}{2}}(\mathrm{div}_\Gamma,\Gamma) \cap \boldsymbol{H}^{-\frac{1}{2}+s}_{\mathrm{pw}}(\mathrm{div}_\Gamma,\Gamma)$

$$\|\boldsymbol{u}-\boldsymbol{u}_\ell\|_{\boldsymbol{H}(\mathbf{curl},\Omega)} + \|\boldsymbol{\phi}-\boldsymbol{\phi}_\ell\|_{\boldsymbol{H}^{-\frac{1}{2}}(\mathrm{div}_\Gamma,\Gamma)} \leq C h^s \left(\|\boldsymbol{u}\|_{\boldsymbol{H}^s_{\mathrm{pw}}(\mathbf{curl},\Omega)} + \|\boldsymbol{\phi}\|_{\boldsymbol{H}^{-\frac{1}{2}+s}_{\mathrm{pw}}(\mathrm{div}_\Gamma,\Gamma)} \right)$$

with a constant $C > 0$.

Proof. Due to Theorem 4.41, Problem 4.39 possesses a unique solution in $[\boldsymbol{H}(\mathbf{curl},\Omega)] \times \boldsymbol{H}^{-\frac{1}{2}}(\mathrm{div}_\Gamma 0,\Gamma)$. Moreover, well-posedness of the discrete Problem 4.43 follows analogously to Corollary 4.11. Indeed, let $\boldsymbol{u} \in \boldsymbol{H}(\mathbf{curl},\Omega)$. We know from [21, Appendix A] that there exists a projection $\Pi : \boldsymbol{H}(\mathbf{curl},\Omega) \to \mathbb{S}^1_{\boldsymbol{p}}(\Omega)$, which commutes with the respective differential operator, namely, $\Pi \circ \mathbf{curl} = \mathbf{curl} \circ \Pi$.
Let $\mathsf{P} : \boldsymbol{H}(\mathbf{curl},\Omega) \to (\boldsymbol{H}(\mathbf{curl}\,\mathbf{0},\Omega))^\perp \subset \boldsymbol{H}(\mathbf{curl},\Omega)$ be an orthogonal projection, which is defined analogously to the one used in the proof of [43, Proposition 3.2]. Then, $\Pi_1 := \Pi \circ \mathsf{P} : \boldsymbol{H}(\mathbf{curl},\Omega) \to [\mathbb{S}^1_{\boldsymbol{p}}(\Omega)] \cong (\mathbb{S}^1_{\boldsymbol{p}}(\mathbf{curl}\,\mathbf{0},\Omega))^\perp \subset \mathbb{S}^1_{\boldsymbol{p}}(\Omega)$ defines a projection, which retains the same convergence rates with respect to h-refinement as the ones given by Π, due to the optimality of orthogonal projections.

Furthermore, for smooth enough functions, the commutativity of the de Rham complex leads to

$$\gamma_{\boldsymbol{n}} \circ \mathbf{curl} = \operatorname{div}_\Gamma \circ \boldsymbol{\gamma}_\times \,.$$

Hence, by using $\gamma_{\mathrm{N}} = \boldsymbol{\gamma}_\times \circ \mathbf{curl}$, we obtain for $\boldsymbol{u}_\ell := \Pi\, \mathbf{curl}\, \boldsymbol{v} = \mathbf{curl}\, \Pi \boldsymbol{v}$

$$\operatorname{div}_\Gamma \gamma_{\mathrm{N}}\, \boldsymbol{v}_\ell = \gamma_{\boldsymbol{n}}\, \mathbf{curl}\, \mathbf{curl}\, \boldsymbol{v}_\ell = 0 \quad \text{ with } \boldsymbol{v}_\ell := \Pi \boldsymbol{v}.$$

Therefore, $\boldsymbol{\psi}_\ell := \gamma_{\mathrm{N}}\, \boldsymbol{v}_\ell \in \mathbb{S}^{1,\perp}_{\widetilde{\boldsymbol{p}}}(\Gamma)$ satisfies $\operatorname{div}_\Gamma \boldsymbol{\psi}_\ell = 0$, i.e., $\boldsymbol{\psi}_\ell \in \mathbb{S}^{1,\perp}_{\widetilde{\boldsymbol{p}},0}(\Gamma)$.
With this, the approximation results of Lemma 4.46 and Theorem 4.44 may be utilized, which leads merely to the asserted a priori estimates. □

In the following, we give an adaptation of Theorem 4.33 and Remark 4.34 to the 3D case, where the possible super-convergence of the solution of the scalar problem in the BEM domain was discussed. For notational simplicity, let

$$\boldsymbol{\mathcal{H}}^s_{\mathrm{v,pw}} := (\boldsymbol{H}(\mathbf{curl}, \Omega) \cap \boldsymbol{H}^s_{\mathrm{pw}}(\mathbf{curl}, \Omega)) \times (\boldsymbol{H}^{-\frac{1}{2}}(\operatorname{div}_\Gamma, \Gamma) \cap \boldsymbol{H}^s_{\mathrm{pw}}(\operatorname{div}_\Gamma, \Gamma))$$

be a product space of patchwise regularity. Its corresponding norm, denoted by $\|\cdot\|_{\boldsymbol{\mathcal{H}}^s_{\mathrm{v,pw}}}$, is defined accordingly to Definition 4.45.

Theorem 4.48. *Let $\mathfrak{F} \in \boldsymbol{\mathcal{H}}'_{\mathrm{v},\ell}$ be a continuous and linear functional. We denote by $\mathbf{u} := (\boldsymbol{u}, \phi) \in \boldsymbol{\mathcal{H}}_{\mathrm{v}} := [\boldsymbol{H}(\mathbf{curl}, \Omega)] \times \boldsymbol{H}^{-\frac{1}{2}}(\operatorname{div}_\Gamma 0, \Gamma)$ the solution of the continuous problem 4.39, and by $\mathbf{u}_\ell := (\boldsymbol{u}_\ell, \phi_\ell) \in \boldsymbol{\mathcal{H}}_{\mathrm{v},\ell} := \mathbb{S}^1_{\boldsymbol{p}}(\Omega) \times \mathbb{S}^{1,\perp}_{\widetilde{\boldsymbol{p}},0}(\Gamma)$ the solution of the discrete problem 4.43. Moreover, let $\mathbf{w} \in \boldsymbol{\mathcal{H}}_{\mathrm{v}}$ be the unique solution of the dual problem*

$$\boldsymbol{b}(\mathbf{v}, \mathbf{w}) = \mathfrak{F}(\mathbf{v}), \tag{4.38}$$

for all $\mathbf{v} \in \boldsymbol{\mathcal{H}}_{\mathrm{v}}$. Then, there exists a constant $C_1 > 0$ such that

$$|\mathfrak{F}(\mathbf{u}) - \mathfrak{F}(\mathbf{u}_\ell)| \leq C_1\, \|\mathbf{u} - \mathbf{v}_\ell\|_{\boldsymbol{\mathcal{H}}_{\mathrm{v}}} \|\mathbf{w} - \mathbf{z}_\ell\|_{\boldsymbol{\mathcal{H}}_{\mathrm{v}}} \tag{4.39}$$

for arbitrary $\mathbf{v}_\ell \in \boldsymbol{\mathcal{H}}_{\mathrm{v},\ell}$, $\mathbf{z}_\ell \in \boldsymbol{\mathcal{H}}_{\mathrm{v},\ell}$. Furthermore, provided $\mathbf{u} \in \boldsymbol{\mathcal{H}}^s_{\mathrm{v,pw}}$ and $\mathbf{w} \in \boldsymbol{\mathcal{H}}^t_{\mathrm{vpw}}$, with $2 < s, t \leq p$, there exists a constant $C_2 > 0$ such that

$$|\mathfrak{F}(\mathbf{u}) - \mathfrak{F}(\mathbf{u}_\ell)| \leq C_2\, h^{s+t} \|\mathbf{u}\|_{\boldsymbol{\mathcal{H}}^s_{\mathrm{v,pw}}} \|\mathbf{w}\|_{\boldsymbol{\mathcal{H}}^t_{\mathrm{vpw}}}. \tag{4.40}$$

Proof. The assertions can be shown analogously to Theorem 4.33. □

Remark 4.49. *In particular, the functional of Theorem 4.48 may be, e.g., the representation formula of the exterior domain* (3.20b)*. Assuming a maximal regularity for* $\mathbf{u}$ *and* $\mathbf{w}$ *in* (4.40)*, i.e., $\mathbf{u} \in \boldsymbol{\mathcal{H}}^p_{\mathrm{vpw}}$ and $\mathbf{w} \in \boldsymbol{\mathcal{H}}^p_{\mathrm{vpw}}$ yields the following pointwise error: For $\boldsymbol{x} \in \Omega^{\mathrm{e}}$, it holds*

$$|\boldsymbol{u}^{\mathrm{e}}(\boldsymbol{x}) - \boldsymbol{u}^{\mathrm{e}}_\ell(\boldsymbol{x})| = |\mathfrak{F}(\mathbf{u}^{\mathrm{e}})(\boldsymbol{x}) - \mathfrak{F}(\mathbf{u}^{\mathrm{e}}_\ell)(\boldsymbol{x})| \leq C h^{2p}, \quad C > 0. \tag{4.41}$$

This suggests that under some regularity assumptions, the convergence rate may double. This behavior is called super-convergence. Analogously to Remark 4.34, the constant C in (4.41) *depends in particular on the fundamental solution $u^*(\boldsymbol{x}, \boldsymbol{y})$. Hence, it tends to infinity, when approaching the boundary. However, suitable numerical schemes similar to [107] may be considered to reduce this non-desirable effect, and profit from the faster convergence.*

5 Numerical validation and results

> The greatest mathematicians, as Archimedes, Newton, and Gauß, always united theory and applications in equal measure.
>
> F. Klein

This chapter consists of two parts. We start in Section 5.1 by validating the theoretical results that we established in the previous chapter. For this, we consider three examples that correspond to Sections 4.1, 4.3 and 4.4, respectively. In the first one, we study the optimal convergence behavior using a standard academic problem, for which we prescribe a smooth solution, and calculate the input data accordingly. Besides the convergence rates in the interior domain, we address the pointwise error associated with the exterior domain to verify the predicted possible super-convergence. For this reason, by considering a linear material we ensure a concrete characterization of the dual problem. Therefore, we expect a doubling of the convergence rates, see Remarks 4.36 and 4.37. Moreover, as mentioned in Remark 4.34, we discuss the effects of numerical integration and the position of the evaluation path on the super-convergence. The second example involves a multiply-connected domain with non-linear materials. Via this experiment, we highlight the advantages of the isogeometric coupling of Finite Element Method (FEM) and Boundary Element Methods (BEMs), which consists in particular in the super-convergence of the solution in a thin air gap, which separates two domains that are filled with non-linear materials. This can be thought of as a simplified 2-pole synchronous machine. To showcase the effects of the field on a non-linear material, we show its saturation effects, which can be given by the magnetic reluctivity. The third example is dedicated to the proof-of-concept of the method in the three-dimensional (3D) case. For simplicity, we restrict ourselves to a simply-connected domain and a uniform magnetization, which leads to a linear system. However, as expected from our theoretical results, our method is also suitable for general applications involving multiply-connected domains with non-linear behavior, as for the two-dimensional (2D) case. Surely, the implementation for the 3D case is more involved, and subjects such as preconditioning, and advanced software engineering techniques have to be set in the foreground. For this, we refer to [61, 62, 71, 72, 111], for instance.
The second part of the chapter, i.e., Section 5.2 is devoted to the coupled discrete electromechanical problem, which we solve as illustrated in Figure 1.3. For this, we consider our non-symmetric FEM-BEM coupling's formulations for parabolic and elliptic problems, according to Sections 4.1 and 4.2. Throughout the section, we employ an isogeometric discretization in space, and use a classical implicit Euler method in the time domain. In particular, we consider three experiments to highlight the following aspects: In the first one, we address practice-oriented non-linear materials. There, the B-H curve is reconstructed from experimental data such that the physical prerequisites of Definition 1.1 are fulfilled. To verify our approach for force computations with the Maxwell Stress Tensor (MST) method, we utilize for benchmarking the commercial software *JMAG* [68]. In the second experiment, we consider an electromechanical problem that is coupled via the mechanical torque, and for which a reference solution for the trajectory can be gained from the computer algebra system *Wolfram Mathematica* [83]. The last experiment is an extension to the previous one to

discuss the effects of conductors in the electrical system.

All results for the 2D problems are obtained by means of an implementation in *MATLAB/Octave* [40, 84]. For this, we used several structures and functionalities from the open-source package *GeoPDEs*, which provides a framework for the implementation of isogeometric methods, see [37, 114]. In particular, this involves all the necessary tools to define the appropriate B-Spline basis functions, e.g., parametrizations, h- and p-refinements etc. For geometrical modelling, we use the *NURBS toolbox*, which is included in *GeoPDEs*, to find multipatch representations of domains via Non-Uniform Rational B-Splines (NURBS) mappings. An example is given in Figure 3.2. The implementation of the FEM part is rather standard, and we use classical assembling techniques for the stiffness and mass matrices. For efficiency purposes, the code is vectorized. Concerning the Boundary Integral Operators (BIOs), we use the integral representations as given in Lemma 3.13, which obviously hold for the B-Splines basis functions. Due to the singularities that may occur during the assembly of the matrices, see Remark 3.14, special integration techniques have to be adopted. For instance, we follow the approach of [7, Section 4.3], where Duffy-type transformations have been considered for identical and neighboring elements. For the single-layer BIO, we further employ for the singular parts a combination of logarithmic and Gaussian quadrature. Otherwise, for regular contributions, we use a standard Gauss-Legendre quadrature. In the 3D case, the only difference is that we use *BEMBEL*, which is a freely available *C++* library, see [38], for an efficient assembly of BIOs in the isogeometric framework.
We employ throughout this chapter only uniform h-refinement, thus the first assumption in Assumption 3.25 is clearly fulfilled. Furthermore, non-linear problems are solved by using a standard Picard iteration method [93].

5.1 Numerical validation of the isogeometric approach

This section is devoted to the numerical validation of the theoretical results of the previous chapter. Therefore, we will consider the following subsections, three complementary examples. In each one of them, we set the emphasis on different specific aspects, which may require for the purpose some simplifications or adaptation. The results and figures of the first two sections have already been published in [42], and those of the last one in [43].

5.1.1 Mexican hat

To verify the convergence rates in the interior domain, an exact solution is needed. Moreover, in order to validate the super-convergence behavior in the exterior domain, concrete knowledge about the dual problem is required. Therefore, let us consider the following academic problem; see [46]: Let $\Omega := (0.25, 0.25)^2$ be a square domain with boundary Γ. Obviously, the second assumption in Assumption 3.25 is satisfied by a single patch representation.

We consider Problem 4.1 with a linear material. For simplicity, let $\mathcal{U} = \mathrm{Id}$. Similar to [46], we prescribe the exact solutions

$$\begin{aligned} u(\boldsymbol{x}) &= \left(1 - 100x_1^2 - 100x_2^2\right) e^{-50(x_1^2+x_2^2)}, && \boldsymbol{x} \in \Omega, \\ u^{\mathrm{e}}(\boldsymbol{x}) &= \log(\sqrt{x_1^2 + x_2^2}), && \boldsymbol{x} \in \Omega^{\mathrm{e}}, \end{aligned}$$

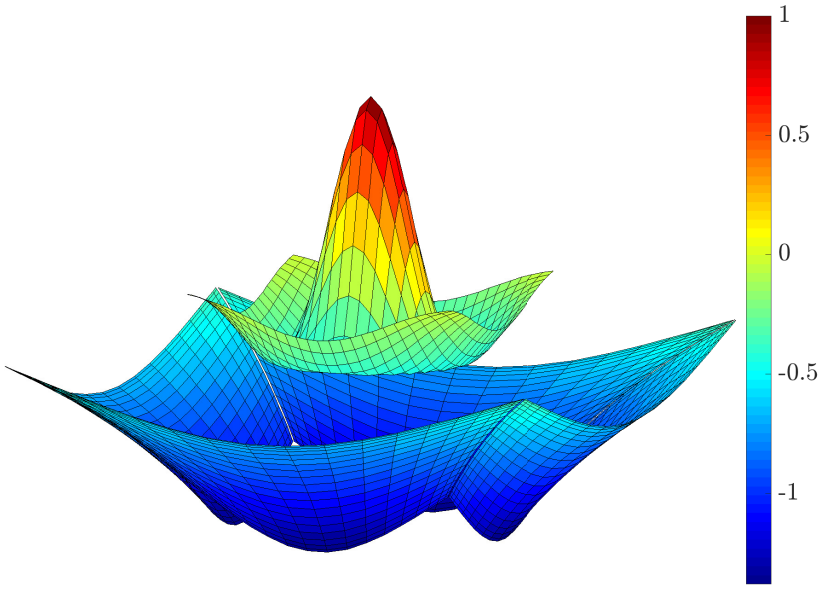

Figure 5.1: Example of Subsection 5.1.1: Solution $\left(u_\ell, u_\ell^{\mathrm{e}}\right) \in \mathbb{S}^0_{\boldsymbol{p}}(\Omega) \times \mathbb{S}^0_{\boldsymbol{p}}(\Omega_{\mathrm{e}}^{\mathrm{e}})$ with degree $p = 2$ and an h-refinement level $\ell = 20$. The exterior solution is represented in $\Omega_{\mathrm{e}}^{\mathrm{e}} := (-0.5, 0.5)\setminus\overline{\Omega}$, and is obtained by the evaluation of 25 points in each of the four exterior patches [42].

where $\boldsymbol{x} = (x_1, x_2)$. Therefrom, the right-hand side f and the jump data $\widehat{u}$ and $\widehat{\phi}$ follow by direct computation. The discrete variational problem corresponds to Problem 4.10 with $\boldsymbol{\mathcal{H}}_\ell = \mathbb{S}^0_{\boldsymbol{p}}(\Omega) \times \mathbb{S}^2_{\widetilde{p}}(\Gamma)$. Remember that $\boldsymbol{p} = (p, p)$ and $\widetilde{p} = p - 1$. By solving the discrete problem, we obtain the solution in the interior domain, from which the interior Dirichlet data $\gamma_0 u_\ell$ can be extracted, together with the exterior conormal derivative $\phi_\ell := \gamma_1^{\mathrm{e}} u_\ell^{\mathrm{e}}$. These Cauchy data together with (4.1c), namely $(\gamma_0^{\mathrm{e}} u_\ell^{\mathrm{e}} = \gamma_0 u_\ell - \widehat{u}, \phi_\ell)$, allow the computation of the solution at any point of the exterior domain using the representation formula (3.19b). For instance, we show in Figure 5.1 the solution of the above discrete problem with $p = 2$ and a level of h-refinement $\ell = 20$. The exterior domain is unbounded, thus, for convenience, we plot the exterior solution only in $\Omega_{\mathrm{e}}^{\mathrm{e}} := (-0.5, 0.5)\setminus\overline{\Omega}$, which consists of 4 patches. There, the depicted solution is obtained from the evaluation of 25 points in each patch.

Next, we want to validate numerically the a priori estimates of Theorem 4.15. Because the norm $\|\cdot\|_{H^{-\frac{1}{2}}(\Gamma)}$ is not computable, we consider the equivalent operator norm $\|\cdot\|_{\mathcal{V}_0}$ instead, see (3.34). Hence, the error is measured with respect to the norm $\sqrt{\|u - u_\ell\|^2_{H(\nabla,\Omega)} + \|\phi - \phi_\ell\|^2_{\mathcal{V}_0}}$. Due to the smoothness of the prescribed solution, we expect an optimal convergence order, i.e., equal to the degree of the considered discrete space $\boldsymbol{\mathcal{H}}_\ell$. In Figure 5.2, the results of the simulations for B-Spline spaces of degree $p = 1, 2, 3, 4$, respectively, confirm this behavior. With the same configuration, let us discuss in the following the possible super-convergence behavior that results in the BEM domain, see Remarks 4.34 and 4.35, and Remark 4.37. With $\mathcal{U} = \mathrm{Id}$, we can easily check that the dual of the bilinear form $a(\mathbf{u}, \mathbf{v})$, see (4.3), coincides with the bilinear form that arises by a Bielak-MacCamy FEM-BEM coupling of Problem 4.1, see [6]. Then, following the same steps as in our analysis guarantees the same a priori estimates of Theorem 4.15. Together with the smoothness of the prescribed solution, the latter consideration should yield a doubling of the convergence rates in the pointwise error. We

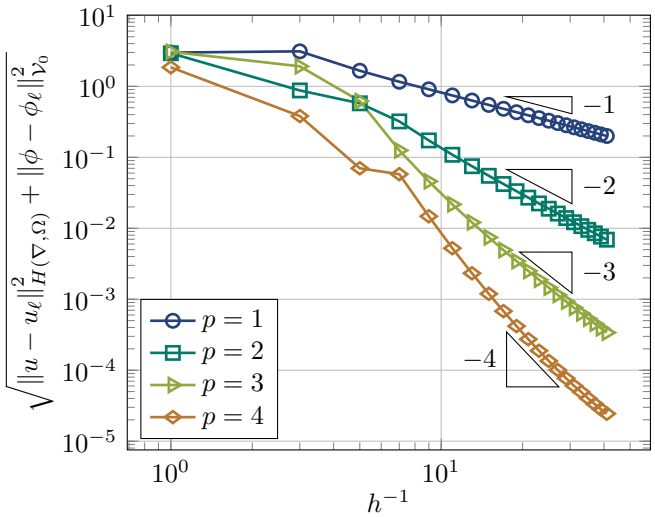

Figure 5.2: Example of Subsection 5.1.1: Convergence of discrete solution $(u_\ell, \phi_\ell) \in \boldsymbol{\mathcal{H}}_\ell$ to the solution $(u, \phi) \in \boldsymbol{\mathcal{H}}$. The considered B-Spline spaces have the degrees $p = 1, 2, 3, 4$, respectively, and the error is presented in the norm $\sqrt{\|\cdot\|^2_{H(\nabla,\Omega)} + \|\cdot\|^2_{\mathcal{V}_0}}$, which is equivalent to the standard $\boldsymbol{\mathcal{H}} = H(\nabla, \Omega) \times H^{-\frac{1}{2}}(\Gamma)$ norm [42].

verify this by using similar functionals to Remarks 4.34 and 4.35, namely,

$$u^{\mathrm{e}}(\boldsymbol{x}) = \mathfrak{F}(\mathbf{u}) := \int_\Gamma u^*(\boldsymbol{x}, \boldsymbol{y})\phi(\boldsymbol{y})\,\mathrm{d}\sigma_{\boldsymbol{y}} - \int_\Gamma \nabla_{\boldsymbol{x}} u^*(\boldsymbol{x}, \boldsymbol{y}) \cdot \boldsymbol{n}(\boldsymbol{y})(\gamma_0 u + \widehat{u})(\boldsymbol{y})\,\mathrm{d}\sigma_{\boldsymbol{y}},$$

and

$$\boldsymbol{b}^{\mathrm{e}}(\boldsymbol{x}) = \mathfrak{F}_b(\mathbf{u}) := \begin{pmatrix} -\int_\Gamma \partial_{x_2} u^*(\boldsymbol{x}, \boldsymbol{y})\phi(\boldsymbol{y})\,\mathrm{d}\sigma_{\boldsymbol{y}} + \int_\Gamma \partial_{x_2}(\nabla_{\boldsymbol{x}} u^*(\boldsymbol{x}, \boldsymbol{y}) \cdot \boldsymbol{n}(\boldsymbol{y}))(\gamma_0 u + \widehat{u})(\boldsymbol{y})\,\mathrm{d}\sigma_{\boldsymbol{y}} \\ \int_\Gamma \partial_{x_1} u^*(\boldsymbol{x}, \boldsymbol{y})\phi(\boldsymbol{y})\,\mathrm{d}\sigma_{\boldsymbol{y}} - \int_\Gamma \partial_{x_1}(\nabla_{\boldsymbol{x}} u^*(\boldsymbol{x}, \boldsymbol{y}) \cdot \boldsymbol{n}(\boldsymbol{y}))(\gamma_0 u + \widehat{u})(\boldsymbol{y})\,\mathrm{d}\sigma_{\boldsymbol{y}} \end{pmatrix},$$

which evaluate the exterior solution u^{e} and $\boldsymbol{b}^{\mathrm{e}} = \widetilde{\mathbf{curl}}\, u^{\mathrm{e}}$ at some point $\boldsymbol{x} = (x_1, x_2) \in \Omega^{\mathrm{e}}$. In particular, we set $N = 20$ uniformly distributed points on the evaluation path Γ_{e}, which we choose as the boundary of $(-0.35, 0.35)^2$, and compute the pointwise errors for u^{e} and $\boldsymbol{b}^{\mathrm{e}}$ by

$$\mathrm{error}_a = \max_{i=1,\dots,N} |u^{\mathrm{e}}(\boldsymbol{x}_i) - u^{\mathrm{e}}_\ell(\boldsymbol{x}_i)|, \qquad \mathrm{error}_b = \max_{i=1,\dots,N} |\boldsymbol{b}^{\mathrm{e}}(\boldsymbol{x}_i) - \boldsymbol{b}^{\mathrm{e}}_\ell(\boldsymbol{x}_i)|,$$

respectively. In Figure 5.3, the expected behavior is confirmed. Moreover, we also readily notice the effect of the leading constant, which depends on the order of singularity related to the kernel $u^*(\boldsymbol{x}, \cdot)$, see the discussion in Remarks 4.34 and 4.35. For instance, by comparing the convergence for $p = 4$ in both Figure 5.3a and Figure 5.3b, which correspond to error_a and error_b, respectively, we see that machine precision is reached for the former at a significantly smaller refinement level compared to the latter. Furthermore, we investigate the effects of position and quality of integration on the constant C of Remark 4.34. We repeat the experiment above with $p = 3$, and evaluate the exterior solution on three evaluation paths, namely, $\Gamma_{\mathrm{e},1} = \partial(-1, 1)^2$, $\Gamma_{\mathrm{e},2} = \partial(-0.35, 0.35)^2$, and $\Gamma_{\mathrm{e},3} = \partial(-0.26, 0.26)^2$. Thereby, the notation ∂D denotes the boundary of D. The results are plotted in Figure 5.4a, where we observe the expected behavior. The evaluation on $\Gamma_{\mathrm{e},1}$ even reaches machine precision. The closer we get to the boundary of Ω, the bigger the super-convergence's con-

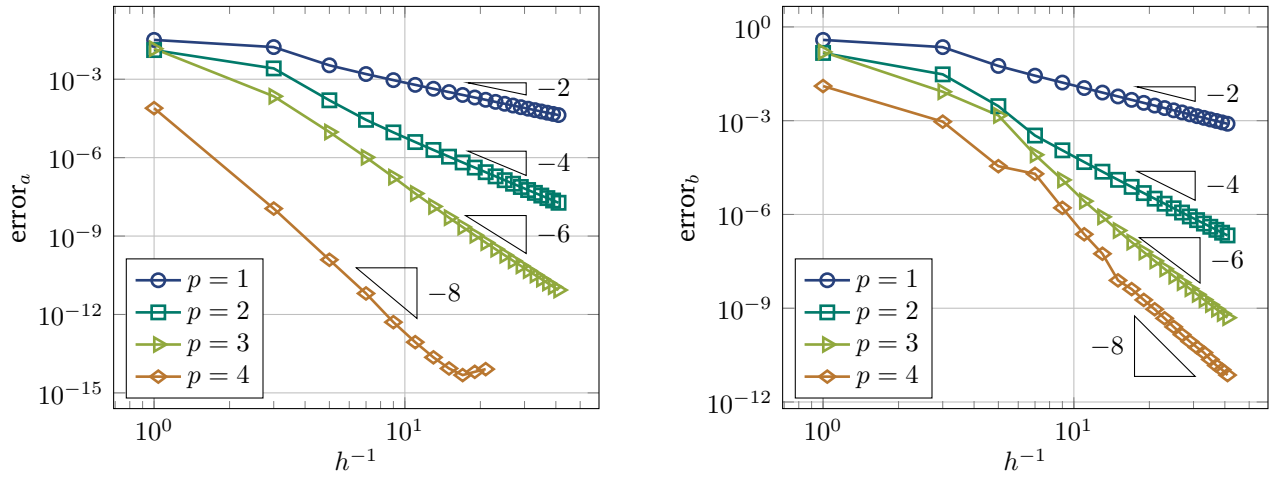

(a) Convergence of the exterior solution with respect to $\text{error}_a = \max_{i=1,\dots,N} |u^{\text{e}}(\boldsymbol{x}_i) - u^{\text{e}}_\ell(\boldsymbol{x}_i)|$. For $p = 4$ the error even achieves machine precision [42].

(b) Convergence of the $\widetilde{\mathbf{curl}}$ of the exterior solution with respect to $\text{error}_b = \max_{i=1,\dots,N} |\boldsymbol{b}^{\text{e}}(\boldsymbol{x}_i) - \boldsymbol{b}^{\text{e}}_\ell(\boldsymbol{x}_i)|$.

Figure 5.3: Example of Subsection 5.1.1: Super-convergence of the example in Subsection 5.1.1. The errors are calculated with $N = 20$ evaluations points on Γ_{e}, which is the boundary of $(-0.35, 0.35)^2$. The considered B-Spline spaces have the degrees $p = 1, 2, 3, 4$, respectively.

stant is. For the closest path $\Gamma_{\text{e},3}$, we notice that the quality of the computation deteriorates. This is made clearer in Figure 5.4b, where we compare the evaluation on $\Gamma_{\text{e},3}$ with different numbers of Gaussian quadrature points $N_{\text{G}} = 25, 50, 100$. For $N_{\text{G}} = 25$, there is practically no improvement of the convergence rates in the BEM domain. We call this observation a saturation effect. It is caused by the approximation of a nearly singular integral by means of Gauss-Legendre quadrature. By increasing the number of quadrature points, we can improve and even restore the optimal super-convergence. However, this has two apparent drawbacks: On one hand, increasing the number of quadrature points is time-consuming. On the other hand, the saturation effects can not be circumvented in the asymptotic area. However, note that there are better-suited alternatives to these types of applications. For instance, [107] proposes special extraction techniques, which avoid or reduce the issue substantially.

In the next section, we want to investigate the super-convergence for a more complicated problem.

5.1.2 A two-pole synchronous machine

In this subsection, the example that we consider can be modeled by Problem 4.26. In particular, we define Ω_1 and Ω_2 analogously to Figure 4.1 but over circular domains. Moreover, Ω^{e} is the bounded domain that separates Ω_1 and Ω_2. We call it the air gap. Concretely, let $B((x_1, x_2); r)$ denote a circular domain with midpoint (x_1, x_2) and radius r. Then, $\Omega_1 = B((0,0); 0.39) \setminus B((0,0); 0.1)$ and $\Omega_2 = B((0,0); 0.6) \setminus B((0,0); 0.4)$. The air gap is then defined formally by $\Omega_{\text{e}} = B((0,0); 0.4) \setminus B((0,0); 0.39)$. In contrast to the previous example, there exists no regular parametrization that can represent Ω_1 and Ω_2 by a single patch. Nevertheless, a multipatch approach similar to Figure 3.2 is straightforward. An exact representation can be obtained by NURBS of degree $p = 2$. A possible representation is depicted in Figure 5.5.

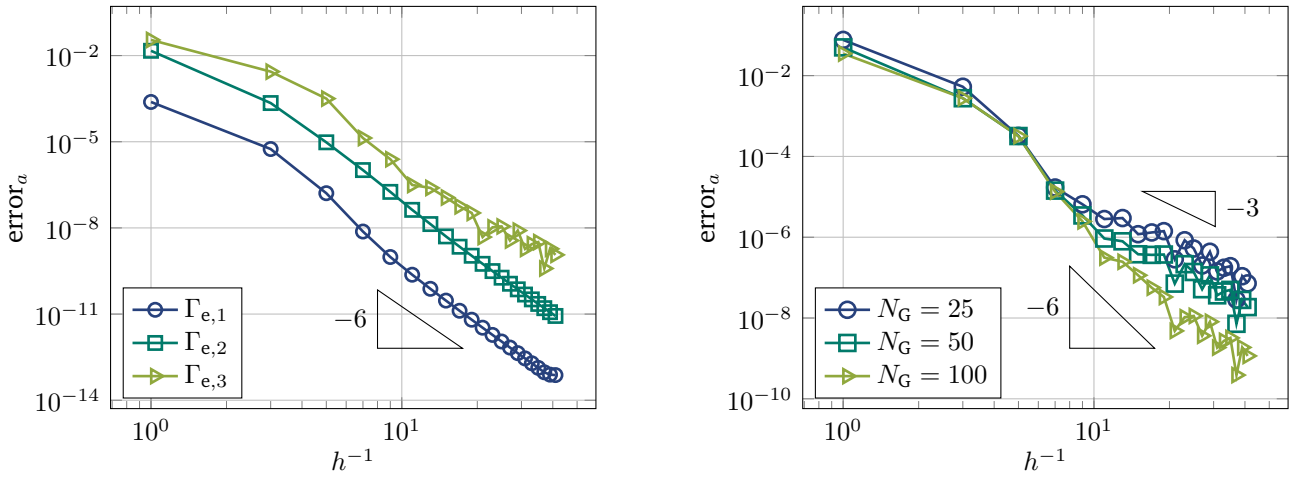

(a) Dependence on the position of the evaluation points, which are taken in $\Gamma_{e,i}$, with $i = 1, 2, 3$. We see an increase of the super-convergence constant the closer to the boundary the paths are.

(b) Dependence on the number of Gaussian points N_G. The evaluation path is thereby $\Gamma_{e,3}$. We observe an amelioration of the undesirable saturation with increasing N_G. For $N_G = 100$, the expected super-convergence is restored to some extent.

Figure 5.4: Example of Subsection 5.1.1: Dependence of the super-convergence on the position of the evaluation points and the number of quadrature points. We use $N = 20$ evaluation points to calculate the $\text{error}_a = \max_{i=1,\dots,N} |u^e(\boldsymbol{x}_i) - u^e_\ell(\boldsymbol{x}_i)|$, and choose the paths $\Gamma_{e,1} = \partial(-1, 1)^2$, $\Gamma_{e,2} = \partial(-0.35, 0.35)^2$, and $\Gamma_{e,3} = \partial(-0.26, 0.26)^2$. The considered B-Spline spaces are of degree $p = 3$ [42].

This example is interesting both from a theoretical and a practical point of view. Indeed, the eigenvalues λ_1 and λ_2 of $C_{\text{ell}}^{\mathcal{U}_i} > \frac{1}{4\lambda_i}$ in Theorems 4.28 and 4.32 are in general not explicitly known. However, we know for circular domains that the values are $\lambda_1 = \lambda_2 = 1$, see [90, Section 3] for more details. This allows us to test the validity of the coupling beyond the above mentioned restriction on $C_{\text{ell}}^{\mathcal{U}_i}$, which seems to be a theoretical one, cf. Remark 4.16. Moreover, it can be thought of as a simplified two-pole synchronous machine [75, Section 5.2]. Domain Ω_1 can then be labeled the rotor and Ω_2 the stator. Typically, these devices are mainly made of ferromagnetic materials, which interact non-linearly with the magnetic field. In practice, the corresponding B-H curve needs to be constructed from experimental data. We postpone this technicality to the next section. Here, we choose the following model for the non-linear material tensors

$$\mathcal{U}_i \nabla u_i := g(|\nabla u_i|)\nabla u_i,\ i = 1, 2, \quad \text{with } g(s) = \begin{cases} \frac{h_c}{b_s} & \text{for } s = 0, \\ \frac{h_c}{s} \tanh^{-1}(\frac{s}{b_s}) & \text{for } 0 < s \leq s_c := b_s - \epsilon, \\ 1 + \beta \exp(-\alpha s) & \text{for } s > s_c, \end{cases} \tag{5.1}$$

and specify the parameters such that the corresponding B-H curve is admissible in the sense of Definition 1.1, and such that it is realistic from a physical perspective. In the model above, the parameters h_c and b_s depend on the material. Moreover, $\epsilon > 0$ can be chosen arbitrarily to fulfill $g(s) < 1$, for all $0 < s \leq s_c$, whereas α, β are expansion coefficients that can be computed by

$$\alpha = \frac{g'(s_c)}{1 - g(s_c)}, \quad \beta = (g(s_c) - 1)\exp(\alpha s_c).$$

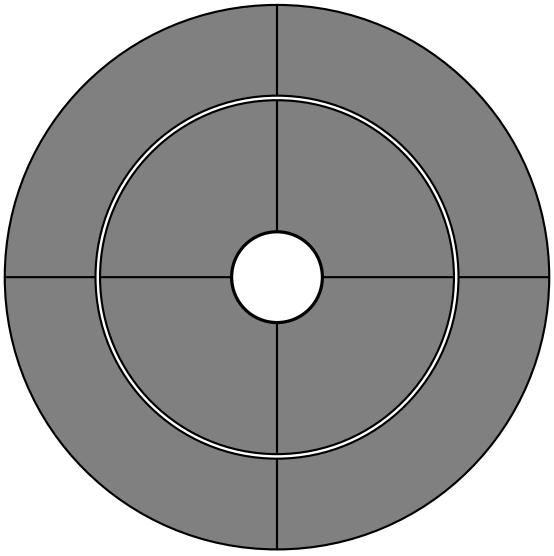

Figure 5.5: A possible multipatch representation for the example of Subsection 5.1.2 with four patches per domain. The interfaces between the patches and boundaries are highlighted by bold lines.

With this, it can be easily verified that g is globally continuously differentiable and strongly monotone in its domain of definition. Concretely, we choose $\epsilon = 10^{-2}$, $h_\mathrm{c} = 3 \cdot 10^{-3}$, and $b_\mathrm{s} = \frac{3}{2}$. In the following, this specific choice is discussed.

Remark 5.1. *On the one hand, note that the non-linear material tensor* (5.1) *in this particular setting leads to* $C_{\mathrm{ell}}^{\mathcal{U}_i} = \frac{h_\mathrm{c}}{b_\mathrm{s}} = 2 \cdot 10^{-3}$*, which clearly violates the condition* $C_{\mathrm{ell}}^{\mathcal{U}_i} > \frac{1}{4}$*. On the other hand, choosing* h_c *and* b_s *such that* $\frac{h_\mathrm{c}}{b_\mathrm{s}} > \frac{1}{4}$ *holds is not realistic in the context of electric machines. With such particular applications in mind, it is primordial to test the numerical validity of the method beyond this theoretical restriction.*

Now, let us prescribe the following input data:

$$\begin{aligned} f_1(\boldsymbol{x}) &= 0 && \text{for } \boldsymbol{x} := (x_1, x_2) \in \Omega_1, \\ f_2(\boldsymbol{x}) &= 100 \sin(\varphi) && \text{for } \boldsymbol{x} := (x_1, x_2) \in \Omega_2, \end{aligned}$$

where φ is the standard angle in a polar coordinate system. In addition, we set the jump conditions to zero, i.e., $\widehat{u}_i = 0$ and $\widehat{\phi}_i = 0$, $i = 1, 2$.
To solve the non-linear discrete Problem 4.31, we use a classical Picard iteration. For a discrete product space $\boldsymbol{\mathcal{H}}_{0,\ell}$ with B-Splines of degree $p = 3$ and at a level of refinement $\ell = 28$, we required 35 iterations to reach the stopping criterion 10^{-10}. The obtained solutions u_1 and u_2 in the interior domains Ω_1 and Ω_2, respectively, are visualized in Figure 5.6a. In the context of electric machines, u_i, $i = 1, 2$ can be interpreted as the axial component of the magnetic vector potential. Hence, the equipotential lines, i.e., the thick continuous black lines in Figure 5.6a are the magnetic field lines. In a post-processing step, we compute the magnetic reluctivity, which is given by the function $g(|\nabla u_i|)$, $i = 1, 2$, in (5.1), to highlight the non-linear behavior of the material. This is depicted in Figure 5.6b.
The next computation is dedicated to the numerical verification of Remark 4.49. For this, we choose the parametrized circle $\Gamma_\mathrm{e} := \partial B(\mathbf{0}; 0.395)$ to be our evaluation path. Similar to the previous subsection, the

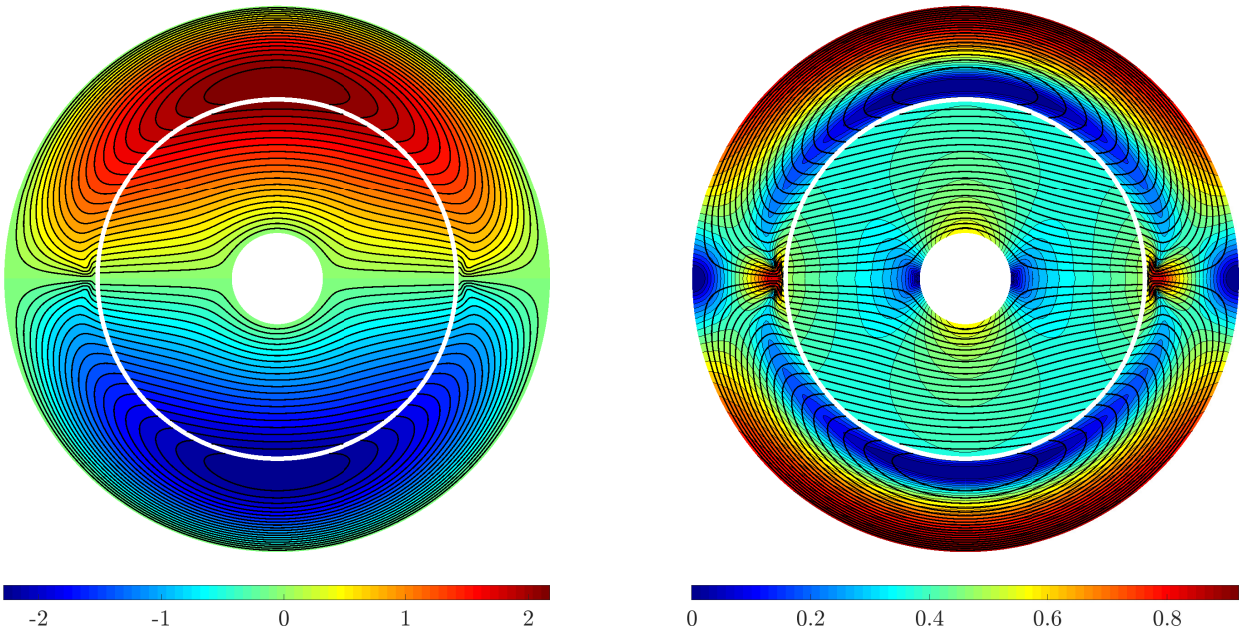

(a) The solutions u_1 and u_2 in the interior domains Ω_1 and Ω_2.

(b) Saturation effects caused by the non-linear material tensors. The color-bar and the thin lines represent the levels of the magnetic reluctivity, which is given by $g(|\nabla u_i|)$ for $i = 1, 2$.

Figure 5.6: Example of Subsection 5.1.2: A simulation of a two-pole synchronous machine with B-Splines of degree $p = 3$, at a refinement level $\ell = 28$. The thick equipotential lines show the magnetic field [42].

evaluation of the solution in a point of Γ_e is performed by means of the functional of Remark 4.34. An analytical solution for our model problem is however not known. Hence, to verify the convergence order, we follow a standard procedure: The mesh of the current solution is successively refined three times. Then, we calculate the corresponding discrete solutions, and apply the Aitkin's Δ^2-extrapolation to this sequence of discrete solutions [5]. This extrapolated value is considered as the reference solution $u^e(\boldsymbol{x}_i)$ in error $= \max_{i=1,\dots,N} |u^e(\boldsymbol{x}_i) - u^e_\ell(\boldsymbol{x}_i)|$ with $N = 20$ evaluations points, and where $u^e_\ell(\boldsymbol{x}_i)$ is the discrete solution at a refinement level ℓ, which can be computed by means of the obtained Cauchy data and the representation formula, see Remark 4.34. This error is visualized in Figure 5.7 for ansatz spaces of degree $p = 2$ and $p = 3$, where we observe an amelioration of the convergence rates. Note that this improvement depends on the quality of the numerical integration, as showcased in Figure 5.4b. For this example, noticeable ameliorations of the convergence rates were only observable for a high number of Gaussian quadrature points. Concretely, we considered $N_G = 400$ points for the assembling of the BEM matrices, which is very time-consuming. As mentioned in the previous subsection, the dominance of the quadrature error for this type of evaluation can be tackled by using special extraction techniques. Moreover, efficient assembly of the BEM matrices based on B-Spline tailored quadrature rules, as given in [2], together with suitable compression methods, see e.g., [39], would accelerate the computation considerably. However, this investigation is beyond the scope of this work.

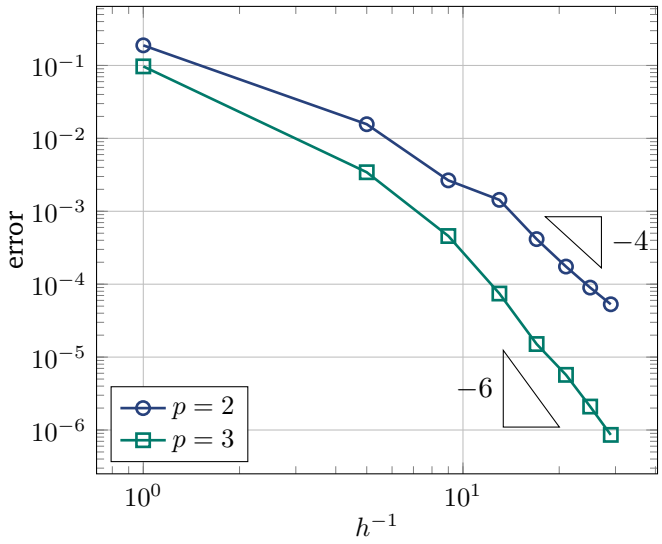

Figure 5.7: Example of Subsection 5.1.2: Convergence of the solution on the evaluation path $\Gamma_{\mathrm{e}} = \partial B(\mathbf{0}; 0.395)$ in the air gap Ω^{e}. Thereby, error $= \max_{i=1,\dots,N} |u^{\mathrm{e}}(\boldsymbol{x}_i) - u^{\mathrm{e}}_{\ell}(\boldsymbol{x}_i)|$ is calculated with $N = 20$ evaluations points [42].

5.1.3 Uniformly magnetized ball

In this subsection, we aim to verify the optimal super-convergence behavior of the isogeometric non-symmetric FEM-BEM coupling in the 3D case with the aid of an academic problem, for which an exact solution can be computed.

The bounded domain Ω is a 3-dimensional ball $B_3(\mathbf{0}\,; R)$, i.e., with radius R and a center that coincides with the origin of the coordinate system. Moreover, we embed a permanent magnetization into Ω. The treatment of such materials follows the discussion illustrated by Figure 1.2a. A sufficiently good approximation can then be obtained by replacing the constitutive law (1.3) by (1.4), which can be written as

$$\boldsymbol{h} = \nu \boldsymbol{b} - \boldsymbol{h}_{\mathrm{c}},$$

where $\boldsymbol{h}_{\mathrm{c}}$ denotes a coercive field, $\boldsymbol{h}$ the magnetic field strength, and $\boldsymbol{b}$ the magnetic flux density. Moreover, the reluctivity $\nu > 0$ is a scalar constant, hence the constitutive law is linear and isotropic. With this consideration and in the absence of an impressed electric current density, we may replace (4.30a) by

$$\mathbf{curl}\, \nu\, \mathbf{curl}\, \boldsymbol{a} = \mathbf{curl}\, \boldsymbol{h}_{\mathrm{c}} \qquad \text{in } \Omega, \tag{5.2}$$

where $\boldsymbol{a}$ is the magnetic vector potential. For simplicity, we choose a normalized reluctivity, i.e., $\nu = 1$[1]. In the exterior domain $\Omega^{\mathrm{e}} := \mathbb{R}^3 \backslash \overline{\Omega}$, the magnetic vector potential $\boldsymbol{a}^{\mathrm{e}}$ satisfies (4.30b). By taking into account the jump conditions (3.2a) and (3.2c), we know that the normal component of $\boldsymbol{b}$ is continuous, whereas a discontinuity is expected in the tangential part of $\boldsymbol{h}$ due to the contribution of the magnetization on the surface. To see this, let $\boldsymbol{h}_{\mathrm{c}}$ represent a uniform unidirectional magnetization. In particular, we choose $\boldsymbol{h}_{\mathrm{c}} = (0, 0, h_{\mathrm{c}})^{\top}$,

[1] Approximately, the model could be seen as NdFeB magnet, where μ_{r} is often taken as $\mu_{\mathrm{r}} = 1.05 \approx 1$.

with $h_c \neq 0$, similar to [67, Chapter 5.10]. There, an analytical solution in terms of magnetic vector potentials in spherical coordinates is provided for both the interior and exterior domains. In our Cartesian coordinate system and for $\boldsymbol{x} = (x_1, x_2, x_3) \in \mathbb{R}^3$, the solutions transform to

$$\boldsymbol{a}(\boldsymbol{x}) = \frac{h_c}{3} (-x_2, x_1, 0)^\top \qquad \text{for } \boldsymbol{x} \in \Omega, \tag{5.3a}$$

$$\boldsymbol{a}^e(\boldsymbol{x}) = \frac{h_c}{3} \left(\frac{R}{r(\boldsymbol{x})}\right)^3 (-x_2, x_1, 0)^\top \qquad \text{for } \boldsymbol{x} \in \Omega^e, \tag{5.3b}$$

where $r(\boldsymbol{x}) = \sqrt{x_1^2 + x_2^2 + x_3^2}$. Moreover, the magnetic flux densities read

$$\boldsymbol{b}(\boldsymbol{x}) = \mathbf{curl}\, \boldsymbol{a}(\boldsymbol{x}) = \frac{2}{3} \boldsymbol{h}_c \qquad \text{for } \boldsymbol{x} \in \Omega, \tag{5.4a}$$

$$\begin{aligned} \boldsymbol{b}^e(\boldsymbol{x}) = \mathbf{curl}\, \boldsymbol{a}^e(\boldsymbol{x}) &= \frac{h_c}{3} \frac{R^3}{r(\boldsymbol{x})^5} \left(3x_1x_3, 3x_2x_3, 2x_3^2 - x_1^2 - x_2^2\right)^\top \\ &= \left(\frac{R}{r(\boldsymbol{x})}\right)^3 \left(\frac{h_c x_3}{r(\boldsymbol{x})} \boldsymbol{n}(\boldsymbol{x}) - \frac{1}{3} \boldsymbol{h}_c\right) \qquad \text{for } \boldsymbol{x} \in \Omega^e. \end{aligned} \tag{5.4b}$$

Thereby, $\boldsymbol{n}(\boldsymbol{x}) = \frac{1}{r(\boldsymbol{x})}(x_1, x_2, x_3)^\top$. Let Γ denote the boundary of Ω. From the expressions above, we can readily verify that $\gamma_{\boldsymbol{n}} \boldsymbol{a} = \gamma_{\boldsymbol{n}} \boldsymbol{a}^e = 0$, $[\![\boldsymbol{\gamma}_D\, \boldsymbol{a}]\!]_\Gamma = \boldsymbol{0}$, and $\operatorname{div} \boldsymbol{a} = \operatorname{div} \boldsymbol{a}^e = 0$, which is in accordance with the physical constraints and the Coulomb gauge (continuity of the normal components and divergence-free property). In addition, we have $[\![\gamma_{\boldsymbol{n}} \boldsymbol{b}]\!]_\Gamma = 0$, and $[\![\boldsymbol{\gamma}_N\, \boldsymbol{a}]\!]_\Gamma = \boldsymbol{n}(\boldsymbol{x}) \times \boldsymbol{h}_c$, for all $\boldsymbol{x} \in \Gamma$. This corresponds to an effective magnetic surface charge density. More details can be found in [67, Chapter 5.10].

To simulate the physical problem described above, we consider the model Problem 4.38 with the adaptation (5.2) to incorporate the permanent magnetization. By applying a direct non-symmetric FEM-BEM coupling, we arrive at a variational formulation according to Problem 4.39. Then, an isogeometric Galerkin discretization yields Problem 4.43 with $\mathbf{u}_\ell := (\boldsymbol{u}_\ell, \boldsymbol{\phi}_\ell) \in \boldsymbol{\mathcal{H}}_{v,\ell} := \mathbb{S}^1_{\boldsymbol{p}}(\Omega) \times \mathbb{S}^{1,\perp}_{\widetilde{\boldsymbol{p}},0}(\Gamma)$. The obtained system of linear equations is singular, due to the infinite-dimensional kernel of the **curl**-operator in the FEM-domain. However, by considering a consistent right-hand side, i.e., divergence-free also on the discrete level, an iterative Conjugate Gradient (CG)-based solver converges properly. A correction of the data can be applied to ensure the discrete consistency, if it is not provided, see [70], for instance. Moreover, the introduction of Lagrange multipliers may be necessary to enforce gauge conditions in the interior domain, see, e.g., [74]. Nevertheless, as demonstrated in the proof of Theorem 4.47, the commutativity of the discrete de Rham complex guarantees that $\boldsymbol{\phi}_\ell \in \mathbb{S}^{1,\perp}_{\widetilde{\boldsymbol{p}},0}(\Gamma)$. Hence, together with the mapping properties of the involved Boundary Layer Potentials (BLPs), the representation formula

$$\mathfrak{F}(\mathbf{u}_\ell)(\boldsymbol{x}) := \boldsymbol{a}^e_\ell(\boldsymbol{x}) = -\left(\boldsymbol{\Psi}_{SL}(\boldsymbol{\phi}_\ell)(\boldsymbol{x}) + \boldsymbol{\Psi}_{DL}(\boldsymbol{\gamma}_D\, \boldsymbol{u}_\ell - \widehat{\boldsymbol{u}}_\ell)(\boldsymbol{x})\right), \quad \boldsymbol{x} \in \Omega^e \tag{5.5}$$

yields a unique exterior solution, which is expected to enjoy a super-convergence behavior, for the same reasons as in Subsection 5.1.1, see also Remark 4.49. In the following experiment, we prescribe (5.3a) and (5.3b) for the interior and exterior problems, respectively. This translates to $\boldsymbol{f} = \boldsymbol{0}$, $\widehat{\boldsymbol{u}} = \boldsymbol{0}$, and $\widehat{\boldsymbol{\phi}} = \boldsymbol{n}(\boldsymbol{x}) \times \boldsymbol{h}_c$, for all $\boldsymbol{x} \in \Gamma$, as right-hand sides. Note that by $\boldsymbol{f} = \boldsymbol{0}$ we mean that there is no impressed current density and that the volume contribution of the magnetization vanishes, i.e., $\mathbf{curl}\, \boldsymbol{h}_c = \boldsymbol{0}$. Moreover, without loss of generality, we choose $h_c = 1$ and $R = 1$. A multipatch representation of the considered ball $B_3(\boldsymbol{0}; 1)$ using seven regular NURBS patches is illustrated in Figure 5.8.

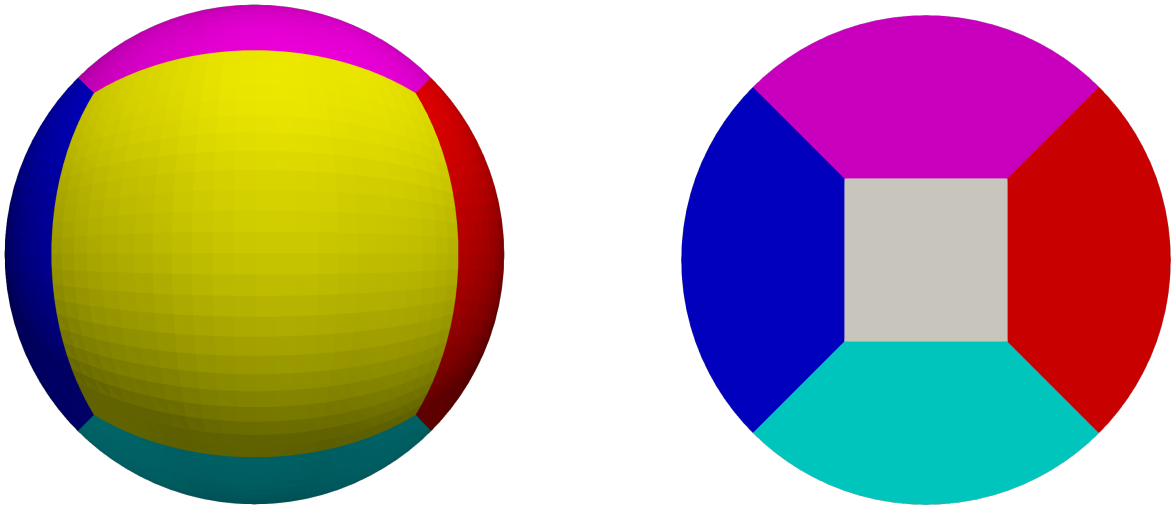

(a) A front view of the sphere.

(b) A cross-section to highlight the interior patch (grey).

Figure 5.8: Multipatch representation of the ball $B_3(\mathbf{0}\,;1)$ from Subsection 5.1.3. It consists of seven volume patches that are glued at interfaces. The patches with a boundary side have the same shape.

To verify the convergence of the magnetic vector potential and the magnetic flux density in the exterior domain, we perform a uniform h-refinement for polynomial degrees $p = 1, 2$. In every refinement level $\ell \geq 0$, the element size h is equal $2^{-\ell}$, where h is the length of a univariate element in the parametric domain. The numerical solution is achieved with a solver's tolerance of 10^{-6}. We used thereby the *BiCGSTAB* solver of *MATLAB/Octave* [40, 84]. In Figure 5.9, we show the obtained interior solution with a polynomial degree $p = 2$ at a refinement level $\ell = 3$.
For the evaluation of the exterior magnetic vector potential $\boldsymbol{a}_\ell^{\mathrm{e}}$ and the magnetic flux density $\boldsymbol{b}_\ell^{\mathrm{e}}$, we choose $N = 20$ equally distributed points on the boundary $\partial B_3(\mathbf{0}\,;1.5)$. Besides (5.5), the evaluation involves the following functional

$$\mathfrak{F}_b(\mathbf{u}_\ell)(\boldsymbol{x}) := \mathbf{curl}\, \boldsymbol{a}_\ell^{\mathrm{e}}(\boldsymbol{x}),$$

which can be derived analogously to the functional of Remark 4.35. With the exact solutions (5.3b) and (5.4b), the pointwise error is then computed by

$$\begin{aligned} \mathrm{error}_a &= \max_{i=1,\dots,N} |\boldsymbol{a}^{\mathrm{e}}(\boldsymbol{x}_i) - \boldsymbol{a}_\ell^{\mathrm{e}}(\boldsymbol{x}_i)|, \\ \mathrm{error}_b &= \max_{i=1,\dots,N} |\boldsymbol{b}^{\mathrm{e}}(\boldsymbol{x}_i) - \boldsymbol{b}_\ell^{\mathrm{e}}(\boldsymbol{x}_i)|, \end{aligned}$$

respectively. In Figure 5.10, we observe a doubling of the convergence rate, as expected from the discussion in Remark 4.49.

The next section is devoted to the electromechanical problem, namely, we inspect the coupled system with

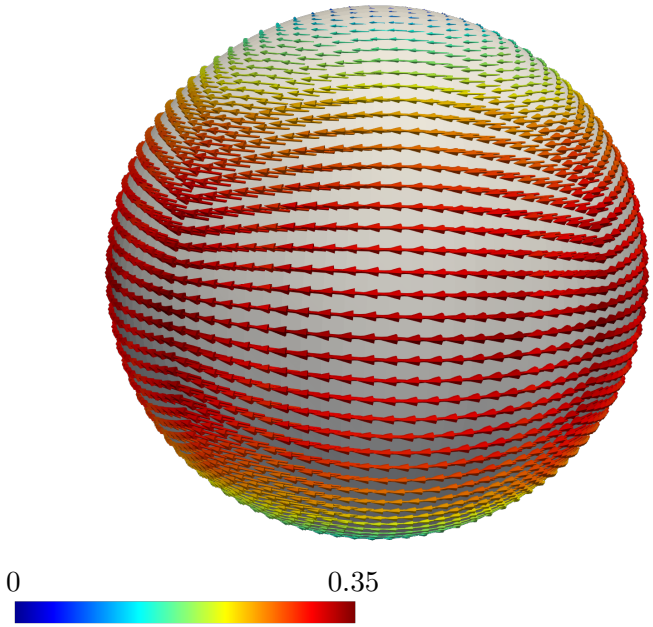

Figure 5.9: Example of Subsection 5.1.3: An interior solution depicted on the boundary of $B_3(\mathbf{0}; 1)$. The arrows encode the solution $\boldsymbol{u}$, and the color bar encodes its magnitude. The considered B-Spline space has the degree $p = 1$, and a refinement level $\ell = 3$.

different magnetic model problems, and address the computation of forces and torques, which represent the coupling of physical quantities.

5.2 The electromechanical problem

In this last section, we address the full discrete coupled system as illustrated in Figure 1.3. The magnetic part may be time-dependent. Then, the model problems follow either Section 4.1 or Section 4.2. In both cases the mechanical problem is given by an ordinary differential equation, see (1.16). We employ a classical implicit Euler method for all time discretizations. In the same spirit of the previous section, we consider three examples and emphasize some specific aspects with each one of them.

5.2.1 Iron plates versus magnet

In this example, we verify our implementation with respect to the computation of forces. In addition, we discuss a standard approach that allows the construction of admissible B-H curves from experimental data. To achieve this, we follow [91]. Recall that we characterized two types of non-linear materials that are relevant for our purpose, which can be classified as either hard or soft magnetic materials, see Subsection 1.1.1. We consider a non-symmetric isogeometric FEM-BEM coupling to solve Problem 4.1 with a domain Ω with

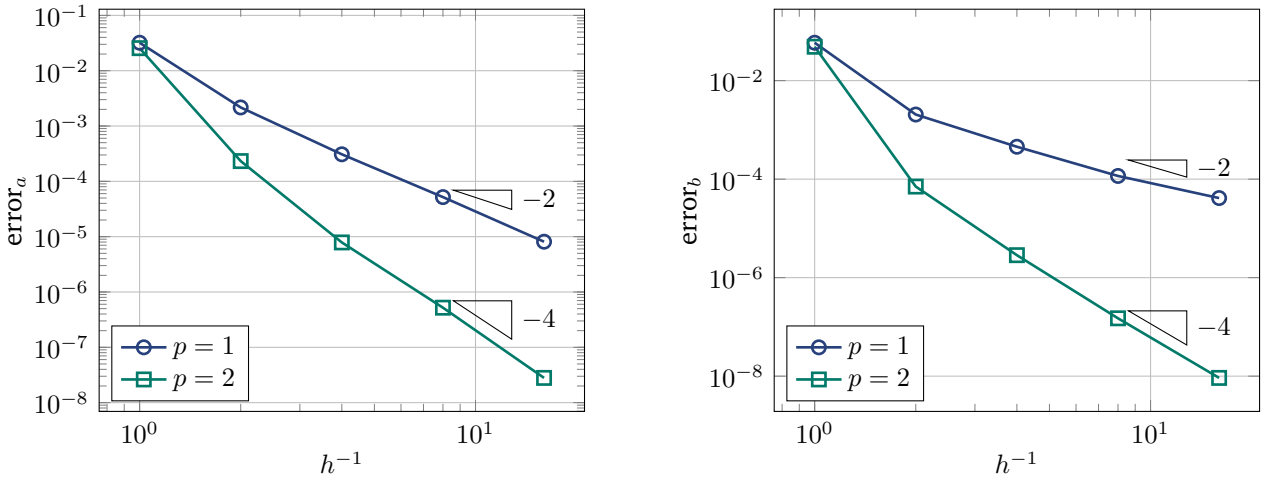

(a) Convergence of the exterior magnetic vector potential. Thereby, $\text{error}_a = \max_{i=1,\dots,N} |\boldsymbol{a}^{\text{e}}(\boldsymbol{x}_i) - \boldsymbol{a}^{\text{e}}_\ell(\boldsymbol{x}_i)|$.

(b) Convergence of the exterior magnetic flux density. Thereby, $\text{error}_b = \max_{i=1,\dots,N} |\boldsymbol{b}^{\text{e}}(\boldsymbol{x}_i) - \boldsymbol{b}^{\text{e}}_\ell(\boldsymbol{x}_i)|$.

Figure 5.10: Example of Subsection 5.1.3: Super-convergence of the exterior solution corresponding to the magnetic vector potential and the magnetic flux density. The considered B-Spline spaces have the degrees $p = 1, 2$, respectively. The evaluation is performed with $N = 20$ points on $\partial B_3(\mathbf{0}; 1.5)$.

several disjoint simply-connected parts.

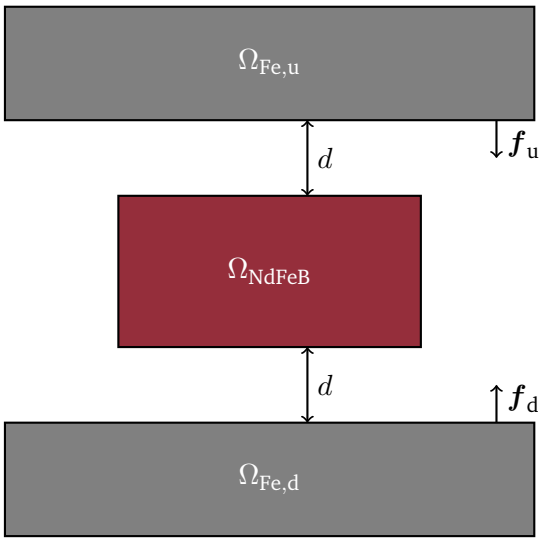

Figure 5.11: Illustration of the domain $\Omega = \Omega_{\text{NdFeB}} \cup \Omega_{\text{Fe,u}} \cup \Omega_{\text{Fe,d}}$ of Subsection 5.2.1, where Ω_{NdFeB} is associated to a Neodymium permanent magnet, and $\Omega_{\text{Fe,u}}$ and $\Omega_{\text{Fe,d}}$ to iron plates. Thereby, d denotes the distance between the iron plates and the magnet, and $\boldsymbol{f}_{\text{u}}$, $\boldsymbol{f}_{\text{d}}$ are the corresponding attractive forces.

In Figure 5.11, we illustrate the arrangement of the connected parts of $\Omega = \Omega_{\text{NdFeB}} \cup \Omega_{\text{Fe,u}} \cup \Omega_{\text{Fe,d}}$ with $\Omega_{\text{NdFeB}} = [-20, 20] \times [-10, 10]$, $\Omega_{\text{Fe,d}} = [-35, 35] \times [-35, -20]$, and $\Omega_{\text{Fe,u}} = [-35, 35] \times [20, 35]$. The previous dimensions are given in cm. Moreover, note that similar to a FEM (or BEM) only approach, using appropriate Boundary Conditions (BCs) to reduce the considered domain in the presence of symmetries is also possible in the context of FEM-BEM couplings, see [81, Section 3.2.2] and [75, Section 3.4.3], for instance.
On the one hand, we associate Ω_{NdFeB} with an NdFeB permanent magnet, which is made of an alloy of Neodymium, iron, and boron. It is the most frequently used strong magnet in electrical machines. Evidently, it is considered as a hard magnetic material, whose hysteresis follows Figure 1.2a. Hence, the constitutive law (1.4) is a good and widely used approximation. For instance, (3.9a) can be linearized in the following sense

$$\mathbf{curl}\, \nu\, \mathbf{curl}\, \boldsymbol{a} = \mathbf{curl}\, \boldsymbol{h}_{\text{c}} + \boldsymbol{j}_{\text{s}},$$

where ν is a constant magnetic reluctivity, and $\boldsymbol{h}_{\text{c}}$ is a coercive field. In our 2D case, the interior problem reads

$$\operatorname{div} \nu \operatorname{grad} a = \operatorname{curl} \boldsymbol{h}_{\text{c}} + j \qquad \text{in } \Omega_{\text{NdFeB}}. \tag{5.6}$$

We choose here the coercive field to be of the form $\boldsymbol{h}_{\text{c}} = (0, 1)^{\top}$, and $\nu = \nu_0 \nu_{\text{NdFeB}} = \frac{\nu_0}{\mu_{\text{NdFeB}}}$ with $\nu_{\text{NdFeB}} = 1.05$. Note that $(0, 1)^{\top}$ means a magnetization in the vertical direction.
On the other hand, $\Omega_{\text{Fe,u}}$ and $\Omega_{\text{Fe,d}}$ are filled with iron. In this case, iron can be considered as a soft magnetic material, whose magnetic behavior follows the magnetization curve of Figure 1.2b. Hence, the non-linearity is handled as in Subsection 5.1.2, if the B-H curve is available in an analytic form. However, this is usually not the case as information is mostly provided by a set of experimentally measured data, from which a closed form for the B-H curve should be gained for simulation purposes. The approach that we consider in our calculations is standard. We refer to [91, Section 3.1] and the literature cited therein. It involves a cubic spline interpolation and an extrapolation as in (5.1). The quality of such an approach depends on that of the measured data, which we assume here to be good enough, for convenience. See the previously cited reference for a possible workaround in case of noisy data, and also [92], for instance. Under this assumption, the used interpolation and extrapolation approaches guarantee an admissible B-H curve in the sense of Definition 1.1. With a sample provided in [91, Table B.1], we illustrate the interpolation process in Figure 5.12.

First, we use the non-linear reluctivity of Figure 5.12b, which follows easily from the corresponding B-H curve, and the permanent magnetization as described in (5.6) for the magnet part to solve Problem 4.1 using a non-symmetric isogeometric FEM-BEM coupling with ansatz spaces of degree $p = 1$ and at a refinement level $\ell = 15$. We consider in this experiment different distances d between the permanent magnet and the iron plates, see Figure 5.11, and compute the attractive force. For convenience, we depict the solution, i.e., the magnetic vector potential, for $d = 5\,\text{cm}$ in Figure 5.13. By symmetry, we know that the attractive forces $\boldsymbol{f}_{\text{u}}$, $\boldsymbol{f}_{\text{d}}$ are equal in magnitude and oppositely directed. In this context, the force is unidirectional, namely, there is only one non-zero component in the vertical direction. Moreover, no forces are exerted on the permanent magnet. To verify our implementation of forces using the Maxwell Stress Tensor (MST) method, see (1.19), we may choose as contour Γ_{e} every closed curve that encloses the considered Region Of Interest (ROI). In this case, our ROI corresponds to $\Omega_{\text{Fe,u}}$. Then we integrate numerically following (1.20). As pointed out in Subsection 1.1.2, all points of Γ_{e} should be contained in the air region. Even though taking the boundary as an integration path is possible, see [77, 81], for instance, it would be counterproductive as the method would not profit from the super-convergence of BEM. Whenever it is possible, choosing a 2π-periodic contour and solving the intergral by the trapezoidal rule is more advantageous, since it is known to yield exponential convergence. Otherwise, we apply standard Gaussian quadrature. We compute the attractive force for $d = 10, 5, 2.5\,\text{cm}$, respectively, and compare our result with a benchmark solution, which

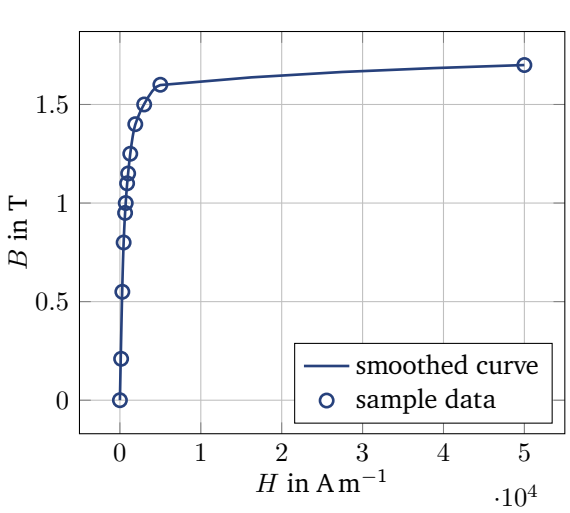

(a) Measured data and interpolated B-H curve.

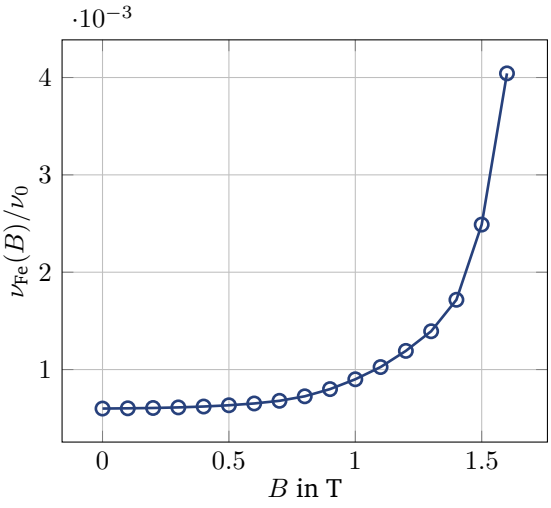

(b) The corresponding normalized reluctivity $\frac{\nu_{\mathrm{Fe}}}{\nu_0}$ to Figure 5.12a.

Figure 5.12: Example of Subsection 5.2.1: Interpolation using a cubic spline of the sample data from [91, Table B.1].

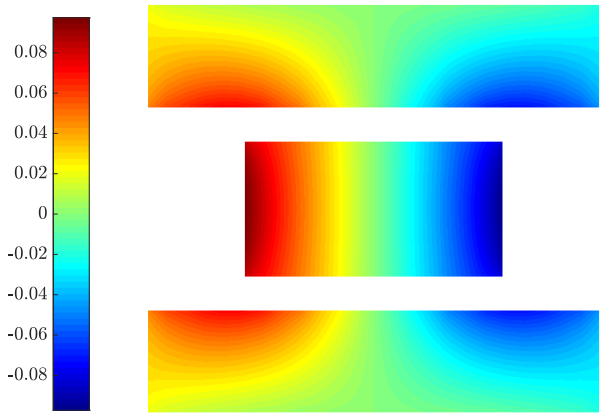

(a) The magnetic vector potential at $d = 5\,\mathrm{cm}$.

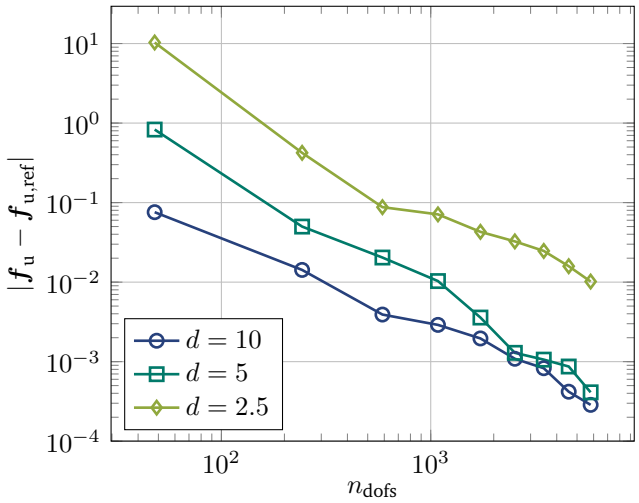

(b) Convergence of the force towards the benchmark solution of JMAG at a distance $d = 10, 5, 2.5\,\mathrm{cm}$. Thereby, n_{dofs} denotes the number of degrees of freedom. The force is expressed in kN.

Figure 5.13: Example of Subsection 5.2.1: Result of the simulation with an ansatz space of degree $p = 1$ and at a refinement level $\ell = 15$.

we compute by using the commercial software *JMAG* [68]. The comparison shown in Figure 5.13b confirms our implementation.

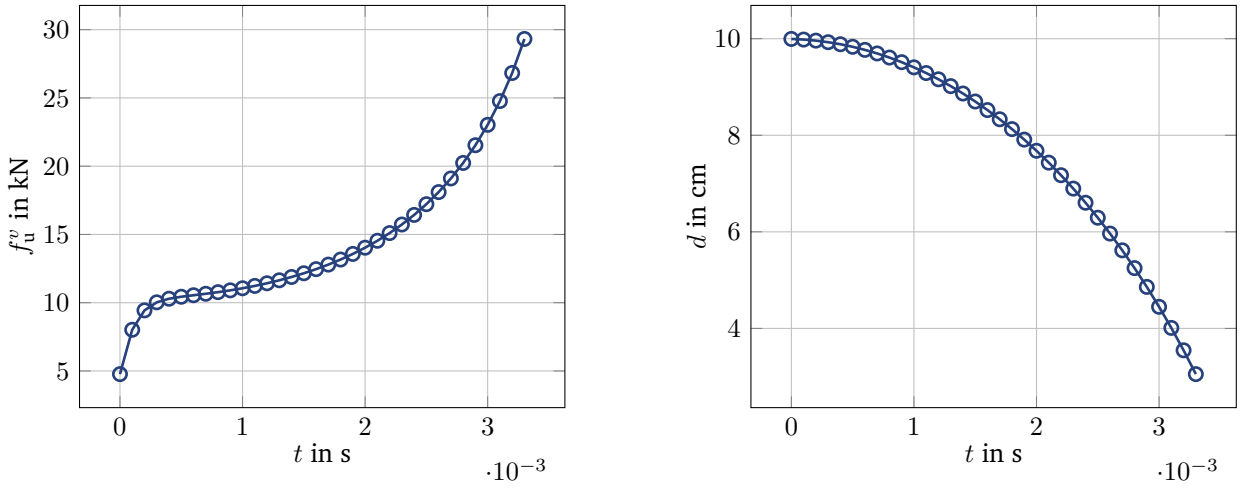

(a) Vertical component of the force f_u^v per time.

(b) Total distance per time.

Figure 5.14: Example of Subsection 5.2.1: The dynamics of the electromechanical problem over a time interval $T = [0, 3.3]$ ms and a time step $\Delta t = 0.1$ ms .

Second, supplementing the problem above with the mechanical system described by the equations of motion (1.16) leads to a movement of the iron plates due to the attractive forces towards the fixed permanent magnet. Because the force is unidirectional, namely, the movement is a pure translation in the vertical direction, we can use the simplified version of Newton's law (1.17). The ordinary differential equation is solved by a classical implicit Euler method. We compute for a time interval $T = [0, 3.3]$ ms with a time step $\Delta t = 0.1$ ms, and a mass $m_{\text{Fe}} = 1$ kg for convenience. The resulting dynamics of the system is plotted in Figure 5.14. In Figure 5.14a, we observe that in the first steps the force increases more rapidly, and sort of stabilizes its growth rate after ≈ 4 steps. The material reacts immediately to a change in the external field. However, the non-linear behavior affects its dynamics. This latency can then be interpreted as the time needed for the material to reach its saturated state. Upon saturation, iron is fully magnetized. In other words it reacts linearly, and produces the expected dynamics. In Figure 5.14b, we depict the corresponding total distance per time, starting from a gap of $d = 10$cm between the iron plates and the magnet. Note that the discussion in Remark 4.34, and its illustration in Subsection 5.1.1 about the quality of integration for close evaluation paths is also relevant in this case.

In the next subsection, we proceed analogously with an example involving the mechanical torque as a coupling quantity of the electromechanical system.

5.2.2 Magnetic pendulum

In electrical and mechanical systems with only one degree of freedom with respect to movement, the coupling quantity is usually either the force, as we saw in the previous subsection, or the mechanical torque. In the following, we give an example to highlight the latter option. In addition, we extend it by including

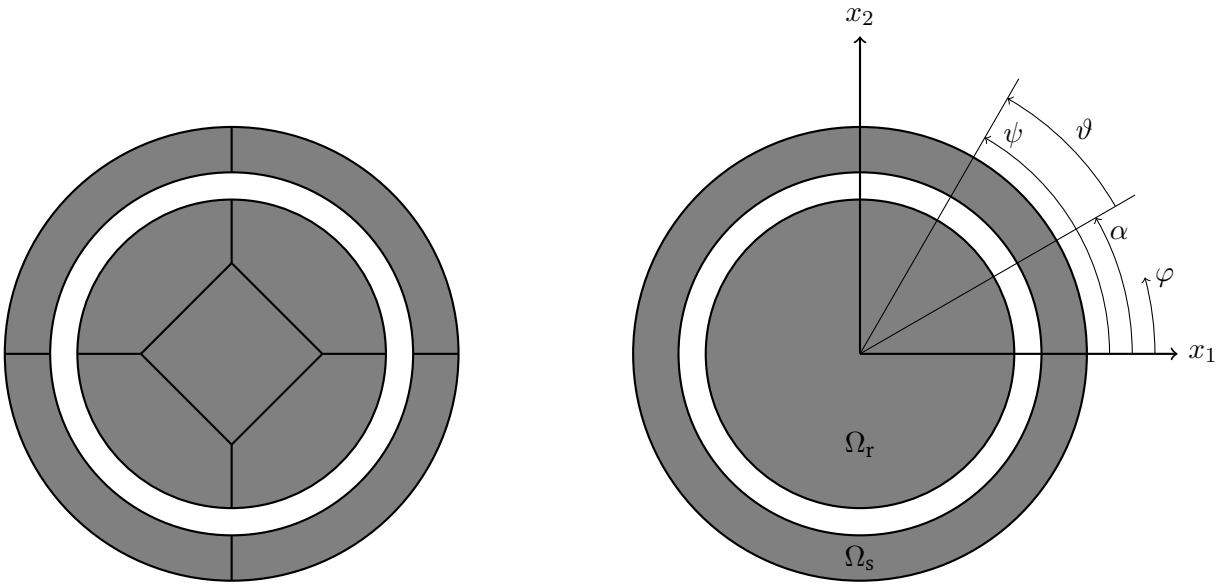

(a) A possible multipatch representation. The patches are delimited with the thick lines.

(b) φ represents the angle in a fixed polar coordinate system, $\alpha := \alpha(t)$ is attached to the rotating field's axis in the stator $\Omega_\mathrm{s} := B(\mathbf{0}; 0.5) \setminus B(\mathbf{0}; 0.4)$, and $\psi := \psi(t)$ to magnetization direction in the rotor $\Omega_\mathrm{r} := B(\mathbf{0}; 0.38)$. We also denote the phase shift between ψ and α by $\vartheta := \psi - \alpha$.

Figure 5.15: An illustration of a multipatch representation of the magnetic pendulum of Subsection 5.2.2, and the considered coordinate systems to describe its dynamics.

conductive regions to test problems of the parabolic type that can be modeled according to Problem 4.17. Both examples have been studied in [75, Section 5.2] with a classical FEM-BEM coupling.

As a starting point, we consider a simplified version of a 2-pole synchronous machine, and assume a permanent magnetization in the rotor $\Omega_\mathrm{r} := B(\mathbf{0}; 0.34)$. Thereby and throughout this section, all geometry dimensions are given in meter. The permanent magnetization can be incorporated into the Partial Differential Equation (PDE) as in (5.6). Furthermore, we impose a rotating current density in the stator, which we define as $\Omega_\mathrm{s} := B(\mathbf{0}; 0.5) \setminus B(\mathbf{0}; 0.4)$. These adaptations allow the interpretation of the problem as analogon to a physical pendulum, for which an approximation of the solution can be obtained by a Taylor series expansion. In Figure 5.15, we illustrate the problem's geometry, introduce the used coordinate systems, and furnish a possible NURBS representation of the domains. Concretely, for $t \geq 0$, we prescribe the rotating current density

$$j = j_0 \sin(\varphi - \alpha(t)) \quad \text{with } \alpha(t) = \omega t$$

in the stator domain Ω_s, and the magnetization

$$\boldsymbol{h}_\mathrm{c} = h_\mathrm{c}(\cos\psi(t), \sin\psi(t))^\top,$$

in the rotor domain Ω_r. Thereby, ω is a constant angular velocity, φ is a coordinate in a standard polar coordinate system, whereas $\alpha(t)$ and $\psi(t)$ designate the rotation field's axis in the stator and the rotor angles, respectively; see Figure 5.15b for an illustration. Let $\vartheta(t) = \psi(t) - \alpha(t)$, $t \geq 0$ denote the phase shift between

the direction of magnetization and the rotating field, cf. Figure 5.15b. The phase shift $\vartheta := \vartheta(t)$ is the solution of the following Initial Value Problem (IVP) [75, Appendix E]:

$$T^2\ddot{\vartheta} + \sin\vartheta = 0 \qquad \text{for } t > 0, \tag{5.7}$$
$$\vartheta = 0 \qquad \text{for } t = 0, \tag{5.8}$$
$$\dot{\vartheta} = -\omega \qquad \text{for } t = 0, \tag{5.9}$$

where T is the time constant of the oscillation. The initial conditions above follow from our initial configuration, which we assume to be

$$\psi = 0 \qquad \text{for } t = 0,$$
$$\dot{\psi} = 0 \qquad \text{for } t = 0.$$

The solution of the IVP (5.7) can be approximated by utilizing the computer algebra system *Wolfram Mathematica* [83], for instance. Therefrom stems our reference solution for ψ.

For an actual calculation, we need to specify the following parameters: the amplitude of the imposed current density j_0, the time constant T, the angular velocity ω, the amplitude of magnetization h_c, and the moment of inertia θ. Thereby, the subsequent relations have to be taken into account,

$$T^2 = \frac{2\theta}{h_\mathrm{c}\pi r^2 j_0 d}, \quad T\omega < 2, \quad \theta = \frac{1}{2}mr^2,$$

see [75, Section 5.2.1] for more details. In the relations above, r denotes the radius of the rotor, m its mass, and d the width of the stator. Henceforth, we choose $T = 10^{-3}\,\mathrm{s}$, $\omega = 10^3\,\mathrm{rad\,s^{-1}}$, $m = 0.1\,\mathrm{kg}$, and $j_0 = 4.82\sqrt{2}\,\mathrm{A\,m^{-1}}$. Note that r and d are readily obtained from the definition of the domains, and that h_c and θ follow from the relations above. For the computation of the torque with the MST method, we consider the contour $\Gamma_\mathrm{e} = \partial B\,(\mathbf{0}; 0.37)$ and integrate using the trapezoidal rule. Furthermore, time discretization is again performed by an implicit Euler method over the time interval $[0, 30]\,\mathrm{ms}$ with 300 time steps.
For the magnetic part of the problem, we consider Problem 4.10 with an ansatz space of degree $p = 2$, which is sufficient for an exact NURBS representation for circular domains. In addition, we choose a refinement level $\ell = 15$. We present our solution of the rotor's position in Figure 5.16, and depict the magnetic vector potential at different time stamps $t = 1.7,\ 3.4,\ 5.1\,\mathrm{ms}$ in Figure 5.17. The results are in concordance with the expectations. In particular, our numerical solution for the position of the rotor coincides with [75, Figure 5.7], and with the selected reference solutions, as shown in Figure 5.16b. As mentioned above, the trajectories that we obtained are characteristic to the undamped case of a physical pendulum. Indeed, the results can be interpreted as follows: At the beginning, i.e., at $t = 0$, the magnetization's direction and the rotating field created in the stator are in phase, i.e., $\vartheta(t) = \psi(t) - \alpha(t) = 0$. Hence, there are no tangential forces and the mechanical torque is also equal to zero. This changes however as soon as $\alpha(t) > 0$. In this case, i.e., when $\vartheta(t) < 0$, the mechanical torque is positive and increases accordingly to the phase shift. This induces an accelerated rotational movement of the rotor, which continues until reaching alignment, i.e., $\vartheta = 0$. Because of the inertia of the rotor, the magnetization's direction outruns the rotating field of the stator, which triggers a deceleration process. The deceleration comes with an increase of the torque in the opposite direction until $\vartheta = 0$ and trails back for the same reason. That is, both processes alternate to give rise to the obtained dynamics.

Let us now consider an extension of the model problem that includes conductive materials, and see how it

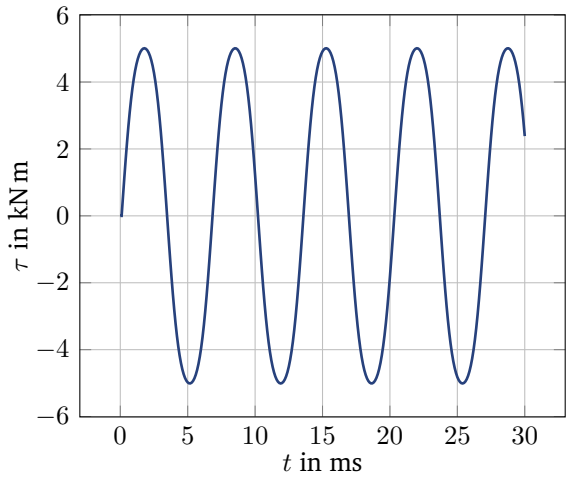

(a) Torque per time.

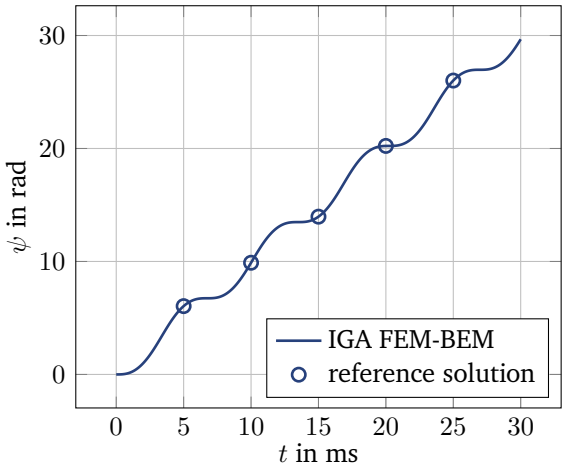

(b) Rotor angle ψ per time.

Figure 5.16: Example of Subsection 5.2.2: Dynamics of the magnetic pendulum computed with a time step of $0.1\,\mathrm{ms}$. The discrete problem corresponds to Problem 4.2 with an ansatz space of degree $p = 2$ and at a level of refinement $\ell = 15$.

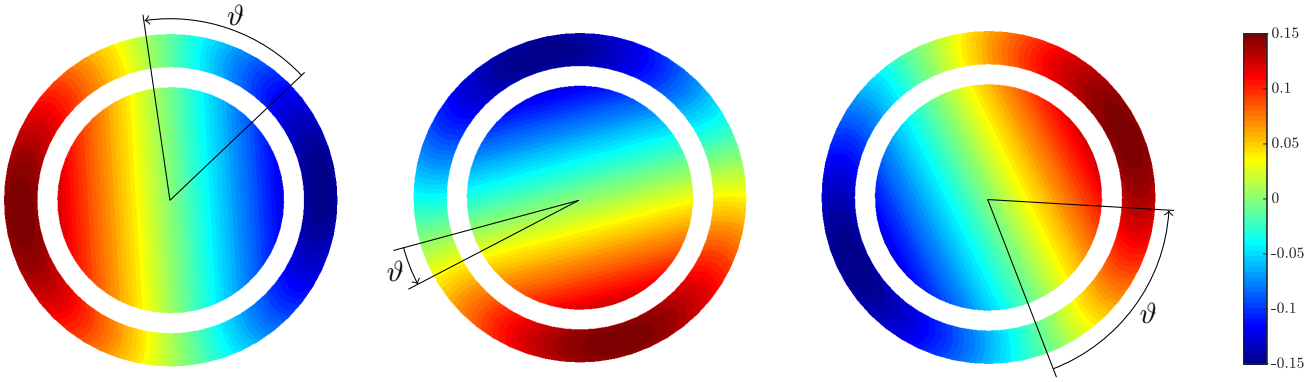

(a) At $t = 1.7\,\mathrm{ms}$ and $\vartheta \approx -54°$. **(b)** At $t = 3.4\,\mathrm{ms}$ and $\vartheta \approx -12°$. **(c)** At $t = 5.1\,\mathrm{ms}$ and $\vartheta \approx 65°$.

Figure 5.17: Example of Subsection 5.2.2: The solution at different time stamps of the discrete Problem 4.10 with an ansatz space of degree $p = 2$ and at a level of refinement $\ell = 15$. The solution is computed over the time interval $[0, 30]\,\mathrm{ms}$ with 300 time steps.

affects the system's dynamics. As depicted in Figure 5.18, we supplement the rotor with 8 damper rods, which will be associated with the conductive materials. We distribute them uniformly along the boundary. Their dimensions can be taken from Figure 5.18b. Moreover, we keep the notation and the coordinate systems of Figure 5.15b. To apply our isogeometric approach, we need to find a new multipatch representation for the rotor. In Figure 5.18a, we propose a possible representation of the rotor's domain that obviously guarantees the parametrizations' regularity, see Definition 3.23. Note that no changes have been made for the stator, and that the underlying equations of the magnetic part of the system correspond now to the parabolic Problem 4.17.

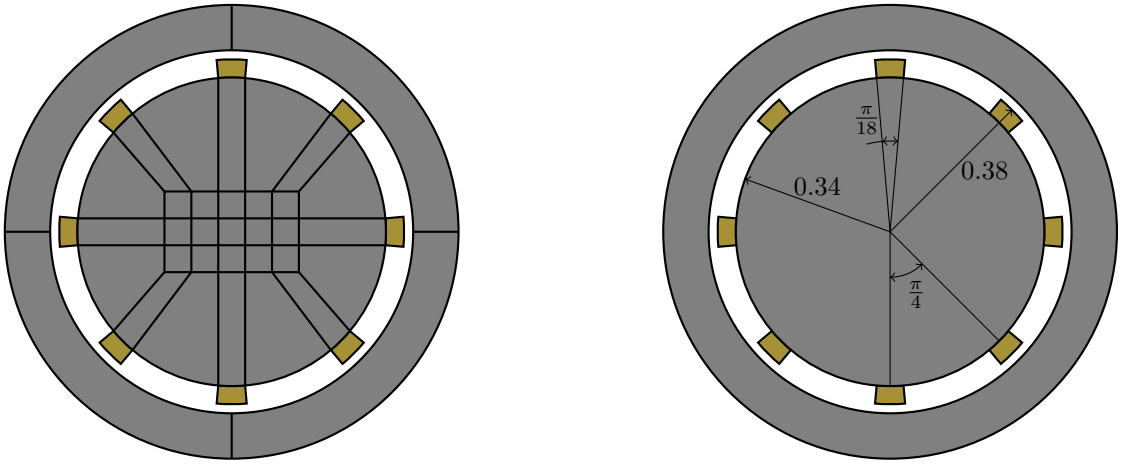

(a) A possible multipatch representation. The patches are delimited with the thick lines.

(b) The dimension and position of the damper rods. The stator's and permanent magnet's dimensions, as well as further notations can be taken from Figure 5.15b.

Figure 5.18: An illustration of a multipatch representation of the magnetic pendulum of Subsection 5.2.2 with eight uniformly distributed damper rods (in gold).

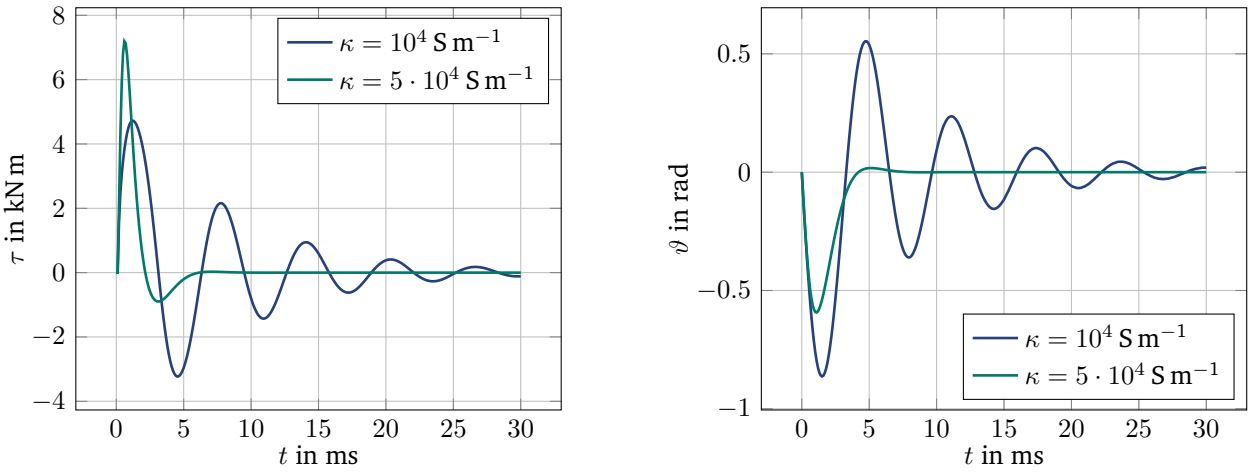

(a) Torque per time.

(b) Phase shift $\vartheta(t) = \psi(t) - \alpha(t)$ per time.

Figure 5.19: Example of Subsection 5.2.2: Dynamics of the magnetic pendulum supplemented by damper rods with electrical conductivity $\kappa = 10^4\,\mathrm{S\,m^{-1}}$, and $\kappa = 5 \cdot 10^4\,\mathrm{S\,m^{-1}}$. The discrete eddy-current problem corresponds to Problem 4.18 with an ansatz space of degree $p = 2$ and at a level of refinement $\ell = 15$.

In the moving conductive rods, we know from the Faraday's law (1.1c) that a current is induced in the presence of the rotating magnetic field. This leads to losses that damp the movement of the rotor, which gives rise to damped oscillations. Depending on the material properties and the chosen configuration, this may lead the magnetization and the rotating field from the stator to be synchronous after a few oscillations. In the

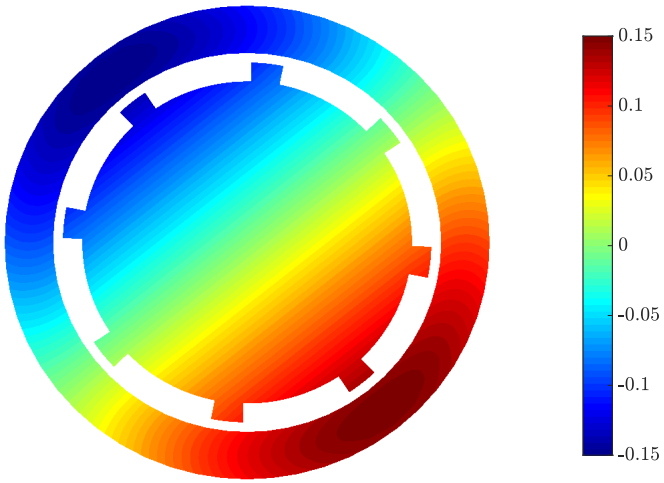

Figure 5.20: Example of Subsection 5.2.2: Vector potential of the magnetic pendulum with the electrical conductivity $\kappa = 5 \cdot 10^4\,\mathrm{S\,m^{-1}}$ with damper rods at $t = 10.1\,\mathrm{ms}$ and $\vartheta = 0$, namely, $\psi = \alpha = 10.1\,\mathrm{rad}$.

following, we test this effect with electrical conductivities $\kappa = 10^4,\ 5 \cdot 10^4\,\mathrm{S\,m^{-1}}$, a contour $\Gamma_\mathrm{e} = \partial B(\mathbf{0}; 0.39)$, and otherwise keep the same configuration from the previous experiment.
The expected dynamics of the magnetic pendulum with conductive rods is shown in Figure 5.19. In Figure 5.19a, we see a decrease in the mechanical torque with increasing time. The damping is clearly more noticeable for the bigger electrical conductivity $\kappa = 5 \cdot 10^4\,\mathrm{S\,m^{-1}}$. Correspondingly, the phase shift between the magnetization and the rotating magnetic field in the stator reduces proportionally inverse to the torque until reaching a synchronous state starting from $t = 10.1\,\mathrm{ms}$ for $\kappa = 5 \cdot 10^4\,\mathrm{S\,m^{-1}}$. This is depicted in Figure 5.19b. For convenience, we show the solution of the eddy-current problem at $t = 10.1\,\mathrm{ms}$ for an electrical conductivity $\kappa = 5 \cdot 10^4\,\mathrm{S\,m^{-1}}$ in Figure 5.20, where the rotor's magnetization and the stator's rotating field are synchronous.

In the next and last chapter, we summarize and comment the main findings of this thesis, and discuss further possibilities to extend and consolidate the presented method, namely, the direct non-symmetric isogeometric FEM-BEM coupling for the simulation of electromechanical energy converters.

6 Summary and prospects for future research

> If... the past may be no Rule for the future, all Experience becomes useless and can give rise to no Inferences or Conclusions.
>
> D. Hume

For the simulation of electromechanical energy converters, we considered a direct non-symmetric coupling of the Finite Element Method (FEM) and the Boundary Element Method (BEM) in an isogeometric setting for several model problems. This turns out to be a promising alternative to classical approaches. Indeed, the coupling combines the advantages of the numerical methods in a complementary way: FEM allows the consideration of non-linear Partial Differential Equations (PDEs) defined over bounded domains, the direct BEM solves problems in unbounded or thin domains, which exhibit linear material behavior, and the isogeometric framework avoids additional approximation errors due to the geometry representation and offers a straightforward h- and p-refinement procedure. Moreover, the coupling facilitates the incorporation of movements without the need of remeshing by allowing the different subdomains to be modeled separately. In addition, the convergence rates in the BEM domain are ameliorated if the dual problem is well-defined and its solution is smooth enough, which is advantageous for the computation of forces and torques using the Maxwell Stress Tensor (MST) method.

To arrive at the model problems for domains with a general topology, we proposed a mathematical approach to derive a vector potential formulation of the eddy-current model, where we considered two types of Boundary Conditions (BCs), which coincide with the electric and magnetic wall BC, respectively. By using results related to the de Rham complex, we obtained the well-known A-formulations from physics and engineering literature. In the three-dimensional (3D) case, the unknown magnetic vector potential is sought for in appropriate quotient spaces, which leads to solutions that have to be understood in the sense of equivalence classes.
To apply Boundary Element Methods, suitable representation formulae have been introduced, which lead to so called Boundary Integral Equations (BIEs) that are defined over the boundaries. An important tool in our analysis consists in estimating the energy of interior domains (FEM domains) in terms of Boundary Integral Operators (BIOs). This can be achieved in the scalar case by using the contractivity of (a shifted version of) the double-layer operator, which is a known result [110]. Analogously, we proved a similar estimate for the Maxwell double-layer operator.

Our analysis is based on the framework of Lipschitz continuous and strongly monotone operators. First, we addressed a two-dimensional (2D) Laplacian interface problem, which arises for instance in the magnetostatic regime. We extended the analysis of [46] to our non-linear setting, and established well-posedness by using an implicit stabilization that yields an equivalent problem, which is proved to be strongly monotone and

Lipschitz continuous. For a particular type of non-linear materials, which are relevant in our applications, we demonstrated the stability of the problem. Moreover, we showed quasi-optimality of the method with respect to a Galerkin discretization. Therefrom, we derived a priori error estimates for conforming B-Spline spaces, by using their approximation properties, which are provided in [21, 25].
Second, we considered an evolution problem in the 2D case. Such problems model the magnetoquasistationary case in a 2D setting. We showed that the properties established for the previous interface problem together with hemicontinuity are sufficient to prove well-posedness. However, note that for the parabolic case, well-posedness can be established without resorting to an implicit stabilization, see [41]. In addition, we provided a stability result analogously to [41].
Third, we studied a possible extension of a Laplacian interface problem to a Boundary Value Problem (BVP) that is suitable to model typical cross sections of electric machines, i.e., the domain consists of two disjoint nested subdomains, separated by an air gap. The model problem involves additionally homogeneous BCs in the outermost and the innermost boundary, respectively, see Figure 4.1 for a visualization. The central idea for the proof of strong monotonicity consisted in expressing the energies of the bounded domains in terms of energies that are related to unbounded problems. For this, auxiliary exterior eigenvalue problems can be defined as in [90]. Furthermore, we addressed the possible amelioration of the convergence rates in the BEM domain, and underlined the conditions that need to be fulfilled to reach super-convergence. The argument involves the dual problem, which arises by using an Aubin-Nitsche argument.
As a last model problem, we considered the magnetostatic case in three dimensions. The steps of the analysis are analogous to the 2D interface problem. However, due to the infinite-dimensional kernel of the **curl** operator consisting of gradient fields, we opted for a formulation of the coupled variational problem in the product space consisting of the quotient space $[\boldsymbol{H}(\mathbf{curl}, \Omega)]$ and its dual, which we characterized as a space of divergence-free vector fields with additional constraints depending on the topology and the considered BCs.

The above mentioned theoretical findings were confirmed by several numerical examples. The first part of the experiments was dedicated to the validation of the isogeometric approach. We verified the optimal behavior of the convergence rates in interior domains as well as the rates of the corresponding Cauchy data and the super-convergence of the solution in the BEM domains. Moreover, we discussed factors that may deteriorate a theoretically possible super-convergence, namely, the position of the evaluation points and in particular the quality of the numerical integration. The second part concerned the coupled electromechanical problem. For illustration purposes, we coupled the magnetic and the mechanical subsystems weakly, and applied a classical implicit Euler scheme for the discretization of time derivatives. The considered examples showcased both the calculation of forces and torques as coupling quantities by using the MST method. Moreover, the underlying equations covered both elliptic and parabolic cases.

Outlook To consolidate isogeometric FEM-BEM couplings for the simulation of electromechanical energy converters, several aspects could be investigated and implemented in future works.

- An analysis of the fully discretized parabolic problem with a higher time order discretization in both 2D and 3D domains is still missing. For this, the results of [47] can be adapted and extended to the non-linear setting with the drawback of the usual higher regularity assumptions in the time component. Alternatively to the method of lines and time-stepping methods, an isogeometric space-time discretization could also be investigated, see, e.g., [80].
- The development and analysis of adaptive isogeoemtric FEM-BEM couplings is to my knowledge still an open problem.

- The development of efficient preconditioning techniques that are tailored for the isogeometric framework would help to make the method more efficient from a practical point of view.
- The optimization and extension of the software implementation is required. From a Technology Readiness Level (TRL) perspective, the developed implementation is around TRL 4, see [28]. Nevertheless, it provides a great starting point to investigate real-world problems and it highlights the benefits of the isogeometric FEM-BEM coupling as a promising alternative for realistic production problems, since it circumvents several practical difficulties encountered with classical approaches.

We also note that a particularly elegant and concise alternative to formulate Maxwell-based 2D and 3D problems can also be achieved by using the language of differential forms. We refer for instance to [76].

A Monotone operators

We provide in this appendix a concise overview on some useful properties of monotone operators. For a more general survey, we refer to [51, 122]. In particular, the different types of continuity and monotonicity are compared in [51, Lemma 6.2] and [51, Lemma 6.4], respectively.

Let H be some Banach space, and let H' be its dual. We denote by $\langle \cdot, \cdot \rangle$ the corresponding duality product.

Definition A.1 (Monotone operators, [122])**.** *The operator $\mathcal{A} : H \to H'$ is called*

- *monotone, if and only if*
$$\langle \mathcal{A}u - \mathcal{A}v, u - v \rangle \geq 0 \qquad \forall u, v \in H.$$
- *strictly monotone, if and only if*
$$\langle \mathcal{A}u - \mathcal{A}v, u - v \rangle > 0 \qquad \forall u, v \in H \text{ and } u \neq v.$$
- *uniformly monotone, if and only if*
$$\exists\, C^{\mathcal{A}}_{\mathrm{UM}}(\|u - v\|_H) : \qquad \langle \mathcal{A}u - \mathcal{A}v, u - v \rangle \geq C^{\mathcal{A}}_{\mathrm{UM}}(\|u - v\|_H)\|u - v\|_H \qquad \forall u, v \in H$$
with $C^{\mathcal{A}}_{\mathrm{UM}} : \mathbb{R}_+ \to \mathbb{R}_+$ being an increasing function that satisfy $C_{\mathrm{UM}}(0) = 0$.
- *strongly monotone, if and only if*
$$\exists\, C^{\mathcal{A}}_{\mathrm{M}} > 0 : \qquad \langle \mathcal{A}u - \mathcal{A}v, u - v \rangle \geq C^{\mathcal{A}}_{\mathrm{M}}\|u - v\|^2_H \qquad \forall u, v \in H.$$

Definition A.2 (Coercive operators, [122])**.** *The operator $\mathcal{A} : H \to H'$ is coercive if*

$$\lim_{\|u\|_H \to \infty} \frac{\langle \mathcal{A}u, u \rangle}{\|u\|_H} \to \infty.$$

Lemma A.3. *Provided $\mathcal{A} : H \to H'$ is strongly monotone, then it is also coercive.*

Proof. First, it is obvious that a strongly monotone operator is also uniformly monotone. For instance, choose $C^{\mathcal{A}}_{\mathrm{UM}}(\|u - v\|_H) = C^{\mathcal{A}}_{\mathrm{M}}\|u - v\|_H$. Then, we refer to [53, Lemma 6] for a proof that uniformly monotone operators are also coercive. □

Definition A.4 (Continuous operators, [122])**.** *The operator $\mathcal{A} : H \to H'$ is called*

- *hemicontinuous, if for all* $u, v, w \in H$

$$\epsilon \mapsto \langle \mathcal{A}(u + \epsilon v), w \rangle$$

  is continuous on $[0, 1]$.

- *Lipschitz continuous, if for all* $u, v \in H$

$$\exists\, C_{\mathrm{L}}^{\mathcal{A}} > 0 : \qquad \|\mathcal{A}u - \mathcal{A}v\|_{H'} \leq C_{\mathrm{L}}^{\mathcal{A}} \|u - v\|_{H}.$$

B Vector potential formulation for the electric wall case

For completeness, we present in the following the analogous vector potential formulation to Section 3.1 in the case of an eddy-current model problem supplemented by an electric wall BC.

For every $t \in T$, $\boldsymbol{b} \in \boldsymbol{H}(\operatorname{div} 0, \Omega)$ and $\boldsymbol{e} \in \boldsymbol{H}(\mathbf{curl}\, \mathbf{0}, \Omega)$. As illustrated in Figure 2.4, the decomposition

$$\boldsymbol{b} = \boldsymbol{b}_{\mathrm{C}} + \boldsymbol{\eta}_1$$

with $\boldsymbol{b}_{\mathrm{C}} \in \boldsymbol{H}_0^{\mathrm{C}}(\operatorname{div} 0, \Omega)$ and $\boldsymbol{\eta}_1 \in \mathbb{H}_1(\Omega)$ is readily obtained. By using Corollary 2.25, there exists a unique vector potential $\boldsymbol{a} \in \boldsymbol{H}_{\mathbf{0}}(\mathbf{curl}, \Omega) \cap \boldsymbol{H}^{\Gamma}(\operatorname{div} 0, \Omega)$, such that

$$\boldsymbol{b} = \mathbf{curl}\, \boldsymbol{a} + \boldsymbol{\eta}_1. \tag{B.1}$$

In addition, due to the time dependence of the vector fields in (3.1a), for instance, $\boldsymbol{a}$ is an element of the Bochner space $\boldsymbol{L}^2(\partial_t, T;\, \boldsymbol{H}_{\mathbf{0}}(\mathbf{curl}, \Omega) \cap \boldsymbol{H}^{\Gamma}(\operatorname{div} 0, \Omega))$.
Now, inserting (B.1) in (3.1a) yields

$$\mathbf{curl}(\boldsymbol{e} + \partial_t \boldsymbol{a}) = -\partial_t \boldsymbol{\eta}_1 = \mathbf{0}.$$

Thereby, we used that for every $t \in T$, $\mathbf{curl}(\boldsymbol{e} + \partial_t \boldsymbol{a}) \in \boldsymbol{H}_0^{\mathrm{C}}(\operatorname{div} 0, \Omega)$. Since $\boldsymbol{H}_0^{\mathrm{C}}(\operatorname{div} 0, \Omega)$ is orthogonal to $\mathbb{H}_1(\Omega)$, i.e., $\boldsymbol{H}_0^{\mathrm{C}}(\operatorname{div} 0, \Omega) \cap \mathbb{H}_1(\Omega) = \{\mathbf{0}\}$, it follows that $\partial_t \boldsymbol{\eta}_1 = \mathbf{0}$.
As a consequence, for all $t \in T$, it follows that $(\boldsymbol{e} + \partial_t \boldsymbol{a}) \in \boldsymbol{H}_{\mathbf{0}}(\mathbf{curl}\, \mathbf{0}, \Omega)$. Then, by the decomposition (2.42a) together with (2.43a), there exists a unique scalar potential $\varphi \in L^2(T;\, H(\nabla, \Omega))$ (up to a constant) and $\boldsymbol{\eta}_2 \in \boldsymbol{L}^2(T;\, \mathbb{H}_2(\Omega))$, such that

$$\boldsymbol{e} + \partial_t \boldsymbol{a} = -\nabla \varphi + \boldsymbol{\eta}_2. \tag{B.2}$$

By inserting $\boldsymbol{e}$ from (B.2) into (3.1e), we arrive at

$$\boldsymbol{j} = \boldsymbol{j}_{\mathrm{s}} + \kappa(-\partial_t \boldsymbol{a} + \boldsymbol{\eta}_2 - \nabla \varphi), \tag{B.3}$$

which gives us a representation of the right-hand side of Ampère's law (3.1b). Moreover, with $\operatorname{div} \boldsymbol{\eta}_2 = 0$ we obtain a continuity condition

$$\operatorname{div}(\boldsymbol{j}_{\mathrm{s}} - \kappa \nabla \varphi) = \operatorname{div}(\kappa \partial_t \boldsymbol{a}) = 0.$$

With this, and for the sake of consistency with Ampère's law, we set $\boldsymbol{j} \in \boldsymbol{H}^{\Gamma}(\operatorname{div} 0, \Omega)$.
Using the constitutive law (3.1d) leads with $\mathbf{curl}\, \boldsymbol{\eta}_1 = \mathbf{0}$ to

$$\mathbf{curl}\, \nu(|\mathbf{curl}\, \boldsymbol{a} + \boldsymbol{\eta}_1|)\, \mathbf{curl}\, \boldsymbol{a} + \kappa \partial_t \boldsymbol{a} - \kappa \boldsymbol{\eta}_2 = -\kappa \nabla \varphi + \boldsymbol{j}_{\mathrm{s}}, \tag{B.4}$$

which is formulated in terms of the vector potential $\boldsymbol{a} \in \boldsymbol{L}^2(\partial_t, T;\, [\boldsymbol{H}_{\boldsymbol{0}}(\mathbf{curl}, \Omega)])$, a scalar potential $\varphi \in L^2(T;\, H(\nabla, \Omega))$ and cohomology vector fields $\boldsymbol{\eta}_1 \in \boldsymbol{L}^2(T;\, \mathbb{H}_1(\Omega))$ and $\boldsymbol{\eta}_2 \in \boldsymbol{L}^2(T;\, \mathbb{H}_2(\Omega))$. Thereby, we used (2.52a), i.e., the identification $\boldsymbol{H}(\mathbf{curl}, \Omega) \cap \boldsymbol{H}^{\Gamma}(\operatorname{div} 0, \Omega) \cong [\boldsymbol{H}_{\boldsymbol{0}}(\mathbf{curl}, \Omega)]$. Similarly to the magnetic wall case of Section 3.1, we may define $\boldsymbol{j}_{\mathrm{in}} = -\kappa \nabla \varphi + \boldsymbol{j}_{\mathrm{s}} \in \boldsymbol{L}^2(T;\, \boldsymbol{H}^{\Gamma}(\operatorname{div} 0, \Omega))$.

Remark B.1. *The topological terms η_1 and η_2 are can be eliminated analogously to Remark 3.1 by restricting $(\boldsymbol{b},\, \boldsymbol{e})$ to $\boldsymbol{L}^2(T;\, \boldsymbol{H}_0^{\mathsf{C}}(\operatorname{div} 0, \Omega)) \times \boldsymbol{L}^2(\partial_t, T;\, [\boldsymbol{H}_{\boldsymbol{0}}(\mathbf{curl}, \Omega)])$.*

List of acronyms

1D one-dimensional
2D two-dimensional
3D three-dimensional
a.e. almost everywhere
AC Alternating Current
BC Boundary Condition
BEM Boundary Element Method
BIE Boundary Integral Equation
BIO Boundary Integral Operator
BLP Boundary Layer Potential
BVP Boundary Value Problem
CAD Computer Aided Design
CG Conjugate Gradient
DC Direct Current
DLP Double-Layer Potential
FEM Finite Element Method
IGA Isogeometric Analysis
IVP Initial Value Problem
MST Maxwell Stress Tensor
NURBS Non-Uniform Rational B-Splines
PDE Partial Differential Equation
PEC Perfect Electric Conductor
PM Permanent Magnet
PMC Perfect Magnetic Conductor
PMSM Permanent Magnet Synchronous Machine
ROI Region Of Interest
SLP Single-Layer Potential

List of symbols

General

Symbol	Meaning	Page
$\mathbb{R}$	the set of real numbers	2
$\mathbb{R}_0^+$	the set of non-negative real numbers	5
$\times$	cross product, Cartesian product	9
$\mathbb{N}_0$	the set of non-negative integers	19
$\langle \cdot, \cdot \rangle_D$	duality product on D	20
$(\cdot, \cdot)_D$	inner product on D	20
$\boldsymbol{\alpha}$	multi-index	21
$\forall$	for all	21
$\exists$	there exists	25
$\exists!$	there exists a unique	25
$\|[v]\|_{[H]}$	quotient norm with $[v] \in [H]$	25
$\ker(\cdot)$	kernel	33
$\mathrm{Im}(\cdot)$	image	33
$.^\perp$	orthogonal complement	35
$.^{\perp,0}$	orthogonal complement in the corresponding null-space	36
$\cong$	isomorphic	40
$[\![\cdot]\!]_\Gamma$	jump from the interior to exterior trace with respect to Γ	57
$\mathbb{N}$	the set of natural numbers	65
det	determinant	69

Physical entities

Symbol	Meaning	Page
$\boldsymbol{d}(\boldsymbol{x}, t)$	electric flux density	2
$\varrho(\boldsymbol{x}, t)$	electric charge distribution	2
$\boldsymbol{b}(\boldsymbol{x}, t)$	magnetic flux density	2
$\boldsymbol{e}(\boldsymbol{x}, t)$	electric field	2
$\boldsymbol{h}(\boldsymbol{x}, t)$	magnetic field	2
$\boldsymbol{j}(\boldsymbol{x}, t)$	electric current density	2
ε	electric permittivity	3
μ	magnetic permeability	3
μ_0	vacuum permeability	3

μ_r	relative magnetic permeability	3
H	oriented magnitude of $\boldsymbol{h}(\boldsymbol{x},t)$	3
B	oriented magnitude of $\boldsymbol{b}(\boldsymbol{x},t)$	3
b_s	magnetic saturation	3
h_c	magnetic coercivity	3
b_r	magnetic remanence	4
$\boldsymbol{b}_\mathrm{r}$	remanent magnetic flux density	4
$\boldsymbol{h}_\mathrm{c}$	coercive field	4
ν	magnetic reluctivity	6
ν_0	vacuum reluctivity	6
κ	electrical conductivity	6
$\boldsymbol{j}_\mathrm{s}$	imposed electric current density	6
$\boldsymbol{k}(\boldsymbol{x},t)$	surface current density	6
$(\boldsymbol{x},\dot{\boldsymbol{x}},\ddot{\boldsymbol{x}},\ldots)$	kinematic variables (position, velocity, acceleration, ...)	8
$\boldsymbol{\omega}_\mathrm{l}$	angular velocity	8
m	mass	9
$\boldsymbol{\Theta}$	inertia tensor	9
$\boldsymbol{f}_\mathrm{M}$	total force	9
$\boldsymbol{\tau}_\mathrm{M}$	total torque	9
f_M	total force (unidirectional)	9
τ_M	total torque (unidirectional)	9
θ	moment of inertia	9
$\mathcal{T}_\mathrm{M}$	Maxwell stress tensor	9
$\boldsymbol{a}$	magnetic vector potential	51
φ	magnetic scalar potential	51
$\boldsymbol{\eta}_1$, $\boldsymbol{\eta}_2$	cohomology vector fields	51
$\boldsymbol{j}_\mathrm{in}$	$-\kappa\nabla\varphi+\boldsymbol{j}_s$	52

Geometric entities

Symbol	Meaning	Page
$\boldsymbol{x}$	an element of the Euclidean space	2
Σ_l	Lagrangian reference frame	8
$\boldsymbol{x}_\mathrm{l}$	coordinates in Σ_l	8
Σ_e	Eulerian reference frame	8
$\boldsymbol{x}_\mathrm{e}$	coordinates in Σ_e	8
$\boldsymbol{x}_\mathrm{e}^0$	coordinates in Σ_e	8
Ψ,Θ,Φ	Eulerian angles	8
$\mathcal{T}(t)$	orthogonal transformation	8
d	dimension of the Euclidean space	18
Ω	a bounded Lipschitz domain in $\mathbb{R}^d$	18
Γ	the boundary of Ω	18
N_Γ	the number of connected boundary parts in Γ	18
N_C	the number of cuts needed to render a connected domain simply-connected	18

D	a placeholder that may refer to $\{\mathbb{R}^d, \overline{\Omega}, \Omega, \Gamma\}$	18
τ_i	a boundary segment Γ	19
$\hat{\boldsymbol{p}}_i$	a local parametrization of Γ	19
Γ_{C_k}	interior cut	35
$\beta_i(\Omega)$	Betti-numbers associated with Ω with $i = 0, \dots, 3$ for $d = 3$	37
Ω^{e}	$\Omega^{\mathsf{e}} = \mathbb{R}^d \backslash \overline{\Omega}$ (if unbounded)	40
$\beta_1(\Gamma)$	Betti-number associated with Γ	45
Γ_{FEM}	union of connected parts of Γ that are associated with the FEM domain	53
Γ_{BEM}	union of connected parts of Γ that are associated with the BEM boundary	53
Ξ ($\boldsymbol{\Xi}$)	univariate (multivariate) knot vector	65
p ($\boldsymbol{p}$)	degree of a univariate (multivariate) B-Spline basis function	65
b_i^p ($b_{\boldsymbol{i}}^{\boldsymbol{p}}$)	univariate (multivariate) B-Spline basis function	65
r_i^p ($r_{\boldsymbol{i}}^{\boldsymbol{p}}$)	univariate (multivariate) Non-Uniform Rational B-Spline basis function	66
w_i ($w_{\boldsymbol{i}}$)	set of univariate (multivariate) weighting functions	66
κ_l	a single patch domain	67
$\boldsymbol{f}_l$	a regular parametrization from $[0,1]^d \to \kappa_l$	67
N_κ	number of patches	68
K	a multipatch representation of either Ω or Γ	67
h	global mesh size	67
$\boldsymbol{c_i}$	control points	68
$\widetilde{\Xi}$ ($\widetilde{\boldsymbol{\Xi}}$)	reduced univariate (multivariate) knot vector	70
$\widetilde{p}$ ($\widetilde{\boldsymbol{p}}$)	reduced degree of a univariate (multivariate) B-Spline basis function	70

Operators, functions, and functionals

Symbol	Meaning	Page
∂_t	partial derivative with respect to time t	2
div	divergence operator	2
curl	curl operator	2
g	a non-linear function describing an admissible B-H curve with Lipschitz continuity constant C_{L}^g and strong monotonicity constant C_{M}^g	5
$\partial_{\boldsymbol{x}}$	partial derivative with respect to $\boldsymbol{x}$	21
$\delta_{\boldsymbol{x}}$	Dirac distribution with support $\boldsymbol{x}$	21
$\mathcal{A}$	a non-linear operator with Lipschitz continuity constant $C_{\mathrm{L}}^{\mathcal{A}}$ and strong monotonicity constant $C_{\mathrm{M}}^{\mathcal{A}}$	26
∇	gradient operator	28
$\mathcal{U}$	a non-linear operator with Lipschitz continuity constant $C_{\mathrm{L}}^{\mathcal{U}}$ and strong monotonicity constant $C_{\mathrm{M}}^{\mathcal{U}}$	29
γ_0	standard trace operator with continuity constant C_0	30
$\gamma_1^{\mathcal{U}}$	conormal derivative with continuity constant C_1	30

$\gamma_{\boldsymbol{n}}$	normal trace operator with continuity constant $C_{\boldsymbol{n}}$	30
$\boldsymbol{\gamma}_{\times}$	tangential trace operator with continuity constant $C_{\times}$	30
$\boldsymbol{\gamma}_{\mathrm{D}}$	Dirichlet trace operator with continuity constant C_{D}	30
$\boldsymbol{\gamma}_{\mathrm{N}}^{\mathcal{U}}$	Neumann trace operator with continuity constant C_{N}	30
Id	identity operator	30
δ_{Γ}	Dirac distribution with support Γ	30
Δ	Laplace operator $\Delta = \operatorname{div}\nabla$	31
∇_{Γ}	surface gradient operator	41
$\mathbf{curl}_{\Gamma}$	surface **curl** operator	41
$\operatorname{curl}_{\Gamma}$	scalar surface curl operator	41
$\operatorname{div}_{\Gamma}$	surface divergence operator	42
$\times\boldsymbol{n}$ ($\boldsymbol{n}\times$)	rotation operator (its adjoint)	43
$\widetilde{\mathrm{Id}}$	augmented identity matrix	53
$\widetilde{\mathbf{curl}}$	2D **curl** operator	53
curl	2D scalar curl operator	53
$u^*(\cdot,\cdot)$	fundamental solution of the Laplace equation	55
Ψ_{SL} ($\boldsymbol{\Psi}_{\mathrm{SL}}$)	single-layer potential (vectorial)	55
Ψ_{DL} ($\boldsymbol{\Psi}_{\mathrm{DL}}$)	double-layer potential (vectorial)	55
$\mathcal{V}_0$ ($\boldsymbol{\mathcal{A}}_0$)	single-layer boundary integral operator (vectorial) with ellipticity constant $C_{\mathcal{V}_0}$ ($C_{\boldsymbol{\mathcal{A}}_0}$)	57
$\mathcal{K}_0$ ($\boldsymbol{\mathcal{C}}_0$)	double-layer boundary integral operator (vectorial) with contraction constant $C_{\mathcal{K}_0}$ ($C_{\boldsymbol{\mathcal{C}}_0}$)	57
$\mathcal{K}_0'$ ($\boldsymbol{\mathcal{B}}_0$)	adjoint double-layer boundary integral operator (Maxwell)	57
$\mathcal{W}_0$ ($\boldsymbol{\mathcal{N}}_0$)	hyper-singular boundary integral operator (vectorial) with ellipticity constant $C_{\mathcal{W}_0}$ ($C_{\boldsymbol{\mathcal{N}}_0}$)	57
$\mathcal{S}^{\mathrm{int}}$ ($\mathcal{S}^{\mathrm{ext}}$)	interior (exterior) Steklov-Poincaré operator	61
$\boldsymbol{\mathcal{S}}^{\mathrm{int}}$ ($\boldsymbol{\mathcal{S}}^{\mathrm{ext}}$)	interior (exterior) vectorial Steklov-Poincaré operator	62
$\mathfrak{F}$	a continuous and linear functional	90

Spaces

Symbol	Meaning	Page
$C^k(D)$ ($\boldsymbol{C}^k(D)$)	space of k-times continuously differentiable functions (vector fields)	19
$C^{\infty}(D)$ ($\boldsymbol{C}^{\infty}(D)$)	space of smooth functions (vector fields)	19
$C^{k,\iota}(D)$ ($\boldsymbol{C}^{k,\iota}(D)$)	space of Hölder continuous functions (vector fields)	19
$C^{0,1}(D)$ ($\boldsymbol{C}^{0,1}(D)$)	space of Lipschitz continuous functions (vector fields)	19
$L^2(D)$ ($\boldsymbol{L}^2(D)$)	space of square integrable functions	20
$\mathcal{D}(D)$ ($\mathcal{D}'(D)$)	space of test functions (distributions)	21
$\boldsymbol{\mathcal{D}}(D)$ ($\boldsymbol{\mathcal{D}}'(D)$)	space of test vector fields (distributions)	21
$W^{k,p}(\Omega)$	Sobolov space, $p \geq 1$, $k \geq 0$	22
$H^s(\Omega)$ ($\boldsymbol{H}^s(\Omega)$)	Hilbert space for functions (vector fields), $s \in \mathbb{R}_+$	22
$H^s_{\mathrm{loc}}(\mathbb{R}^d\backslash\overline{\Omega})$	space with local H^s-behavior	23
$L^2_{\mathrm{loc}}(\mathbb{R}^d\backslash\overline{\Omega})$	space with local L^2-behavior	23

$H^s(\Gamma)$	Hilbert space on a Lipschitz boundary, $s \in [-1,1]$	23
$L^2(\Gamma)$	$H^0(\Gamma)$	23
$L^2(T;\, H(D))$	Bochner space with instantaneous values in $H(D)$	24
$\boldsymbol{L}^2(T;\, \boldsymbol{H}(D))$	Bochner space with instantaneous values in $\boldsymbol{H}(D)$	24
$L^2(\partial_t, T;\, H(D))$	Bochner space with continuous weak time derivative (functions)	24
$\boldsymbol{L}^2(\partial_t, T;\, \boldsymbol{H}(D))$	Bochner space with continuous weak time derivative (vector fields)	24
$[H]$	quotient space for a generic Hilbert space H	25
$H(\nabla, \Omega)$	energy space with respect to ∇	28
$\boldsymbol{H}(\mathbf{curl}, \Omega)$	energy space with respect to **curl**	28
$\boldsymbol{H}(\mathrm{div}, \Omega)$	energy space with respect to div	28
$H_\lambda(\nabla, \Omega)$	$\{v \in H(\nabla, \Omega) :\, \gamma_0 v = \lambda\}$	32
$\boldsymbol{H}_{\boldsymbol{\lambda}}(\mathbf{curl}, \Omega)$	$\{\boldsymbol{v} \in \boldsymbol{H}(\mathbf{curl}, \Omega) :\, \boldsymbol{\gamma}_\times \boldsymbol{v} = \boldsymbol{\lambda}\}$	32
$\boldsymbol{H}_\lambda(\mathrm{div}, \Omega)$	$\{\boldsymbol{v} \in \boldsymbol{H}(\mathrm{div}, \Omega) :\, \gamma_{\boldsymbol{n}} \boldsymbol{v} = \lambda\}$	32
$H_\lambda(\nabla, \Omega, \Gamma_i)$	$\{v \in H(\nabla, \Omega) :\, \gamma_0 v = \lambda \text{ on } \Gamma_i\}$	32
$\boldsymbol{H}_{\boldsymbol{\lambda}}(\mathbf{curl}, \Omega, \Gamma_i)$	$\{\boldsymbol{v} \in \boldsymbol{H}(\mathbf{curl}, \Omega) :\, \boldsymbol{\gamma}_\times \boldsymbol{v} = \boldsymbol{\lambda} \text{ on } \Gamma_i\}$	32
$\boldsymbol{H}_\lambda(\mathrm{div}, \Omega, \Gamma_i)$	$\{\boldsymbol{v} \in \boldsymbol{H}(\mathrm{div}, \Omega) :\, \gamma_{\boldsymbol{n}} \boldsymbol{v} = \lambda \text{ on } \Gamma_i\}$	32
$H(\nabla \mathbf{0}, \Omega)$	$\{v \in H(\nabla, \Omega) :\, \nabla v = \mathbf{0}\}$	33
$\boldsymbol{H}(\mathbf{curl}\, \mathbf{0}, \Omega)$	$\{\boldsymbol{v} \in \boldsymbol{H}(\mathbf{curl}, \Omega) :\, \mathbf{curl}\, \boldsymbol{v} = \mathbf{0}\}$	33
$\boldsymbol{H}(\mathrm{div}\, 0, \Omega)$	$\{\boldsymbol{v} \in \boldsymbol{H}(\mathrm{div}, \Omega) :\, \mathrm{div}\, \boldsymbol{v} = 0\}$	33
$\boldsymbol{H}_0(\mathrm{div}\, 0, \Omega)$	$\{\boldsymbol{v} \in \boldsymbol{H}(\mathrm{div}\, 0, \Omega) :\, \gamma_{\boldsymbol{n}} \boldsymbol{v} = 0\}$	34
$[H(\nabla, \Omega)]$	$H(\nabla, \Omega)/\mathbb{R}$	34
$[\boldsymbol{H}(\mathbf{curl}, \Omega)]$	$\boldsymbol{H}(\mathbf{curl}, \Omega)/\nabla(H(\nabla, \Omega))$	34
$[\boldsymbol{H}(\mathrm{div}, \Omega)]$	$\boldsymbol{H}(\mathrm{div}, \Omega)/\,\mathbf{curl}(\boldsymbol{H}(\mathbf{curl}, \Omega))$	34
$\boldsymbol{H}_{\mathbf{0}}(\mathbf{curl}\, \mathbf{0}, \Omega)$	$\{\boldsymbol{v} \in \boldsymbol{H}(\mathbf{curl}\, \mathbf{0}, \Omega) :\, \boldsymbol{\gamma}_\times \boldsymbol{v} = \mathbf{0}\}$	37
$\mathbb{H}_1(\Omega)$	first de Rham cohomology space associated with Ω	37
$\mathbb{H}_2(\Omega)$	second de Rham cohomology space associated with Ω	37
$\boldsymbol{H}_0^{\mathsf{C}}(\mathrm{div}\, 0, \Omega)$	$\{\boldsymbol{v} \in \boldsymbol{H}(\mathrm{div}\, 0, \Omega) :\, \langle \gamma_{\boldsymbol{n}} \boldsymbol{v}, 1 \rangle_{\Gamma_{C_k}} = 0 \quad \forall\, k = 1, \ldots, N_{\mathsf{C}}\}$	38
$\boldsymbol{H}^{\Gamma}(\mathrm{div}\, 0, \Omega)$	$\{\boldsymbol{v} \in \boldsymbol{H}(\mathrm{div}\, 0, \Omega) :\, \langle \gamma_{\boldsymbol{n}} \boldsymbol{v}, 1 \rangle_{\Gamma_k} = 0 \quad \forall\, k = 1, \ldots, N_{\Gamma}\}$	38
$\boldsymbol{H}_{\mathsf{D}}^{\frac{1}{2}}(\Gamma)$	$\boldsymbol{\gamma}_{\mathsf{D}}(\boldsymbol{H}^1(\Omega))$	42
$\boldsymbol{H}_{\times}^{\frac{1}{2}}(\Gamma)$	$\boldsymbol{\gamma}_\times(\boldsymbol{H}^1(\Omega))$	42
$\boldsymbol{H}_{\mathsf{t}}^{\frac{1}{2}}(\Gamma)$	space of tangential fields with regularity $\frac{1}{2}$	42
$\boldsymbol{H}^{-\frac{1}{2}}(\mathrm{curl}_\Gamma, \Gamma)$	$\{\boldsymbol{\psi} \in \boldsymbol{H}_{\mathsf{D}}^{-\frac{1}{2}}(\Gamma) : \mathrm{curl}_\Gamma\, \boldsymbol{\psi} \in H^{-\frac{1}{2}}(\Gamma)\}$	42
$\boldsymbol{H}^{-\frac{1}{2}}(\mathrm{div}_\Gamma, \Gamma)$	$\{\boldsymbol{\psi} \in \boldsymbol{H}_{\times}^{-\frac{1}{2}}(\Gamma) : \mathrm{div}_\Gamma\, \boldsymbol{\psi} \in H^{-\frac{1}{2}}(\Gamma)\}$	42
$\boldsymbol{H}^{-\frac{1}{2}}(\mathrm{curl}_\Gamma\, 0, \Gamma)$	$\{\boldsymbol{\psi} \in \boldsymbol{H}^{-\frac{1}{2}}(\mathrm{curl}_\Gamma, \Gamma) : \mathrm{curl}_\Gamma\, \boldsymbol{\psi} = 0\}$	44
$\boldsymbol{H}^{-\frac{1}{2}}(\mathrm{div}_\Gamma\, 0, \Gamma)$	$\{\boldsymbol{\psi} \in \boldsymbol{H}^{-\frac{1}{2}}(\mathrm{div}_\Gamma, \Gamma) : \mathrm{div}_\Gamma\, \boldsymbol{\psi} = 0\}$	45
$\mathbb{H}_1(\Gamma)$	first de Rham cohomology space associated with Γ	45
$H_\star^{-\frac{1}{2}}(\Gamma)$	$\{\psi \in H^{-\frac{1}{2}}(\Gamma) : \langle \psi, 1 \rangle_\Gamma = 0\}$	46
$[H^{-\frac{1}{2}}(\Gamma)]$	$H^{-\frac{1}{2}}(\Gamma)/\mathbb{R}$	46
$[\boldsymbol{H}^{-\frac{1}{2}}(\mathrm{curl}_\Gamma, \Gamma)]$	$\boldsymbol{H}^{-\frac{1}{2}}(\mathrm{curl}_\Gamma, \Gamma)/\boldsymbol{H}^{-\frac{1}{2}}(\mathrm{curl}_\Gamma\, 0, \Gamma) \cap \boldsymbol{H}_{\times}^{\frac{1}{2}}(\Gamma)$	46
$\mathbb{S}^0_{\boldsymbol{p}}(\Omega)$	$H(\nabla, \Omega)$ conforming B-Spline space	69
$\mathbb{S}^1_{\boldsymbol{p}}(\Omega)$	$\boldsymbol{H}(\mathbf{curl}, \Omega)$ conforming B-Spline space	69
$\mathbb{S}^2_{\boldsymbol{p}}(\Omega)$	$\boldsymbol{H}(\mathrm{div}, \Omega)$ conforming B-Spline space	69
$\mathbb{S}^3_{\boldsymbol{p}}(\Omega)$	$L^2(\Omega)$ conforming B-Spline space	69
$\mathbb{S}^0_{\widetilde{\boldsymbol{p}}}(\Gamma)$	$H^{\frac{1}{2}}(\Gamma)$ conforming B-Spline space	70

$\mathbb{S}^{1,\parallel}_{\widetilde{\boldsymbol{p}}}(\Gamma)$	$\boldsymbol{H}^{-\frac{1}{2}}(\mathrm{curl}_\Gamma, \Gamma)$ conforming B-Spline space	70
$\mathbb{S}^{1,\perp}_{\widetilde{\boldsymbol{p}}}(\Gamma)$	$\boldsymbol{H}^{-\frac{1}{2}}(\mathrm{div}_\Gamma, \Gamma)$ conforming B-Spline space	70
$\mathbb{S}^{2}_{\widetilde{\boldsymbol{p}}}(\Gamma)$	$H^{-\frac{1}{2}}(\Gamma)$ conforming B-Spline space	70
$\mathbb{S}^{1,\perp}_{\widetilde{\boldsymbol{p}},0}(\Gamma)$	$\{\boldsymbol{\psi} \in \mathbb{S}^{1,\perp}_{\widetilde{\boldsymbol{p}}}(\Gamma) : \mathrm{div}_\Gamma \boldsymbol{\psi} = 0\}$	70
$\boldsymbol{\mathcal{H}}$	$H(\nabla, \Omega) \times H^{-\frac{1}{2}}(\Gamma)$	75
$\boldsymbol{\mathcal{H}}_\mathrm{T}$	$L^2(\partial_t, T;\, H(\nabla, \Omega)) \times L^2(T;\, H^{-\frac{1}{2}}(\Gamma))$	82
$\boldsymbol{\mathcal{H}}_0$	$H_0(\nabla, \Omega_1, \Gamma_{0,1}) \times H_0(\nabla, \Omega_2, \Gamma_{0,2}) \times H_\star^{-\frac{1}{2}}(\Gamma)$	86
$\boldsymbol{\mathcal{H}}_\mathrm{v}$	$[\boldsymbol{H}(\mathbf{curl}, \Omega)] \times \boldsymbol{H}^{-\frac{1}{2}}(\mathrm{div}_\Gamma\, 0, \Gamma)$	93
$\mathbb{S}^1_{\boldsymbol{p}}(\mathbf{curl}\,\mathbf{0}, \Omega)$	$\{\boldsymbol{v}_\ell \in \mathbb{S}^1_{\boldsymbol{p}}(\Omega) :\ \mathbf{curl}\,\boldsymbol{v}_\ell = \mathbf{0}\}$	97

Bibliography

[1] R. A. Adams and J. J. F. Fournier, *Sobolev spaces*. Elsevier, 2003.

[2] A. Aimi, F. Calabro, M. Diligenti, M. L. Sampoli, G. Sangalli, and A. Sestini, *Efficient assembly based on B-spline tailored quadrature rules for the IgA-SGBEM*, *Computer Methods in Applied Mechanics and Engineering*, vol. 331, pp. 327–342, 2018.

[3] C. Amrouche, C. Bernardi, M. Dauge, and V. Girault, *Vector potentials in three-dimensional non-smooth domains*, *Mathematical Methods in the Applied Sciences*, vol. 21, no. 9, pp. 823–864, 1998.

[4] D. N. Arnold, R. S. Falk, and R. Winther, *Finite element exterior calculus, homological techniques, and applications*, *Acta Numerica*, vol. 15, pp. 1–155, 2006.

[5] K. E. Atkinson, *An introduction to numerical analysis*. John Wiley & Sons, 1969.

[6] M. Aurada, M. Feischl, T. Führer, M. Karkulik, J. M. Melenk, and D. Praetorius, *Classical FEM-BEM coupling methods: nonlinearities, well-posedness, and adaptivity*, *Computational Mechanics*, vol. 51, no. 4, pp. 399–419, 2013.

[7] A. Bantle, *On high-order NURBS-based boundary element methods in two dimensions-numerical integration and implementation*, PhD Thesis, Universität Ulm, 2015.

[8] M. Bebendorf, *Approximation of boundary element matrices*, *Numerische Mathematik*, vol. 86, no. 4, pp. 565–589, 2000.

[9] J. Bielak and R. C. MacCamy, *An exterior interface problem in two-dimensional elastodynamics*, *Quarterly of Applied Mathematics*, vol. 41, no. 1, pp. 143–159, 1983.

[10] Z. Bontinck, J. Corno, S. Schöps, and H. De Gersem, *Isogeometric Analysis and Harmonic Stator-Rotor Coupling for Simulating Electric Machines*, *Computer Methods in Applied Mechanics and Engineering*, vol. 334, 2017. DOI: 10.1016/j.cma.2018.01.047.

[11] A. Bossavit, *Computational electromagnetism: variational formulations, complementarity, edge elements*. Academic Press, 1998.

[12] ——, *Magnetostatic problems in multiply connected regions: some properties of the curl operator*, *IEE Proceedings A (Physical Science, Measurement and Instrumentation, Management and Education, Reviews)*, vol. 135, no. 3, pp. 179–187, 1988.

[13] ——, *On the numerical analysis of eddy-current problems*, *Computer Methods in Applied Mechanics and Engineering*, vol. 27, no. 3, pp. 303–318, 1981.

[14] F. Bruckner, C. Vogler, M. Feischl, D. Praetorius, B. Bergmair, T. Huber, M. Fuger, and D. Suess, *3D FEM-BEM-coupling method to solve magnetostatic Maxwell equations*, *Journal of Magnetism and Magnetic Materials*, vol. 324, no. 10, pp. 1862–1866, 2012, ISSN: 0304-8853. DOI: https://doi.org/10.1016/j.jmmm.2012.01.016.

[15] A. Buffa, *Hodge decompositions on the boundary of nonsmooth domains: the multi-connected case*, *Mathematical Models and Methods in Applied Sciences*, vol. 11, no. 09, pp. 1491–1503, 2001.

[16] A. Buffa, H. Ammari, and J.-C. Nédélec, *A justification of eddy currents model for the Maxwell equations*, *SIAM Journal on Applied Mathematics*, vol. 60, no. 5, pp. 1805–1823, 2000.

[17] A. Buffa and P. J. Ciarlet, *On traces for functional spaces related to Maxwell's equations Part I: An integration by parts formula in Lipschitz polyhedra*, *Mathematical Methods in the Applied Sciences*, vol. 24, no. 1, pp. 9–30, 2001.

[18] ——, *On traces for functional spaces related to Maxwell's equations Part II: Hodge decompositions on the boundary of Lipschitz polyhedra and applications*, *Mathematical Methods in the Applied Sciences*, vol. 24, no. 1, pp. 31–48, 2001.

[19] A. Buffa, M. Costabel, and C. Schwab, *Boundary element methods for Maxwell's equations on non-smooth domains*, *Numerische Mathematik*, vol. 92, no. 4, pp. 679–710, 2002.

[20] A. Buffa, M. Costabel, and D. Sheen, *On traces for H(curl,Ω) in Lipschitz domains*, *Journal of Mathematical Analysis and Applications*, vol. 276, no. 2, pp. 845–867, 2002, ISSN: 0022-247X. DOI: https://doi.org/10.1016/S0022-247X(02)00455-9.

[21] A. Buffa, J. Dölz, S. Kurz, S. Schöps, R. Vázquez, and F. Wolf, *Multipatch approximation of the de Rham sequence and its traces in isogeometric analysis*, *Numerische Mathematik*, vol. 144, no. 1, pp. 201–236, 2020.

[22] A. Buffa and R. Hiptmair, *Galerkin boundary element methods for electromagnetic scattering*, in *Topics in computational wave propagation*, Springer, 2003, pp. 83–124.

[23] A. Buffa, R. Hiptmair, T. von Petersdorff, and C. Schwab, *Boundary element methods for Maxwell transmission problems in Lipschitz domains*, *Numerische Mathematik*, vol. 95, no. 3, pp. 459–485, 2003.

[24] A. Buffa, G. Sangalli, and R. Vázquez, *Isogeometric analysis in electromagnetics: B-splines approximation*, *Computer Methods in Applied Mechanics and Engineering*, vol. 199, no. 17-20, pp. 1143–1152, 2010.

[25] A. Buffa, R. H. Vázquez, G. Sangalli, and L. Beirão da Veiga, *Approximation estimates for isogeometric spaces in multipatch geometries*, *Numerical Methods for Partial Differential Equations*, vol. 31, no. 2, pp. 422–438, 2015.

[26] C. Carstensen and E. P. Stephan, *Adaptive coupling of boundary elements and finite elements*, *RAIRO Modélisation Mathématique et Analyse Numérique*, vol. 29, no. 7, pp. 779–817, 1995.

[27] M. Cessenat, *Mathematical methods in electromagnetism: linear theory and applications*. World Scientific, 1996, vol. 41.

[28] R. L. Clay, S. J. Marburger, T. G. Trucano, and M. S. Shneider, *Modeling and Simulation Technology Readiness Levels*. United States. Department of Energy, 2006.

[29] J. Corno, C. de Falco, H. De Gersem, and S. Schöps, *Isogeometric simulation of Lorentz detuning in superconducting accelerator cavities*, *Computer Physics Communications*, vol. 201, pp. 1–7, 2016.

[30] M. Costabel, *A symmetric method for the coupling of finite elements and boundary elements*, *The Mathematics of Finite Elements and Applications, VI (Uxbridge, 1987)*, pp. 281–288, 1988.

[31] ——, *Boundary integral operators on Lipschitz domains: elementary results*, *SIAM Journal on Mathematical Analysis*, vol. 19, no. 3, pp. 613–626, 1988.

[32] J. A. Cottrell, T. J. Hughes, and Y. Bazilevs, *Isogeometric analysis: toward integration of CAD and FEA*. John Wiley & Sons, 2009.

[33] L. B. Da Veiga, A. Buffa, G. Sangalli, and R. Vázquez, *Mathematical analysis of variational isogeometric methods*, *Acta Numerica*, vol. 23, pp. 157–287, 2014.

[34] R. Dautray and J.-L. Lions, *Mathematical analysis and numerical methods for science and technology: volume 1 physical origins and classical methods*. Springer Science & Business Media, 2012.

[35] ——, *Mathematical analysis and numerical methods for science and technology: volume 3 Spectral Theory and Applications*. Springer Science & Business Media, 1999, vol. 3.

[36] B. Davat, Z. Ren, and M. Lajoie-Mazenc, *The movement in field modeling*, *IEEE Transactions on Magnetics*, vol. 21, no. 6, pp. 2296–2298, 1985.

[37] C. de Falco, A. Reali, and R. Vázquez, *GeoPDEs: a research tool for isogeometric analysis of PDEs*, *Advances in Engineering Software*, vol. 42, no. 12, pp. 1020–1034, 2011.

[38] J. Dölz, H. Harbrecht, S. Kurz, M. Multerer, S. Schöps, and F. Wolf, *Bembel: The fast isogeometric boundary element C++ library for Laplace, Helmholtz, and electric wave equation*, *SoftwareX*, vol. 11, p. 100 476, 2020.

[39] J. Dölz, S. Kurz, S. Schöps, and F. Wolf, *Isogeometric boundary elements in electromagnetism: Rigorous analysis, fast methods, and examples*, *SIAM Journal on Scientific Computing*, vol. 41, no. 5, B983–B1010, 2019.

[40] J. W. Eaton, D. Bateman, S. Hauberg, and R. Wehbring, *GNU Octave version 5.1.0 manual: a high-level interactive language for numerical computations*, 2019.

[41] H. Egger, C. Erath, and R. Schorr, *On the nonsymmetric coupling method for parabolic-elliptic interface problems*, *SIAM Journal on Numerical Analysis*, vol. 56, no. 6, pp. 3510–3533, 2018, ISSN: 0036-1429. DOI: 10.1137/17M1158276.

[42] M. Elasmi, C. Erath, and S. Kurz, *Non-symmetric isogeometric FEM-BEM couplings*, *Advances in Computational Mathematics*, vol. 47, no. 61, 2021. DOI: https://doi.org/10.1007/s10444-021-09886-3.

[43] ——, *The Johnson-Nédélec FEM-BEM coupling for magnetostatic problems in the isogeometric framework*, 2021. arXiv: 2110.04150 [math.NA].

[44] S. Engleder, *Boundary Element Methods for Eddy Current Transmission Problems*, PhD Thesis, Institut für Numerische Mathematik, Graz University of Technology, 2011.

[45] C. Erath, *Coupling of the finite volume element method and the boundary element method: an a priori convergence result*, *SIAM Journal on Numerical Analysis*, vol. 50, no. 2, pp. 574–594, 2012, ISSN: 0036-1429. DOI: 10.1137/110833944.

[46] C. Erath, G. Of, and F. Sayas, *A non-symmetric coupling of the finite volume method and the boundary element method*, *Numerische Mathematik*, vol. 135, no. 3, pp. 895–922, 2017.

[47] C. Erath and R. Schorr, *Stable Non-symmetric Coupling of the Finite Volume Method and the Boundary Element Method for Convection-Dominated Parabolic-Elliptic Interface Problems*, *Computational Methods in Applied Mathematics*, pp. 1–22, 2019. DOI: 10.1515/cmam-2018-0253.

[48] L. C. Evans, *Partial differential equations*, *Graduate Studies in Mathematics*, vol. 19, no. 2, 1998.

[49] P. Fernandes and G. Gilardi, *Magnetostatic and electrostatic problems in inhomogeneous anisotropic media with irregular boundary and mixed boundary conditions*, *Mathematical Models and Methods in Applied Sciences*, vol. 7, no. 07, pp. 957–991, 1997.

[50] P. Fernandes and I. Perugia, *Vector potential formulation for magnetostatics and modelling of permanent magnets*, *IMA Journal of Applied Mathematics*, vol. 66, no. 3, pp. 293–318, 2001.

[51] J. Franců, *Monotone operators. A survey directed to applications to differential equations*, *Aplikace Matematiky*, vol. 35, no. 4, pp. 257–301, 1990.

[52] A. Frangi, P. Faure-Ragani, and L. Ghezzi, *Magneto-mechanical simulations by a coupled fast multipole method-finite element method*, in *Computational Fluid and Solid Mechanics 2003*, Elsevier, 2003, pp. 1347–1349.

[53] M. Galewski, *On variational nonlinear equations with monotone operators*, *Advances in Nonlinear Analysis*, vol. 10, no. 1, pp. 289–300, 2021.

[54] J. F. Gieras, *Electrical Machines: Fundamentals of Electromechanical Energy Conversion*. CRC Press, 2016.

[55] V. Girault and P.-A. Raviart, *Finite Element Methods for Navier-Stokes Equations: Theory and Algorithms*. Springer Series in Computational Mathematics. Springer-Verlag, Berlin-Heidelberg, 1986.

[56] M. González, *Fully discrete FEM-BEM method for a class of exterior nonlinear parabolic–elliptic problems in 2D*, *Applied Numerical Mathematics*, vol. 56, no. 10-11, pp. 1340–1355, 2006.

[57] W. Hafla, A. Buchau, and W. M. Rucker, *Accuracy improvement in nonlinear magnetostatic field computations with integral equation methods and indirect total scalar potential formulations*, *COMPEL - The International Journal for Computation and Mathematics in Electrical and Electronic Engineering*, 2006.

[58] G. W. Hanson and A. B. Yakovlev, *Operator theory for electromagnetics: an introduction*. Springer Science & Business Media, 2013.

[59] A. Hatcher, *Algebraic topology*. Cambridge University Press, 2005.

[60] R. Hiptmair, *Finite elements in computational electromagnetism*, *Acta Numerica 2002*, vol. 11, no. 11, p. 237, 2002.

[61] ——, *Symmetric coupling for eddy current problems*, *SIAM Journal on Numerical Analysis*, vol. 40, no. 1, pp. 41–65, 2002.

[62] R. Hiptmair and J. Ostrowski, *Coupled boundary-element scheme for eddy-current computation*, *Journal of Engineering Mathematics*, vol. 51, no. 3, pp. 231–250, 2005.

[63] ——, *Generators of $H_1(\Gamma_h, \mathbb{Z})$ for Triangulated Surfaces: Construction and Classification*, *SIAM Journal on Computing*, vol. 31, no. 5, pp. 1405–1423, 2002.

[64] B.-Y. Hou and B.-Y. Hou, *Differential geometry for physicists*. World Scientific Publishing Company, 1997, vol. 6.

[65] T. Hughes, J. Cottrell, and Y. Bazilevs, *Isogeometric analysis: CAD, finite elements, NURBS, exact geometry and mesh refinement*, *Computer Methods in Applied Mechanics and Engineering*, vol. 194, no. 39, pp. 4135–4195, 2005, ISSN: 0045-7825. DOI: https://doi.org/10.1016/j.cma.2004.10.008.

[66] N. Ida and J. P. A. Bastos, *Electromagnetics and calculation of fields*. Springer Science & Business Media, 2013.

[67] J. D. Jackson, *Classical electrodynamics*. Wiley, New York, 1975.

[68] JMAG-Designer. (2021). *JSOL-Corporation*, [Online]. Available: https://www.jmag-international.com/products/jmag-designer/ (visited on 09/09/2021).

[69] C. Johnson and J. C. Nédélec, *On the coupling of boundary integral and finite element methods*, *Mathematics of Computation*, vol. 35, pp. 1063–1079, 1980.

[70] H. Kanayama, R. Shioya, D. Tagami, and H. Zheng, *A numerical procedure for 3-D nonlinear magnetostatic problems using the magnetic vector potential*, *Theoretical and Applied Mechanics*, vol. 50, pp. 411–418, 2001.

[71] L. Kielhorn, T. Rüberg, and J. Zechner, *Robust FEM-BEM Coupling for LS-DYNA®'s EM module*, *International LS-DYNA® Users Conference*, 2018.

[72] ——, *Simulation of electrical machines: a FEM-BEM coupling scheme*, *COMPEL-The International Journal for Computation and Mathematics in Electrical and Electronic Engineering*, 2017.

[73] A. Kufner, O. John, and S. Fucik, *Function spaces*. Springer Science & Business Media, 1977, vol. 3.

[74] M. Kuhn and O. Steinbach, *Symmetric coupling of finite and boundary elements for exterior magnetic field problems*, *Mathematical Methods in the Applied Sciences*, vol. 25, no. 5, pp. 357–371, 2002.

[75] S. Kurz, *Die numerische Behandlung elektromechanischer Systeme mit Hilfe der Kopplung der Methode der finiten Elemente und der Randelementmethode*. VDI-Verlag, 1998.

[76] S. Kurz and B. Auchmann, *Differential forms and boundary integral equations for Maxwell-type problems*, *Fast Boundary Element Methods in Engineering and Industrial Applications*, pp. 1–62, 2012.

[77] S. Kurz, J. Fetzer, T. Kube, G. Lehner, and W. M. Rucker, *BEM-FEM coupling in electromechanics: A 2-D watch stepping motor driven by a thin wire coil*, *Applied Computational Electromagnetics Society Journal*, vol. 12, pp. 135–139, 1997.

[78] S. Kurz, J. Fetzer, G. Lehner, and W. M. Rucker, *A novel formulation for 3D eddy current problems with moving bodies using a Lagrangian description and BEM-FEM coupling*, *IEEE Transactions on Magnetics*, vol. 34, no. 5, pp. 3068–3073, 1998.

[79] L. D. Landau and E. M. Lifshitz, *Course of Theoretical Physics*, *Electrodynamics of Continuous Media*, vol. VIII: Electrodynamics of Continuous Media, 1984.

[80] U. Langer, S. E. Moore, and M. Neumüller, *Space–time isogeometric analysis of parabolic evolution problems*, *Computer Methods in Applied Mechanics and Engineering*, vol. 306, pp. 342–363, 2016.

[81] V. Leconte, *Simulation des convertisseurs électromécaniques*, PhD Thesis, Institut National Polytechnique de Grenoble-INPG, 2000.

[82] R. C. MacCamy and M. Suri, *A Time-Dependent Interface Problem for Two-Dimensional Eddy Currents*, *Quarterly of Applied Mathematics*, vol. 44, pp. 675–690, 1987.

[83] *Mathematica, version 12.0*, Champaign, IL, Wolfram Research, Inc. 2019.

[84] MATLAB, *version 7.10.0 (R2019a)*. Natick, Massachusetts: The MathWorks Inc., 2019.

[85] J. C. Maxwell, *VIII. A dynamical theory of the electromagnetic field*, *Philosophical Transactions of the Royal Society of London*, no. 155, pp. 459–512, 1865.

[86] S. May, M. Kästner, S. Müller, and V. Ulbricht, *A hybrid IGAFEM/IGABEM formulation for two-dimensional stationary magnetic and magneto-mechanical field problems*, *Computer Methods in Applied Mechanics and Engineering*, vol. 273, pp. 161–180, 2014.

[87] W. McLean, *Strongly elliptic systems and boundary integral equations*. Cambridge University Press, 2000.

[88] P. Monk, *Finite element methods for Maxwell's equations*. Oxford University Press, 2003.

[89] G. Of and O. Steinbach, *Is the one-equation coupling of finite and boundary element methods always stable?*, *ZAMM-Journal of Applied Mathematics and Mechanics/Zeitschrift für Angewandte Mathematik und Mechanik*, vol. 93, no. 6-7, pp. 476–484, 2013.

[90] ——, *On the ellipticity of coupled finite element and one-equation boundary element methods for boundary value problems*, *Numerische Mathematik*, vol. 127, no. 3, pp. 567–593, 2014.

[91] C. Pechstein, *Multigrid-Newton-methods for nonlinear magnetostatic problems*, Master's Thesis, Johannes Kepler University of Linz, Institute of Computational Mathematics, Linz, 2004.

[92] C. Pechstein and B. Jüttler, *Monotonicity-preserving interproximation of B–H-curves*, *Journal of Computational and Applied Mathematics*, vol. 196, no. 1, pp. 45–57, 2006.

[93] E. Picard, *Mémoire sur la théorie des équations aux dérivées partielles et la méthode des approximations successives*, *Journal de Mathématiques Pures et Appliquées*, vol. 6, pp. 145–210, 1890.

[94] L. Piegl and W. Tiller, *The NURBS book*. Springer Science & Business Media, 2012.

[95] D. Pusch and J. Ostrowski, *Robust FEM/BEM coupling for magnetostatics on multiconnected domains*, *IEEE Transactions on Magnetics*, vol. 46, no. 8, pp. 3177–3180, 2010.

[96] S. Reitzinger, B. Kaltenbacher, and M. Kaltenbacher, *A note on the approximation of BH curves for nonlinear magnetic field computations*, *Johannes Kepler University Linz*, 2002.

[97] S. Rjasanow and O. Steinbach, *The fast solution of boundary integral equations*. Springer Science & Business Media, 2007.

[98] S. Rjasanow and L. Weggler, *ACA accelerated high order BEM for Maxwell problems*, *Computational Mechanics*, vol. 51, no. 4, pp. 431–441, 2013.

[99] U. Römer, *Numerical approximation of the magnetoquasistatic model with uncertainties and its application to magnet design*, PhD Thesis, Institut für Theorie Elektromagnetischer Felder, Technische Universität Darmstadt, 2015.

[100] W. Rudin, *Functional analysis*. McGraw-Hill, New York, 1973.

[101] P. Salgado and V. Selgas, *A symmetric BEM-FEM coupling for the three-dimensional magnetostatic problem using scalar potentials*, *Engineering Analysis with Boundary Elements*, vol. 32, no. 8, pp. 633–644, 2008.

[102] S. J. Salon, *Finite element analysis of electrical machines*. Kluwer Academic Publishers Boston, 1995, vol. 101.

[103] S. A. Sauter and C. Schwab, *Boundary Element Methods*. Springer, Berlin, Heidelberg, 2011.

[104] F. Sayas, *The validity of Johnson–Nédélec's BEM–FEM coupling on polygonal interfaces*, *SIAM Journal on Numerical Analysis*, vol. 47, no. 5, pp. 3451–3463, 2009.

[105] K. Schmidt, O. Sterz, and R. Hiptmair, *Estimating the eddy-current modeling error*, *IEEE Transactions on Magnetics*, vol. 44, no. 6, pp. 686–689, 2008.

[106] R. Schorr, *Numerical Methods for Parabolic-Elliptic Interface Problems*, PhD Thesis, Technische Universität Darmstadt, 2019.

[107] C. Schwab and W. Wendland, *On the extraction technique in boundary integral equations*, *Mathematics of Computation*, vol. 68, no. 225, pp. 91–122, 1999.

[108] O. Steinbach, *A note on the stable one-equation coupling of finite and boundary elements*, *SIAM Journal on Numerical Analysis*, vol. 49, no. 4, pp. 1521–1531, 2011.

[109] ——, *Numerical approximation methods for elliptic boundary value problems: finite and boundary elements*. Springer Science & Business Media, 2007.

[110] O. Steinbach and W. L. Wendland, *On C. Neumann's Method for Second-Order Elliptic Systems in Domains with Non-smooth Boundaries*, *Journal of Mathematical Analysis and Applications*, vol. 262, no. 2, pp. 733–748, 2001, ISSN: 0022-247X. DOI: https://doi.org/10.1006/jmaa.2001.7615.

[111] ——, *The construction of some efficient preconditioners in the boundary element method*, *Advances in Computational Mathematics*, vol. 9, no. 1, pp. 191–216, 1998.

[112] T. Steinmetz, S. Kurz, and M. Clemens, *Domains of validity of quasistatic and quasistationary field approximations*, *COMPEL-The International Journal for Computation and Mathematics in Electrical and Electronic Engineering*, 2011.

[113] R. Touzani and J. Rappaz, *Mathematical Models for Eddy Currents and Magnetostatics: With Selected Applications*. Springer Netherlands, 2014.

[114] R. Vázquez, *A new design for the implementation of isogeometric analysis in Octave and Matlab: GeoPDEs 3.0*, *Computers & Mathematics with Applications*, vol. 72, no. 3, pp. 523–554, 2016, ISSN: 0898-1221. DOI: https://doi.org/10.1016/j.camwa.2016.05.010.

[115] C. Von Westenholz, *Differential forms in mathematical physics*. Elsevier, 2009.

[116] L. Weggler, *High order boundary element methods*, PhD Thesis, Universität des Saarlandes, 2011.

[117] D. Werner, *Funktionalanalysis*. Springer, 2006.

[118] J. Wloka, *Partial Differential Equations*. Cambridge University Press, 1987.

[119] F. Wolf, *Analysis and Implementation of Isogeometric Boundary Elements for Electromagnetism*. Springer Nature, 2021.

[120] E. H. Zarantonello, *Solving functional equations by contractive averaging*. Mathematics Research Center, United States Army, University of Wisconsin, 1960.

[121] E. Zeidler, *Nonlinear Functional Analysis and its Applications II/A: Linear Monotone Operators*. Springer, 1986.

[122] ——, *Nonlinear Functional Analysis and its Applications II/B: Nonlinear Monotone Operators*. Springer, 1986.

Acknowledgements

First and foremost, I would like to thank Prof. Stefan Kurz and Prof. Christoph Erath for their highly efficient and valuable supervision. I am very grateful for the support you gave me during this thesis both on the scientific and personal levels. Your feedback and inputs were utterly helpful.
A necessary condition to accomplish a PhD is to start one. Therefore, I reiterate here my gratitude to Stefan for giving me this opportunity, and also to Prof. Sergej Rjasanow for supervising my master thesis, which I consider as my first real encounter with the world of numerical mathematics. For this nice encounter, I am still very thankful. I also would like to thank Prof. Sebastian Schöps for several reasons. Thank you for co-examining this work, and for the pleasant working atmosphere you provide in the CEM workgroup. At some times, I did almost forget that I am actually not a member of the CEM group. Contributors to this friendly and enjoyable atmosphere are of course all actual and former CEMler. I really enjoyed your company, and in particular the not so scientific discussions. Thank you! On the same note, I thank all TEMFler, and my former colleagues of the Graduate School of Computational Engineering. I think I forgot to organize another Kicker tournament! Sorry!

Apart from the academic world, I am extremely grateful to my mother Raoudha, and to my father Zied, from whom I got my interest in science. Thank you for your unconditional support and motivation! Moreover, I would like to thank my sisters Faten and Nadia, and my brother Tarek very much for their motivating feedback on this work, as well as for everything else. In particular, thank you Nadia for your contribution to considerably ameliorate the writing style in some parts of this work.
Furthermore, I thank all my friends and roommates for their extracurricular support by providing me with the needed distractions every now and then. Last but not least, I am very grateful to Pegi for reading and improving considerably the writing style of the whole treatise, and for the valuable support especially all along the writing process. Thank you very much!

This work is supported by the *Excellence Initiative* of the German Federal and State Governments and the *Graduate School of Computational Engineering* at TU Darmstadt.